A Contribution to Optimal Scheduling of Real-World Trigeneration Systems using Economic Model Predictive Control

Von der Fakultät Maschinenwesen

der Technischen Universität Dresden

zur Erlangung des akademischen Grades

Doktoringenieur (Dr.-Ing.)

angenommene Dissertation

von

M.Sc. Parantapa Sawant

geboren am 22.12.1987 in Sangli (Indien)

Acknowledgement

Index

List of selected abbreviations

AdC	Adsorption Chiller
BAC	Building Automation and Control
BEMS	Building Energy Management System
BLM	Base Load Matching
CCHP	Combined Cooling, Heating, and Power
CC	Compression Chiller
CHP	Combined Heating and Power
CL	Cooling Load
COP	Coefficient of Performance
CTES	Cold Thermal Energy Storage
EER	Energy Efficiency Ratio
EL	Electrical Load
EPMS	Energy Plant Management System
FEL	Following Electrical Load
FLM	Full Load Matching
FTL	Following Thermal Load
HiL	Hardware-in-the-Loop
HL	Heating Load
HMI	Human-Machine-Interface
HP	Heat Pump
HTES	Hot Thermal Energy Storage
INES	Institute of Energy Systems Technology
LG	Load Generators
MAE	Mean Absolute Error
MILP	Mixed Integer Linear Problem
MINLP	Mixed Integer Nonlinear Problem
MIOCP	Mixed Integer Optimal Control Problem
MPC	Model Predictive Control
NLP	Nonlinear Problem
NRMSRE	Normalised Root Mean Squared Relative Error
NTU-ε	Number of Transfer Units – Effectiveness
OC	Outdoor Coil
ODE	Ordinary Differential Equations
OPC	OLE for Process Control
PID	Proportional Integral Derivative Control
PLC	Programmable Logic Controller
RCV	Relative Change-of-Value
RHP	Reversible Heat Pump
SNSE	Sum of Normalised Squared Error
TC	Test Chamber

List of selected symbols and indices

Symbols

Symbol	Meaning	Common unit
A	Area	m^2
$\boldsymbol{b}$	Binary control vector	-
$\boldsymbol{c}$	Vector of time-varying parameters	-
c_p	Specific heat capacity	kJ/(kg·K)
C	Heat capacity rate	W/K
COP	Coefficient of performance	-
$Cost$	Total cost for consumption of a final energy	€
C_r	Heat capacity rate ratio	-
CT_i	Temperature of ith layer in cold tank	°C
d	Thickness	m
dt	Integration interval	s
D	Diameter of tank	m
e	Control difference	-
E	Mayer term	-
f	General function	-
g	Equality constraint function	-
h	Inequality constraint function	-
H	Height of tank	m
HCV	Higher calorific value	kWh/m^3
HT_i	Temperature of ith layer in hot tank	°C
J	Cost function	-
k	Overall heat transfer coefficient of the tank envelope	W/(m^2·K)
K_s	Gain of controlled system	-
K_p	Proportional gain of PID controller	-
L	Lagrange term	-
m	Mass of water in one tank layer	kg
$\dot{m}$	Mass flow	kg/h
N	Number	-
NTU	Number of transfer units	-
$\boldsymbol{p}$	Vector of constant parameters	-
P	Power	kW
Q	Energy thermal	kWh

Symbols (continued)

Symbol	Meaning	Common unit
r	Rate or price of final energy	€/kWh or €/m^3
r^2	Coefficient of determination	-
RPM	Rotational speed	RPM
$\mathbb{R}$	Set of real numbers	-
$\boldsymbol{s}$	Vector of slack variables	-
$sLCOE$	Simple levelised cost of energy	€/kWh
S	On-off switch	-
t	Time, time period	h
Δt	Time-step	s
T	Temperature	°C
T_v	Derivative-action time of PID controller	s
T_n	Integral-action time of PID controller	s
T_s	Time-constant of controlled system	s
T_t	Dead time	s
u	Manipulated variable	-
$\boldsymbol{u}$	Vector of continuous controls	-
U	Overall heat transfer coefficient	W/(m^2·K)
V	Voltage	V
$\dot{v}$	Volume flow	m^3/h
W	Energy electrical	kWh
W_s	Weighting matrix for slack variables	-
$\boldsymbol{x}$	Vector of states	-
x	Independent variables in regression analysis	-
$\dot{x}$	Time derivative of a system state	-
$\mathbb{X}$	Set of admissible states	-
$\boldsymbol{y}$	Vector of outputs	-
y	Measured value	-
y^*	Dependent variable in regression analysis	-
y^*	Predicted value	-
$\bar{y}$	Arithmetic mean of measured values	
$\bar{y}^*$	Arithmetic mean of predicted values	
z	Height of one layer in the tank	m
$\mathbb{Z}$	Set of integer values	-
$a,b,c,d,e,e^*,f,f^*,g,g^*,h$	Coefficients of regression for different models	-

Symbol	Meaning	Common unit
β	Coefficients of regression in regression analysis	-
δ	Binary parameter	-
ε	Heat exchanger effectiveness	-
$\mathcal{L}$	Lagrangian function	-
λ	Heat conductivity	W/(m·K)
λ	Lagrange multiplier vector for equality constraints	-
μ	Lagrange multiplier vector for inequality constraints	-
η	Efficiency	-
ρ	Density	kg/m^3

Indices

Subscript	Meaning
air	Ambient air
aprx	Approximate
AdC	Adsorption chiller
amb	Ambient
aux	Auxiliary or ancillary
b	Brine
buy	Buying from grid
c	Condenser circuit of the reversible heat pump
c	Cold fluid entering heat exchanger
cool	Cooling
CC	Compression chiller
CHP	Combined heating and power
CL	Cooling load
CT	Cold tank
e	Evaporator circuit of the reversible heat pump
eff	Effective
el	Electrical or electricity
ext	Exterior
EL	Electrical load
EMPC	Economic-MPC
EPEX	EPEX SPOT SE day-ahead auction electricity prices
EWERK	Two-price electricity tariff structure of the local grid operator

Indices (continued)

Subscript	Meaning
f	Feed-line leaving a component
f	Final time-step
fc	Forecast
fe	Final energy
fuel	Related to fuel consumed by CHP
grid	Related to electricity grid
h	Hot fluid entering heat exchanger
heat	Heating
H	High temperature circuit
HL	Heating load
HP	Heat pump
HT	Hot tank
HX	Heat exchanger
init	Initial
IMG	Related to INES micro-grid
lb	Lower bound
loss	Thermal losses
L	Low temperature circuit
LG	Load generator
max	Maximum
meas	Measured
min	Minimum
M	Medium temperature circuit
MPC	Related to tests with MPC
n_b	Number of binary controls
n_c	Number of time-varying parameters
n_p	Number of time-constant parameters
n_s	Number of slack variables
n_u	Number of inputs or controls
n_x	Number of states
n_y	Number of outputs
nom	Nominal value
opt	Optimal
OC	Outdoor coil
prev	Previous solution
r	Return-line entering a component
ref	Related to tests with reference controller
relx	Relaxed value with respect to binary controls
RHP	Reversible heat pump
sell	Selling to grid

Subscript	Meaning
sim	Simulated
SNSE	Sum of normalised squared error
total	Total value
th	Thermal
TC	Test chamber
ub	Upper bound
w	Water
i,j,k	Serial variables

Glossary of terms

For the purposes of this dissertation, the following terms and definitions apply:

Availability of controller framework

Availability is a representative metric for the probability that the controller framework will provide a practical schedule for the plant during the period of a test and will not fail to control the individual components.

Bang-bang control

When the solution of the optimal control problem switches from one extreme restriction (upper bound or lower bound) to another (i.e. is strictly never in between the bounds), then that solution is referred to as a bang-bang solution.

Building automation and control system

A building automation and control system is typically a computer-based hierarchical framework, comprising of all engineering tools and services facilitating automatic control, monitoring, optimisation, operation, human intervention, and management to achieve a good building performance.

Building energy management system

A building energy management system is typically a computerised system that is an integrated part of the building automation and control, for monitoring and controlling all energy-related building services plant and equipment.

Consumption-related costs

Consumption-related or demand-related costs is the cost group in total cost of a plant that must be paid for consumption of final energies like electricity and fuel.

Control architecture

Control architecture refers to the strategy to combine the model based controllers with the capabilities of an existing building automation and control system into a coherent framework and is described using a flow chart.

Control logic

Is an underlying part of the control architecture and describes the operation of a controller using flow charts and state diagrams.

Control loop

Is the combination of the controlled system and the controller with a closed chain of action.

Energy plant management system

The element of a building energy management system focussing specifically on scheduling of the heating and/or cooling plant refers to the energy plant management system.

Final energy

Final energy is the generic term for the energy in the form of fuel or electricity from a grid converted by the heating and/or cooling plant into useful energy for the end user. It includes the auxiliary energy and electrical consumption of the individual components in the plant.

Functional tests

Refers to the rudimentary functional performance testing done with the individual components and the entire system during the commissioning phase and conventional controller development phase.

Grid-supportive operation

Grid-supportive or grid-reactive operation means the economically optimal scheduling of a heating and/or cooling plant with respect to a variable electricity price reflecting the grid's status in terms of consumption and generation profiles, grid congestion, and utilisation of grid connectivity.

Grey-box modelling

Is a modelling methodology to program HVAC models by combining a physics based mathematical structure and data based curve fits.

Internal control logic

The control logic programmed on embedded controllers inside the components to improve their performance under part-load operation or for their operational safety is defined as internal control logic. The controller is set at default-values and is not accessible to end user in most cases.

Manipulated variable

The manipulated variable or control signal is the output of the controller and input of the controlled system to influence the value of the controlled variable.

Mixed integer nonlinear problem

Refers to a special class of optimisation problems where the objective function and/or constraint equations are twice differentiable in the decision variables which are either real or integer values.

Model based control

An open-loop control algorithm that uses the output of the controlled system's simulation model to generate a manipulated variable is defined as model based control. This type of control is typically used in reactive control since the controlled system lacks any elements (e.g. storages) that can be predictively controlled.

Model predictive control

Model predictive control is an optimal feedback control technique that is based on the repeated solution of an open-loop optimal control problem where at each sampling instance an optimisation problem is solved to predict and optimise the system's future behaviour and only the first control action is implemented at the real process. At next instance the horizon is adjusted and the entire process is repeated. See also "Optimal control".

Optimal control

With reference to dynamic systems, optimal control is the application of mathematical algorithms to find a control law for the system such that an optimal criterion is achieved under the restriction of constraints on that system. The policy for developing the optimal controller could be open-loop or a closed feedback loop and may include estimation of the system states too.

Outdoor coil

The outdoor coil is a dry-cooled electric fan recooler acting as both heat sink and heat source for the thermal chiller and heat pump respectively.

Process variable

Process variables are the typical physical parameters in an industrial plant that are monitored during operation and describe the status of the plant e.g. circuit temperatures or volume flows.

Simple levelised cost of energy

The simple levelised cost of energy is a version of the popular metric "levelised cost of energy" and is applied to calculate cost of useful energy based only on the consumption-related costs of final energy over the duration of the monitoring campaign. The capital-related costs, operation-related costs, other costs, and discount rate factors over the long-term life of the plant are not included in the scope of this work.

Supervisory controller

The modern definition of a supervisory controller replaces the older version of human supervised controller and outlines an automation-based system within the building automation and control system facilitating the automatic control of a plant on the field level.

Switching point

In control of heating or cooling plants with multiple components, the operation mode can be switched from one component to another based on a pre-defined logic using the switching point. Typically, the switching logic is based on ambient temperature and referred to as bivalent operation using the bivalency point.

System state

A dynamic process variable that characterises a dynamic system by predicting its evolution over time through solution of differential equations is defined as a system state. For instance, temperature of a storage tank or state of charge in a battery.

Trigeneration systems

Trigeneration systems or combined cooling, heating, and power systems are technically an extension of cogeneration systems wherein the waste heat of cogeneration is used to produce cooling in thermal chillers.

Useful energy

Useful energy is the generic term referring to the energy required by the end user for satisfying the electricity, heating, cooling, and air conditioning requirements.

1   Introduction

"Fridays for Future" and "Coal Exit Commission" are a few recent developments amongst a long-standing list of projects, which are helping to accelerate the "Energy Transition" in Europe economically, socially, and politically. The sustainable shift to renewables will require an integrated development of the system with coupling of the energy, transport, and building sectors in combination with storage technologies (BMWi, 2018; Kalz et al., 2018; Klein et al., 2016). The far-reaching motivation of this work is to support this shift in the buildings and districts sector by facilitating their action as flexible prosumers (producers and consumers), intelligent storage systems, or decentralised micro-grids. This will ensure greater adaptability to variable renewable technologies and grid-supportive operation of building energy systems.

The latest "Energy Transition Monitoring Report" targets a decrease of 80% by 2050 in the primary energy consumption for buildings in comparison with 2008 (BMWi, 2018). Energy systems like trigeneration shown in *Fig. 1-1* contribute to reduction of primary energy use through simultaneous production of three useful energies in buildings (electricity, heating, and cooling) from a single fuel source using high efficiency conversion devices (Angrisani et al., 2016; Liu et al., 2014). Additionally, they offer the technical flexibility for aligning local power generation and demand, thereby achieving a good building performance and integration of variable renewable energies. However, most of the installed systems are conventionally operated and do not effectively contribute to the above targets (EBC-IEA, 2016).
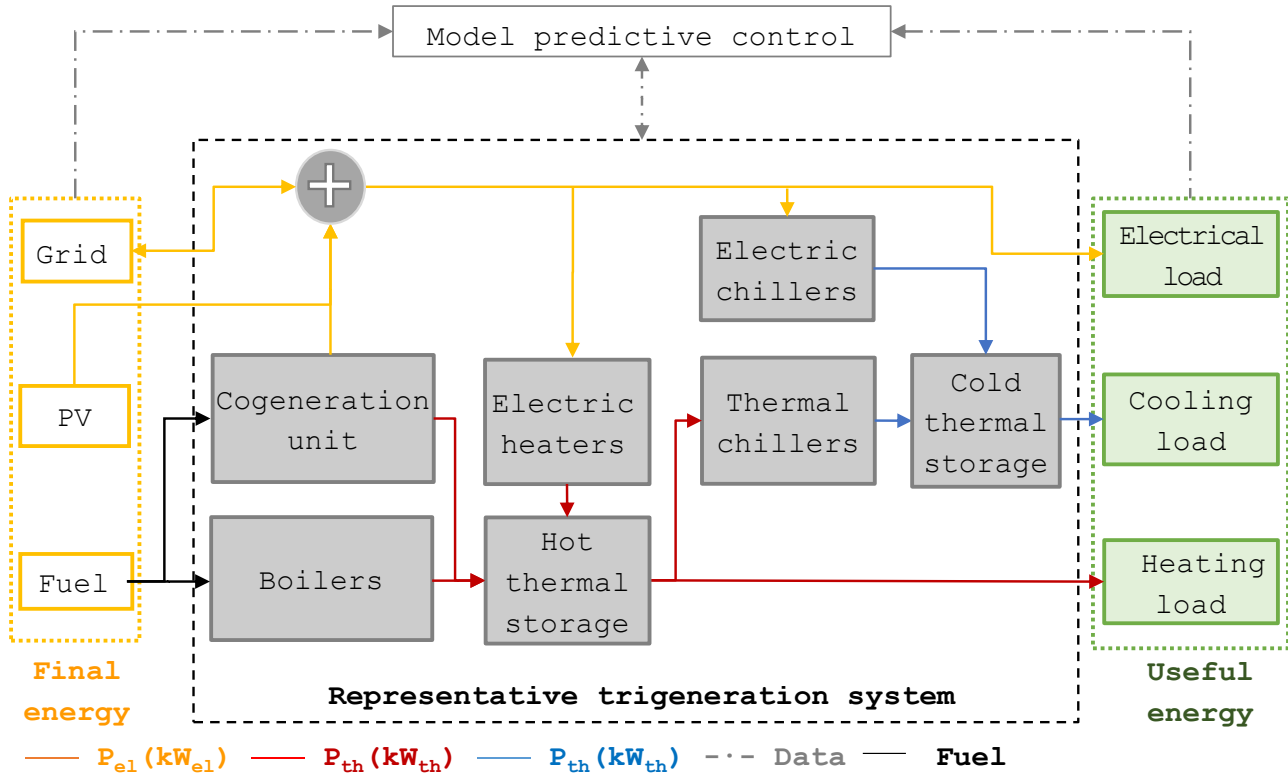
Fig. 1-1 Schematic representation of a building trigeneration system and MPC for its optimal operation

Applying optimisation algorithms for the operation of a decentralised trigeneration system has shown promising results for their energy-efficient, sector-coupled (power-to-heat or gas-to-electricity) and grid-reactive scheduling (Al Moussawi et al., 2016; Andiappan, 2017; Cho et al., 2014; Gu et al., 2014; Jradi and Riffat, 2014). Researchers have quantified potential economic benefits of 29% (Cho et al., 2009b), 8.5% (Chandan et al., 2012), 9.5% to 26% (Kim and Edgar, 2014), 49% to 84% (P. Liu et al., 2013) and 8% to 100% (Facci et al., 2014) by applying optimal control instead of conventional control to a wide range of stand-alone trigeneration systems or to micro-grids utilising trigeneration systems. Also, a reduction of 50% in thermal energy wastage of a residential PV-trigeneration system (Liu et al., 2014) and upto 24% in primary energy consumption and CO_2 emissions of a large-scale trigeneration plant (Ortiga et al., 2013) is reported.

However, a common consensus in the research community regarding gaps in the status of optimum operation of micro-scale trigeneration systems available on the market is the lack of demonstration projects using advanced controllers like *model predictive control* (MPC) (Cho et al., 2014; Dagdougui et al., 2012; Jradi and Riffat, 2014; Rong and Su, 2017; Wang and Ma, 2008). The core motivation of this dissertation is to overcome the corresponding challenges identified in the literature namely:

- lack of experimentally validated models that can simulate the wide range of nonlinear operating conditions of such systems with sufficient accuracy and are yet simple enough for application in MPC,

- development and demonstration of a control architecture that combines an optimal controller with a standard *building automation and control* (BAC) system.

What is the contribution of this work? Based on existing theoretical and practical approaches in building technologies, an *energy plant management system* (EPMS) using MPC with novel component models and constraint formulations is developed and demonstrated. Additionally, a qualitative and quantitative comparison with conventional control in an experimental set-up is done. The scientific and engineering results should aid mathematical algorithm developers in providing practically relevant solutions and system designers in deciding the type of control strategy for a green-field or retrofit scenario.

The structure of the dissertation is shown in *Fig. 1-2*.

Part A Technical background	Chap. 2: State-of-art and scope
	Chap. 3: MPC in building automation and control
	Chap. 4a: Experimental set-up
Part B MPC development	Chap. 4b: Control oriented component models
	Chap. 5: Test case with a MBC towards developing a MPC
	Chap. 6: Optimal control framework
Part C Real-world demonstration	Chap. 7: Experiments on economic-MPC of a trigeneration system
	Chap. 8: Comparison of MPC with conventional control
Part D Summary	Chap. 9: Conclusion and outlook

Fig. 1-2 Structure of dissertation

2 State-of-Art and Scope

In this chapter, the state-of-art for trigeneration systems in terms of technologies used, their conventional control strategies, optimisation techniques, and component models is presented and the scope of this work is formulated. The results of a detailed literature research are distributed into three sections. The first section reviews the potential of trigeneration systems as key solutions for energy transition in the building heating and cooling sector and the need for their optimal control. In the second section, the application of mathematical algorithms either for their synthesis, their sizing, or their operation are described. Finally, an analysis of existing models for components of a trigeneration system is given.

2.1 Trigeneration systems

Trigeneration or combined cooling, heating, and power (CCHP) systems typically generate electricity, useful heating, and cooling simultaneously from a single fuel source. Here, the thermal or electrical/mechanical energy from the cogeneration or combined heating and power (CHP) process is used further to produce cooling for processes or spaces by installing thermal chillers, electric chillers or both. Traditionally, only cogeneration systems were used in industries but since the early 1980s, various chillers have been integrated to form a trigeneration system for municipal cooling and heating. More recently, with advent of decentralisation and micro-grids, building level systems have gained attention especially in hotels, hospitals, shopping malls, restaurants, food storage, server rooms, and multi-residential dwellings and communities.

The energy (electricity and thermal) requirement of the building sector (residential, public, and commercial) in IEA countries, is approximately 32% of total final energy demand (Al Moussawi et al., 2016). Considering this existing high energy requirement and projected worldwide increase especially in warmer, but economically developing countries it is apparent that energy efficient and environment friendly innovative systems like trigeneration will play an important role in a sustainable low-carbon energy future. Their potential also derives from the fact that many countries already have policies supporting the installation of CHP systems for example, the combined heat and power act in Germany or the European emissions trading scheme (BMWi, 2018). In the context of the German energy system, it is reported that in addition to facilitating development of micro-grids in the future, CCHP systems also have a potential of covering 41% to 53% of the total cooling demand in industries and 15% in buildings using process waste heat or CHP waste heat (Heinrich et al., 2014).

Comprehensive information regarding the basics of trigeneration technologies, system configurations, performance evaluation metrics and policies supporting their growth are available in the reviews of Jradi, Liu, Murugan and Wu (Jradi and Riffat, 2014;

Liu et al., 2014; Murugan and Horák, 2016; Wu and Wang, 2006). In *Fig. 2-1* a summary of these works with respect to the CCHP benefits is shown.

Decentralised energy supply: Advanced trigeneration systems can be deployed as on-site power plants in a decentralised energy set-up with the following benefits:

- possibility to form micro-grids where they interact with the main grid to provide demand response or peak-shaving services while satisfying the local electrical and thermal loads,
- improved capability for integration of local renewable energy sources,
- avoiding transmission and distribution losses of a centralised grid and external risks to security of supply by using smaller, flexible, and dispersed systems,
- increasing reliability of energy supply since decentralised CCHP systems can run multiple fuel types and support the central grid during power cuts,
- providing alternative options for challenging locations with power shortages or no connection to the central grid especially when they also have cooling and/or heating loads.

Overall system efficiency: Since an energy cascade is developed with multiple useful energy carriers, lesser primary energy is needed for obtaining the same amount of electricity and thermal output in comparison to conventional separate production. This is represented in different criteria in the literature, for example, primary energy savings ratio, fuel energy savings ratio, trigeneration primary energy saving, and energy utilisation factor (Cho et al., 2014). Consequently, the energy efficiency is also improved compared to conventional methods, where electricity from large-scale central power plants is used separately to satisfy the electric lighting and chiller requirements and boilers are used for thermal loads.

Reduced emissions: A reduction of greenhouse gas emissions is estimated in cases where modern prime mover technologies, like fuel cells and micro-turbines are combined with thermal chillers and penetration of renewable energy systems is supported.

Higher flexibility: Due to different permutations and combinations of technologies available for synthesising a CCHP plant, designers of such systems have the flexibility to develop industry or building specific solutions. A greater flexibility in operation is also possible because modern day technologies like micro-turbines and thermal chillers have reliable internal controllers to modulate their outputs, thereby allowing grid-supportive operation of such systems. Trigeneration systems facilitate installation of larger CHPs and their prolonged operation by using excess heat (especially in summer months). This enhances the flexible operation of the systems all-year round.

Lower operational costs: When correctly designed and operated, CCHP systems that couple various energy sectors for application in scenarios with permanent electrical, heating, and cooling loads lead to lower operational costs.
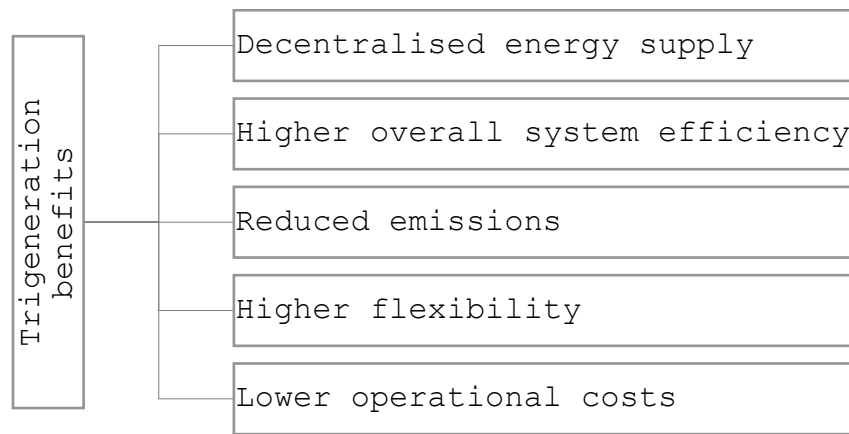
Fig. 2-1 Summary of trigeneration system benefits

This work is meant to provide the tools for exploiting the higher flexibility of trigeneration systems and support their deployment in a decentralised set-up. Through economic scheduling, reduction in consumption-related costs (e.g. energy costs) should be expected.

2.2 Classification of trigeneration systems

Trigeneration systems can be usually classified into five categories depending on: the type of cogeneration unit, type of chiller, type of storage, type of back-up systems, and size of the plant[1], as shown in *Fig. 2-2* (no particular order). A recent review paper provides further insight into the topic of classification of trigeneration systems and the features of the different types of technologies (Al Moussawi et al., 2016). The following section highlights a few of these aspects.
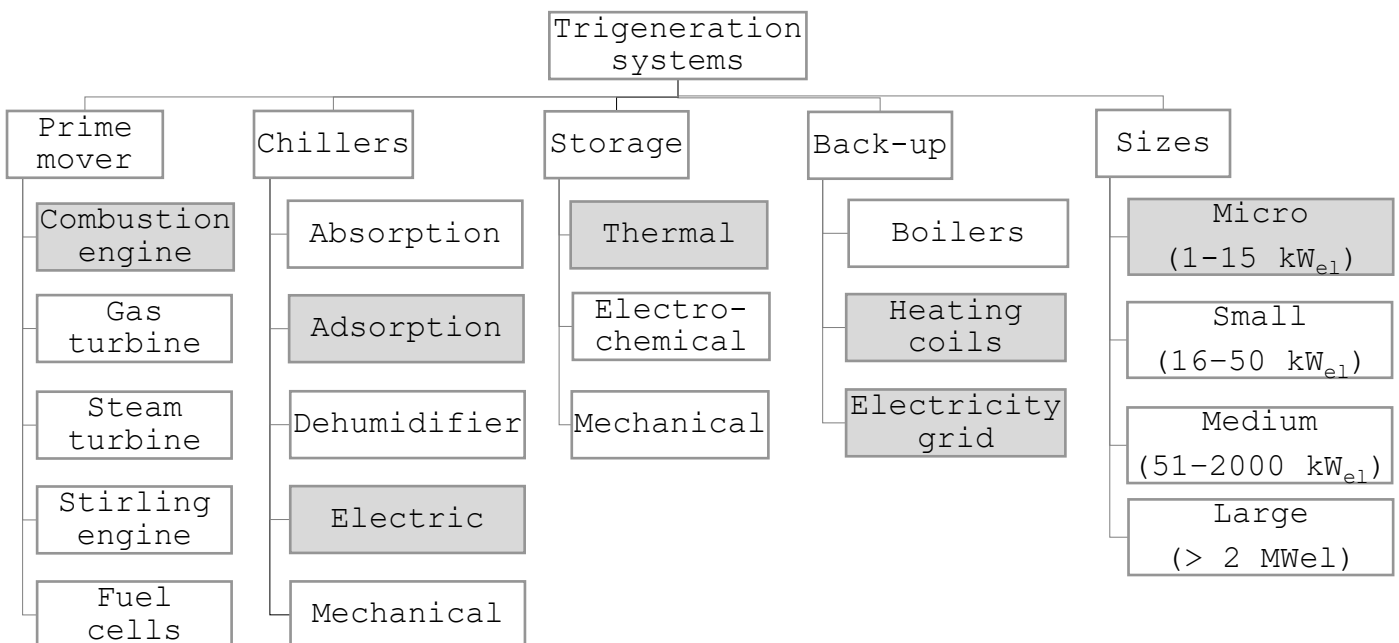
Fig. 2-2 An example of trigeneration system classification (technologies in this work are highlighted)

---

[1] The scope of this work considers trigeneration systems based typically on a cogeneration unit. Definition in glossary of terms.

Prime mover: It is the most basic element of a CCHP plant and can be defined as a machine that transforms energy from thermal, electrical or pressure form to mechanical form. This could either be a combustion-based engine or turbine whose motion is coupled to a generator for producing electricity or an electro-chemical energy conversion device like fuel cell. The underlying technology for combustion engines and turbines is very mature and modern systems like Stirling engines, solid oxide fuel cells, and polymer electrolyte fuel cells are slowly penetrating the CHP market. Any of these options can be chosen to meet diverse demands and limitations depending on the application scenario. This is especially true for cases with restrictions on regional emissions, noise regulations, or installation procedure. Gas turbines and steam turbines systems ranging from several hundred kilowatts to several hundred megawatts have been in operation in industries and other commercial applications for several decades. Recently, micro-turbines ranging from 30 to 400 kW_{el} and combustion engines ranging from 5 to 20 kW_{el} are serving building applications. Discussions based on theoretical and experimental analysis of trigeneration systems with different prime movers from an energetic, exergetic, economic, environmental or integrated point of view can be found in the literature (Jradi and Riffat, 2014; Liu et al., 2014).

Chillers: CCHP systems have either thermally, electrically, or mechanically driven chillers. Thermally driven chillers are principally used in trigeneration systems but sometimes mass-produced electric chillers are also installed as peak load components to reduce the initial investment costs of the system and to achieve a higher electrical cooling to cool load ratio (Angrisani et al., 2012; M. Liu et al., 2013). Most electric chillers are based on the vapour-compression cycle and can be operated as reversible heat pumps. The main types of thermally driven chillers are closed cycle-absorption or adsorption based and open cycle-desiccant dehumidifiers. The choice of the chillers primarily depends on the temperature range of the driving heat. Absorption chillers using high-temperature waste heat from combustion turbines are the most established in industry. However, in the past decade, adsorption chillers are gaining much attention due to their ability to use low-temperature driving heat and using only water as the refrigerant. Adsorption working pairs like silica gel-water, zeolite-water, and activated carbon-methanol with ca. 15 kW_{th} cooling capacity are available on the market. They can use the low-temperature driving heat (60 to 90 °C) from micro-scale CHPs or rooftop solar thermal systems and are practical for smaller buildings. In addition, the typical chilled water output temperature of adsorption chillers is between 12 to 16 °C and can be used effectively in HVAC systems like thermally activated building systems (TABS) or radiant floor cooling. Further information on the working principle and operating characteristics of these chillers is available in the literature (Chua et al., 2013; Núñez, 2010; Zhai and Wang, 2009).

Storage: Thermal or electrical storages are integrated in CCHP plants to balance production-demand mismatches, extend operational hours of a CHP and aid in reducing CO_2 emissions. Depending upon the application and load-scenario, the storages could be thermal, electro-chemical, or mechanical. In building technologies, the most common are water storage tanks and in micro-grids stationary battery packs are used as

electro-chemical storages. In the near future, a greater number of electric vehicles may also be integrated into micro-grids for use as storage systems. It has been shown that storage provides an additional degree of freedom in optimal scheduling problems and helps alleviate the negative effects of variability in energy demands and fluctuating renewable energy generation (Cole et al., 2012; Zhao et al., 2015).

Back-up technology: Another classification of CCHPs is the type of back-up used to cover the peak electrical or thermal loads. Peak cooling loads are satisfied by installing conventional chillers and peak heating loads are generally covered with back-up boilers or electric heating coils. Back-up systems are either connected to the storage tanks or directly influence the feed-line temperatures of the HVAC distribution circuit. Excess electrical loads are mostly satisfied by purchasing electricity from the local grid.

Sizes (scales): CCHP systems are installed in different sizes (capacities). The nomenclature for their size-based classification varies in different parts of the world but in the German context, micro-scale systems are between 1-15 kW_{el}, small-scale are 16-50 kW_{el}, medium-scale are 51-2000 kW_{el}, and bigger capacities are considered large-scale (Seifert, 2013). Micro-scale and small-scale systems together are sometimes called mini-scale and are estimated to reach a production of ca. 3 TWh_{el} per annum by 2030 in Germany (Seifert et al., 2015). CCHP systems are frequently deployed in medium-scale applications in small industries and commercial complexes with gas turbines or engines as prime movers and absorption based thermal chillers. Large-scale systems are ideal for bigger industries or university campuses and residential districts. However, in the past decade small-scale and micro-scale systems have attracted considerable interest especially in terms of grid flexibility and demand side management for buildings having less cooling load. Combustion engines and fuel cells are typical prime movers in this scale. The intersection technology between novel decentralised energy systems (on-site renewable energy systems) and conventional CCHP (large-scale centralized cogeneration units) mostly lies in the range of relatively small capacity distributed CCHP units with advanced prime mover and thermally activated technologies.

Designers or planners of such plants meticulously select the type of technologies and size of components based on various factors like fuel available at the location, load and temperature profiles of the HVAC distribution components, subsidiary policies etc. A standard procedure for sizing the components is based on the load duration curve and type of operation modes such as monovalent or bivalent operation. In monovalent operation, a single component provides the required thermal energy in all possible operating states. In bivalent operation, either two or more components cover the entire thermal load in alternative modes or by running in parallel.

2.3   Conventional control of trigeneration systems

For any application scenario and configuration of the trigeneration system, the operation strategy is a critical factor governing the system's overall performance. Typical control strategies in the building sector are shown in *Fig. 2-3.*

The two main types of configurations are the full load matching (FLM) and the base load matching (BLM). The selection is done during the planning phase of the system because this influences the size of the CHP unit. Based on the type of configuration the two main control strategies are the following electrical load (FEL) and following thermal load (FTL) modes.

FLM-FEL strategy: The CHP is designed and operated such that it generates all the electricity needed to satisfy the electrical demand of the building, including that of the compression chiller and other auxiliary equipment. The waste heat is used to satisfy all or part of the building's thermal load or is used to drive a thermal chiller. If necessary, the peak heating loads are satisfied with a back-up boiler that is typically controlled using a hysteresis dead-band controller to maintain a set tank-temperature. In contrast, excess heat is discarded to the environment through cooling towers or open-air cooling tanks. This control strategy is mostly applied in island systems since no connection to the grid is mandatory and is sometimes called electrical demand management.
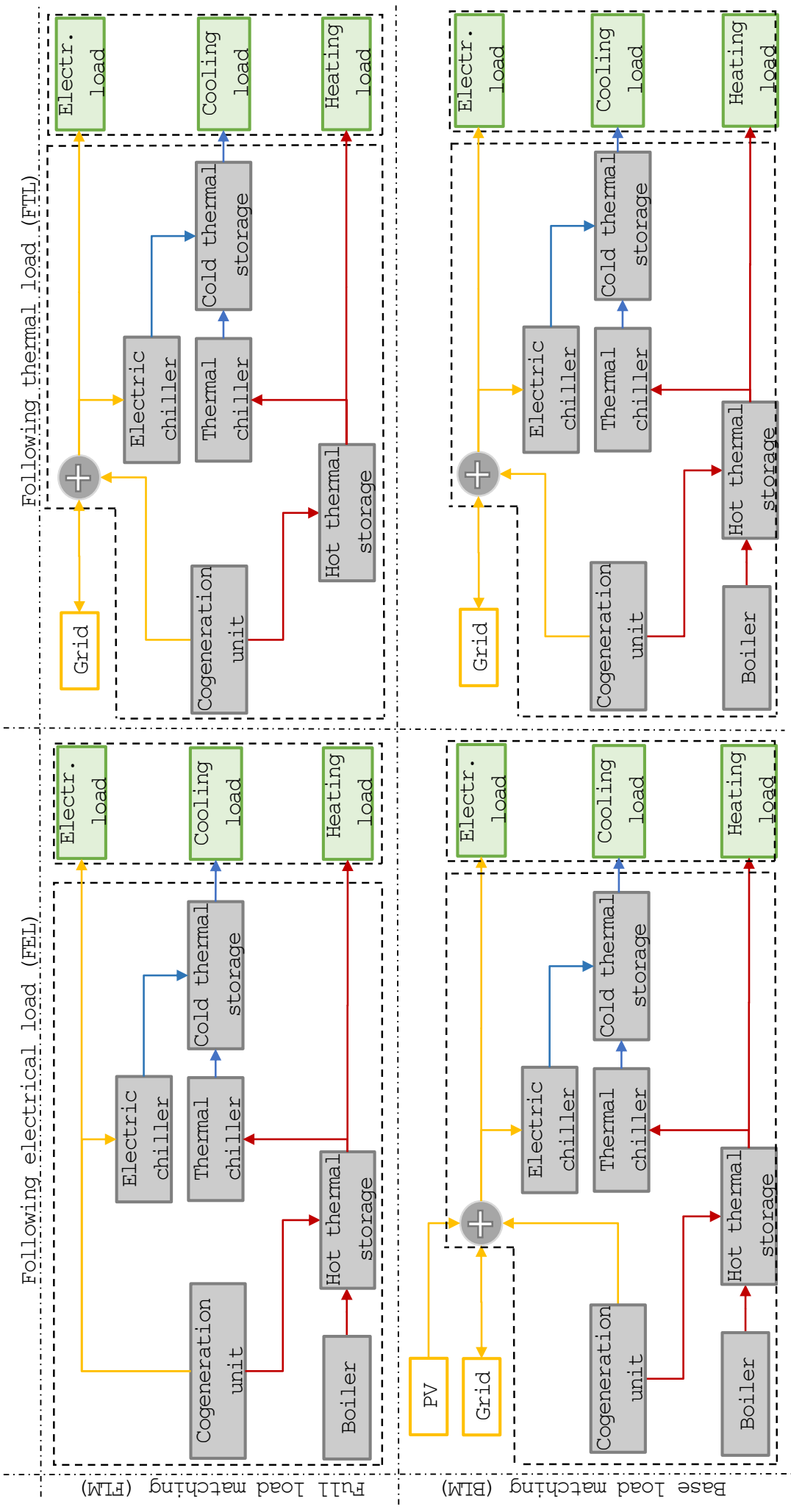
Fig. 2-3 Typical conventional control strategies of a CCHP system based on system configuration[1], with BLM-FTL selected in this work

BLM-FEL strategy: Unlike the previous strategy, here the CHP is designed and operated to cover only a part of the entire electrical load and the remaining is covered through back-up systems. In this control strategy, the CHP operates more often under full-load conditions as it covers the base load. The heating and cooling loads are satisfied by the CHP and back-up boilers operating either in parallel or alternatively. In current developments, this strategy integrates PV or other renewable systems in combination with battery storages as back-up for electrical loads forming the platform for a micro-grid.

FLM-FTL strategy: Under this operating strategy, the CHP alone satisfies the building's complete heating load including the driving heat requirement of the thermal chillers. Accordingly, the chillers can completely satisfy the cooling load. Thus, the CCHP system is self-sufficient in terms of the thermal demand and the electricity demand is satisfied either completely or partly by the cogeneration unit. Excess electricity is ingested back into the grid or shortage of electricity is bought from the grid. This option might not be available in all scenarios and accordingly other arrangements like battery storages are made. Since the focus of this strategy is on thermal loads it is also sometimes called the thermal demand management.

BLM-FTL strategy: Contrary to the previous control strategy, here the CHP satisfies only a part of the entire heating load and the remaining is covered by back-up systems like boilers or heating coils. Sometimes in modern micro-grids, a reversible heat pump is installed as back-up system to increase the system's flexibility for interaction with the grid. Most conventional CCHP systems in buildings are operated using this strategy as various operating modes are possible.

The BLM-FTL is chosen as the conventional control strategy in this work and is compared with the optimal controller. It is often deployed in standard plants and gives the possibility to analyse the operation of a CCHP system that uses different types of components. The components are operated alternatively due to the type of hydraulic connections in the lab that limit the operation of all heating (cooling) components simultaneously (Further details in *Section 4.1* and *Appendix B.4*).

A comprehensive explanation of the conventional design process and control strategies is given in the works of Badea et al. (Badea, 2014). These conventional strategies may not produce the best possible operation of the system and can lead to considerable wastage of energy (M. Liu et al., 2013; P. Liu et al., 2013). Economically optimal conditions are dependent not only on the load demand but also on fuel prices and electricity prices. Additionally, information on the weather forecasts or predictive usage of storage capacities should be included in a system-wide control strategy (Cho et al., 2014). Thus, optimal operation strategy of a CCHP could be effective when it uses mathematical models and optimisation techniques, with the objective of minimising costs, energy consumption, and/or emissions.

2.4 Optimisation of trigeneration systems

In recent years the focus of the research community working with trigeneration systems has shifted from experimental analysis of such systems and their components to the optimisation of these systems (Andiappan, 2017; P. Liu et al., 2013; Rong and Su, 2017). Mathematical algorithms are applied in optimisation of trigeneration systems mainly in the following three scenarios (Andiappan, 2017):

Synthesis of the system: For selection of the different technologies in the plant. To plan and configure a CCHP system especially in a micro-grid is extremely complex because of the various factors affecting its techno-commercial performance such as demand for multiple energies, operating strategies, efficiencies of components and variations in fuel and electricity prices. Often linear optimisation problems using investment costs, regulatory policies and multiple energy balancing capabilities are solved at this level.

Design of the system: Further technical details such as component sizes and operational limits are considered and minimisation of investment and operational costs, energy usage, and/or net emissions is targeted.

Real-time operation: This involves the scheduling of the components and calculating the optimal set-points for circuit temperatures or volume flows of the plant equipment.

The optimisation of a plant's real-time operation is highly relevant from an engineering implementation perspective. A direct comparison with conventional control of a predesigned plant using standard industrial components is possible and the potential gains of an optimal controller like MPC in a retrofit scenario can be assessed. Furthermore, the adaptation of results from a retrofit scenario to a green-field scenario can be a more practical approach. Hence, the emphasis in this work is on *development and demonstration of MPC for economic scheduling of a trigeneration plant*.

The state-of-art in this field was established though a sophisticated analysis of the literature published between 2005 to 2020. The focus was on the field of MPC for building energy plants, optimisation of trigeneration systems, optimal scheduling, or economic dispatch of energy systems. The results of this analysis are presented in the radar-chart in *Fig. 2-4* and the complete table with the literature for this analysis is in the *Appendix A*.
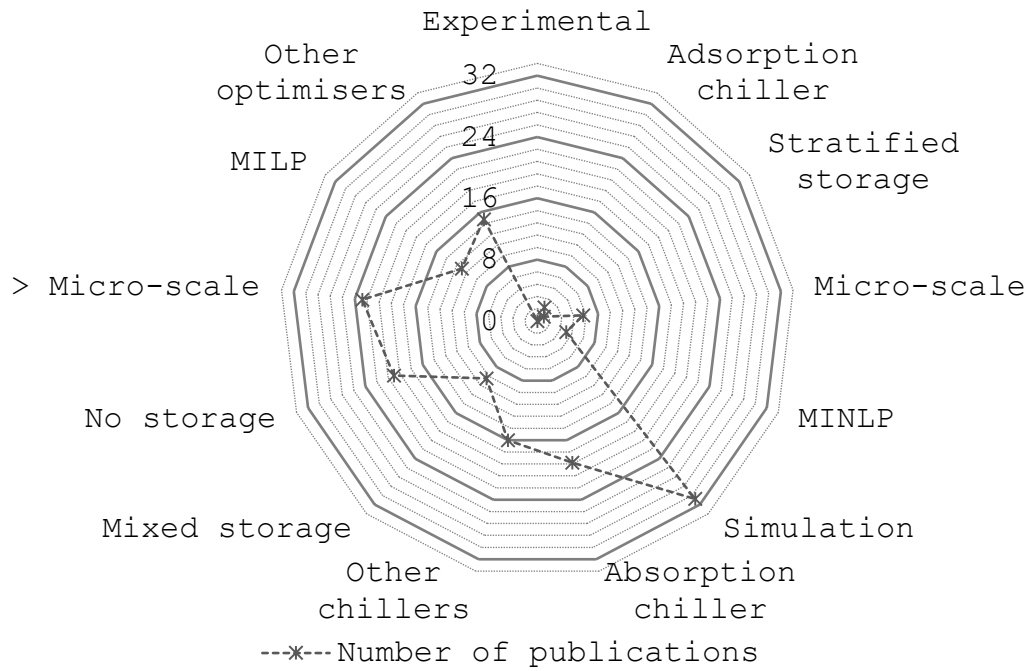
Fig. 2-4 Analysis of the literature available on optimisation for operation of trigeneration systems (33 references out of a total 133 references matched the analysis criteria for further investigation)

Majority of the work in operation optimisation or optimal control of trigeneration systems is performed in a simulation environment. The focus of the simulation studies is to demonstrate the theoretical potential of optimal control for stand-alone or grid-connected CCHP systems. Mixed integer linear problems (MILP) or other optimisation algorithms like genetic algorithms and quadratic programming are often used for this purpose. These methods are suitable for studies limited to simulation because tracking the exact interactions between components and their performance curves, which are often nonlinear, are not as critical as when working with real components. Also, a well formulated MILP and quadratic programming problem often reaches a global optimum owing to convexity of linear constraints and can be solved with extremely fast and effective commercially available software (Urbanucci, 2018). The need to simplify the optimisation problem for these complex systems is reflected in the number of studies using no storage tanks or mixed storage tanks. Due to the popularity of medium-scale and large-scale CCHPs more studies are done with such systems and they typically deploy absorption-based chillers and/or electric chillers.

On the other hand, a less tackled field of research is the experimental demonstration of optimal control or MPC based strategies for building energy source side (scheduling) in comparison to control of distribution equipment (Bruni et al., 2015). This gap is also identified in works that establish the need for a real-time supervisory controller using optimisation in conjunction with MPC (Jradi and Riffat, 2014; Rong and Su, 2017). Resulting from the lack of experimental demonstrations there are fewer studies with mixed integer nonlinear problems (MINLP) and stratified tank models. These would be otherwise consequential to represent the nonlinear dynamics of the components and tracking the temperature distribution of the stratified storage tank which is often a system-state or a decision variable of the optimisation problem (Urbanucci, 2018).

The deployment of micro-scale and small-scale CCHPs in micro-grids and zero energy buildings is a relatively new concept with fewer research projects and ensuing from this, is the absence of research on adsorption chillers as their efficiency and applicability is primarily established only on these scales (Zhai and Wang, 2009).

2.5 Modelling of trigeneration systems

Mathematical models of the components form the corner stone of the MPC framework. Accuracy (model value) and complexity (model cost) are two of their most important traits and a correct balance has to be found between these traits. As stated in the literature, this is often a field of science in its own right and the decision on the complexity of the model must be made by the developers based on the intended application scenario of the models (Trčka and Hensen, 2010; Whiten, 2013). *A rise in complexity must justify the value of the model as it increases the cost of the model.*

Literature research of existing models was done with a special focus on the main components in this work. These are a silica gel-water *adsorption chiller* (AdC), a fuel oil *combined heating and power* unit (CHP), fan based *dry-cooled outdoor coil* (OC), air-water-electric *reversible heat pump* (RHP), and water based hot and cold *thermal energy storages* (HTES/CTES). The primary search was for models already applied in the field of optimisation of trigeneration systems and this was done using keywords such as "Optimisation of Trigeneration/CCHP", "CCHP Models", and "CCHP/Trigeneration MPC". For components like AdC and OC further investigation was necessary due to lack of models with the above keywords and specific keywords such as "Models for HVAC simulation and control", "Adsorption chiller models", and "Cooling tower models" were used. The key online searches were done using *Mendeley*, *Science Direct*, and *Google Scholar*. Some of the models were part of published libraries or software packages such as *TRNSYS*, *EnergyPlus*, *HVACSIM+*, or *Modelica Building Systems*.

A selected cross-section of papers is shown in *Table 2-1* where the models are sorted according to different factors for identifying approaches that could be adapted in this work.

Firstly, the technology of the component used in the study is identified. The models are then classified based on their methodology and class. Both linear and nonlinear models as ordinary differential equations (ODE) or differential algebraic equations (DAE) with varying level of details and applications are found in the literature.

Another important classification is between scientific law based (e.g. physics or chemistry) *white-box models*, data driven *black-box models* or a mixture of both as *grey-box models*. These are summarised in *Fig. 2-5*. In white-box or forward approach, the relationships between model input, output, and parameters are derived using laws of physics or chemistry and a detailed calculation of the thermodynamic or electro-chemical processes for individual parts of a machine is done. In black-box or inverse approach, large sets of system performance data under varying operational modes or special tests are evaluated to establish input-output relationships.

In grey-box modelling, either the first law of thermodynamics and the principle of mass and energy balance are applied for developing the mathematical structure of the models and any missing variables are quantified through data fitting methods, or a black-box model frame is used and mathematical constraints are placed on model parameters and variables (Sohlberg, 2003).

Grey-box methodology is a compromise between white-box models and black-box models and can provide good generalisation capabilities while maintaining a high level of accuracy (Afram and Janabi-Sharifi, 2015a; Bohlin, 1994). These models are also robust to disturbances, have auto-tuning capabilities, and need fewer assumptions to set-up. This is an advantage over data-driven algorithms like artificial neural networks for developing black-box models, showing promising results but having limitations on generalisation capabilities and less robustness to disturbances (Afram and Janabi-Sharifi, 2015b).

Further in *Table 2-1*, the main outputs of the model are identified and compared with the outputs necessary for MPC based scheduling of the trigeneration system in this work. The size (scope) and complexity of the model is expressed in terms of the system states, parameters, and number of curve fits needed to simulate the component and its interactions (Trčka and Hensen, 2010). Finally, the models are analysed for their application e.g. for real-time optimal control or in-depth component level simulation by studying the model objective and validation status.
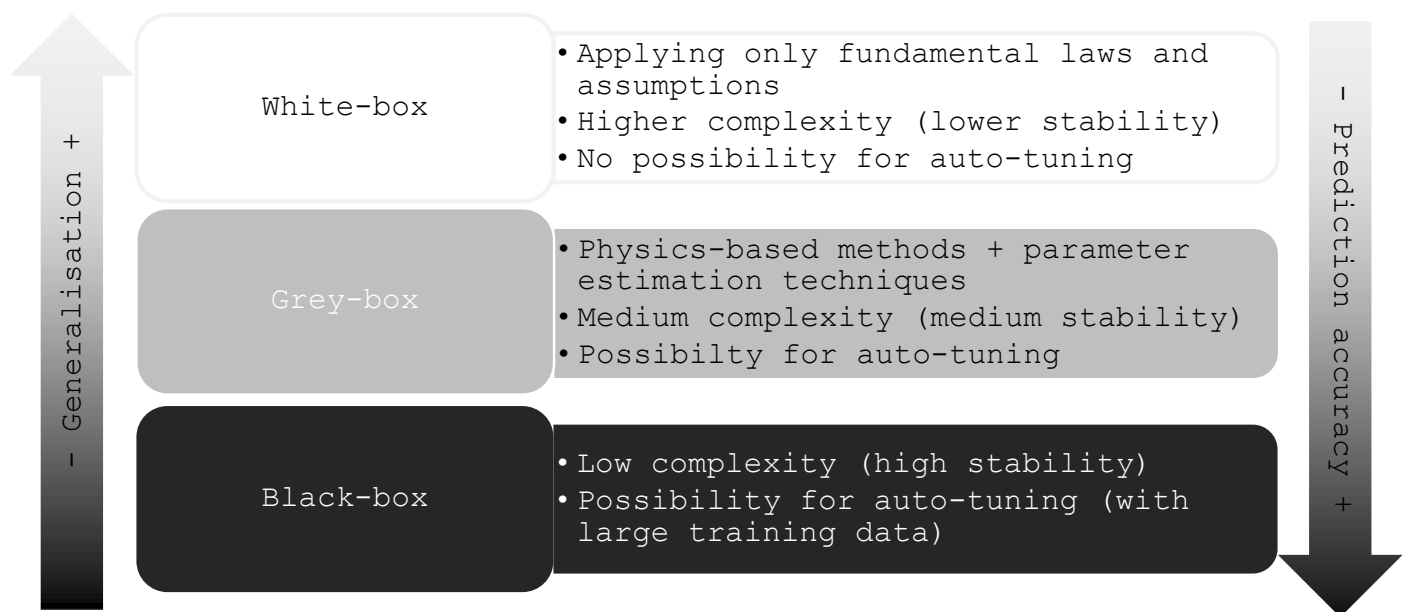
Fig. 2-5 Classes in HVAC modelling

For the AdC, simulation models were already developed in the 1980s and their modifications have been used recently. The focus of these models is to simulate the machine's performance for varying inlet temperatures or varying switching and cycle times. The newer studies include the internal controllers responsible for switching the adsorption-desorption cycles between two chambers for continuous cooling operation. These models display the periodic behaviour of the AdC and are quantitatively validated.

The theoretical approach of these models is to use the linear driving force (LDF) kinetic equation for the adsorption-desorption rate, modelling of heat exchangers and thermodynamic mass and energy balance. Simplified models using linear energy balance or curve fits for the coefficient of performance (COP) as a function of the part-load ratio have also been developed recently. These are specifically for the purpose of system-wide optimal control of trigeneration systems using AdCs.

For the CHP, simulation models for different technologies such as gas turbines or combustion engines applied in optimal control studies are available. These are mostly static black-box or grey -box models. A few dynamic models also exist that either use a step-response analysis or do an energy conversion and heat transfer calculation from the fuel to the engine block and then cooling system. In most cases, only a visual validation of these models is available under the assumption that visual accuracy is sufficient for application in MPC.

For the OC, which is principally a dry-cooling tower with variable-speed fan motors, validated simulation models exist in the literature. Based mostly on the Merkel's theory, the recent models also use the number of transfer unit – effectiveness method that is analogous to heat exchanger modelling. These models are static and highly nonlinear. In combination with the fan laws, the power consumption of the fan motors is also calculated.

For the RHP, static grey-box and black-box models are often applied in optimal control problems. A few dynamic models employing mass and energy balance over the internal components of a vapour-compression chiller (evaporator, condenser, expansion valve, and compressor) are used for detailed simulation of the transient behaviour of the machine and its part-load operation. Most of the validated models calculate the cooling power, power input and circuit temperatures.

For the HTES/CTES, 1-dimensional and 2-dimensional stratified tank models are available with different levels of accuracy and complexity. The application of these models is mostly in simulation of building HVAC systems to depict the temperature distribution in the tanks. For application in optimisation problems a mixed tank model is often used as observed in the previous sections (*cf. Fig. 2-4*)

Table 2-1 Classification of the literature for HVAC systems modelling

Component	Modelling class & methodology	Main outputs	Size & complexity of model	Objective of study or model	Validation results	Reference
AdC: Silica gel–water	• Nonlinear dynamic white-box models • LDF kinetic equation for adsorption and desorption rate • Pressure and enthalpy-based mass and energy balance	• Cooling power • Circuit temperatures • COP	• > 20 parameters • > 4 states	Study effects of following parameters on the AdC performance: • operating temperatures • switching time • cycle time	Visual, quantitative (APE, RMSE)	(Chua et al., 1999; Li and Wu, 2009; Saha et al., 1995; Sakoda and Suzuki, 1984)
Silica gel–water	• Nonlinear dynamic grey-box model using PDEs • LDF kinetic equation for adsorption and desorption rate • Resistance-capacitance heat exchanger model • Pressure and enthalpy-based mass and energy balance	• Cooling power • Circuit temperatures • COP	• 10 parameters • 2 curve fits • > 4 states	Parameterisation of an AdC and simulation of its periodic behaviour	Quantitative (NSD)	(Schicktanz and Núñez, 2009)
–	• Nonlinear dynamic white-box model • DAE formulations • Density and temperature-based mass and energy balance	• Cooling power • Circuit temperatures • COP	• 22 parameters • 10 differential states • 2 algebraic states	Application in optimal control of an AdC by controlling the cycle times	–	(Gräber et al., 2011)
–	• Nonlinear static grey-box model • Curve fit of COP as a function of part-load ratio • Implicit energy balance equation	• Cooling power • COP	• 0 states • 1 parameter and 1 parameter set	Application in an MINLP algorithm for multi-objective operational optimisation of a micro-CCHP system	–	(Wu et al., 2012)
–	• Linear static grey-box model • Energy balance • Constant heat recovery ratio and COP of machine	• Cooling power	• 1 state	Application in an NLP algorithm to solve an economic-MPC for optimal scheduling of primary HVAC equipment	–	(Zhao et al., 2015)
CHP: Gas engine	• Linear static grey-box models • Linear interpolation or quadratic regression of predefined parameters for different load factors	• Cost of operation • Power output • Fuel input	• > 2 parameters	Application in an MILP or MINLP algorithm for cost based optimisation to design and operate a CCHP	–	(Bracco et al., 2013; Cho et al., 2009a; Ren et al., 2008)

2-State-of-Art and Scope

Component (continued)	Modelling class & methodology	Main outputs	Size & complexity of model	Objective of study or model	Validation results	Reference
Gas turbine CHP with internal PID control	• Nonlinear static black-box model • Regression based static input-output relationships • Reduced order modelling	• Fuel input • Exhaust gas mass flow & temperature	• 3 parameter sets (10 total)	Application in an NLP algorithm to solve a cost-based look-ahead optimisation problem for operating strategy	Visual	(Chandan et al., 2012)
Gas engine micro-CHP	• Nonlinear dynamic input-output black-box model • Transfer function using step-response analysis	• Power output	• 1 state	Application in active voltage management using a proportional integral controller	Visual	(Hidalgo Rodriguez et al., 2012)
Gas engine micro-CHP with internal mass flow controller	• Nonlinear dynamic grey-box model • Curve fits for part-load behaviour • Mass and energy balance over engine and heat exchanger	• Feed-line & engine temp. • Power output • Fuel input • Variable mass flow	• > 5 component parameters • 3 parameter sets (fitting coefficients)	Simulation of the dynamic behaviour of a micro-CHP including its part-load behaviour and internal control logic	Visual	(Seifert, 2013)
General PGU	• Nonlinear static grey-box models • Curve fits for part-load behaviour • Linearisation using discretisation • Energy balance	• Power output • Fuel consumption	• > 2 parameters	Application in a linearised MINLP or GA for cost-based capacity and configuration optimisation of a CCHP system	–	(Li et al., 2014; Zhou et al., 2013)
Gas engine	• Linear static grey-box model • Prime mover capacity factor, heat recovery factor and heat to power ratio are used • Energy balance	• Power output • Fuel consumption	• 4 parameters	Application in a GA for multi-objective design optimisation of a medium-scale CCHP system	–	(Kavvadias and Maroulis, 2010)
Gas engine	• Nonlinear static black-box models • Energy balance	• Power output • Fuel input	• > 4 parameters	Application in backward dynamic programing for operation optimisation to reduce costs	–	(Facci et al., 2014)
CC: Counter-flow wet cooling tower	• Empirical linear model • Interpolation of range and wet-bulb temperature catalogue data • Lagrange interpolation or 2nd degree curve fits	• Outlet water temperature	• 9 parameters	Static simulation of a cooling tower system for design and analysis	–	(Stoecker, 1989)

Component (continued)	Modelling class & methodology	Main outputs	Size & complexity of model	Objective of study or model	Validation results	Reference
Counter-flow wet cooling tower	• Merkel's Theory • NTU-effectiveness method • Levenberg-Marquardt method for parameter identification	• Heat rejection rate	• 3 parameters • 1 state	Real time optimisation of operating cooling towers	Visual, quantitative (RMSRE)	(Jin et al., 2007)
Wet and dry cooling towers	• Pressure-enthalpy based energy balances • Initial temperature difference method • Fan laws	• Condenser pressure • Water Use • Parasitic fan and pump power	• > 15 Parameters • > 10 Curve fits	Simulation of cooling tower behaviour in a Rankine cycle steam power plant	–	(Wagner and Gilman, 2011)
Counter-flow wet cooling tower	• Nonlinear static white-box models • Analogy to sensible heat exchanger • Mass and energy balance • NTU-effectiveness • Fan laws	• Heat rejection rate • Fan power • Output temperatures	• 4 parameters	Determining performace of a cooling tower for design purposes	–	(Bergman et al., 2011; Mitchell and Braun, 2013)
RHP: Water-to-water heat pump	• Nonlinear static grey-box models • Parameter estimation from catalogue data • Mass and energy balance over chiller internal components	• Heating power and power input • Circuit temperatures	• > 10 Parameters	Application in energy calculation and/or building simulation programs	Visual, quantitative (RMSE)	(Jin and Spitler, 2002)
Air cooled compression chiller	• Nonlinear static grey-box models • Parameter estimation from catalogue data and experimental results • Pressure-enthalpy based mass and energy balance over chiller internal components	• Cooling power and power input • COP	• > 10 Parameters	Application in calculation of cooling energy generated and power input required for a air-cooled chiller with limited catalogue data	Visual	(Lemort et al., 2009)
-	• Nonlinear static grey-box models • Look up tables of manufacturer data • Energy balance	• Cooling power and power input • Circuit temperatures • COP	• > 5 parameter sets	Application in a nonlinear optimisation of CCHP operation using mass flow and chilled water temperature as variables. Simulation of a GSHP	Visual, quantitative (MAPE)	(Ma et al., 2009; Salvalai, 2012)
Electric compression chiller	• Nonlinear dynamic grey-box models • Polynomial fit of COP to Carnot efficiency	• Cooling power and power input • COP	• > 10 Parameters • 1 Curve fit	Application in a building HVAC system simulation within Modelica enviroment	–	(Wetter, 2009)

2-State-of-Art and Scope

Component (continued)	•Modelling class & methodology	•Main outputs	•Size & complexity of model	Objective of study or model	Validation results	Reference
Electric compression chiller	•Nonlinear dynamic grey-box models •Polynomial fit of COP to Carnot efficiency •Mass and energy balance over chiller internal components	•Cooling power and power input •COP •Circuit temperatures	•> 10 Parameters •1 Curve fit	Application in a building HVAC system simulation within Modelica environment	–	(Wetter, 2009)
Compression chiller (electric and mechanical)	•Nonlinear static black-box models •Model identification using least squares	•Cooling power •Circuit temperatures	•> 5 parameters	Application in the controller development of the chiller's variable speed compressor. Application in a dynamic programming algorithm for optimal scheduling of a trigeneration plant in a simulation environment	Quantitative (percentage error)	(Facci et al., 2014; Romero et al., 2011)
Water cooled electric compression chiller	•Nonlinear static grey-box models •Pressure-enthalpy based thermodynamic balance •Semi-empirical models of chiller internal components	•Cooling power and power input •COP •Circuit temperatures	•> 10 parameters	Application for developing practical model based supervisory control of a HVAC plant comprising of this chiller	Quantitative (RMSE and MAE)	(Jin et al., 2011)
Electric compression chiller	•Linear static grey-box models •Regression analysis for compressor power •Mass flow is decision variable	•Cooling power and power input	•< 5 Parameters •1 Curve fit	Application in a nonlinear optimisation for operation of a trigeneration plant	Visual	(Chandan et al., 2012)
Electric compression chiller	•Linearised state-space dynamic models •Mass and energy balance over chiller internal components	•Cooling power and power input •COP •Circuit temperatures	•6 states •> 20 parameters	Simulation of transient behaviour of machine under different perturbations and initial conditions	Quantitative (AE)	(Yao et al., 2013)
HITES/CTES: Stratified small-scale tank	•1-dimensional dynamic multilayer models •Fourier's equation for heat flow •Mass and energy balance per layer •If-Else logic for effective flow •Effective vertical heat conductivity	•Temperature distribution	•1 state per layer •< 8 parameters	Simulation of the transient temperatures in a stratified tank. A simplified 2-layer model with 1 state per layer in nonlinear MPC	Visual	(Dwivedi, 2009; Eicker, 2006; Ma et al., 2009)

Component (continued)	Modelling class & methodology	Main outputs	Size & complexity of model	Objective of study or model	Validation results	Reference
Mixed large-scale tank	• Mass and energy balance • Figure-of-merit concept • Tank charging and discharging rate as control variable	• State-of-charge of tank • Tank temperature	• 1 state	Application in a MILP algorithm for dynamic optimisation of a chilled water plant design or in a MINLP algorithm for optimal design of a district heating network	–	(Henze et al., 2008; Tveit et al., 2009)
Stratified tank	• Multinode model with heat conduction only	• Temperature distribution	• < 10 Parameters	Application in a building HVAC system simulation within Modelica environment	–	(Wetter, 2009)
Stratified large-scale tank	• Numerical 2-dimensional transient model • Computational fluid dynamics for solving PDEs • Navier-Stokes equations for mass, momentum and energy • Temperature distribution modelling	• Temperature distribution • Velocity fields	• 4 states per layer • > 10 parameters	Simulate charging and discharging process of a heat storage and evaluate suitable time-steps for simulations.	Quantitative (APE)	(Streckiene et al., 2011)
Stratified tank	• Nonlinear dynamic DAE model for a 2-layer tank • Mass and energy balance per layer • Regression based delay times	• Temperature distribution	• > 10 Parameters • 2 states	Application in a nonlinear optimisation for operation of a trigeneration plant	Visual	(Chandan et al., 2012)

AE (Absolute Error), APE (Absolute Percentage Error), CCHP (Combined Cooling, Heating, and Power), COP (Coefficient of Performance), DAE (Differential Algebraic Equations), DP (Dynamic Programming), GA (Genetic Algorithm), GSHP (Ground Source Heat Pump), LDF (Linear Driving Force), MAE (Mean Absolute Error), MAPE (Mean Absolute Percentage Error), MILP (Mixed Integer Linear Problem), MINLP (Mixed Integer Nonlinear Problem), NLP (Nonlinear Problem), NSD (Normalised Standard Deviation), NTU (Number of Transfer Units), PDE (Partial Differential Equation), PGU (Power Generation Unit), RMSE (Root Mean Squared Error), RMSRE (Root Mean Squared Relative Error)

2.6   Summary and outlook

The review of scientific journals, project reports, and brochures in this chapter concluded that trigeneration systems are capable of: (a) facilitating the development of micro-grids, (b) covering a major part of the cooling requirement, and (c) reducing primary energy consumption. Additionally, theoretical studies in the field of optimal control of these systems presented a high potential for their economic and energy efficient operation. Despite that, the experimental demonstration and comparison of optimal control with conventional control for scheduling of CCHPs using standard industrial components and practices were identified as gaps in this field of research. This was noticed especially for micro-scale systems deploying stratified tanks and adsorption chillers.

Analysis of previous literature also revealed the multitude of existing models that were classified as per their methodologies, complexity, and objectives. With this regard, the shortlisted literature is analysed further in this dissertation to filter out the best approaches for developing *control-oriented component models*.

The scope of this work is fixed within the vast field of HVAC systems research to the development and demonstration of an *MPC based supervisory controller* for the generation side of a building HVAC system, also referred to as optimal scheduling of the primary HVAC equipment. The emphasis being on engineering-oriented methodologies that support generalisation and execution in practice while facilitating a closest-possible comparison to conventional control techniques.

However, before proceeding further with developing and implementing the MPC within the *building automation and control* system, the basic concepts of these tools and technologies are clarified in the next chapter.

3   MPC in Building Automation and Control

The need for practical implementation of MPC for scheduling of CCHPs was recognised in the previous chapter. MPC is a collection of control techniques that merge optimisation tools, forecast data, and physical constraints. The different factors affecting its performance as a supervisory controller in a building automation and control system are studied in this chapter. The sought-after characteristics of control-oriented models in real-world applications are highlighted and mathematical concepts used in this work are introduced. The theoretical explanation is based on textbook material, technical standards, and scientific publications on optimal control and numerical optimisation.

3.1   Building automation and control

The central management, monitoring, and optimisation of building technology for achieving a well-matched interaction of the architecture, HVAC equipment, indoor comfort, and safety is described as *building automation and control* (BAC). Complex interactions of electrical and mechanical plants in large non-residential buildings are commonly monitored and controlled using BAC systems for improving the building performance and energy efficiency. In standard practice, the BAC system is divided into three levels (as seen in *Fig. 3-1*) with different equipment at each level and industrial communication protocols for data transfer between them.
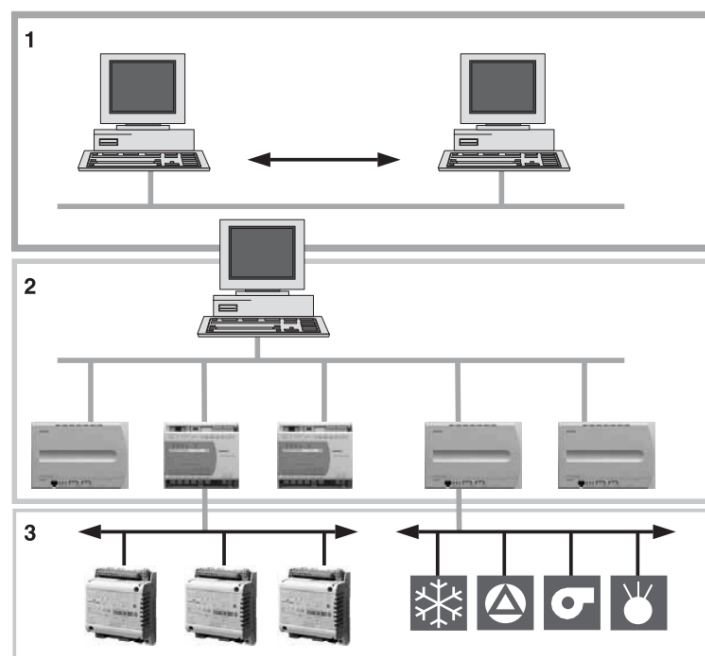
Fig. 3-1 Three levels of a hierarchical BAC system: (1) Management level, (2) Automation level, and (3) Field level[1]

---

(1) Management level: A central computer is used for monitoring and synchronising the operation of the lower levels and in some cases coordination with management level of other plants. It runs a *supervisory controller*, which typically, provides set-points to the lower level controller and switches plant groups following a scheduling program. The scheduling program could be either a rule-based method, a performance map-based method, or an optimal control approach that yields reduction in energy consumption while simultaneously tracking thermal comfort. Exchange of data/information with third party systems, e.g. cloud-based databases, also occurs on the management level.

(2) Automation level: Open and closed loop controllers operate the plant at set-points received from the management level. These lower level controllers can operate the plant independently using conventional control strategies if the supervisory controller fails. In addition to measurement and control, the other tasks for automation are switching, visualisation, counting, and monitoring. Typical hardware on this level is a programmable logic controller (PLC), modular input/output devices (I/O modules), relay switches, potentiometers, and electrical safety components amongst others. These are normally located in the control panel of the plant that is easily accessible to the operator. Binary signals are processed and transmitted to the management level directly, while analogue signals are converted into digital signals before transmission.

(3) Field level: The process variables (temperatures, volume flow etc.) are measured via sensors, while the positioning of valves, dampers, and switching of components is completed via actuators. The sensor data are transmitted to the automation level as feedback signal to indicate the status of the system including monitoring equipment. At the field level, it is possible to control individual zones of a building using equipment such as radiator valves, fan coil units, mixing dampers etc.

One of the major technical challenges is establishing the BAC network for transfer of data/information, both intra- and inter-level and with other external systems. Principally, a system-specific data bus permits exchange either horizontally or vertically, with each level operating with the data assigned to that level. As per the technical standard on building automation and control *VDI 3814*, standard data bus systems and communication protocols like *Modbus*, *M-Bus* or *BACnet* are used for this purpose. They help in transferring data of varying complexity, in integration of heterogeneous plants, and in central operation and monitoring. Using existing infrastructure (LAN/WAN) and facilitating a flexible installation are both possible due to standard communication systems. Depending on the scenario, either a single computer combines the operation on the management or automation level or each of these levels has a separate computer.

Optimisation based *building energy management systems*, are capable of operating complex building HVAC systems over a wide range while still satisfying physical constraints and thermal comfort (Bruni et al., 2015). When applied specifically for the supervisory control and scheduling of the heating and/or cooling plant the energy management system is referred to as the *energy plant management system* (EPMS),

energy production plant management (EPPM), or *energy production system management* (EPSM) (Figueiredo and Martins, 2010).

3.2 MPC basics

MPC is, "an on-line (process accompanying) optimisation-based control technique that optimises a performance index or cost function over a prediction (control) horizon by taking advantage of a dynamic nominal process model while accounting for process constraints" (Elliott, 2008).

It originated in the late 1970s and gained popularity for application particularly in chemical and process industries. With progress in algorithms and computing power, its field of application has extended to robotics and energy (Elliott, 2008). The term MPC covers control strategies that have a typical structure comprising of prediction model, objective function, prediction horizon, and constraints. The advantages of MPC have been summarised in the literature as follows (Afram and Janabi-Sharifi, 2014a; Camacho and Bordons, 2007; Gu et al., 2014):

- variety of processes with dynamics ranging from simple to more complex ones can be controlled using a similar framework,
- integration of a system model and disturbance model allows for anticipatory control rather than reactive control, leaving room for a wide range of operating conditions,
- depending on the scenario, multiple control objectives such as energy conservation or reduction of control effort can be followed simultaneously due to the usage of a cost function,
- treatment of constraints and uncertainties (weather and load forecasts) is conceptually simple and the number of physical constraints can be extended easily during the design process when the framework already exists,
- slow-moving processes with delays can be effectively controlled,
- multivariable cases can be handled, making it suitable for multiple-input multiple-output systems,
- application in a hierarchical building automation and control is possible at both supervisory and local levels,
- experienced plant operators with limited exposure to control theory can still contribute in designing and tuning the controller due to its intuitive concepts,
- improvement in computing power and advancement of optimisation algorithms can be exploited,
- information on future references can be exploited more effectively compared to conventional controllers,
- adding new constraints and parameters to an existing MPC formulation can be less time-consuming compared to editing the control logic of an existing rule-based reference controller,

- it is possible to deploy MPC in both green-field and retrofit scenarios especially when machine learning algorithms are implemented for online parameterisation of the models and develop a generalizable controller.

On the other hand, the disadvantages or challenges faced in MPC application are listed below:

- computation hardware capable of running the (often demanding) optimisation solvers should be available,
- longer computation times especially in presence of constraints and complex process dynamics considerably limits the type of processes to which it can be applied,
- ensuring real-time operation may need excessive simplification of the numerical problem and implementing suboptimal solutions which may not always be justified,
- stability and robustness analysis of the control loop is still an active field of academic research and the results can only be applied to very small processes,
- in case of nonstandard scenarios, computer programming and system modelling expertise is necessary due to lack of directly applicable industrial software packages.

A block diagram for possible MPC implementation on a plant is shown in *Fig. 3-2*.
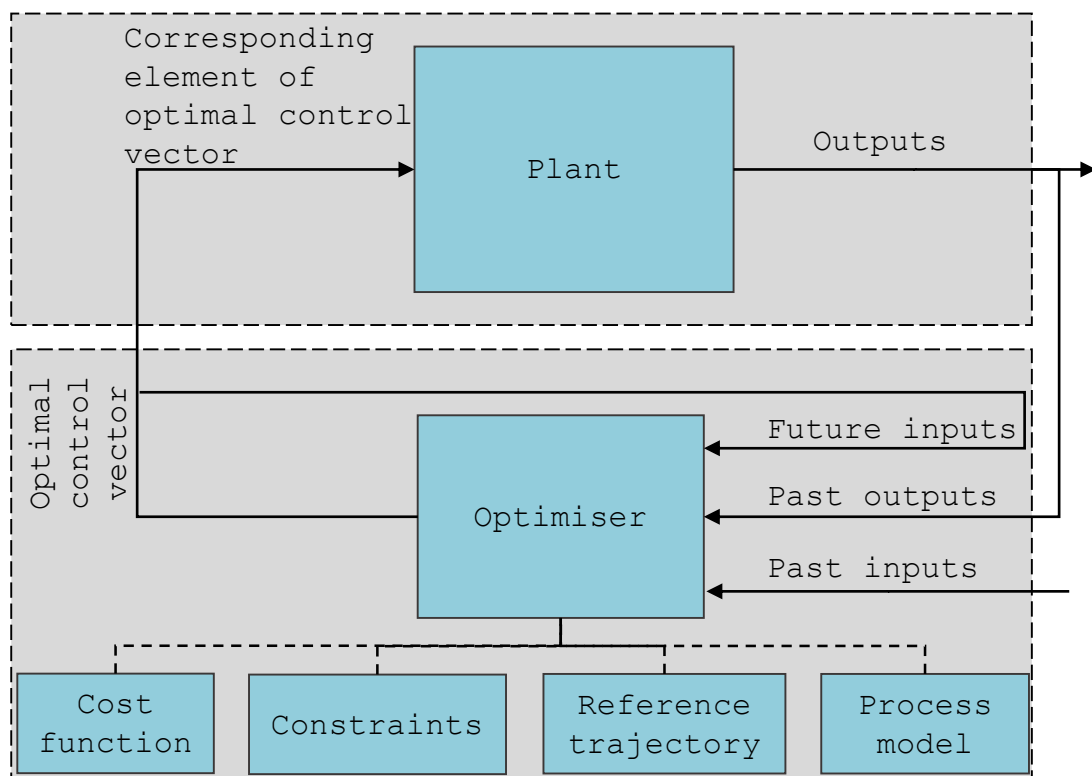
Fig. 3-2 Block diagram of a MPC control loop with solid arrows representing flow of input/output information and dashed lines representing mathematical constituents of the optimiser

At a given sampling time, a process model predicts the outputs of a plant based on its past inputs, past outputs, and future inputs over the entire prediction horizon. The predicted output is compared to a reference trajectory generating a vector of future errors. The optimiser uses this information to generate an optimal solution or optimal control vector that minimises a cost function in presence of disturbances and constraints over the prediction horizon. Only the first element for each corresponding manipulated

variable from the entire control vector is supplied to the plant as the control signal. The control loop repeats at sampling intervals including the time needed for solving the algorithm. Thus, it is important to find fast solutions within a small part of the sampling time length. The new loop uses updated measurements as past outputs and past inputs, the optimal control vector as future inputs, and a new prediction horizon shifted by the sampling time length. Only at the first sampling instance, the problem is initialised with apriori initial control signals to calculate the initial states for the MPC.

The repetitive nature of the MPC loop and the logic behind its denotation as *receding horizon control* is expressed in *Fig. 3-3*, with,

- k − discrete variable referring to a specific sampling instance,
- N_u − control horizon,
- N_p − prediction horizon.

The current state of the controlled variable and its predicted output under the influence of the manipulated variable over the control and prediction horizons is seen in both figures. For this example, an N_u equivalent to 6 time-steps and N_p equivalent to 10 time-steps is taken. The reference set-point for the controlled variable is fixed at 100.

In the top figure, at instant $k = 0$, the MPC generates an optimal control vector (comprising of the manipulated variable values) for 10 time-steps in the future with values for the manipulated variable u changing for 6 time-steps before being constant for the remaining 4 steps. The value of the manipulated variable $u(k_0) = 3$ is applied for the duration of one time-step i.e. the duration of one sampling instance or sampling time, after which the above process is iterated and the horizons are shifted forward by one sampling time as shown in the bottom figure. The new control vector in the bottom figure is clearly different from the above figure to accommodate for disturbances, prediction inaccuracies, or uncertainties in the system over the previous sampling time.
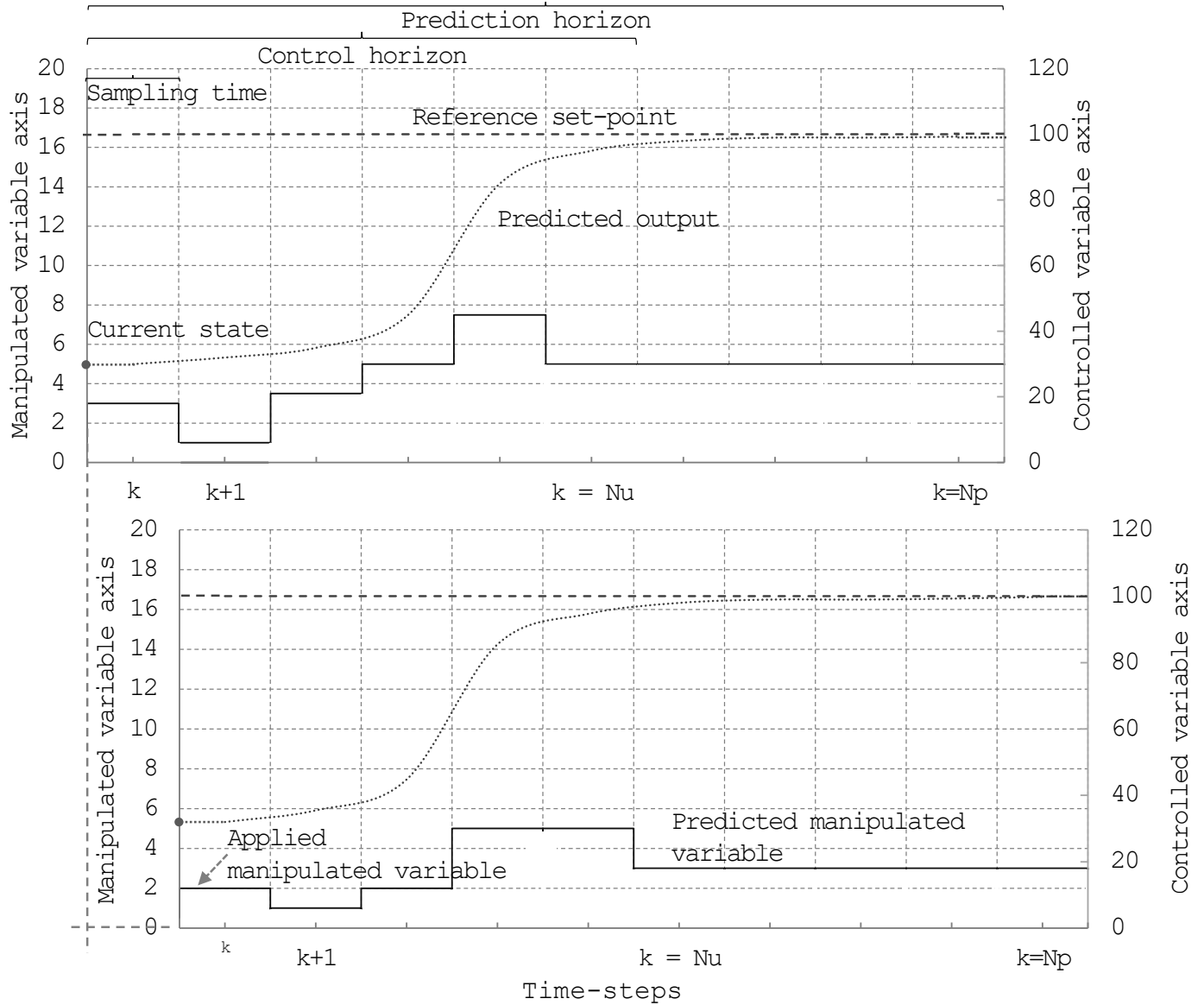
Fig. 3-3 The receding horizon scheme with a displacement by one time-step in the bottom figure

The receding horizon strategy, where at each instant only the first element of the control signal vector is applied while a new control signal is generated at the next time instant is the main difference between MPC and open-loop optimal control. This strategy is able to reduce a system's sensitivity to uncertainties and model mismatch and is often implemented in MPC formulations. The horizons, characteristics of the objective function, and the penalties on the errors and control actions play a significant role in any MPC implementation. These aspects are discussed in the next sections especially in the context of BAC.

3.3 Application of MPC in an energy plant management system (EPMS)

The application of MPC in an EPMS can be derived from the basic principle of MPC for buildings as shown in *Fig. 3-4* (Široký et al., 2011). Time-varying parameters for the MPC problem are extracted from databases, internet back-end services, or forecast models. Energy prices are typically used in the cost function for reduction in demand-related

costs whereas the weather and load forecasts are used by the system models. Comfort criteria for the building users or physical aspects of the components are formulated as constraints of the MPC problem. The models, cost function, and constraints are formulated into an optimisation problem that generates a control signal for the energy plant at each sampling instance. The control signal could be an optimal schedule (on-off time series) for the energy plant's primary components like cogeneration and heat pumps or set-points for the secondary equipment like fan-coil speed, damper rates, and pump speeds. The real-time weather and load requirement (occupancy, production schedule or human influences) that physically affect the system states and could deviate from the forecast values are referred to as disturbances. The energy plant operates for one time-step with the latest control signal and the effect of such disturbances is captured in the next iteration when instantaneous measurements of the system states are sent back to the MPC loop.
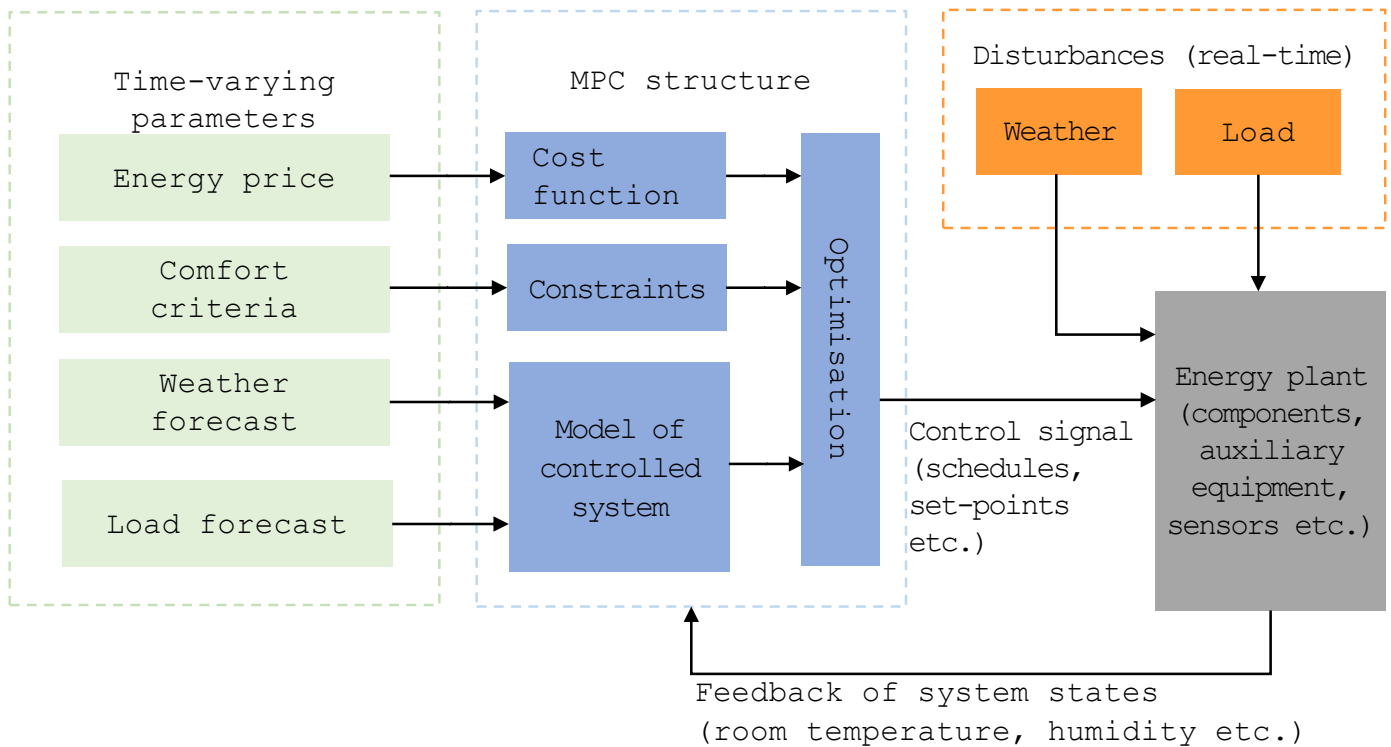
Fig. 3-4 MPC application in supervisory control of an energy plant.

Multiple MPC-typologies for supervisory control of a variety of processes are reported in the literature (Serale et al., 2018). When the uncertainties are unknown but bounded and the calculated control strategy maintains stability and performance specification for all possible variations then a *robust-MPC* is formed. Alternatively, if the disturbances and constraints are included as random variables with a given probability distribution and a stochastic dynamical model of the process is used to predict all possible output scenarios, then a *stochastic-MPC* is developed. Depending on the application scenario, the MPC control law might be solved in real-time using *implicit-MPC* techniques or offline programming algorithms could be applied to provide a lookup table as the control law using *explicit-MPC* techniques. Explicit-MPC can be applied when small sample times are needed or the computing power is limited.

3.3.1 Models for MPC based EPMS

Models form the consequential building block of an energy plant MPC as they mathematically connect the power consumption, system states, and consumption-related costs. Their development and parameterisation is often the most time-consuming and challenging part of the MPC formulation.

The three categories of models for an MPC based EPMS are:

- detailed simulation model of the building and energy plant, in case the scenario demands a closed loop simulation before applying the controls to a real system or in absence of a real system,
- forecast models for the uncontrollable disturbances such as weather or energy price that may affect the output of the system or the optimiser,
- control-oriented models for the plant components.

Various models in the above categories can also be classified into *white-box, black-box* or *grey-box models* (*cf. Chapter 2.5*) and are of interest to both industry and academia to simulate on their application-specific detail level.

In the first category, comprehensive component models in libraries such as *EnergyPlus*, *TRNSYS*, *CARNOT ToolBox*, and *ESP-r* (Afram and Janabi-Sharifi, 2014b) can be used to develop simulation models of a system and analyse the performance of a controller. However, it is unlikely for these models to be used for development of optimal control due to their computation efforts and nontrivial identification processes.

In the second category, forecast models are often used for the following disturbances in EPMS:

- weather conditions,
- occupancy conditions,
- energy grid information.

For design optimisation problems, commonly available data sets such as representative meteorological year and standard load duration curves for building demand and occupation patterns are used. However, for real-time applications, a more accurate representation of the disturbances is achieved by using online or offline forecast models. Online forecasts often use an application programming interface (API) to back-end services, mostly running their own complex prediction algorithms. Offline prediction methods use data collected onsite and can involve complex statistical approaches to forecast the disturbances for a particular scenario. In most cases, the output of the above models is integrated into the dynamic building model and their impact on the system response is directly captured.

Regarding the third category of models in controller development, artificial neural network tools are most prominent amongst black-box approaches and are widely researched in the academic field. Even so, limitations are foreseen in their practical application due to the large amount of data needed for training these models and the

operation of the systems outside of that training range (Afram and Janabi-Sharifi, 2015b).

Simplified physical models and grey-box models have shown significant potential for control-oriented modelling of HVAC primary and secondary equipment (Wang and Ma, 2008). Grey-box models may show only sufficient accuracy compared to the high accuracy of black-box models but they have higher generalisation capability due to their physics based structure (Afram and Janabi-Sharifi, 2015b). For example, the resistance-capacitance electrical network analogy or constrained transfer function approach is often used for modelling the thermodynamics of a building zone, where real-time measurements from the BAC can be used for parameterisation of the models.

In terms of system theory and control engineering, most controllable dynamical systems with outputs can be represented (approximately) in their ODE form as shown in (3.1) and (3.2) (Diehl, 2014a). $x(t) \in \mathbb{X} \subseteq \mathbb{R}^{n_x}$ is the state vector, n_x is the number of states, and set $\mathbb{X}$ denotes the set of admissible states. $\dot{x}(t)$ is the time derivative of the state. $u(t) \in \mathbb{U} \subseteq \mathbb{R}^{n_u}$ is the vector of all manipulated variables and $y(t) \in \mathbb{Y} \subseteq \mathbb{R}^{n_y}$ is the vector of system outputs where n_u is the number of inputs or controls and n_y is the number of outputs. For $t \in [t_0, t_{\mathrm{f}}]$:

$$\dot{x}(t) = f(x(t), u(t)) \tag{3.1}$$

$$y(t) = g(x(t), u(t)) \tag{3.2}$$

The functions $f : \mathbb{R}^{n_x \times n_u} \to \mathbb{R}^{n_x}$ and $g : \mathbb{R}^{n_x \times n_u} \to \mathbb{R}^{n_y}$ establish the mathematical relation between the system states, controls, and outputs.

(3.3) and (3.4) show the state-space formulation of a continuous linear time invariant (LTI) system under the assumption that the process could be sufficiently simulated with a linear model or by linearization around a steady state of the nonlinear model (Diehl, 2019). This formulation is frequently used in control and automation for system analysis and controller design (Felsmann, 2002). $A \in \mathbb{R}^{n_x \times n_x}$ and $B \in \mathbb{R}^{n_x \times n_u}$ are the state matrix and control matrix respectively, whereas $C \in \mathbb{R}^{n_y \times n_x}$ and $D \in \mathbb{R}^{n_y \times n_u}$ are the output and disturbance matrices respectively.

$$\dot{x}(t) = Ax(t) + Bu(t) \tag{3.3}$$

$$y(t) = Cx(t) + Du(t) \tag{3.4}$$

The ability of models to describe the system behaviour with adequate accuracy and computation speed over the length of the prediction horizon greatly influences the quality (stability & practicality) of the controller. For instance, in a practical application the solution time of the MPC problem should be far less than the sample time length. The following characteristics are sought-after in the models to be applied in an EPMS (*Fig. 3-5*) (Sawant et al., 2020a).

```
                                    ┌─────────────────────────┐
                                    │ 1a. Capture dynamic     │
                                    │    characteristics      │
                                    └─────────────────────────┘
                                    ┌─────────────────────────┐
                    ┌──────────────┐│ 1b. Capture part-load   │
                    │ 1. Field level││    behaviour /          │
                    │ control       ││   internal control logic│
                    └──────────────┘└─────────────────────────┘
                                    ┌─────────────────────────┐
┌──────────────┐                    │ 1c. Practical           │
│ Sought after │                    │   parameterisation      │
│characteristics│                   │    capabilities         │
└──────────────┘                    └─────────────────────────┘
                                    ┌─────────────────────────┐
                                    │ 1d. Adaptability to     │
                                    │    component design     │
                                    └─────────────────────────┘
                                    ┌─────────────────────────┐
                                    │ 2a. Lower complexity    │
                    ┌──────────────┐│   (more stability)      │
                    │ 2. Optimisation└─────────────────────────┘
                    └──────────────┐┌─────────────────────────┐
                                    │ 2b.Sufficient accuracy  │
                                    └─────────────────────────┘
                                    ┌─────────────────────────┐
                                    │ 2c. Continuous          │
                                    │    differentiability    │
                                    └─────────────────────────┘
```
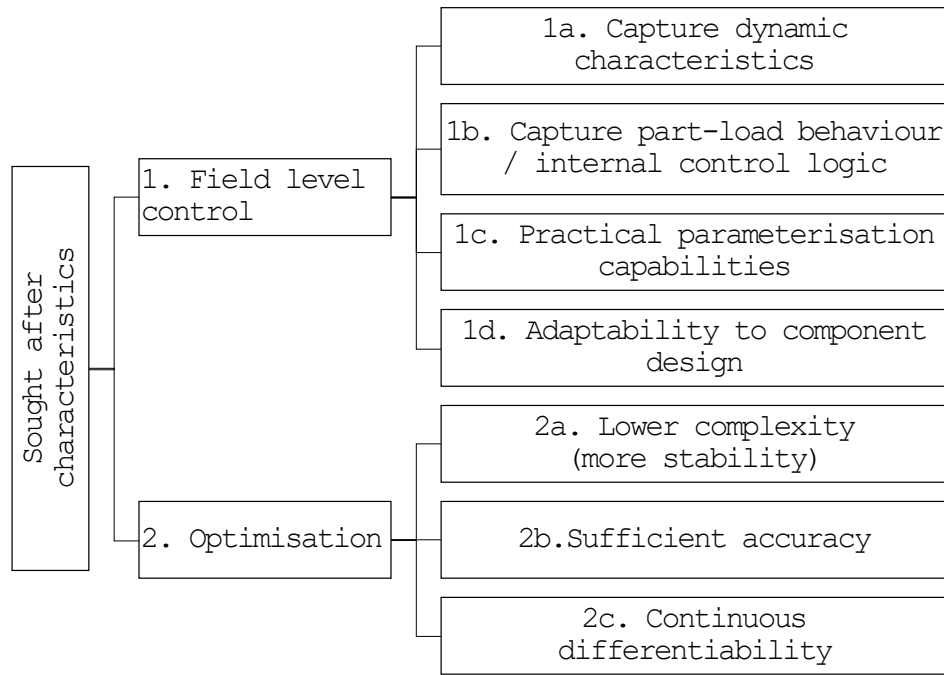
Fig. 3-5 Sought-after characteristics of models for MPC based energy plant management system (EPMS)

1a. Capture dynamic characteristics: When working with actual components, a switch from one operating point to another often has a dynamic effect on the system states, and should be included in the component models for improving their controllability (Afram and Janabi-Sharifi, 2015a; Zhou et al., 2013). For example, limitations of following an entirely static modelling approach are reported in the literature due to their excessive parameterisation-data requirements and higher inaccuracies especially for thermal storage models (Gu et al., 2014). In the context of MPC, if the components exhibit slow dynamic behaviours and settling times much longer than the sampling time interval, then this behaviour should be simulated accordingly.

1b. Capture part-load behaviour / internal control logic: If the components operate at lower efficiencies under part-load or have an internal control logic that uses low-level controllers to improve their performance under part-load, then the appropriate output should be simulated by their models. This increases the model's accuracy and suitability for controller design both on the local and supervisory level.

1c. Practical parameterisation capabilities: The basis for modelling the components should allow practical parameterisation of the components. This includes parameters that are promptly available from data sheets, can be collected during the commissioning phase of the plant, or are based on data that is collected in standard monitoring practices.

For example, regression-based models should not use data for fitting the parameters that needs specialised instrumentation or disassembly of the components. Practical parameterisation capabilities reduce the need for component-data measured inside a machine or in other inaccessible locations and usually lower the set-up and computation time (Jin and Spitler, 2002). They also facilitate the application of MPC in both retrofit and green-field scenarios. However, when sufficient catalogue data is not available or unexpected operational ranges are simulated then an extrapolation of empirical models

can lead to inaccuracies. Semi-empirical models are preferred in this case due to their ability for operation outside the fitting range (Lemort et al., 2009).

1d. Adaptability to component design: The constructional design of a component might strongly influence its performance and interoperability. The models of such components should have the ability to adapt to the type of design.

For instance, the height at which water enters and leaves a storage tank depends on its hydraulic connections, or the type of heat transfer depends on the heat exchanger installed in the tank.

2a. Lower complexity: Chandan et al. denoted the unsuitability of detailed HVAC simulation models for direct use in an MPC structure due to their large computation times and challenges in parameterisation (Chandan et al., 2012). For instance, a higher order model increases its complexity but does not necessarily fit the data better and may lead to over-fitting the training data (Afram and Janabi-Sharifi, 2015b). If no significant benefit is gained by increasing the model order, then a lower order model should be selected. Another example is the number of system states. With each new state and control the size of the entire optimisation problem increases by a factor of the total number of sampling intervals over the entire forecast horizon, leading to an expansion of the state- and control spaces. The number of states and controls in the component models should be limited to only those necessary for calculating outputs relevant for the particular optimisation problem.

2b. Sufficient accuracy: The required accuracy of models depends on the available system knowledge and on aspects of the real system that are relevant for accomplishment of the simulation objectives. There is no comprehensive guideline on model selection and a balance must be found between the model complexity and potential error in performance prediction (Trčka and Hensen, 2010). The models needed for receding horizon MPC of thermal systems (which typically demonstrate slow dynamics) do not need to be of high accuracy as black-box models used for component level simulations in design problems. Since MPC gives means to adjust the control and react to uncertainties or model mismatch due to the update of system information after every sampling time, the models need to predict (only) process variables relevant for the plant's control and safety with sufficient accuracy (Lefort et al., 2013; Široký et al., 2011).

2c. Continuous differentiability: The models need to be continuously differentiable when their application is in gradient-based optimisation methods as described in *Section 3.3.6* (Biegler, 2010). This can also increase the applicability of more efficient solvers that do not have to handle discontinuities (Imsland et al., 2010). For example, "If-Else" clauses should not be used to describe the different operation regions or change in operational status of machines but alternative strategies should be used for approximating such clauses with continuous functions as implemented in *Section 4.9.1* (Beck and Fischer, 1994).

The models developed for the INES Trigeneration system with the above characteristics are discussed in *Section 4.4*.

3.3.2 Cost function

A cost function establishes the link between the control actions of a system, the events occurring in that system, and the costs of performing those tasks in a mathematical form. Often it is a quadratic formulation and aims at minimising the deviation from a reference trajectory and the predicted control effort simultaneously. This form is used in a *tracking-error-MPC*. An explicit solution can be obtained for a quadratic cost function if the model is linear and there are no constraints on the system (Camacho and Bordons, 2007). However, in the presence of constraints the solution is often obtained after multiple iterations with advanced numerical algorithms. The cost function J_{TE} formulated using (3.5) is a typical cost function for tracking error problems:

$$J_{TE} = \sum_{k=1}^{N_r} w_{r_k^*}(r_k - r_k^*)^2 + \sum_{k=1}^{N_u} w_{u_k} u_k{}^2 \tag{3.5}$$

where,

r_k – kth reference variable in N_r number of variables

r_k^* – kth controlled variable in N_r number of variables

$w_{r_k^*}$ – weighting coefficient reflecting the relative importance of r_k^*

u_k – kth manipulated variable in N_u number of variables

w_{u_k} – weighting coefficient penalising control actions through manipulated variable u_k

In theory, a cost function in the form of a *Lyapunov function* for a closed loop system is ideal to increase the control loop's stability (Ellis et al., 2014). However, stability is generally not a critical factor in practical building systems with slow moving dynamics (Široký et al., 2011) and different types of cost functions or their combinations are used in MPC-based BAC (Afram and Janabi-Sharifi, 2014a). For example:

- weighted sum of tracking error and control effort,
- quadratic cost function for tracking the error and control effort,
- sum of operational costs,
- sum of the tracking error (e.g. room-temperature control, energy conservation),
- energy consumption,
- thermal comfort violation cost.

The weighting coefficients help to achieve a trade-off between competing objective combinations, such as maximising thermal comfort and minimising energy consumption or minimising tracking error and control actions simultaneously.

In some cases, a dynamic cost function is used wherein the magnitude of the weights can vary over the prediction horizon depending on the available incentives. Some studies combine different types of cost functions for solving two or more MPC problems to control different aspects of the complete system. For instance, Lefort et al. proposed a hierarchical MPC to combine the slow-moving dynamics of an energy plant scheduling problem with the fast-dynamics of room temperature control to reduce the total energy

consumption (Lefort et al., 2013). The scheduling problem was solved with a relaxed cost function for a large scheduling horizon of 7 hours and scheduling sampling time of 5 minutes and the temperature control problem was solved with a tracking error cost function for a short horizon of 5 minutes and a sampling time of 30 seconds.

When the MPC scheme uses a continuous economic cost function as shown in (3.6), that unifies economic optimisation with process control by applying economically driven signals such as operating costs or energy costs then it is referred to as *economic-MPC* (Ellis et al., 2014). The function $l_e \colon \mathbb{R}^{n_x \times n_u} \to \mathbb{R}$ is a continuous function that is used as a measure of the instantaneous process costs, which depending on the type of process, is expressed in monetary or productivity terms. For $t \in [t_0, t_f]$, a typical economic-MPC cost function J_{EMPC} is given as:

$$J_{\mathrm{EMPC}} = \int_{t_0}^{t_f} l_e(\boldsymbol{x}(t), \boldsymbol{u}(t)) \, \mathrm{d}t \qquad (3.6)$$

It does not have a conventional quadratic form with magnitude of the tracking error and control actions but considers the process economics and thus cannot be used as a traditional Lyapunov function to prove closed-loop stability (Serale et al., 2018).

The cost function used in this work for minimisation of consumption-related costs is formulated in *Chapter 6*.

3.3.3 Constraints and slacks

MPC is also referred to as constrained control due to its ability for handling constraints placed on the manipulated variables, system states, and equipment characteristics. These constraints give the mathematical formulation of an MPC problem an engineering perspective as they often have a physical motivation. For example, in HVAC systems, constraints can be placed on (a) equipment characteristics e.g. damper rate limits, compressor speeds, machine switching, temperature based operation limits, or on (b) physical quantities e.g. air-flow, thermal comfort range, tank charge/discharge rates and temperatures (Bürger et al., 2017; Elliott, 2008; Henze et al., 2005).

Such range constraints are often represented as inequalities whereas fixed constraints such as storage sizes or thermal capacity of machines are represented as equalities. In some studies, a terminal constraint with a terminal weight is also introduced to satisfy a particular configuration of the system state like battery state-of-charge or tank temperature at the end of the prediction horizon (Ma et al., 2009).

Although constraints make the solution of an optimisation problem reality-oriented, the time needed for the solution of constrained and robust cases can be various orders of magnitude higher than unconstrained cases (Camacho and Bordons, 2007). Inequality constraints form the so-called path constraints for the optimiser and should be relaxed to improve the feasibility of the problem in real-world applications (Serale et al., 2018). This can be especially necessary when a problem has both integer and continuous control and the solution cannot be obtained by adjusting the continuous controls alone.

A prominent method is the usage of *slack variables* to allow constraint violations but with a weight or penalty cost in the cost function. Thus, higher the cost of using a slack variable, the further the solution of the problem moves towards the hard boundary i.e. towards an infeasible region in the optimisation space. However, the advantage of using slacks is a higher computational robustness of the problem by avoiding unfeasible conditions for the optimiser (Lefort et al., 2013; Široký et al., 2011).

For instance, the outputs of a system collected in a vector Y can be restricted between minimum and maximum values using the following formulation (Bruni et al., 2015):

$$Y_{\min} \leq Y \leq Y_{\max} \tag{3.7}$$

This *hard constraint* can be relaxed to *soft constraints* by introducing a vector of slack variables s_Y of the same shape as Y and satisfying (3.8) and (3.9).

$$Y \leq Y_{\max} + s_Y \tag{3.8}$$

$$Y \geq Y_{\min} - s_Y \tag{3.9}$$

where, $s_Y \geq 0$, and $s_Y \in \mathbb{R}^{n_Y}$ and is a result of the optimisation. A stage-cost penalty $(Y_s = s_Y^{\mathrm{T}} W_s s_Y)$ is then added to the cost function that helps to achieve a trade-off between constraint violation and objective value.

The detection of such constraints in a system needs operational experience and engineering know-how. In practice, operating manuals of the machines and results of commissioning tests are analysed to detect any design and operational limits that are then formulated as constraints.

The identification and implementation of constraints with respect to this work is discussed in *Chapter 4* and *Chapter 6* in further detail.

3.3.4 Horizons

The three main horizons for an MPC problem are:

- prediction horizon – length of time for which the system output is computed,
- control horizon – length of time for which the control vector is computed,
- control sampling time or control time-step – length of time during which the control signal remains unchanged or length of time after which MPC loop is repeated.

The selection of the horizon is fundamental for a practical MPC implementation and is influenced by the controlled system's characteristics like time constants and dynamics. Longer prediction horizons give more forecast data or information to the optimiser but may not lead to additional benefits because the accuracy of forecasts inherently worsens over the horizon, and so does the quality of the solution due to model mismatch and uncertainties. On the other hand, shorter horizons reduce the computation effort but also adversely affect the reliability of the controller by possibly neglecting important dynamics of the system. Splitting the horizon into many control steps leads to a higher accuracy of the simulation because of the increased number of discretisations but also makes the problem larger and requiring longer computation times.

Different combinations are possible for the horizon lengths but most importantly the control horizon is smaller or equal to the prediction horizon and the control sampling time is smaller than the control horizon. Typically, for MPC of slower building systems a prediction horizon of 24 hours and a sampling time of 15 minutes to 1 hour is used and for faster HVAC systems a shorter sampling time of 1-5 minutes is used (Serale et al., 2018). In some cases, the sampling times are varying over the prediction horizon making the time grid non-equidistant (Bürger, 2020). For instance, the time grid could be finer in the near future on the horizon (e.g. 5 minutes for next 1 hour on a 24-hour horizon) and broader as time progresses on the prediction horizon (e.g., 15 minutes for remaining 23 hours). This helps to reduce the total number of discretisations and thus the size of the problem whilst maintaining higher accuracy of the solution for near future and acceptable lower accuracy for distant future. Unlike the receding horizon MPC, if the prediction horizon does not shift or recede but instead reduces as time progresses towards the end of the horizon the scheme is identified as *shrinking horizon MPC* e.g. batch processes in chemical industries.

The choice of the horizon lengths and formulation of the MPC problem for this work is described in *Chapter* 6 and *Chapter* 7.

3.3.5 Control architecture

MPC is applied in BAC for control of various HVAC subsystems and processes. For instance, either the minimisation of HVAC energy consumption in general is targeted or the zone temperatures and humidity in single-zone or multi-zone buildings are controlled (Bracco et al., 2014; Oldewurtel et al., 2010; Široký et al., 2011; Zhao et al., 2015). The control architecture is adapted according to the type of system or process being controlled.

In addition to the *direct control* of actuators and the *hierarchical approach* for implementing MPC, a *cascaded MPC* scheme is also discussed in the literature (Huang, 2011). Instead of having a supervisory layer, multiple layers run optimisations at the same frequency.

A further classification of control architectures is based on the practical implementation of the MPC itself. This is possible either in centralised, decentralised, or distributed configurations (Serale et al., 2018). In a *centralised configuration* an individual MPC provides the optimal solution for an entire system by considering the various inputs on temperatures, occupancy etc. from all the zones and their interactions. Although this may lead to better modelling of the system dynamics and more energy conservation, the problem complexity and technical irregularities increase with size of the system. In a *decentralised configuration,* each zone or subsystem has its own MPC controller reducing the size of the optimisation problem and increasing the ability to operate independently in case of failure of a central controller. However, due to the isolation from the MPC of the other zones a wastage of energy and inherent loss of valuable information occurs. The mutual interactions are considered unknown external disturbances to the models. A *distributed configuration* is considered as a potential

solution for large-scale dynamically coupled buildings where the individual zone-MPCs share necessary information with others for their optimisation problem. Although the computation effort is reduced compared to a central controller, the implementation of software and hardware to operate this configuration is not straightforward.

3.3.6 Optimisation techniques

The elementary theoretical explanation in this section derives from textbooks, course material, and scientific publications on optimal control and numerical optimisations (Camacho and Bordons, 2007; Diehl, 2016; Rawlings; et al., 2019). In principle, MPC is a form of optimal feedback control via real-time optimisations. Depending on the attributes of an optimisation problem, it can be broadly classified as shown in *Fig. 3-6*.
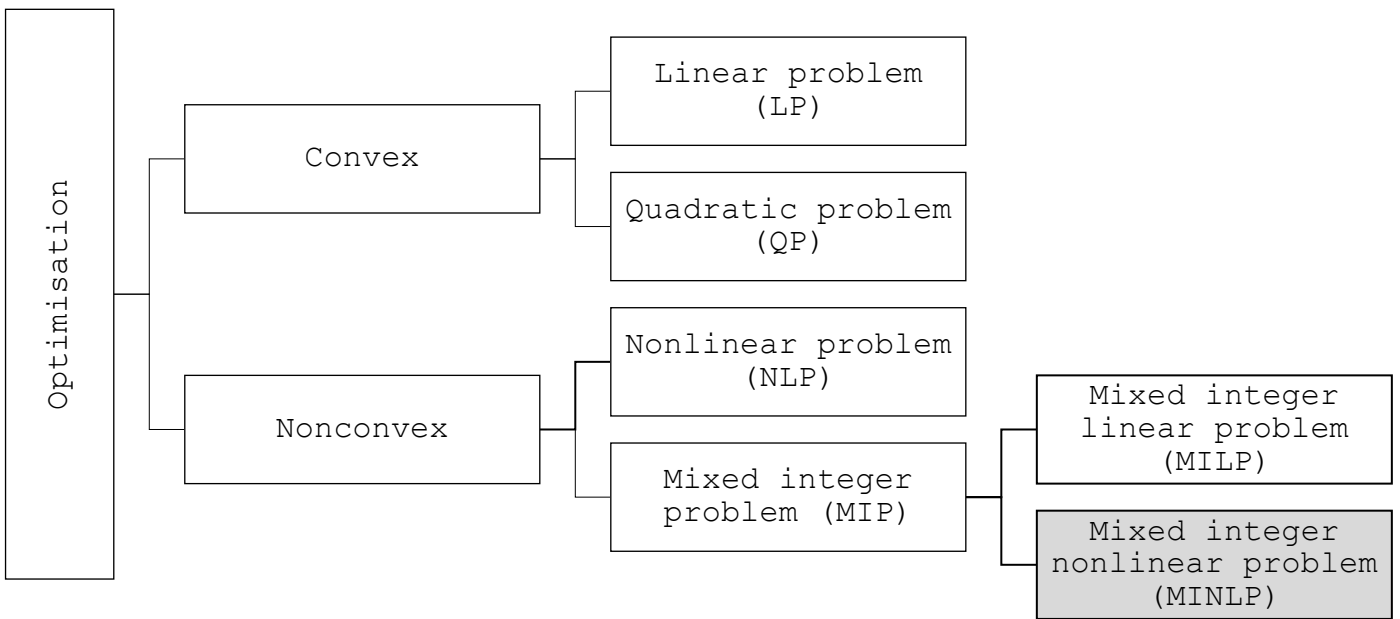
Fig. 3-6 Main classes of an optimisation problem with MINLP as focus of this work

A convex optimisation problem has a convex feasible set and a convex objective function. A local solution is always a global solution and is achieved relatively easier compared to nonconvex problems (Diehl, 2016). Linear problems (LP) and quadratic problems (QP) with a convex objective are two important subclasses of convex problems. In LPs, the objective and all constraints are linear functions of the decision variables and in QPs, only the objective is a quadratic function. Algorithms like *simplex* and *active set method* are widely used for solution of LPs and QPs respectively.

The other important class of optimisation problems is nonconvex problems and nonlinear problems (NLP) typically belong to this class. Gradient-based methods like *interior point methods* are widely used to find the local minimum in NLPs. Optimal control problems with underlying nonlinear dynamic systems are fundamentally NLPs. Optimisation problems with both real and integer decision variables ($u \in \mathbb{Z}$) are called mixed integer problems (MIP) and can never be convex due to the nonconvexity of the set of integers. If the objective function and/or the constraints are nonlinear in the

decision variables, then the special class of MIP is called a mixed integer nonlinear problem (MINLP) and if they both are linear in the decision variables, then it is a mixed integer linear problem (MILP). The typical solution algorithms for MIPs are branch-and-bound, tabu and scatter search, and evolutionary algorithms (Bussieck and Pruessner, 2003).

It is pointed out in previous studies that NLPs and MIPs perform better for optimisation of energy systems and give more practice-oriented solutions than LPs. For instance, one study clearly demonstrated higher operating hours of a favourable component (heat pumps in this case) for economic reasons when performing NLP and MIP optimisation over strictly LP optimisation (Ommen et al., 2014).

In the field of infinite dimensional mixed integer optimisation, continuous time optimal control formulations are described as *mixed integer optimal control problems* (MIOCP). Their solution is challenging due to the combinatorial nature of the integer variables and is especially difficult when complementary conditions are present (e.g. multiplication of switches) leading to non-smoothness (Diehl, 2014a). The derivative or gradient information cannot be used with confidence to determine direction of increase or decrease. Most solution methods use types of convex relaxation of the integer variables where part of the $\boldsymbol{u}$ are fixed to specific integer values and part of them are relaxed.

In a broad sense, it is not trivial to determine the best-suited algorithm for a certain type of model or problem. For the scheduling problem of a CCHP micro-grid, consisting of multiple objectives and mixed binary and continuous variables, experts recommend to focus on improving stability and computation time to satisfy the requirements in real-world applications (Gu et al., 2014). A typical MIOCP formulation for minimising a continuous cost function with a stage cost $L(\boldsymbol{x}(t), \boldsymbol{u}(t))$ or *Lagrange term* and a terminal cost $E(\boldsymbol{x}(t_\mathrm{f}))$ or *Mayer term* is shown in (3.10).

$$\min_{\boldsymbol{x}(\cdot), \boldsymbol{u}(\cdot)} \int_{t_0}^{t_\mathrm{f}} L\big(\boldsymbol{x}(t), \boldsymbol{u}(t)\big)\mathrm{d}t + E(\boldsymbol{x}(t_\mathrm{f})) \tag{3.10a}$$

subject to, for $t \in [t_0, t_\mathrm{f}]$:

$$\boldsymbol{x}(0) - x_0 = 0, \tag{3.10b}$$

$$\dot{\boldsymbol{x}}(t) - f(\boldsymbol{x}(t), \boldsymbol{u}(t)) = 0, \tag{3.10c}$$

$$g\big(\boldsymbol{x}(t), \boldsymbol{u}(t)\big) = 0, \tag{3.10d}$$

$$h\big(\boldsymbol{x}(t), \boldsymbol{u}(t)\big) \leq 0, \tag{3.10e}$$

$$r\big(\boldsymbol{x}(t_\mathrm{f})\big) \leq 0. \tag{3.10f}$$

Where, $\boldsymbol{u}(t)$ are the controls (both integer and continuous) and $\boldsymbol{x}(t)$ the states. The initial state x_0 is determined using (3.10b). Under the assumption that the initial state x_0 and all the controls $u_0 \dots u_{t_\mathrm{f}}$ are known, the remaining states of the system can be simulated with (3.10c). Equality constraints are formulated in (3.10d), path constraint inequalities $h(\boldsymbol{x}(t), \boldsymbol{u}(t))$ in (3.10e) and the terminal constraint $r\big(\boldsymbol{x}(t_\mathrm{f})\big)$ in (3.10f).

Direct methods are the most widespread and successfully used techniques for the solution of MIOCPs (Diehl, 2014a). These methods begin with transforming the continuous time dynamic system into a discrete time system by means of parametric functions to break down the original problem into finite dimensional NLPs and then solve these sparse NLPs ("first discretise, then optimise").

Essentially two approaches are used: *simultaneous approach* e.g. *direct multiple shooting* and *direct collocation* or *sequential approach* e.g. *direct single shooting.* The differences in the approaches are primarily in the methods used for the solution of the state trajectories after the problems are discretised. The simultaneous approach discretises the original problem both in controls and states on a fixed grid. The resulting large sparse NLPs are then solved by structure-exploiting solvers that solve both the simulation and the optimisation problem simultaneously by using x_k and u_k as the optimisation variables. The sequential approach on the other hand, eliminates nearly all states by forward simulation. It keeps the x_0 and $U = \left[u_0^{\mathrm{T}}, \ldots, u_{N-1}^{\mathrm{T}}\right]^{\mathrm{T}}$ as variables and then solves the simulation problem and the optimisation problem sequentially.

The mathematical solution process for the NLPs formed in the above problems involves its *Lagrangian function* that can help to identify its extreme values (Felsmann, 2002) and is formulated as in (3.11).

$$\mathcal{L}(\boldsymbol{\omega}, \boldsymbol{\lambda}, \boldsymbol{\mu}) = F(\boldsymbol{\omega}) + \boldsymbol{\lambda}^{\mathrm{T}} G(\boldsymbol{\omega}) + \boldsymbol{\mu}^{\mathrm{T}} H(\boldsymbol{\omega}) \tag{3.11}$$

Where, $\boldsymbol{\omega}$ is collection of all the variables i.e. $\boldsymbol{\omega} = (x_0, u_0, x_1, \ldots, u_{N-1}, x_N)$ and $\boldsymbol{\lambda} \in \mathbb{R}^{n_g}$ and $\boldsymbol{\mu} \in \mathbb{R}^{n_h}$ are the *Lagrange multipliers*. The functions $G(\boldsymbol{\omega})$ and $H(\boldsymbol{\omega})$ collect all the equality and inequality constraints respectively while $F(\boldsymbol{\omega})$ is a copy of (3.10a).

Observing the *Karush-Kuhn-Tucker* (KKT) optimality conditions, for $\boldsymbol{\omega}^*$ as a solution of the NLP the Lagrange multipliers $\boldsymbol{\lambda}^*$ and $\boldsymbol{\mu}^*$ satisfy (3.12):

$$\nabla \mathcal{L}(\boldsymbol{\omega}^*, \boldsymbol{\lambda}^*, \boldsymbol{\mu}^*) = 0 \tag{3.12a}$$

$$G(\boldsymbol{\omega}^*) = 0 \tag{3.12b}$$

$$H(\boldsymbol{\omega}^*) \leq 0 \tag{3.12c}$$

$$\boldsymbol{\mu}^* \geq 0 \tag{3.12d}$$

$$\boldsymbol{\mu}^* H = 0 \tag{3.12e}$$

The KKT conditions can be solved using *Newton-type gradient-based methods*. In these methods, gradients of the constraint functions are needed to form *the Jacobian matrix* and, in some cases, the second order derivative of the Lagrangian function is needed to form the *Hessian matrix*. The derivatives can be calculated by using the methods of symbolic differentiation, finite-differences, or algorithmic differentiation in various computer programs. The *algorithmic differentiation* method exploits the fact that each differentiable function is composed of several elementary operations that could be programmed using efficient symbolics and embedded functions in a structured programming language(Andersson et al., 2019).

Due to the application of these derivate-based approaches for calculating first and second order derivatives to check for optimality conditions the continuous differentiability of the models should be assured.

A challenge still remains if switching decisions are involved in the original optimal control problem because the discretisation leads to control variables that inherit the integrality condition (Sager, 2009). Convex relaxation of the problem is recommended for solving the resulting MINLPs within time scales appropriate for real-time applications because global optimisation algorithms are often not capable of identifying a global solution within acceptable computation times for engineering practice (Andiappan, 2017).

One approach for solving MINLPs of such types in practical computation times is the *combinatorial integral approximation method* which generates an approximate solution of the MINLP by solving a sequence of subproblems which are less hard to solve than the original problem (Sager, 2009; Sager et al., 2011). In short, first a relaxed version of the MINLP is solved with binary constraints dropped, which is an NLP, to obtain a relaxed binary solution $b_{\text{relx}} \in [0,1]$. Afterwards, an approximated binary solution $b_{\text{aprx}} \in \{0,1\}$ is computed from b_{relx} by solving the so-called *combinatorial integral approximation problem* which is a MILP like the one shown in (3.13). Here, the deviation of the strict integer values from the relaxed solution of the NLP is minimised by minimising the difference in the area under the two curves.

$$\min_{u^*} \max_{j=1 \dots n_b} \max_{i=1 \dots N} \left| \sum_{k=1}^{i} (b_{\text{relx}\,j,k} - b_{j,k}) \Delta t_k \right| \tag{3.13a}$$

subject to:
$$\sigma_{j,\max} \geq \sum_{i=1}^{n_{t-1}} |b_{j,i} - b_{j,i+1}|, \tag{3.13b}$$

$$b_{j,i} \in \{0,1\}. \tag{3.13c}$$

where, Δt_k is the control discretisation grid and (3.13b) is the formulation for maximum switching constraints with $\sigma_{j,\max}$ as maximum number of switches. $b_{\text{relx}\,j,i} \in [0,1]$ and $b_{j,i} \in \{0,1\}$.

The MILP is solved using branch and bound algorithms applied within the solver routines used in this work. An NLP is then solved again (gradient-based methods) using the fixed binary control to fit the states and continuous controls.

Another method to find suitable approximations is the *sum-up rounding* highlighted in (3.14) (Sager, 2009).

$$b_{j,i} = \begin{cases} 1, & if \ \sum_{k=0}^{i} b_{\text{relx}\,j,k} \Delta t_k - \sum_{k=0}^{i-1} b_{j,k} \Delta t_k \geq 0.5 \Delta t_i \\ 0, & else \end{cases} \tag{3.14}$$

where, $\Delta t_i = t_{i+1} - t_i$, $j = 1 \dots n_b, i = 1 \dots N$ and N is the total number of discretisations. $b_{\text{relx}\,j,i} \in [0,1]$ and $b_{j,i} \in \{0,1\}$.

However, if the constraints of the problem depend explicitly on the integer variables as in the case of switching constraints (e.g. maximum switching of a machine) or costs on fixed control grid, then the sum-up rounding method is not applicable, as it cannot directly consider such constraints.

3.4   Summary and outlook

Building automation and control systems are typically divided into three levels: management, automation, and field level. Different types of *energy management systems* or *supervisory controllers* operate on the management level to control a variety of systems e.g. heating plants, ventilation systems or air-conditioning systems. In this work, the supervisory controller is applied for optimal scheduling of the micro-scale trigeneration system (energy plant) on the field level. This particular application of a supervisory controller for the HVAC primary side or energy plant in a building is referred to as the *energy plant management system*.

In this chapter, the different attributes of an MPC and optimisation techniques to solve it were presented in a condensed form. Particularly, the sought-after characteristics in *control-oriented models* e.g. practical parameterisation and continuous differentiability were summarised. An *economic-MPC* framework with *grey-box models* is considered most practical for thermal energy plants with slow-dynamics and is explored further in this dissertation. Three main issues are mentioned in the literature regarding application of economic-MPC: (a) feasibility of the optimisation problem, (b) stability of the closed-loop system and (c) the closed-loop performance. These are handled using simplified mathematical algorithms and engineering solutions discussed in later chapters. Additionally, the MPC framework is developed in a *hierarchical and centralised architecture* where the management layer synchronises an operation with the lower level controllers. For real-time application, *implicit-MPC* techniques with a *receding horizon* and a *variable length time -steps* are applied. A *mixed integer optimal control problem* is solved using *direct collocation* for discretization of the problem and the *combinatorial integral approximation method* with *branch-and-bound* routines for solving the resulting MINLP. The solution of this optimal control problem including operational constraints with *slack variables* provides on-off switching sequences for the components that are used directly for the lower-level controller. Open-source forecast data from third party platforms is used for the MPC.

With the above outlook on solving the MPC problem for economic scheduling of a micro-scale trigeneration system, the most important steps of developing the models for MPC and the experimental set-up for their evaluation is explained in the following chapter.

4 Experimental Set-Up and Component Models

Models form the virtual representation of a plant that is controlled by MPC and their development is the most resource intensive phase during the controller design process. In this chapter, the models for the trigeneration system at the Institute of Energy Systems Technology are developed and evaluated. The experimental set-up with the building automation and control framework used for parameterisation and evaluation of the models is also described. The modelling methodology and evaluation is illustrated with one example for the functional tests and simulation results for each main operation mode. Results of both, qualitative and quantitative analysis are presented. The novelty in developing control-oriented models and experimentally evaluating their technical feasibility for implementation in MPC of a complex energy system is highlighted. Finally, the technical challenges faced during commissioning of this complex plant are listed and corresponding lessons learned for planning of future systems are documented.

4.1 Experimental set-up of the trigeneration system at INES

A micro-scale trigeneration system with a combustion engine cogeneration unit, an adsorption based thermal chiller, a reversible heat pump, a compression chiller, hot and cold thermal storages, and two-way connection to the electricity grid was installed at the *Institute of Energy Systems Technology* (INES) at *Offenburg University of Applied Sciences*. The planning and construction of the plant including the installation of the *building automation and control* (BAC) system was done within the framework of this doctoral thesis using the in-house competencies of the institute.

4.1.1 Basic and detailed engineering

During the basic engineering phase, the component technologies and capacities, hydraulic connections, instrumentation and load profiles were decided based on the following overall aims of the laboratory set-up:

- comparing conventional and optimal control,
- application in small- and medium-scale industries and buildings,
- comparing thermal and electric chillers,
- analysing a thermal and electric chiller cascade,
- integration of the existing test chamber (TC) with a thermally activated building system (TABS) and ceiling cooling system (Pfafferott et al., 2016) as thermal loads.

In the detailed engineering phase, piping, pump calculations, and instrumentation plans for the plant were prepared (see *Appendix B*). The effects on the MPC performance due to design decisions for fulfilling these multiple aims and possible improvements are elaborated in *Section 4.12* of this chapter.

A concise explanation of the system is given in the block flow diagram in *Fig. 4-1*. Final energies in the form of combustion fuel (FUEL) and electricity from the local low-voltage grid (GRID) are converted to three useful energies: heating, cooling, and electricity by the components on the energy source side. The combined heating and power (CHP) unit converts fuel to electrical power and high temperature heating power. The adsorption chiller (AdC) uses this as the driving energy to produce cooling power. Additionally, a reversible heat pump (RHP) consumes electricity to operate either as a heat pump (HP) producing low temperature heating power or as a compression chiller (CC) producing cooling power. Both the AdC and RHP interact with the same outdoor coil (OC) in a medium temperature circuit. The heating and cooling produced on the source side is stored in stratified water storage tanks, hot thermal energy storage (HTES) and cold thermal energy storage (CTES). They also act as the connecting points for all the flows between source and supply side. On the supply side, the TC and two thermostats generate a reference heating load (HL) and cooling load (CL) that are covered with low temperature heating or high temperature cooling from the thermal storages respectively. The electrical load (EL) comprises of an imaginary reference load profile and electricity can be purchased or fed-into the local low-voltage grid.
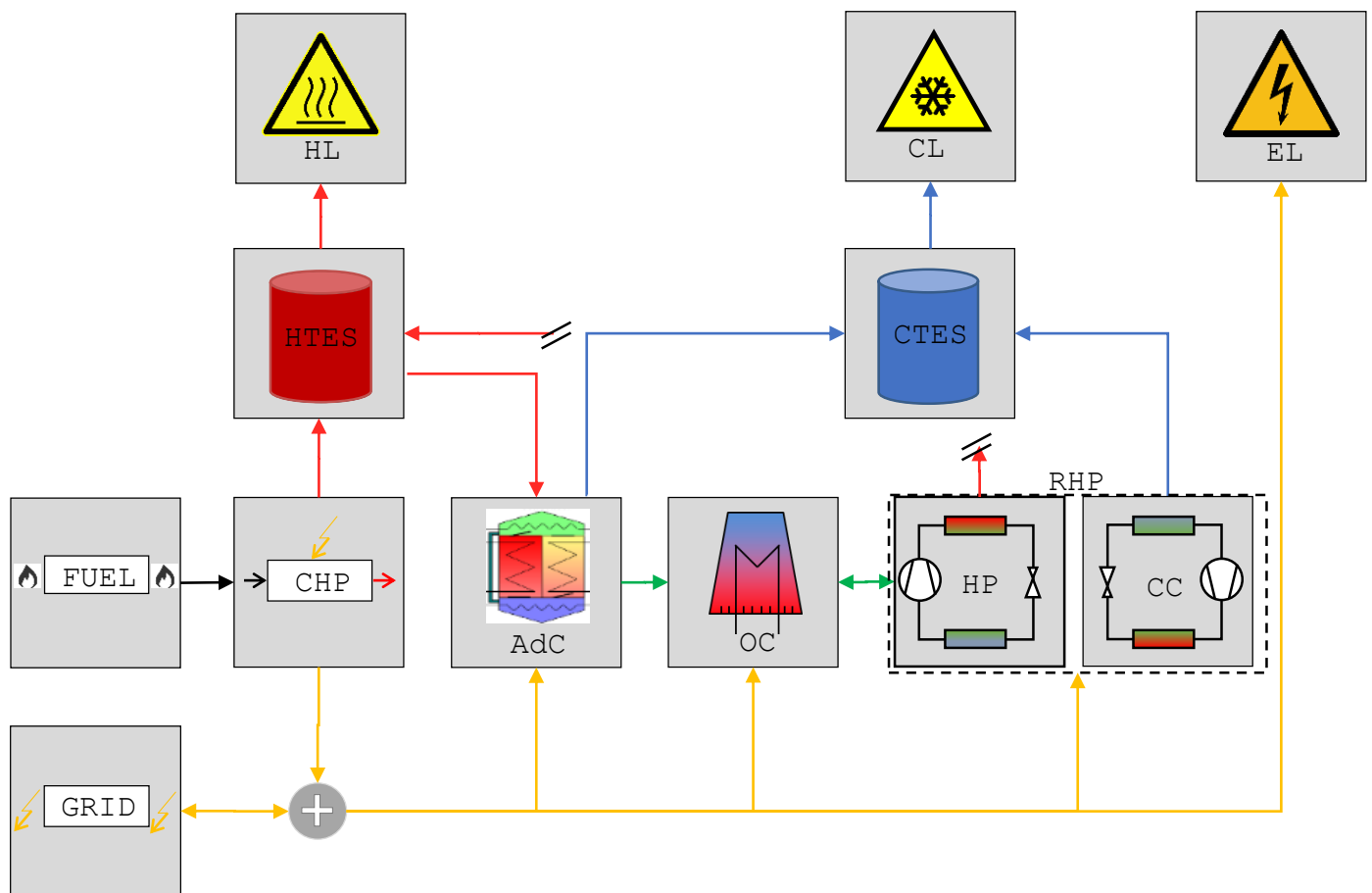
Fig. 4-1 Block flow diagram of the INES trigeneration system

The main technical specifications from the data sheets or commissioning documentation of the individual components are given in *Table 4-1*.

Table 4-1 Main specifications of the primary components

Component	Specification	Value
AdC:	Nominal cooling power	10 kW$_{th}$
	Nominal coefficient of performance	0.45
	Operating range in temperature circuit: • low • medium • high	 • 8 – 18 °C • 22 – 45 °C • 55 – 95 °C
	Recommended volume flow in temperature circuit: • low • medium • high	 • 1.7 m³/h • 4.3 m³/h • 1.6 m³/h
	Set-point for chilled water temperature	12 °C
	Power consumption	0.12 kW$_{el}$
CHP:	Standard heating power	10.5 kW$_{th}$
	Standard electrical power	5.3 kW$_{el}$
	Thermal efficiency (higher calorific value)	66%
	Electrical efficiency	30%
	Safety shut-down temperature in return-line	73 °C
	Auxiliary power consumption	0.14 kW$_{el}$
	Nominal fuel-oil consumption	1.8 l/h
OC:	Heat exchanger area	521.8 m²
	Maximum rotational speed	480 RPM
	Maximum power consumption	0.90 kW$_{el}$
	Control voltage signal	0 – 10 V
	Overall heat transfer coefficient	26 W/(m²·K)
RHP:	Nominal cooling power	12.9 kW$_{th}$
	Nominal heating power	16.7 kW$_{th}$
	Nominal power input	3.8 kW$_{el}$
	Nominal energy efficiency ratio (cooling mode)	3.44
	Nominal coefficient of performance (heating mode)	4.45
	Nominal water flow in evaporator circuit	37 l/min
	Nominal water flow in condenser circuit	48 l/min
CTES and HTES:	Volume	ca. 1500 l
	Diameter without insulation	1 m
	Height without insulation	2.2 m
	Thickness of tank wall	0.0125 m
HiL:	Heating power of the thermostats together	18 kW$_{th}$
	Cooling power of the thermostats together	10 kW$_{th}$
	Tolerance in temperature control	0.01 K
	Total energy dissipation area in test chamber	ca. 34 m²
	Average cooling power dissipation in test chamber	70 W/m²
	Average heating power dissipation in test chamber	90 W/m²

The main components, heat exchangers (HX), piping, and the instrumentation are shown in *Fig. 4-2*. The PLC, switch systems, electrical safety equipment, and signal converters are installed in the wall mounted electric switching cabinet (ESC).

On far right, the workstation computer (WS) and thermostats and TC with TABS for emulating thermal loads connected as hardware-in-the-loop (HiL) are also shown.

Fig. 4-2 (a) View from left of the lab (b) View from right of the lab

The components do not operate all at once but seven different modes of operation are possible depending on the combination of components, hydraulic connections, and thermal loads. Further details of these operating modes are given in *Appendix B*. The changeover operation from one mode to another takes 140 seconds. The hydraulic connections (switchover valves) are limited to covering only the HL or CL at a time.

4.1.2 BAC system for the INES lab

The acquisition and distribution of data plays a key role in MPC of complex building energy systems. The data acquisition system was integrated into the BAC framework (*cf. Chapter 3*) as shown in *Fig. 4-3*. The BAC consists of three levels: *field level, automation level, and management level*.
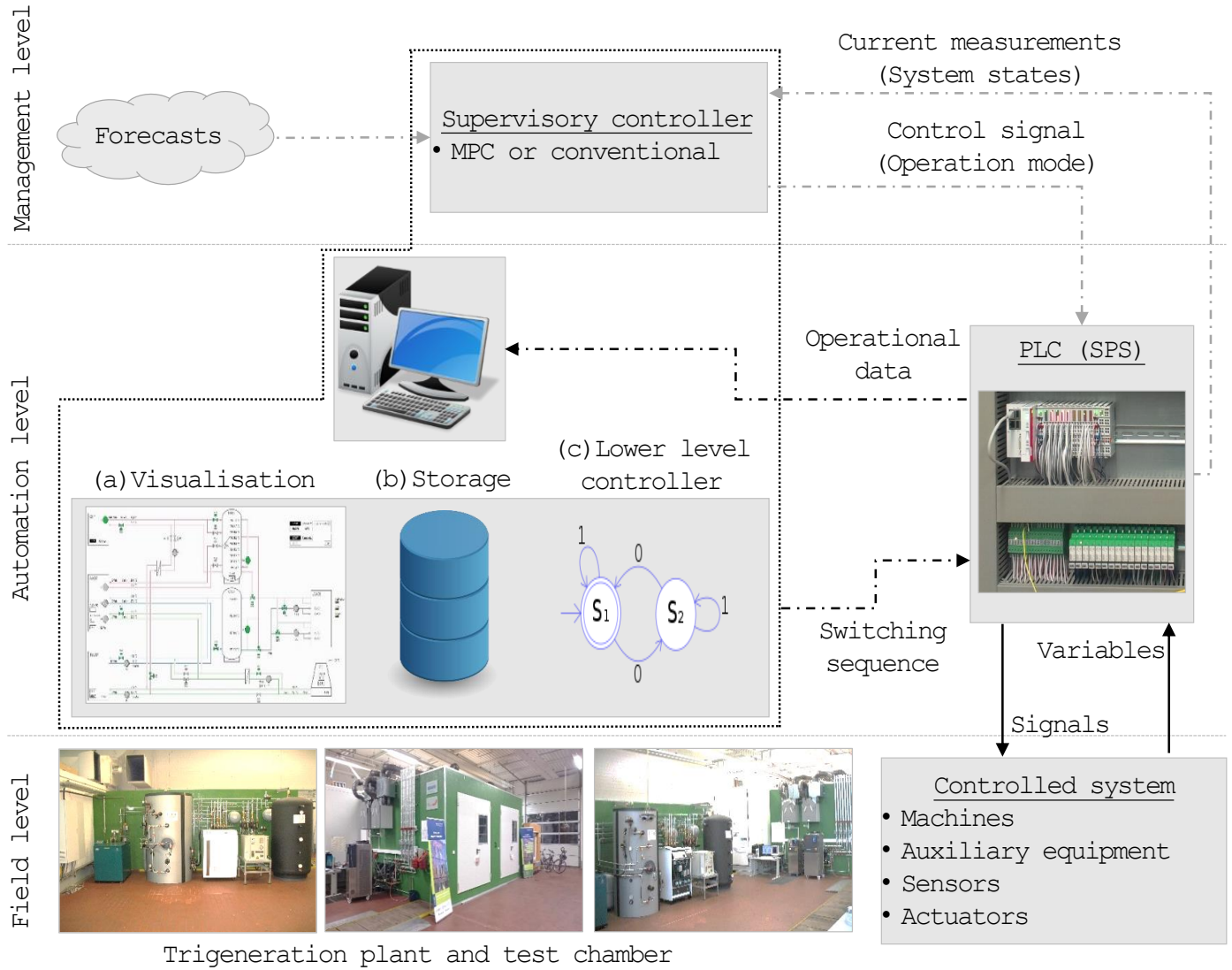
Fig. 4-3 BAC system for the INES trigeneration lab to run both conventional and optimal control. *Dash-dotted arrows represent only digital signals whereas solid arrows represent analogue and digital signals. Grey lines are part of the supervisory control loop and black lines are part of the monitoring loop. The dotted line box represents the workstation computer executing tasks of both management and automation level.*

With this framework, the plant can be operated using a supervisory controller based on either MPC or a conventional logic (for comparison purposes) from the management level. Here, the supervisory controller chooses from one of the seven possible operation modes (refer *Appendix B.3*) for the real-plant on the field level. It is programmed in the *Python* environment and sends its control signal, the operation mode, to PLC on the automation level. A lower-level controller programmed in the *LabVIEW®* environment uses the operation mode value in its sequential control logic to perform the state-based actions and transition tasks. This includes opening/closing valves, providing set-points to the components in a predetermined sequence, and a safety shut-down logic. A complete functional description of the lower-level controller is given in *Appendix B.4*. Sensor data from the field level is passed onto the PLC in the monitoring loop and is then used as system states on the management level or as operational data on the automation

level. For example, as shown in *Fig. 4-4*, the HMI on the automation level visualises current monitoring data, displays alarms, and also functions as an operator's panel.

The data flow represented by dash-dotted arrows use only digital signals and standards necessary for OPC, API, SQL communication, whereas, solid arrows use both digital and analogue signals e.g. M-Bus and resistance and voltage signals. Additionally, the grey lines are part of the supervisory control loop that repeats once every sampling instance and black lines are part of the monitoring loop that repeats continuously every 300 ms. The WS executing tasks on management and automation level is the same desktop computer represented as a box with dotted line and communicates as an OPC Client with the OPC server in the PLC. The MPC uses either internet-based services or local databases for collecting the necessary forecast values for energy prices, weather, and expected loads.

Table 4-2 lists the standard industrial instrumentation used for measuring the operational data.

The ambient temperature sensor (T_{amb}) was installed close to the OC on the west facing side of the building. A 2-lead wire resistance compensation equivalent to 2 K was made for the 15 m distance between the sensor and the ESC (IET Labs Inc., 2016).

The monitoring loop repeated every 300 ms but data was logged only after change-of-value using a logging dead-band of 2% of previous value. The logging resolution of temperature, volume flow, and power was 0.1 °C, 0.00 m³/h, and 0.1 kW respectively. The logged data was interpolated on a 60 seconds time interval to a CSV file for analysis.

Table 4-2 Instrumentation in INES trigeneration lab

Physical parameter	Units	Instrument	Accuracy
Ambient temperature	°C	PT-100 (2-lead circuit) with thermal radiation shield	± 0.1 K
Circuit temperatures (Water)	°C	PT-500 Class B (2-lead circuit)	± 0.30 + 0.0050|T_{meas}| K
Circuit temperatures (Glycol-water)	°C	PT-100 Class B (2-lead circuit)	± 0.30 + 0.0050|T_{meas}| K
Electricity consumption	kW$_{el}$	3-phase energy meters	Class 1 and 2 of IEC 1036
Fuel consumption	l/h	Mechanical roller counter with Reed-impulse generator	± 1%
Storage temperatures (9 in HTES and 4 in CTES)	°C	PT-1000 Class B (2-lead circuit)	± 0.3 K to ± 0.8 K
Thermal power	kW$_{th}$	Electronic heat meter	± 1.5%
Volume flow (Water)	m³/h	Ultrasonic flow meters	± $(2 + 0.02 \frac{\dot{v}_{max}}{\dot{v}_{meas}})$%
Volume flow (Glycol-water)	m³/h	Multi-jet turbine meters with Reed-impulse generator	± $(3 + 0.05 \frac{\dot{v}_{max}}{\dot{v}_{meas}})$%

IEC (International Electro-technical Commission)

4-Experimental Set-Up and Component Models
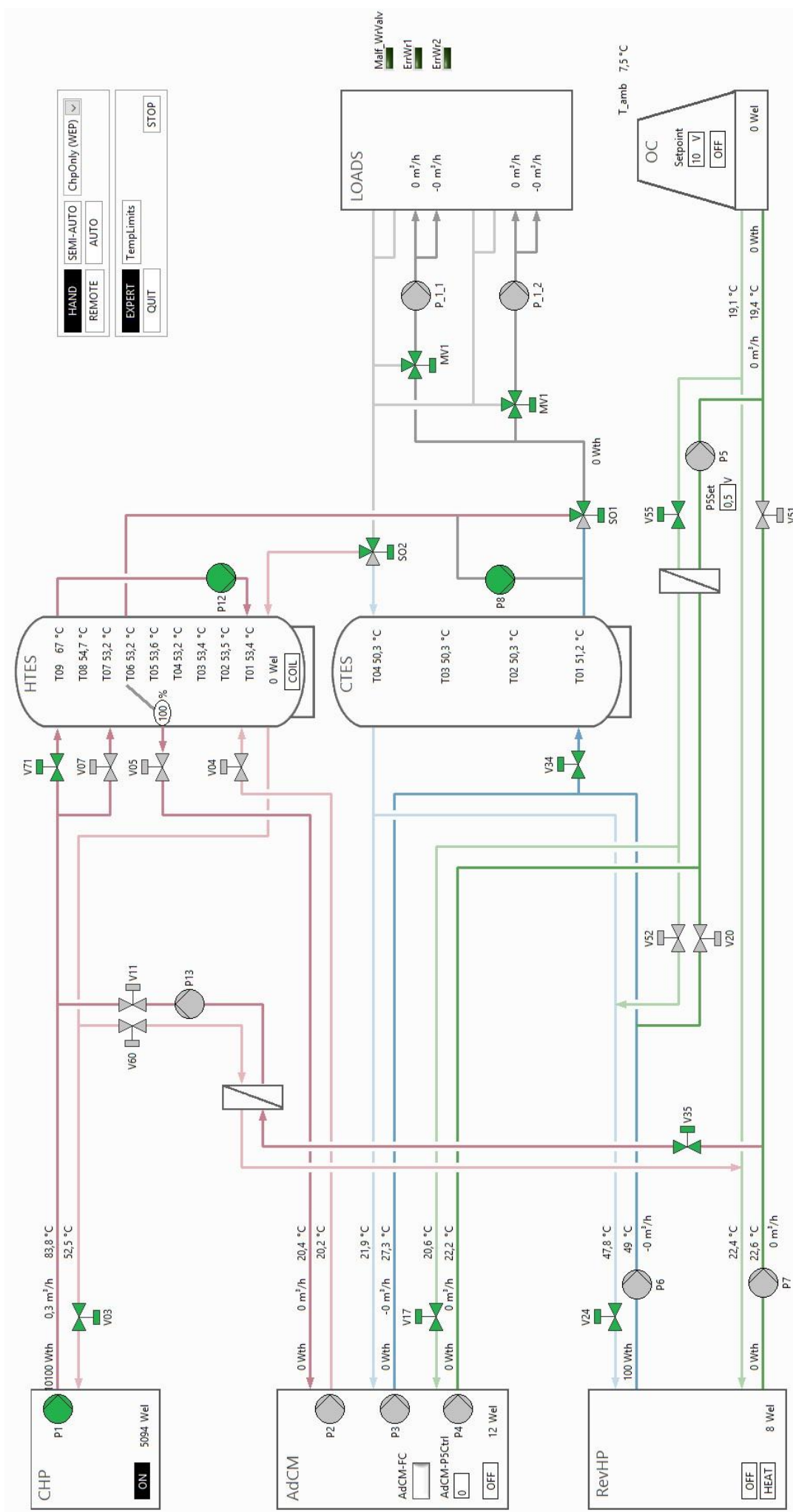
Fig. 4-4 Screenshot of the HMI displaying current values, active components, valves, and pumps in hand mode scenario. Sequential control logic of the lower-level controller is in Appendix B

4.1.3 Conventional control

A variation of the base load matching – following thermal load (BLM-FTL) strategy was chosen for conventional control (*cf. Chapter 2*). The CHP and AdC covered the base thermal loads and HP and CC covered the peak loads. The switching point was specified separately for the winter and summer tests. In summer, either the AdC's maximum cooling power (CHP's standard heating power multiplied by AdC's coefficient of performance) or 75% of maximum cooling load was used as the switching point. In winter, either the CHP's standard heating power or 75% of maximum heating load was used as the switching point.

The FTL operation was realised over a hysteresis dead-band control of the tank-temperatures. The switching occurs only when the lower and upper dead-band limits are reached or else the previous status of the component continues. *Table 4-3* and *Table 4-4* summarise the switching logic for the components using conventional control for summer and winter tests respectively. Further description of the control logic and tuning of these parameters is given in *Appendix* B.4.

Table 4-3 BLM-FTL for summer with switching point

Tank temperatures [°C]	Current cooling load [kW$_{th}$]	AdC	CC	CHP
$T_{CT1} \geq T_{CT1,max}$	$\leq$ Switching point	On	Off	–
$T_{CT1} \geq T_{CT1,max}$	$\geq$ Switching point	Off	On	–
$T_{CT4} \geq T_{CT4,min}$	–	Off	Off	–
$T_{HT6} \leq T_{HT6,min}$	–	–	–	On
$T_{HT1} \geq T_{HT1,CHP,max}$	–	–	–	Off

Table 4-4 BLM-FTL for winter with switching point

Tank temperatures [°C]	Current heating load [kW$_{th}$]	CHP	HP
$T_{HT6} \leq T_{HT6,min}$	$\leq$ Switching point	On	Off
$T_{HT6} \leq T_{HT6,min}$	$\geq$ Switching point	Off	On
$T_{HT1} \geq T_{HT1,CHP,max}$	–	Off	–
$T_{HT1} \geq T_{HT1,HP,max}$	–	–	Off

T_{CT1} (Temperature at bottom of CTES), $T_{CT1,max}$ (Set-point for maximum T_{CT1}), T_{CT4} (Temperature at top of CTES), $T_{CT4,min}$ (Set-point for minimum T_{CT4}), T_{HT1} (Temperature at bottom of HTES), $T_{HT1,CHP,max}$ (Set-point for maximum T_{HT1} during CHP operation), $T_{HT1,HP,max}$ (Set-point for maximum T_{HT1} during HP operation), T_{HT6} (Temperature corresponding to HL supply from HTES), $T_{HT6,min}$ (Set-point for minimum T_{HT6})

4.2   Load profiles for application scenarios

In industrial applications, forecast data for building loads is generated using past data or building simulation models (*cf. Chapter 3.3.1*).

In absence of a real building scenario or a detailed building simulation model, deterministic load forecasts available in the literature were used in this work. Additionally, a deterministic load forecast enabled a comparison of the conventional and optimal operation of the plant under almost-identical loads. Different studies were

identified that used 24-hour thermal and electric seasonal load profiles for techno-economic analysis or for optimisation of trigeneration systems. *Table 4-5* summarises a few examples and the complete list is in *Appendix C*.

Table 4-5 Examples of CCHP related studies with seasonal 24-hour electrical and thermal load profiles

Type of building	Aim of study	System specification	Peak summer loads	Peak winter loads	Peak transi-tion loads	Reference
Hospital-2	CCHP operation optimisation	•Area:83,745 m² •CHP:4.0 MW$_{el}$ •CC:4.2 MW$_{th}$ •Boiler:3.5 MW$_{th}$ •Absorption chiller:4 MW$_{th}$ •Average hourly demands	•EL ~ 2.0 MW$_{el}$ •HL ~ 2.0 MW$_{th}$ •CL ~ 4.0 MW$_{th}$	•EL ~ 2.0 MW$_{el}$ •HL ~ 3.5 MW$_{th}$ •CL ~ 0.0 MW$_{th}$	•EL ~ 2.0 MW$_{el}$ •HL ~ 2.3 MW$_{th}$ •CL ~ 0.0 MW$_{th}$	(Facci et al., 2014)
Hotel-1	Influence of part-load behaviour on optimal design and operation of CCHP	•Area:60,000 m² •CHP:1.46 MW$_{el}$ •Boiler:0.9 MW$_{th}$ •Absorption chiller:1 MW$_{th}$ •Hourly load of representative days	•EL ~ 2.1 MW$_{el}$ •HL ~ 1.3 MW$_{th}$ •CL ~ 4.7 MW$_{th}$	•EL ~ 1.7 MW$_{el}$ •HL ~ 4.7 MW$_{th}$ •CL ~ 0.6 MW$_{th}$	•EL ~ 1.8 MW$_{el}$ •HL ~ 1.0 MW$_{th}$ •CL ~ 1.7 MW$_{th}$	(Zhou et al., 2013)
Hotel-2	Influence of average and peak energy demands and uncertainty on CCHP performance	•Area:78,200 m² •CHP:2 MW$_{el}$ and 3.5 MW$_{th}$ •CC:2 MW$_{th}$ •Boiler:1.5 MW$_{th}$ •Absorption chiller:3 MW$_{th}$ •Average hourly demands	•EL ~ 1.9 MW$_{el}$ •HL ~ 1.8 MW$_{th}$ •CL ~ 3.7 MW$_{th}$	•EL ~ 1.5 MW$_{el}$ •HL ~ 4.2 MW$_{th}$ •CL ~ 0.6 MW$_{th}$	•EL ~ 1.5 MW$_{el}$ •HL ~ 2.4 MW$_{th}$ •CL ~ 1.4 MW$_{th}$	(Li et al., 2008)
Office building	Sensitivity analysis of trigneration primary energy savings ratio	•CHP:330 kW$_{el}$ •CC:560 kW$_{th}$ •Boiler:515 kW$_{th}$ •AdC:515 kW$_{th}$	•EL ~ 280 kW$_{el}$ •HL ~ 0.9 kW$_{th}$ •CL ~ 500 kW$_{th}$	•EL ~ 280 kW$_{el}$ •HL ~ 335 kW$_{th}$ •CL ~ 150 kW$_{th}$	•EL ~ 280 kW$_{el}$ •HL ~ 224 kW$_{th}$ •CL ~ 400 kW$_{th}$	(Chicco and Mancarella, 2007)
University campus-1	Micro-CCHP real-time operation optimisation	•Area: 279 m² •CHP: 15 kW$_{el}$ •AdC: 35 kW$_{th}$ •TRNSYS generated hourly demands	•EL ~ 9.8 kW$_{el}$ •HL ~ 0.0 kW$_{th}$ •CL ~ 12.9 kW$_{th}$	•EL ~ 6.2 kW$_{el}$ •HL ~ 11.2 kW$_{th}$ •CL ~ 0.0 kW$_{th}$	•EL ~ 9.8 kW$_{el}$ •HL ~ 3.0 kW$_{th}$ •CL ~ 2.9 kW$_{th}$	(Cho et al., 2009a)

The load profiles varied as per the system specifications and were normally for much larger systems compared to the INES trigeneration lab. A linear scaling by interpolation between minimum and maximum (user-defined) experimental loads was done against the minimum and maximum values in the literature profiles.

The choice of the minimum and maximum value for the load profiles was made with one of the following methods:

- peak load was a corresponding component's maximum capacity,
- peak load was 125% of a corresponding component's maximum capacity,
- peak load was maximum load that thermostats and TC can generate together,
- peak load was thermal power for a temperature difference of 5 K in the TC's circuit,
- minimum thermal load was fixed at 1.5 kW_{th} (arising from TC in steady state).

As an example, daily load profiles of a non-residential, non-industrial building during different seasons (Chicco and Mancarella, 2007) are scaled down in *Fig. 4-5*. The reference summer, winter, and transitional profiles with a maximum cooling load (CL) of 500 kW_{th}, heating load (HL) of 333 kW_{th} and electrical load (EL) of 280 kW_{el} are shown on the left-hand side of the figure. A downscaled load pattern for experiments in the INES lab is shown on the right-hand side. A maximum CL of 12 kW_{th} and a minimum CL of 1.5 kW_{th} is chosen for the scaling as cooling loads dominate the load profiles in non-residential buildings. The CL profile is interpolated using the ratio between peak reference value and peak INES value to match the profile from the literature. Accordingly, the EL profile is interpolated between 6.6 kW_{el} and 3 kW_{el}. The HL in winter is interpolated between 8.0 and 2.9 kW_{th}.

It is observed that the electrical load (EL) does not exhibit significant variations between seasons. The maximum EL is often two times the minimal load and this pattern is kept in the INES profiles too. A peak in EL is observed during morning hours (07:00 to 10:00), and is presumably due to activities in buildings like hospitals, hotels or office spaces, rather than due to the climate conditions.

On the other hand, the thermal profiles are more irregular between seasons and the CL peak in summer is greater than the HL peak in winter, which is typical in non-residential buildings. In the reference case, the HL ratio between maximum and average demand is 2.2 during summer, 1.3 during winter, and 1.4 during transition. This is often due to the higher average HL during winter and transition seasons and the lower average HL in summer for hot water requirements or other thermally driven processes. However, in the INES profile no HL is generated during summer due to the technical limitations of the lab (*cf. Section 4.1.1*). A heating load is generated in transition season for simulation purposes only.

The CL ratio between maximum and average demand in the reference case is 2.7 during summer, 6.5 during winter, and 4.0 during transition. It is most likely due to the higher average CL during summer season, while in other seasons non-residential buildings may have a CL only at a particular time of the day for activities requiring

indoor-climate control. In the INES profile, no CL is generated during winter for experiments and CL could be simulated in transition season.
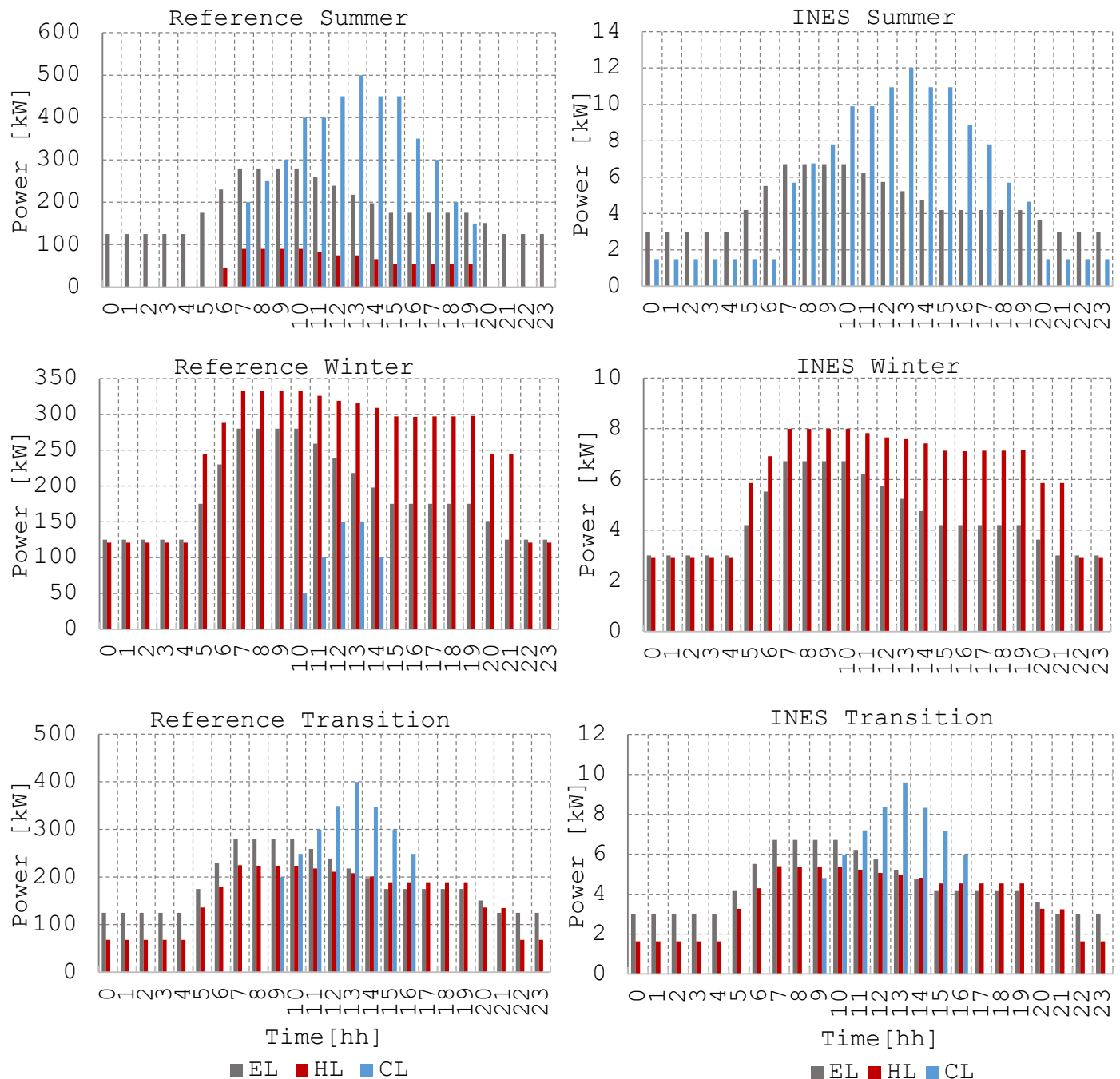
Fig. 4-5 Reference load profiles and scaled down version for INES experiments

Depending on the application scenario the loads decrease or increase on a weekend and this was achieved by a simplistic approach of multiplying the weekday pattern with a scaling factor (Tichi et al., 2010). For instance, a deterministic profile for an office building over an entire week in summer starting from Wednesday could be synthesised as shown in *Fig. 4-6*. The cooling load and electrical load is higher during office hours (07:00 to 19:00) especially on a weekday and significantly reduces over the weekend. The load is 0.5 times the weekday load on a Saturday and 0.45 times the weekday load on a Sunday.
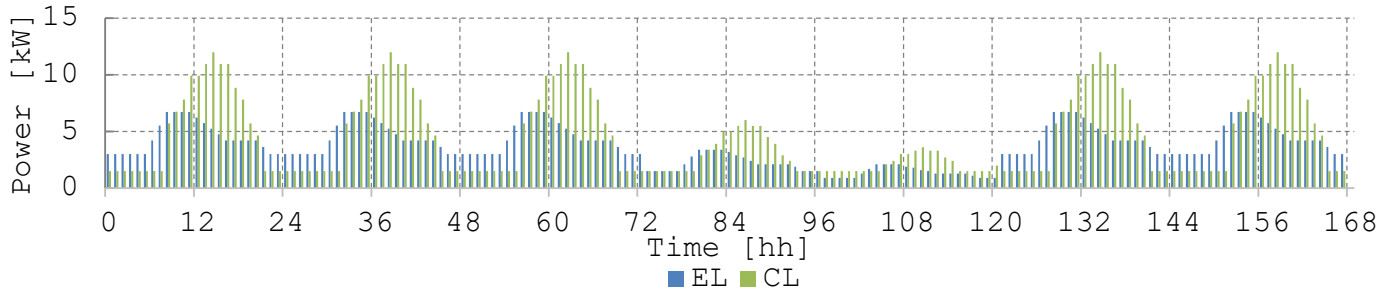
Fig. 4-6 Office building load profile for a summer week starting on a Wednesday midnight

Further examples for load profiles used in the experiments are given in *Appendix C.*

4.3 Energy prices

Market prices of the input variables for the economic optimisation problem, namely electricity and fuel prices or rates were forecasted using different methods described in the following subsections.

4.3.1 Electricity-price forecast

Similar to the load profiles, deterministic electricity buying and selling rates or prices ($r_{el,buy}$ and $r_{el,sell}$) were used in this work. Three different price signals were synthesised:

Based on two-price tariff structure of the local grid operator (E-Werk Mittelbaden AG, 2019): A higher daytime price or rate of 0.287 €/kWh$_{el}$ from 07:00 to 22:00 and a lower night-time rate of 0.222 €/kWh$_{el}$ from 22:00 to 07:00 was set for buying electricity $r_{el,buy,EWERK}$. The selling rate $r_{el,sell,EWERK}$ was taken as a constant value of 0.151 €/kWh$_{el}$ considering a base load price of 0.063 €/kWh$_{el}$, 0.008 €/kWh$_{el}$ avoided grid costs, and a micro-CHP bonus of 0.08 €/kWh$_{el}$ (BMWi, 2016; Schicktanz et al., 2011). A weekly price profile is shown in *Fig. 4-7*.

Based on linear interpolation of EPEX SPOT SE day-ahead auction prices (EPEX SPOT SE, 2008): The day-ahead auction price is based on an aggregated demand-supply curve of a broad geographical region. It is assumed for sake of brevity that this price captures an ideal energy market with all complex interactions in the energy grid including that of variable renewable energies and local grid costs. The hourly price in €/MWh$_{el}$ for the big energy market was reduced to a signal in €/kWh$_{el}$ for the INES experiments. The EPEX buying rate $r_{el,buy,EPEX}$ and selling rate $r_{el,sell,EPEX}$ were then generated by linearly interpolating between the maximum and minimum day-ahead auction price against the highest and lowest grid operator prices. As shown in *Fig. 4-7*, the $r_{el,sell,EPEX}$ follows the profile of $r_{el,buy,EPEX}$ due to the demand-supply concept.

Based on linear interpolation of price signal from the INES micro-grid (Sawant et al., 2019): The optimisation tool of the INES micro-grid (IMG) generates a price signal considering the local photovoltaic generation, the consumption-related costs of the CHP and its peak-shaving operation (Dongol et al., 2018). This price signal was also

interpolated like EPEX prices to generate a buying rate $r_{el,buy,IMG}$ and selling rate $r_{el,sell,IMG}$. As shown in *Fig. 4-7*, the signal has a higher buying to selling ratio and does not follow the EPEX pattern but captures the IMG operation status including the local PV generation and load cycles.
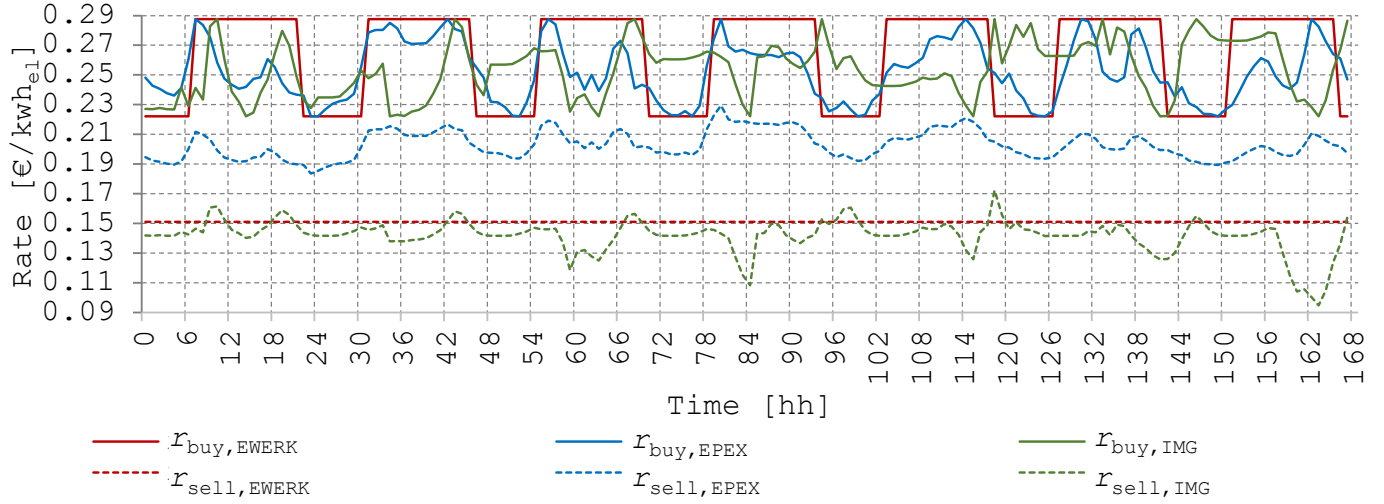
Fig. 4-7 Examples of three different electricity buying and selling rates synthesised for experiments

4.3.2 Fuel-price forecast

The price or rate of fuel r_{fuel} was set at 0.72 €/m^3 or 0.06 €/kWh using data from the German market for a gas based CHP (Bundesnetzagentur, 2019). This was input as a constant parameter in the MPC formulation but could be extended as a time-varying parameter (like electricity prices) for industrial applications in future.

4.4 Control-oriented component models

Control-oriented models for the components of the system are the corner stone of an MPC problem and should have characteristics such as an accuracy-complexity balance and continuous differentiability (*cf. Chapter 3.3.1*). To identify models that satisfy these characteristics a qualitative examination of the modelling approaches available in the literature (*cf. Chapter 2.5*) was done. Individual component models were then developed using the grey-box methodology and simulation results of the combined system for different operating modes were compared against measured data.

4.4.1 Qualitative analysis of existing models

Recurring approaches were identified in the literature and only one example per approach was selected. Secondly, only models focussing on application in optimisation of trigeneration systems were selected. The subsequent list of models was then thoroughly analysed for desired characteristics and *Table 4-6* summarises the results.

It is observed that models used in optimal scheduling mostly consider only static process variables like electrical power or cooling capacities and do not consider dynamic

states like storage temperatures or hydraulic circuit temperatures. On the other hand, existing models that satisfy these requirements are either physics-based models with a component level simulation focus making them very complex, or have rule-based controllers making them not continuously differentiable.

Nevertheless, the qualitative analysis revealed important modelling features that are adapted in this work and are described below:

AdC: Wu et al. calculate the coefficient of performance as a second degree function of the part-load ratio (Wu et al., 2012). However, the regression coefficients are technically infeasible to identify as they require significant amount of operational data of the machine under part-load and make the approach impractical for model parameterisation. A modification of this approach is adapted in this work with the curve fits using product data from manufacturer's data sheets for a more practical parameterisation.

CHP: In Seifert's model for a CHP the internal control logic for the cooling pump influencing the mass flow of water is appropriately simulated with a second degree curve fit of the water inlet temperature and electrical power of CHP (Seifert, 2013). However, the dynamic behaviour of the thermal power output is simulated with a mass and energy balance over the individual components like heat exchanger and engine block of the CHP and make the model very complex for application in a system-level MPC. The approach to simulate the internal control logic is adapted from Seifert's work while simulation of the thermal output is adapted from a simpler step-response based model (Hidalgo Rodriguez et al., 2012).

RHP: The models developed by Salvalai and Jin et al. use product data for equation-fitting to represent part-load behaviour of reversible heat pumps and are adapted in this work (Jin and Spitler, 2002; Salvalai, 2012).

HTES & CTES: U.Eicker presented a 1-D stratified tank model using the *Fourier's equation* (Eicker, 2006). Although accurate and of medium complexity the model is not continuously differentiable due to the usage of "If-Else" clauses. The approach is adapted while modifying the clauses to avoid their discontinuities.

Deriving from the above qualitative analysis and findings in *Chapter 2* and *Chapter 3,* the grey-box methodology was chosen to model the system. It facilitates the adaption of model features identified in the qualitative analysis and applying engineering know-how of the specific system to develop control-oriented component models. Grey-box models are not only of sufficient accuracy and simplicity, but are also considered suitable for application in practice oriented economic-MPC (Sohlberg, 2003). Accordingly, the models are evaluated in *Section 4.11* for their ability to:

- simulate the system response to input variables (component switches),
- predict fuel and electricity consumption with sufficient accuracy,
- simulate process variables that are usually measured in a plant e.g. tank temperatures.

4.4.2 Application of grey-box modelling methodology

For the grey-box modelling approach, regression analysis (Fumo and Rafe Biswas, 2015) and step-response analysis (Diehl, 2019) were used for fitting apriori data and determining the dynamics or part-load properties of the components. Both these methods make it possible to choose data sets that are either readily available in the manufacturer's catalogues or can be collected during commissioning of the equipment.

Regression analysis: Regression analysis is a method to find a polynomial relationship among response or dependent variables and explanatory or independent variables. A regression is linear when the polynomial is linear in the coefficients. However, the regression could be univariate if only one independent variable exists as in (4.1) or multivariate if multiple independent variables are considered as in (4.2). The polynomial itself could be a first degree or a higher degree polynomial depending on the characteristics of the data that is being fit.

$$y^* = \beta_0 + \beta_1 x_1 + \beta_2 x_1{}^2 \tag{4.1}$$

$$y^* = \beta_0 + \beta_1 x_1 + \beta_2 x_2 + \beta_3 x_1 x_2 + \beta_4 x_1{}^2 + \beta_5 x_2{}^2 \tag{4.2}$$

where,

y^* – Dependent variable (predicted value in models)

$\beta_1, \beta_2 \dots \beta_5$ – Coefficients of regression

x_1, x_2 – Independent variables

$y, \beta, x \in \mathbb{R}$

A linear regression was done to minimise a sum of normalised squared error (SNSE) problem as shown in (4.3), subject to, the polynomials (4.1) or (4.2) for fitting apriori data and estimating the coefficients of regression.

$$\min_{\beta}(J_{\text{SNSE}} = \sum_{i=1}^{N} \left(\frac{y_i - y_i^*}{y_i}\right)^2) \tag{4.3}$$

where,

J_{SNSE} – Cost function for the SNSE problem

y_i – i[th] measured value

y_i^* – i[th] predicted value

The generalised reduced gradient search algorithm (via *Microsoft Excel's Data Solver*® Add-On) was applied for solving the above optimisation problem(Lasdon et al., 1976).

Step-response analysis: The dynamic response of a controlled system can be described via the manipulated variable step-response or the interference variable step-response. A manipulated variable step-response is more common in practice and is characterised by the time-constant of controlled system T_s and the transfer coefficient or gain K_s. In building technologies, very often the behaviour of a first order lag or system with one

storage element (PT-1 element) is observed. The input/output differential equation for this system is given in (4.4).

$$T_s \, \dot{y}_i^* + y_i^* = K_s u \qquad\qquad (4.4)$$

where,

y_i^* – Controlled variable or system output (predicted value in models)

u – Manipulated variable (component switch)

K_s – Gain i.e. proportion of change in y_i^* to change in u

T_s – Time-constant i.e. time taken for 63.2% of total y_i^* change to be achieved

Simulation in Modelica: Different software such as *MATLAB, R*, and *Modelica* were preliminarily evaluated for simulating the system. The signal-oriented (causal) approach in MATLAB/Simulink was deemed unsuitable for a system-level simulation, which typically involves solution of many implicit equations. R is significantly suited for statistical analysis but was deemed unsuitable to develop energy system models due to lack of appropriate libraries and complex structure. Another critical factor for choosing the modelling tool was to use an open-source software.

The Modelica language was chosen for developing and testing the models because of various reasons:

- it allows declaration of equations (algebraic or differential), facilitating modelling of real-world physical objects directly in the language (Schicktanz and Núñez, 2009),

- the *OpenModelica* compiler facilitates implicit modelling and generalisation of the equations leading to simpler models and simulation that is more efficient,

- Modelica is an object-oriented language with a general class concept, which allows for reusability, interoperability, and hierarchical structuring that is relevant for physically-oriented energy systems' simulation(Kofránek et al., 2008),

- it allows for cross-domain interaction and user-friendly plotting and analysis,

- the models can be evaluated using well-established compilers and integration methods like *Dassl* or *Runge-Kutta* in OpenModelica and then exported to the Python environment.

Table 4-6 Qualitative analysis of selected literature on trigeneration system models

Reference (years ascending)	Component dynamics	Part-load behaviour / internal control logic	Practical parameterisation capabilities	Adaptability to component design	Complexity	Accuracy	Continuous differentiability
AdC:							
(Li and Wu, 2009)	Yes	Yes / Yes	No	–	High	High	No
(Schicktanz and Núñez, 2009)	Yes	Yes / Yes	No	–	High	High	Yes
(Gräber et al., 2011)	Yes	Yes / Yes	No	–	High	High	Yes
(Wu et al., 2012)	No	Yes / No	No	–	Low	Low	Yes
(Zhao et al., 2015)	No	No / No	No	–	Low	Low	Yes
CHP:							
(Ren et al., 2008)	No	Yes / No	No	–	Medium	Low	Yes
(Hidalgo Rodriguez et al., 2012)	Yes	No / No	Yes	–	Low	Medium	Yes
(Bracco et al., 2013)	No	Yes / No	No	–	Medium	Low	Yes
(Seifert, 2013)	Yes	Yes / Yes	Yes	–	High	High	Yes
(Li et al., 2014)	No	Yes / No	No	–	Low	Low	Yes
RHP:							
(Jin and Spitler, 2002)	No	Yes / –	Yes	–	High	High	Yes
(Ma et al., 2009)	No	Yes / –	Yes	–	Medium	High	Yes
(Wetter, 2009)	Yes	Yes / –	No	–	High	High	Yes
(Salvalai, 2012)	No	Yes / –	Yes	–	Medium	High	Yes
(Facci et al., 2014)	No	Yes / –	No	–	Medium	High	Yes
HTES & CTES:							
(Eicker, 2006)	Yes	–	Yes	No	Medium	High	No
(Henze et al., 2008)	Yes	–	Yes	No	Low	Low	Yes
(Ma et al., 2009)	Yes	–	Yes	No	Low	Low	No
(Wetter, 2009)	Yes	–	Yes	Yes	Medium	High	No
(Chandan et al., 2012)	Yes	–	Yes	No	High	Medium	Yes

Dynamics: If the models represent dynamics of the system using ODE or DAE? Part-load/internal controller: If model represents part-load behaviour through physics-based relations or curve fits / If any internal controller for pumps and valves is represented? Practical parameterisation: Data for curve fits is practically available? Complexity: High (number of states > 3 or number of unique parameters > 10), Medium (number of states > 5), Low (number of states > 1 or number of unique parameters ≤ 1 and number of unique parameters < 3). Accuracy: High (black-box model or visual and quantitative validation), Medium (visual validation or application in simulation), Low (no validation and application in MILP)

Input / output equations for the individual components were directly programmed in the *OpenModelica Connection Editor* using elemental libraries like SI Units and connectors as shown in *Fig. 4-8* (Asghar and Tariq, 2010; Fritzson, 2014).

Nomenclature from process engineering was used, wherein flows leaving a component were designated *feed-line* (subscript "f"), and flows entering a component were designated *return-line* (subscript "r"). For the AdC with multiple temperature circuits, *high temperature circuit* is denoted with an extension "H" in the subscript, *medium temperature circuit* with "M", and *low temperature circuit* with "L". Similarly, for the RHP the *condenser circuit* is denoted with a subscript "c" and the *evaporator circuit* with "e".

General assumptions and formulations: Founded on engineering know-how and apriori knowledge of the system, the following general assumptions for the modelling of this complex energy plant were made:

- heat losses and pressure losses through pipes and components are negligible for one time-step (typically 15 minutes) of MPC for thermal systems,
- specific heat capacities and densities of all fluids are constant,
- simulation of the delay due to changeover operation (140 seconds) from one mode to another is insignificant due to the inclusion of minimum runtime constraints, longer sampling times, and slow dynamics of thermal systems (described in *Chapter 6*),
- ideal conservation of mass,
- at full load real power is the nominal power of the equipment,
- internal controllers of components are ideal and reliable,
- volume flows in the circuits are constant (other than for CHP and loads) and maintained at nominal flows,
- accurate forecast of ambient temperature and building thermal loads are available over the entire simulation horizon.

Throughout the simulations, the mass flow $\dot{m}$ (kg/h) induced in a machine's hydraulic circuit during operation was computed depending on the machine's control input as follows (4.5):

$$\dot{m} = S\dot{v}\rho \tag{4.5}$$

Where, S is the on-off switch for the corresponding machine and a binary control variable in the optimisation problem, $\dot{v}$ is the volume flow (m^3/h) and ρ is the density of the fluid (kg/m^3).

This formulation has two advantages; firstly, when the machines are switched off, then no mass flow occurs between components and storage tanks ensuring that storage-temperatures are not affected. Secondly, the decision variables occur a reduced number of times in the MPC formulation itself since they are avoided in the mass and energy balance equations for the individual models.
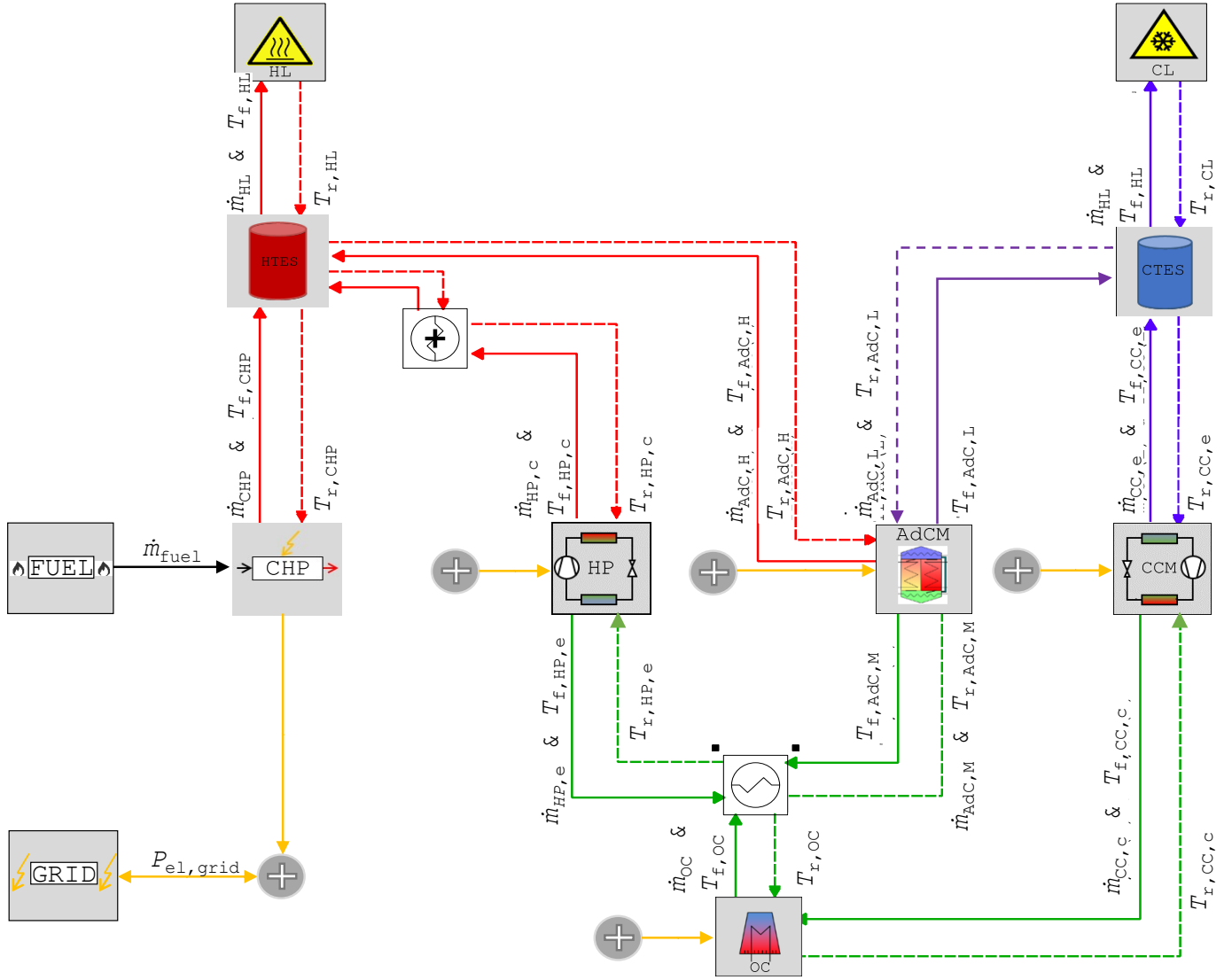
Fig. 4-8 Model of the INES trigeneration system in OpenModelica

4.5 Adsorption chiller (AdC)

The silica-gel water AdC is of type "eCoo" by *Fahrenheit GmbH* and operates on the principle of sorption of silica-gel while the cooling effect is produced by evaporation of water as the refrigerant (Fahrenheit GmbH, 2014). The functional construction of the machine is divided into three circuits as depicted in *Fig. 4-9*:

- Circuit 1: High temperature (driving circuit in red),
- Circuit 2: Medium temperature (recooling circuit in green),
- Circuit 3: Low temperature (chilled water circuit in blue).

Also shown here are the recooler (OC in this case) and a glycol-water system separation (HX in this case) integrated in the recooling circuit.

To produce continuous cooling effectively the machine has two adsorbing chambers (one in each module) that undergo the adsorption/desorption and heat recovery phases. Its operation is achieved through internal switching of 3-way-mixing valves and pumps

using complicated control algorithms leading to the distinctive cyclic behaviour of the three circuit temperatures, as reported in the literature (Wu and Wang, 2006).
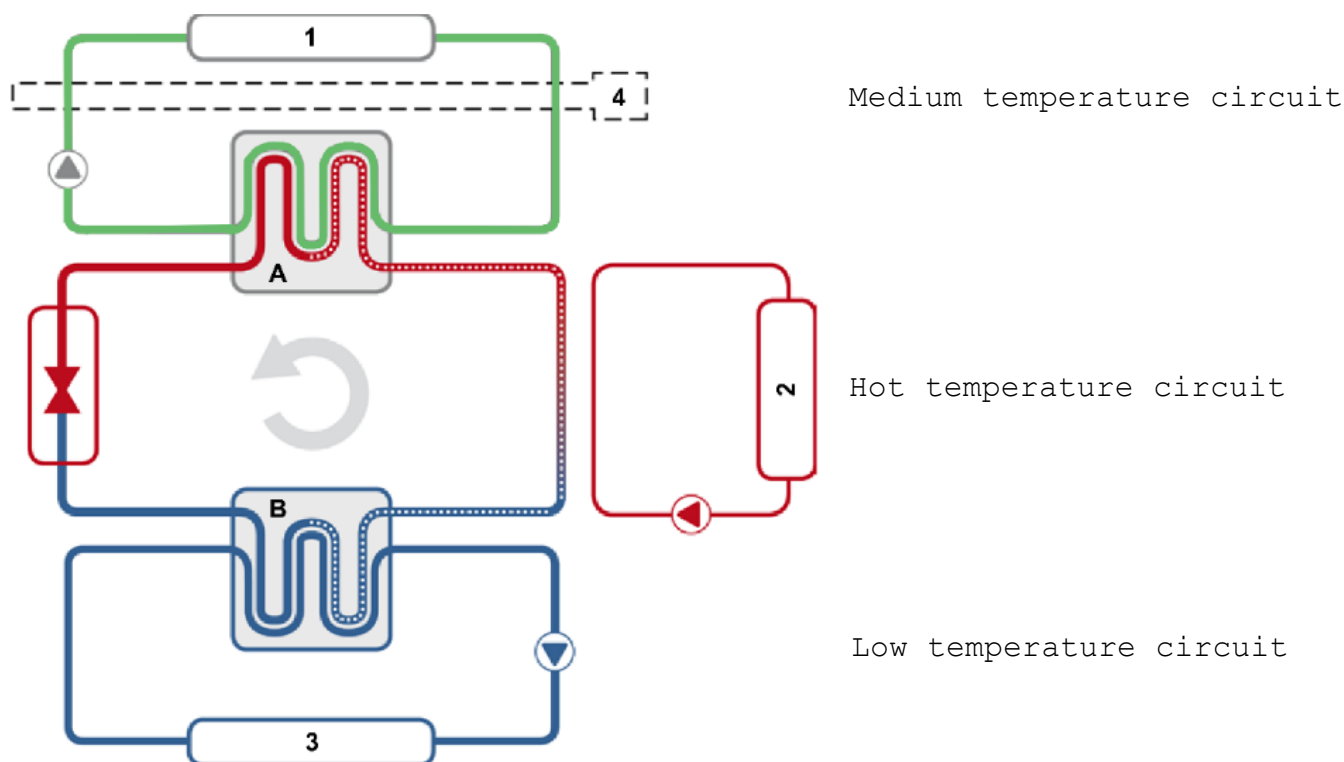
Fig. 4-9 Functional construction of a single adsorption module (Fahrenheit GmbH, 2014). A (Condenser), B (Evaporator), 1(Recooler, here OC), 2 (Driving heat source, here CHP), 3 (Cooling load), 4 (Glycol-water system separation, here HX).

The sequence of events for one entire cycle can be divided into four phases. *Fig. 4-10* shows the first phase and other phases are explained using the same figure.
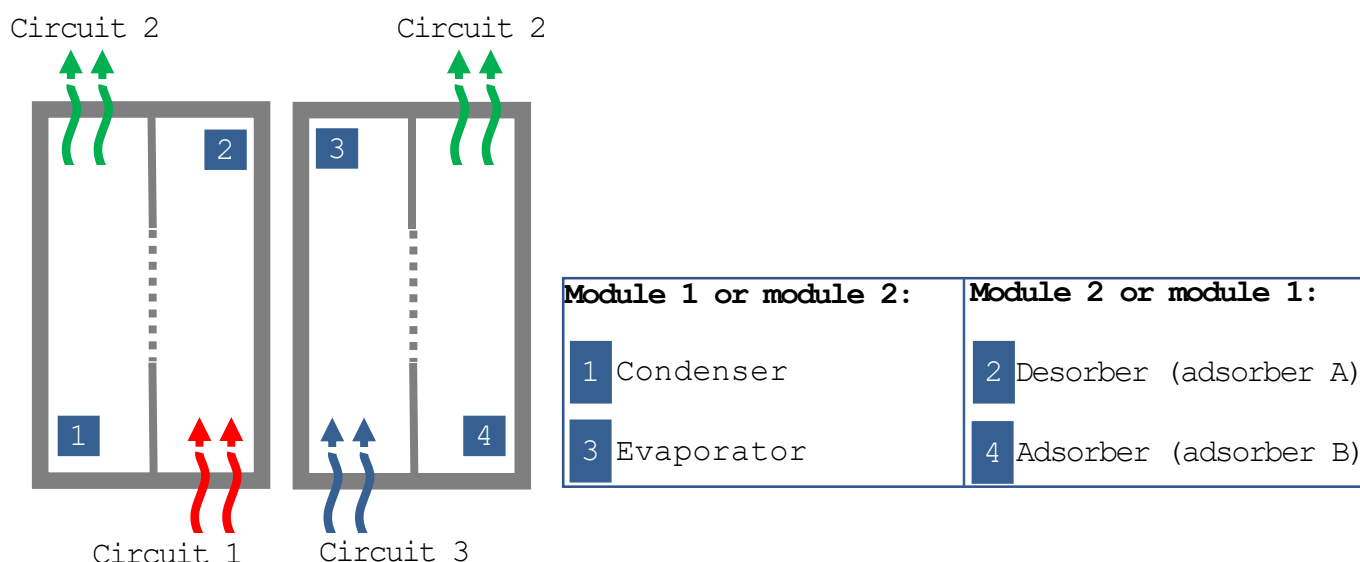
Fig. 4-10 Sequence of events in the processing chambers of the two modules during Phase 1 (Fahrenheit GmbH, 2014)

The operational sequence for a single module consists of the following 4 phases:

Phase 1 (Desorption/Adsorption): Hot water from the source in Circuit 1 enters the completely charged adsorber A or desorber (2). This desorbs or expels the adsorbed refrigerant from the inner surface of the silica-gel into the condenser (1). Here it is condensed to liquid state by removing the heat over Circuit 2 to the environment.

Concurrently, heat from the CL evaporates the refrigerant in the evaporator (3) that is led to adsorber B (4) via Circuit 3. As these vapours are adsorbed the exothermic process releases heat which is also removed together with the heat of liquefaction via Circuit 2.

Phase 2 (Heat recovery): Instantly after phase 1, the 3-way-mixing valves are positioned such that recooling water flows into the previously desorbed adsorber A. As the recooling water increases in temperature it is not immediately pumped into Circuit 2 but continues to be pumped in Circuit 1. On the other hand, the return-line of the now charged adsorber B is routed to the Circuit 2.

This phase ends when a specific temperature difference is achieved between the return-lines of the two adsorbers benefitting the flow of refrigerant vapours. This circulation of the cooling and heating medium between the hot and cold adsorber helps recover the sensible heat of the hot adsorber and increasing the thermal efficiency of the system (Wang et al., 2010).

Phase 3 (Adsorption/Desorption): Adsorber A now begins to adsorb refrigerant vapour while hot water begins to flow through the charged adsorber B for desorbing it. The process continues as in phase 1.

Phase 4 (Heat recovery): Immediately after phase 3, the 3-way-mixing valves are repositioned such that the recooling water now enters the adsorber B which was desorbed in phase 3. The process continues as in phase 2.

4.5.1 AdC functional tests

Step-responses, hydraulic checks, and commissioning tests were used to establish the AdC's operational parameters and interpret the complex physical interactions from an engineering perspective.

As an example, results from a test started with a homogeneous initial temperature of 82 °C in the HTES, 17 °C in the CTES, no charging (discharging) of HTES (CTES), and using a 7-minute average to filter the AdC's periodic behaviour are shown in *Fig. 4-11* and *Fig. 4-12*.

Fig. 4-11 (a) indicates four temperatures in the CTES (T_{CT1} to T_{CT4} with T_{CT1} at the bottom) and nine temperatures in the HTES (T_{HT1} to T_{HT9} with T_{HT1} at the bottom). The feed-line and return-line temperatures in the high temperature ($T_{f,AdC,H}$ & $T_{r,AdC,H}$) and low temperature circuits ($T_{f,AdC,L}$ & $T_{r,AdC,L}$) are also represented. The AdC is switched on at Time $=$ 10 min.

Hydraulic connection of AdC to the tanks and their thermal stratification: $T_{f,AdC,H}$ enters the bottom of the HTES while $T_{r,AdC,H}$ is extracted from a layer between T_{HT8} and T_{HT7}[1]. The characteristic thermal stratification behaviour is observed in the two tanks as they cool down with lower layers cooling faster and a shifting thermocline. A big thermocline is formed between T_{HT7} and T_{HT9} after 150 minutes since T_{HT9} is not used by the AdC. The stratification in CTES is not large because the temperature difference in the low-temperature circuit is smaller.

Dampening of AdC's cyclic behaviour in the tanks: Although an average is used for the $T_{f,AdC,H}$, cyclic behaviour of the AdC is still noticed and is dampened due to the buffer effect of the mass of water in that layer. The dampening effect is evident with the lower change-of-value in the corresponding tank temperature T_{HT1}. Similarly, cyclic behaviour in the feed-line of the low temperature circuit $T_{f,AdC,L}$ is dampened in the corresponding CTES layer T_{CT1}. This information is of high relevance for modelling the component and is significantly handled later in this section.

Shut-down phase has negligible effect on tank temperatures: The machine is switched off at Time = 236 min, following which the circuit temperatures change due to the machine's shut-down phase but have a negligible effect on the tank temperatures.

The 7-minute averages of thermal powers in the three circuits are shown in *Fig. 4-11 (b)*.

No significant cooling in start-up phase: Subsequent to switching the AdC on at Time = 10 min, the start-up phase of the machine runs until approx. Time = 22 min. In these 12 minutes the driving power in the high temperature circuit $P_{th,AdC,H}$, shown in red, is very high in comparison to the cooling power $P_{th,AdC,L}$, shown in blue.

Performance at nominal capacities: Once the normal operation starts from Time = 23 min then the $P_{th,AdC,L}$ is closer to the nominal capacities of the machine. Up to Time = 105 min the conditions for $T_{r,AdC,H}$ and $T_{r,AdC,L}$ are favourable and the $P_{th,AdC,L}$ is highest. $P_{th,AdC,H}$ is approximately twice of $P_{th,AdC,L}$ indicating a coefficient of performance (COP) in the region specified by manufacturer.

---

[1] A retrofit construction in the HTES in Autumn 2017 now facilitates extraction of hot water between T_{HT9} and T_{HT8}
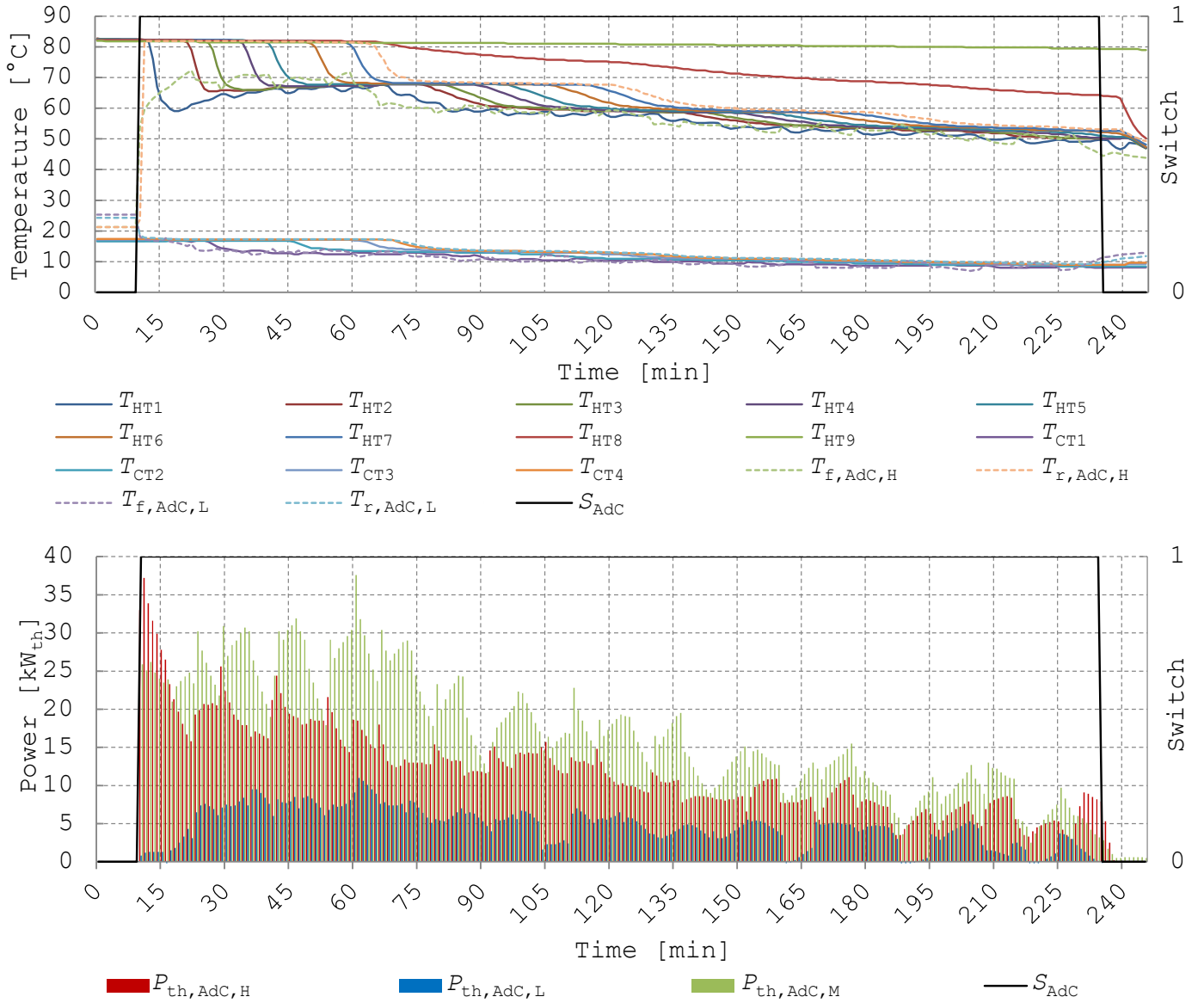
Fig. 4-11 (a) AdC's circuit temperatures with corresponding HTES and CTES temperatures (b) Thermal powers in the three AdC circuits. Data from a test on 12th May 2017 starting at 10:51 (Time = 0 min)

Longer cycle times during part-load operation: As the test proceeds the HTES and CTES are cooled down and unfavourable conditions arise. The $P_{th,AdC,H}$ and COP_{AdC} reduces and to compensate loss of capacity, the cycle time and switching time between cycles are elongated by the internal controller of the machine. Under favourable conditions almost 2 cycles are completed in 15 minutes, for instance, the three peaks between Time = 45 min and 75 min. Under unfavourable conditions only 1 cycle is completed every 15 minutes, e.g. the operation between Time = 165 to 180 min.

Heat extraction to environment through OC: The combined heat of liquefaction and exothermic adsorption is extracted to the environment through the OC over the medium temperature circuit and is approximately equal to the sum of energies flowing in the high temperature and low temperature circuits. This information is further investigated at end of this section.

No cooling in shut-down phase: The shut-down phase or end-phase lasting ca. 3 minutes after the machine is switched off at Time $= 236$ min is also shown. The $P_{\text{th,AdC,H}}$ and $P_{\text{th,AdC,M}}$ are active for finally desorbing both modules while no cooling is produced.
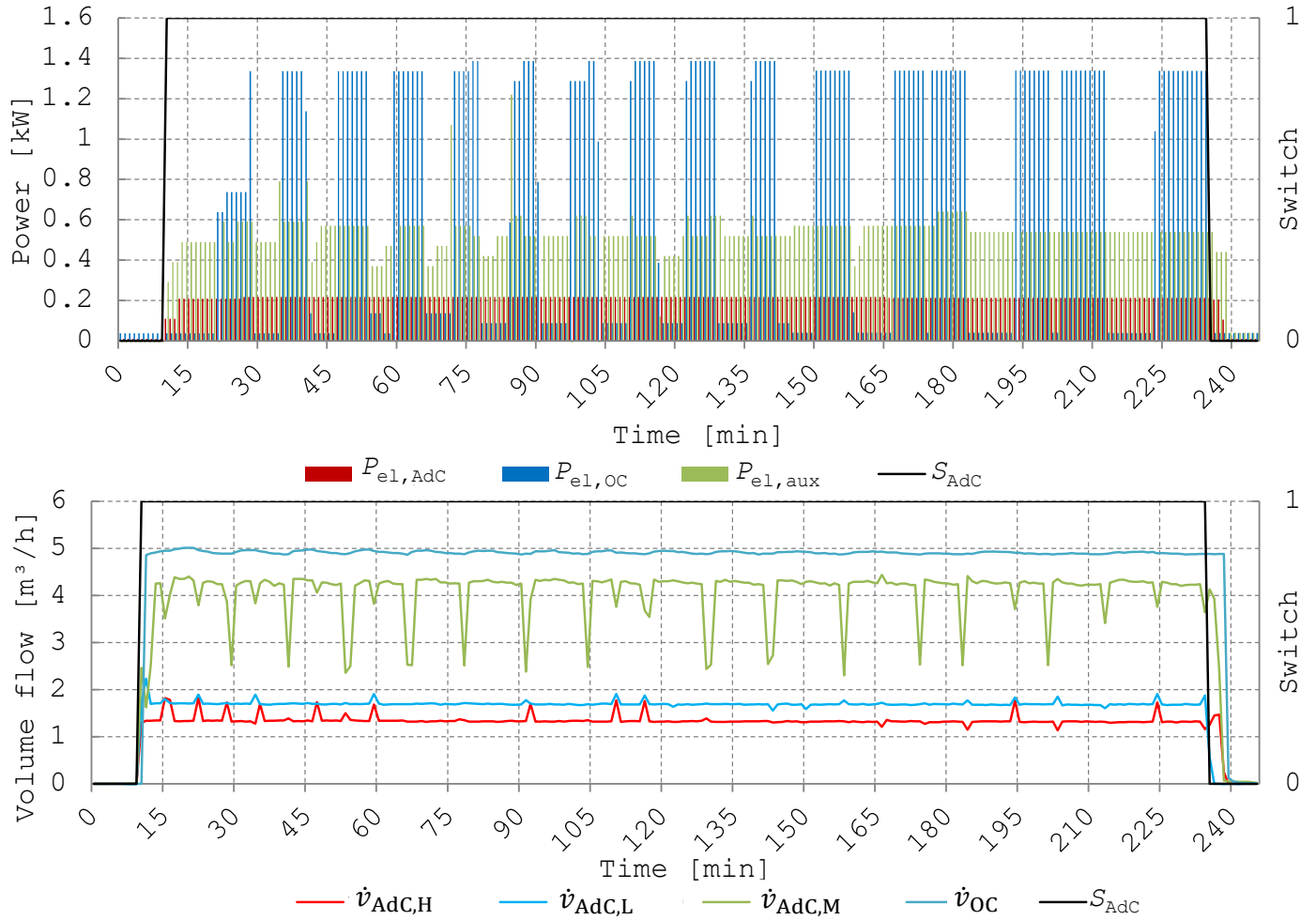
Fig. 4-12 (a) Electrical power consumption during AdC operation (b) Volume flows during AdC operation. Data from a test on 12th May 2017 starting at 10:51 (Time = 0 min)

The electrical consumption and volume flows during the AdC's operation are recorded in *Fig. 4-12.*

Constant electrical consumption and volume flows: The low electrical consumption of the AdC is seen in *Fig. 4-12 (a)* with a constant $P_{\text{el,AdC}}$ of 0.2 kW_{el} coming mostly from the three internal pumps generating volume flows $\dot{v}_{\text{AdC,L}} = 1.7 \text{ m}^3/\text{h}$, $\dot{v}_{\text{AdC,M}} = 4.3 \text{ m}^3/\text{h}$, and $\dot{v}_{\text{AdC,H}} = 1.3 \text{ m}^3/\text{h}$ as shown in *Fig. 4-12 (b)*. These values are close to their nominal values given in *Table 4-1* and are mostly constant during plant operation. Fluctuations occur shortly during a phase change controlled internally by the embedded AdC controller.

Auxiliary consumption: The embedded controller also regulates the speed of the OC, which then consumes electricity $P_{\text{el,OC}}$ between 1.38 kW_{el} and 0.04 kW_{el}[1]. The system separation pump produces a volume flow $\dot{v}_{\text{OC}} = 4.9 \text{ m}^3/\text{h}$ in the OC circuit. The auxiliary

---

[1] The new recooler installed in Summer 2018 consumes a maximum $P_{\text{el,OC,max}}$ of 0.9 kW_{el} and minimum of 0.1 kW_{el}

consumption of the plant, $P_{el,aux}$ including the pump in the system separation unit is approx. 0.5 kW$_{el}$ during AdC operation.

Active volume flows in end-phase: After the AdC is switched off, $\dot{v}_{AdC,L}$ is immediately 0 m^3/h but $\dot{v}_{AdC,H}$, $\dot{v}_{AdC,M}$, and $\dot{v}_{OC}$ are active for a few more minutes. This corresponds to the end-phase behaviour of the machine and correspondingly minimal electrical consumption is noticed.

Dampening of the cyclic behaviour and energy balance between three circuits: The dampening of the cyclic behaviour due to the buffer effect of water storage and release of liquefaction and adsorption heat to the environment are important patterns from the modelling perspective. The earlier pattern is described in detail in *Fig. 4-13* and the latter in *Fig. 4-14*.

In *Fig. 4-13 (a)*, direct values of $T_{f,AdC,H}$ are shown to highlight its vast fluctuations or high change-of-value due to the AdC's cyclic operation. The water enters the HTES at the bottom corresponding to T_{HT1} but the change-of-value in this layer is not as high. The relative change-of-value (RCV) between two continuous measurements of $T_{f,AdC,H}$ and T_{HT1} was analysed for almost 24 hours of steady state operational data and is summarised in *Fig. 4-13 (b)*. It is observed that only 35% of the data for $T_{f,AdC,H}$ had a RCV of less than 1% and 18% of data has a RCV of more than 9% especially when the phases changed. On the other hand, irrespective of the operation phase the RCV for T_{HT1} is mostly lower than 1% expressing the strong reduction in fluctuations and 100% of the data is lower than 3% as noticed in the cumulative curves.
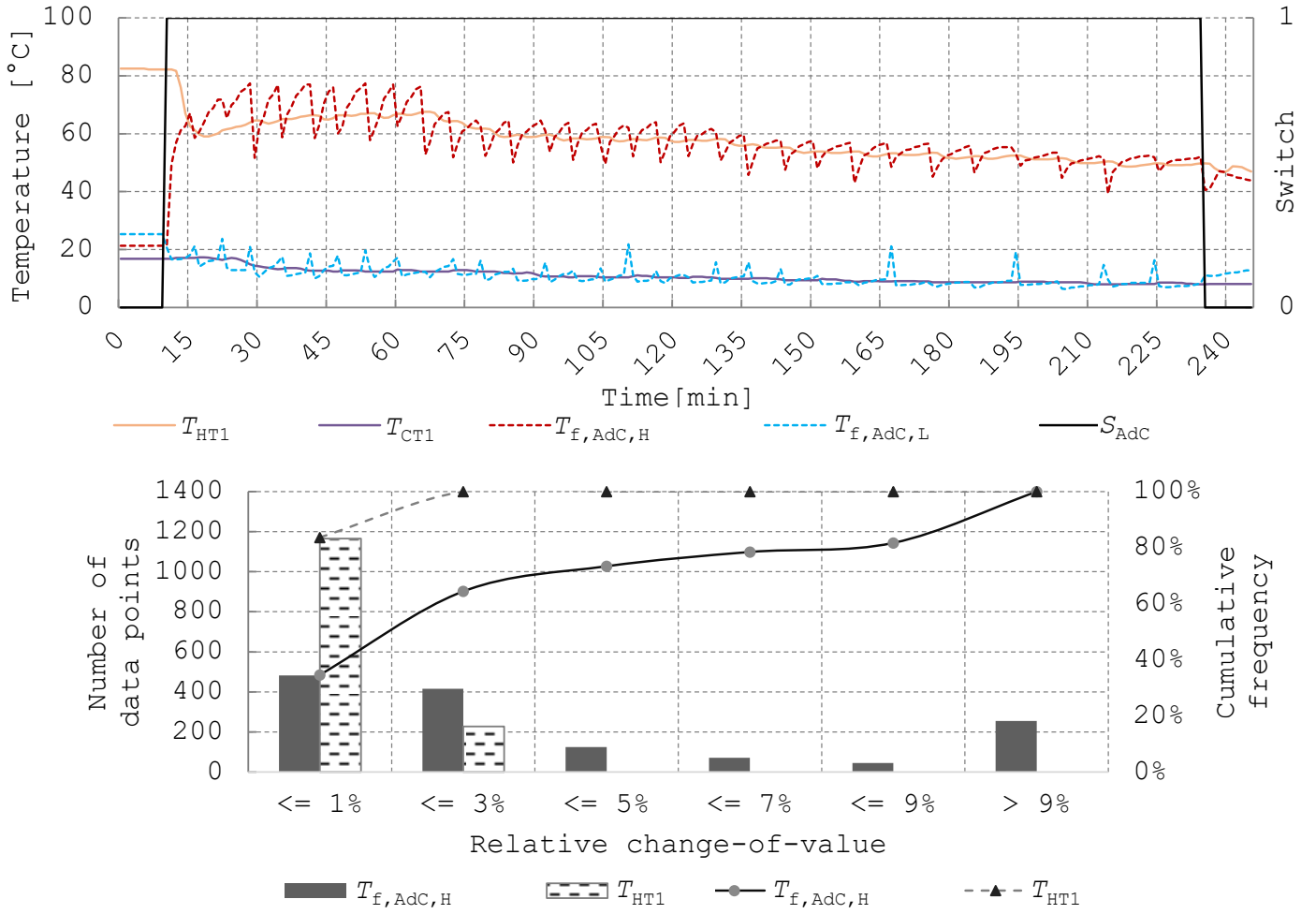
Fig. 4-13 (a) Measurements of AdC outlet temperatures connected to T_{HT1} ($T_{f,AdC,H}$) and T_{CT1} ($T_{f,AdC,L}$) (b) Number of data points and cumulative frequency for the relative change-of-value (RCV) between two continuous measurements of $T_{f,AdC,H}$ and T_{HT1} for 24 hours of steady state data

In *Fig. 4-14,* the 7-minute average thermal powers in the recooler circuit or medium temperature circuit $P_{th,AdC,M}$, in the high temperature circuit $P_{th,AdC,H}$, and low temperature circuit $P_{th,AdC,L}$ are shown. It is noticed that $P_{th,AdC,M}$ at a given point in time is approximately equal to the sum of $P_{th,AdC,H}$ and $P_{th,AdC,L}$. More importantly, the absolute error for energy balance in the three circuits ($|Q_{th,AdC,M} - (Q_{th,AdC,H} + Q_{th,AdC,L})|$) for almost 24 hours of steady state operational data is less than 1.2%.
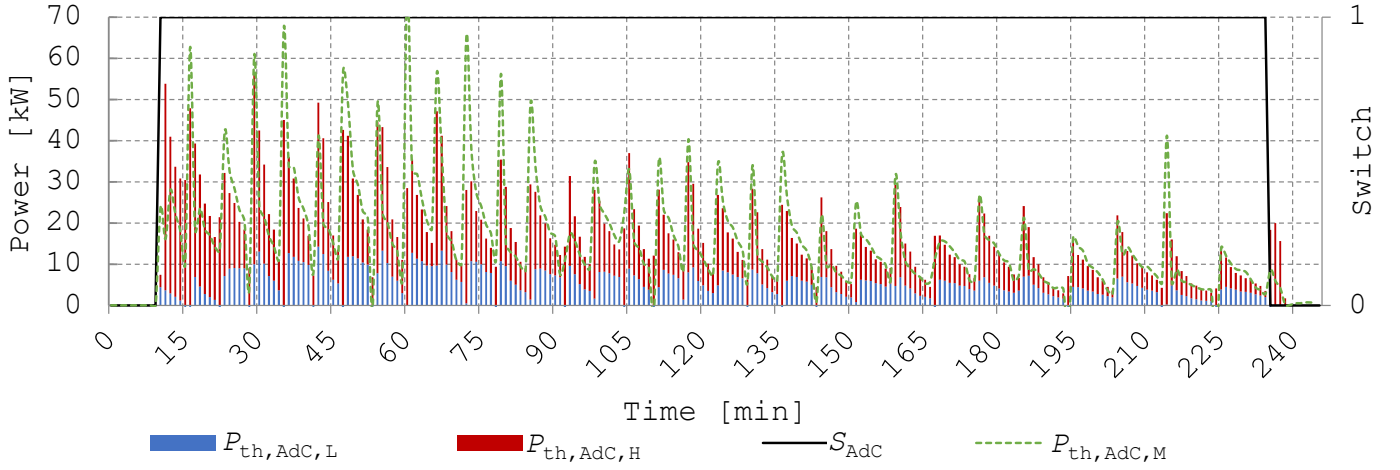
Fig. 4-14 Thermal power balance in the three AdC circuits

4.5.2 AdC model

The modelling of an AdC's internal dynamics is extremely complex and has been included only in a few models as shown in *Table 4-6.* Then again, the complexity of these models makes them ineffective for a system-wide optimisation and simplified models should be developed. On the other extreme, a highly simplified linear energy balance model that assumes a constant COP does not capture the part-load behaviour of the machine, which is highly dependent on its inlet temperatures (Zhao et al., 2015). As seen in *Chapter 3*, a balance of complexity and accuracy must be achieved to develop a practical AdC model that is part of an entire system being optimally scheduled. Using the knowledge gained from the above experiments, an information flow diagram for the model of an AdC was prepared as shown in *Fig. 4-15*.
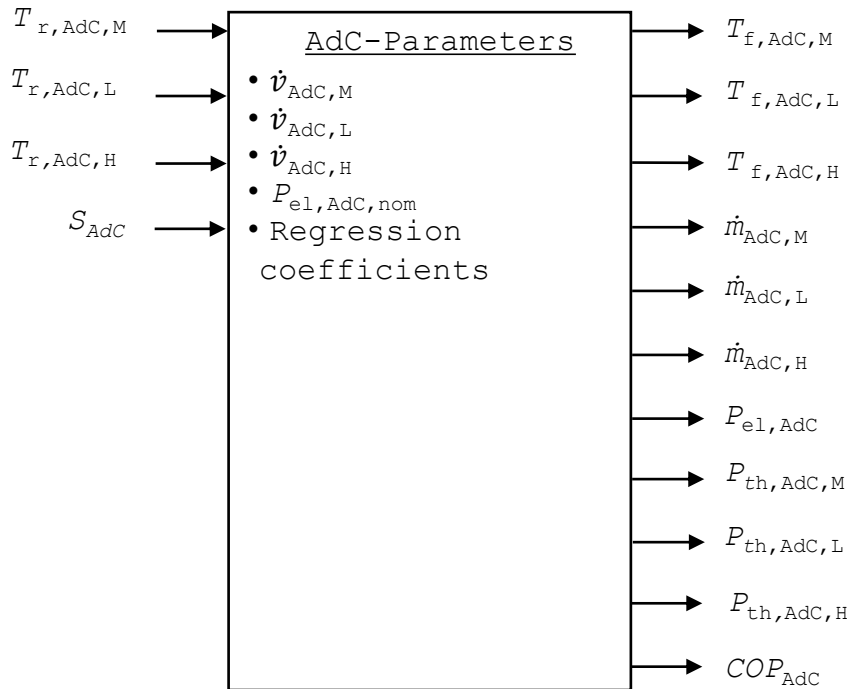
Fig. 4-15 Information flow diagram of the AdC model with reduced parameters and its switch as input

Based on the functional tests and the literature research, the following important assumptions for the modelling of this component were made:

- for typical AdC based trigeneration systems, adequate storage (hot and cold) capacities are often planned and these smoothen the cyclic temperature pattern due to their damping effect, thus making it unnecessary to model this pattern in detail (Bürger et al., 2017; Sawant and Pfafferott, 2017),
- the thermal power in the recooler circuit $P_{th,AdC,M}$ is approximately equal to the sum of thermal power in the high temperature circuit $P_{th,AdC,H}$ and the cooling power $P_{th,AdC,L}$ (Bürger et al., 2017; Sawant and Pfafferott, 2017),
- manufacturer's catalogues of widely used industrial AdCs provide characteristic curves for cooling capacity and COP depending on inlet temperatures in the three circuits (Fahrenheit GmbH, 2014; Invensor GmbH, 2019).

Considering the above findings and assumptions, regression analysis was applied to fit the cooling power and COP of the AdC as second degree functions of the three inlet temperatures as shown in (4.6) and (4.7) respectively.

$$P_{th,AdC,L} = a_1 + a_2 T_{r,AdC,L} + a_3 T_{r,AdC,H} + a_4 T_{r,AdC,M} + a_5 T_{r,AdC,L} T_{r,AdC,H} +$$
$$a_6 T_{r,AdC,H} T_{r,AdC,M} + a_7 T_{r,AdC,L} T_{r,AdC,M} + a_8 T_{r,AdC,L}^2 + a_9 T_{r,AdC,H}^2 + a_{10} T_{r,AdC,M}^2 \qquad (4.6)$$

$$COP_{AdC} = b_1 + b_2 T_{r,AdC,L} + b_3 T_{r,AdC,H} + b_4 T_{r,AdC,M} + b_5 T_{r,AdC,L} T_{r,AdC,H} +$$
$$b_6 T_{r,AdC,H} T_{r,AdC,M} + b_7 T_{r,AdC,L} T_{r,AdC,M} + b_8 T_{r,AdC,L}^2 + b_9 T_{r,AdC,H}^2 + b_{10} T_{r,AdC,M}^2 \qquad (4.7)$$

The coefficients of regression a_1 to a_{10} and b_1 to b_{10} were found by using the empirical data from manufacturer's data sheets shown in *Fig. 4-16* and the values for the regression coefficients are given in the *Appendix D*.
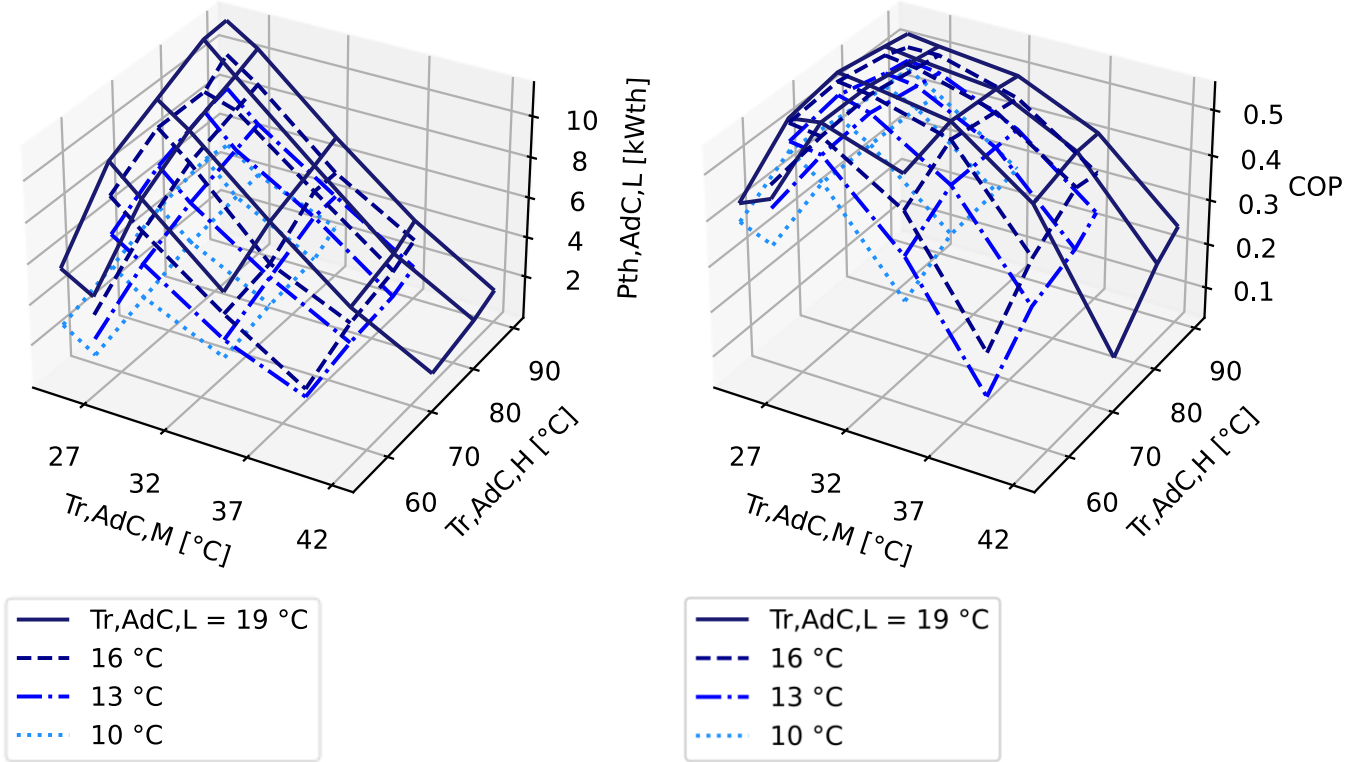
Fig. 4-16 Empirical data of AdC cooling power and COP at different inlet temperatures in the three circuits

It is noticed that the $P_{\text{th,AdC,L}}$ and COP_{AdC} tend to reduce with increasing $T_{\text{r,AdC,M}}$ and lower $T_{\text{r,AdC,L}}$ and $T_{\text{r,AdC,H}}$. The data collected during functional tests also represented this behaviour (*cf. Section 4.5.1*).

The results of the regression analysis to minimise the sum of normalised squared error (SNSE) are summarised in *Fig. 4-17*.
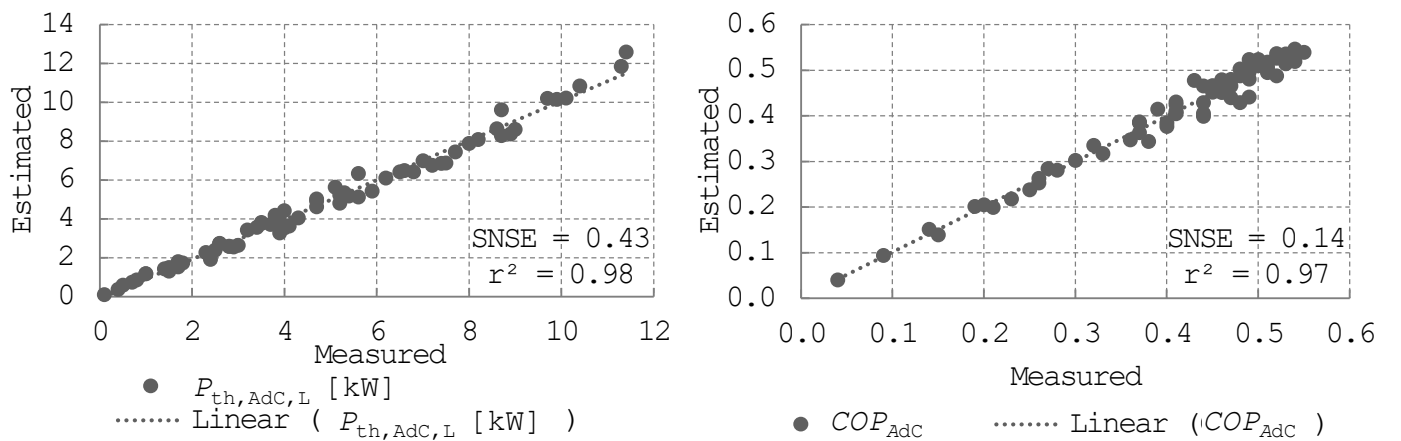
Fig. 4-17 Results of regression analysis for measured AdC data

Using the values of $P_{\text{th,AdC,L}}$ and COP_{AdC} the thermal input to the machine $P_{\text{th,AdC,H}}$ was calculated with (4.8) and the assumption regarding $P_{\text{th,AdC,M}}$ resulted in (4.9).

$$P_{\text{th,AdC,H}} = \frac{P_{\text{th,AdC,L}}}{COP_{\text{AdC}}} \qquad (4.8)$$

$$P_{\text{th,AdC,M}} = P_{\text{th,AdC,H}} + P_{\text{th,AdC,L}} \qquad (4.9)$$

Using the calculated thermal powers and applying the first law of thermodynamics, the feed-line temperatures for each circuit were calculated as in (4.10), (4.11), and (4.12).

$$T_{\text{f,AdC,L}} = T_{\text{r,AdC,L}} - \frac{P_{\text{th,AdC,L}}}{\rho_{\text{w}} \dot{v}_{\text{AdC,L}} c_{p,\text{w}}} \qquad (4.10)$$

$$T_{\text{f,AdC,H}} = T_{\text{r,AdC,H}} - \frac{P_{\text{th,AdC,H}}}{\rho_{\text{w}} \dot{v}_{\text{AdC,H}} c_{p,\text{w}}} \qquad (4.11)$$

$$T_{\text{f,AdC,M}} = T_{\text{r,AdC,M}} + \frac{P_{\text{th,AdC,M}}}{\rho_{\text{w}} \dot{v}_{\text{AdC,M}} c_{p,\text{w}}} \qquad (4.12)$$

The volume flows in the three circuits $\dot{v}_{\text{AdC,L}}$, $\dot{v}_{\text{AdC,M}}$, and $\dot{v}_{\text{AdC,H}}$ are constant parameters of the model. A division by zero was avoided by using these constant volume flows instead of actual mass flows in the equations above. The actual mass flows in the three circuits were calculated using (4.5) shown earlier and were zero when the machine was off.

The AdC's electrical consumption was calculated with (4.13).

$$P_{\text{el,AdC}} = S_{\text{AdC}} P_{\text{el,AdC,nom}} \qquad (4.13)$$

4.6   Combined heating and power (CHP)

The combustion engine CHP is of the type "Dachs HR5.3" by *SenerTec GmbH* (SenerTech GmbH, 2014) and operates on fuel-oil. A single cylinder (580 cm^3), 4-stroke Otto-cycle engine drives an asynchronous electrical generator converting mechanical energy to electricity (*Fig. 4-18*). The waste heat produced by the engine and the generator is transferred to cooling water that is circulated in a closed circuit by the internal cooling pump into the HTES. The CHP works parallel to the grid, always generating electricity and heat simultaneously. *VDE-AR-N 4105* standards are followed to supervise the electricity feed-in to the grid using an embedded controller. The controller also maintains the electrical safety system, fuel input, and cooling water volume flow.
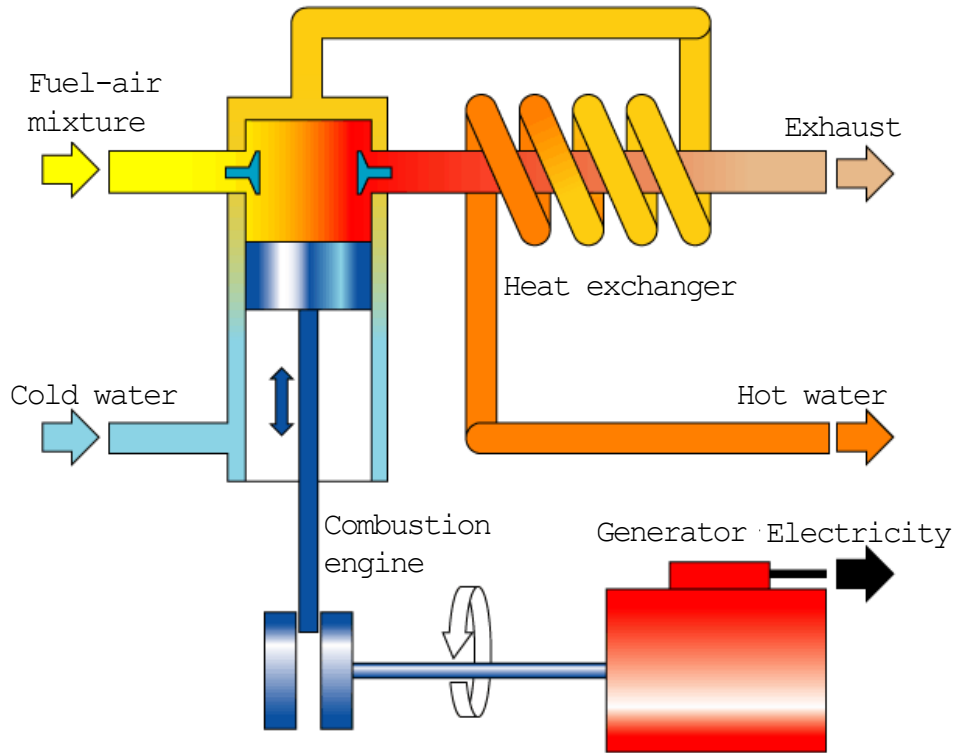
Fig. 4-18 Basic process of a combustion engine CHP[1]

4.6.1 CHP functional tests

The results of a sample functional test started with a homogeneous initial temperature of 21 °C in the HTES are shown in *Fig. 4-19*.

The response of thermal power $P_{th,CHP}$ and electrical power $P_{el,CHP}$ is shown in *Fig. 4-19 (a)*.

Quasi-static response of electrical power: The CHP is switched on at Time = 11 min. The $P_{el,CHP}$ in blue has a quasi-static response and approximately reaches its nominal value $P_{el,CHP,nom}$ of 5.3 kW$_{el}$ after 7 minutes of operation. This includes a 25 seconds delay time due to the internal start-up checks by the embedded controller.

Slow dynamic response of thermal power: $P_{th,CHP}$ in red displays a slow dynamic as it approximately reaches its nominal value $P_{th,CHP,nom}$ of 10.5 kW$_{th}$ after almost 60 minutes of operation. This is a typical PT-1 first order lag behaviour often demonstrated by thermal systems (Diehl, 2019).

Fig. 4-19 (b) indicates the nine temperatures in the HTES (T_{HT1} to T_{HT9} with T_{HT1} at the bottom) as solid lines. The feed-line and return-line temperatures in CHP-HTES circuit ($T_{f,CHP}$ & $T_{r,CHP}$) are also represented as dashed lines. $T_{f,CHP}$ increases rapidly from 21 °C to 65 °C after 5 minutes of turning on the CHP and then plateaus out to 72 °C till Time = 60 min.

---

[1] This figure by unknown author is used under the CC-BY-SA license.

Hydraulic connection of CHP to HTES and thermal stratification: The hot $T_{\text{f,CHP}}$ enters the top of the HTES (above T_{HT9}) while cold $T_{\text{r,CHP}}$ is extracted from the bottom (below T_{HT1}). The characteristic thermal stratification behaviour is observed during heating of the HTES with higher layers heating first and a shifting thermocline.

Embedded controller adjusts cooling water volume flow: Until Time = 446 min, the embedded controller maintains a temperature difference of almost 50 °C in the feed-line and return-line by controlling the coolant volume flow $\dot{v}_{\text{CHP}}$. A second stratification step is observed as the T_{HT1} increases after all above layers are heated and the $T_{\text{f,CHP}}$ increases further to around 80 °C. The $\dot{v}_{\text{CHP}}$ also increases with a higher $T_{\text{r,CHP}}$ due to the internal control logic.

Safety shut-down: After the $T_{\text{r,CHP}} > 74$ °C at Time = 728 min the internal controller shuts-down the CHP due to overheating risks even though the S_{CHP} is 1. A mixing of stratified temperatures occurs as the cooling pump continues circulating water for emergency cooling of the CHP.

Constant fuel consumption: The CHP consumes 1.8 l/h of fuel-oil immediately after it is turned on and has a constant fuel consumption (SenerTech GmbH, 2014). However, for the scope of this work the fuel consumption is calculated based on a gas CHP and using the nominal power outputs and higher calorific value (HCV) of 12 kWh/m^3 (Bundesnetzagentur, 2019), a constant gas consumption $\dot{v}_{\text{fuel}}$ of 1.4 m^3/h is used instead of fuel-oil consumption.
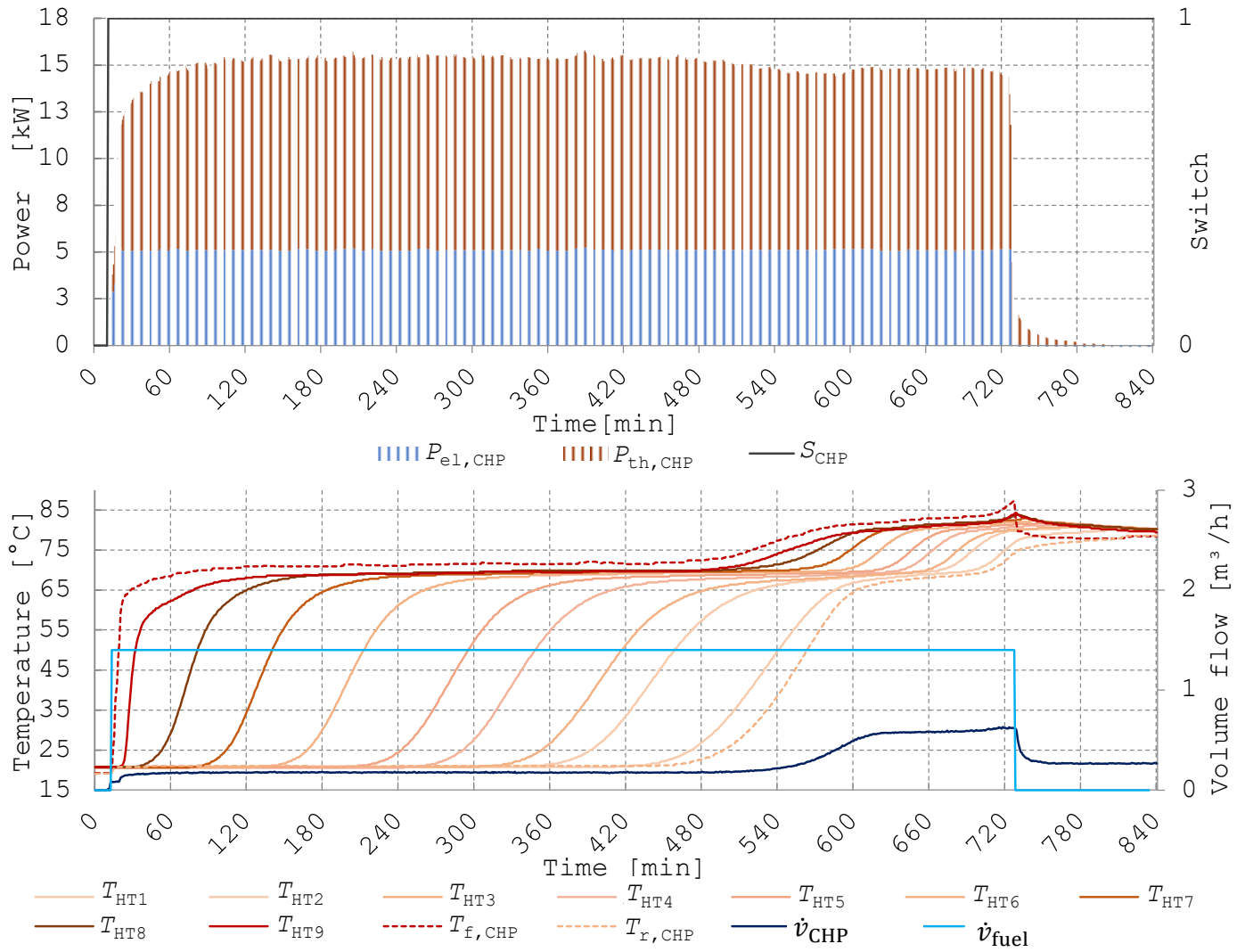
Fig. 4-19 (a) Electrical and thermal power of CHP. Data from a test on 09th May 2017 starting at 11:51 (Time = 0 min). (b) CHP's circuit temperatures, volume flows, and corresponding HTES temperatures

4.6.2 CHP model

Most models used for optimisation (*Table 4-6*) do not integrate the control logic or dynamic behaviour identified in experiments above and are simply linear fits of apriori data. Some models use the black-box approach requiring many high-quality data sets for parameterisation thus making it difficult to generalise the models for other systems. Another approach is to depict the dynamic behaviour through a mass and energy balance over the engine block and the heat exchanger, thereby increasing the number of system states and parameters (complexity) for modelling the CHP. An information flow diagram for the CHP model is shown in *Fig. 4-20*.
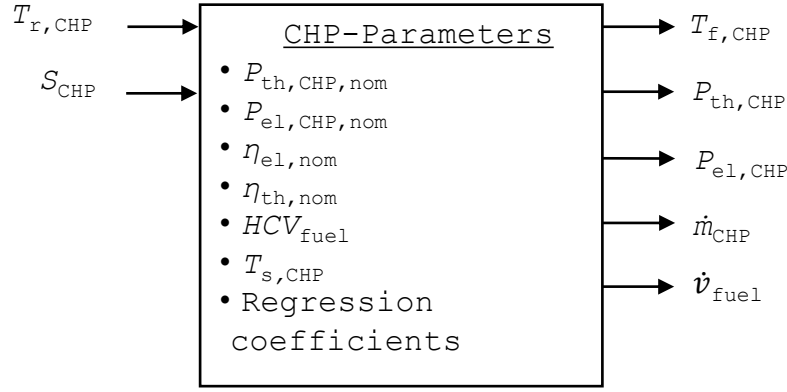
Fig. 4-20 Information flow diagram of the CHP model with its switch as input

Based on experimental work and previous literature research, following assumptions were made:

- the delay time of ca. 25 seconds for electrical output after start-up can be neglected since the length of the sampling time and forecast horizon for a 15-minute electricity price based MPC is significantly larger than the delay time interval itself,
- part-load behaviour is negligible and constant efficiencies can be assumed if an internal controller improves the micro-CHP's performance especially for optimisation of systems using thermal storages (Zhou et al., 2013),
- higher calorific value of fuel HCV_{fuel} is used for calculation,
- a complete combustion of fuel occurs in the CHP.

Considering the above findings and assumptions, the internal controller of the CHP was modelled as shown in (4.14).

$$\dot{v}_{CHP} = c_1 + c_2 T_{r,CHP} + c_3 T_{r,CHP}^2 \tag{4.14}$$

The coefficients of regression c_1 to c_3 were found by using experimental data over 77 hours of CHP operation with different initial temperatures and cold and warm starts and their values are given in the _Appendix D_. Most data available for $T_{r,CHP}$ was between 15 - 25 °C and 30 - 45 °C and the fit of $\dot{v}_{CHP}^*$ for using this data is seen in _Fig 4-21_. These are indeed the typical return-line temperatures to be expected during CHP operations when connected to a HL.
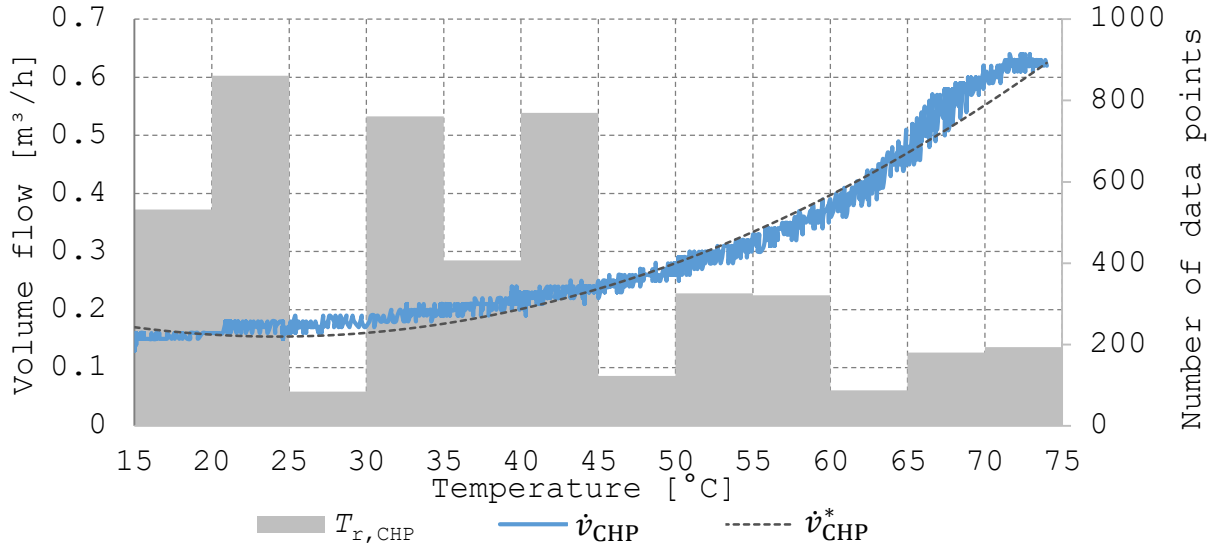
Fig. 4-21 Regression fit of CHP's volume flow against the return-line temperature

The results of the regression analysis to minimise the SNSE are summarised in *Fig. 4-22*.
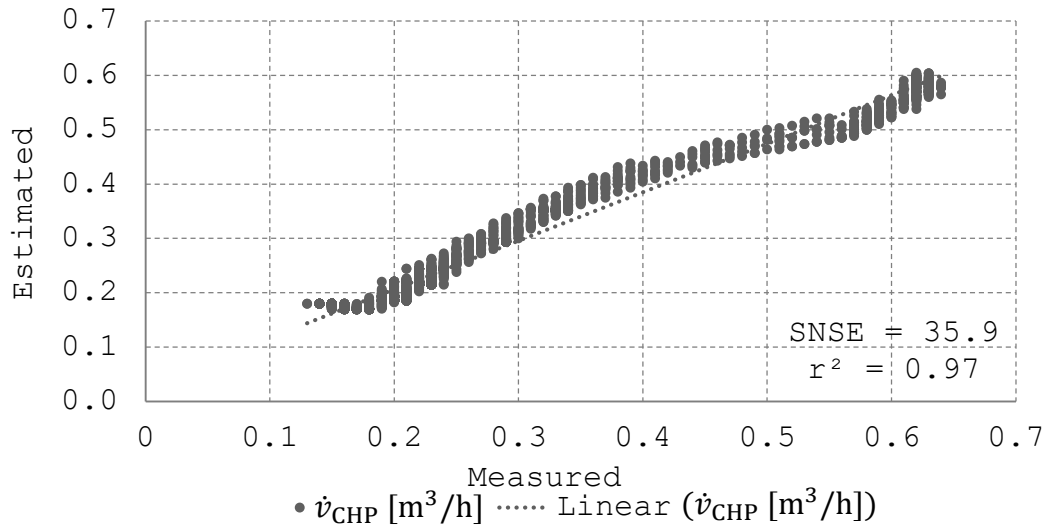
Fig. 4-22 Results of regression analysis for CHP volume flow fit

The dynamic behaviour of the CHP was modelled as shown in (4.15):

$$\frac{dP_{th,CHP}}{dt} = \frac{P_{th,CHP,nom}S_{CHP} - P_{th,CHP}}{d_1}$$

(4.15)

Here d_1 represents the average time-constant of the CHP system that was determined by performing step-response analysis over multiple tests with varying initial temperatures. The manipulated variable was S_{CHP} and controlled variable or system output was $P_{th,CHP}$. Results of a sample step-response test are shown in *Fig. 4-23*. A time-constant $T_{s,CHP}$ of 660 seconds (11 minutes), delay time $T_{t,CHP}$ of 300 seconds (5 minutes), and a gain $K_{s,CHP}$ of 10.2 kW$_{th}$ (approximately equal to $P_{th,CHP,nom}$) are observed.
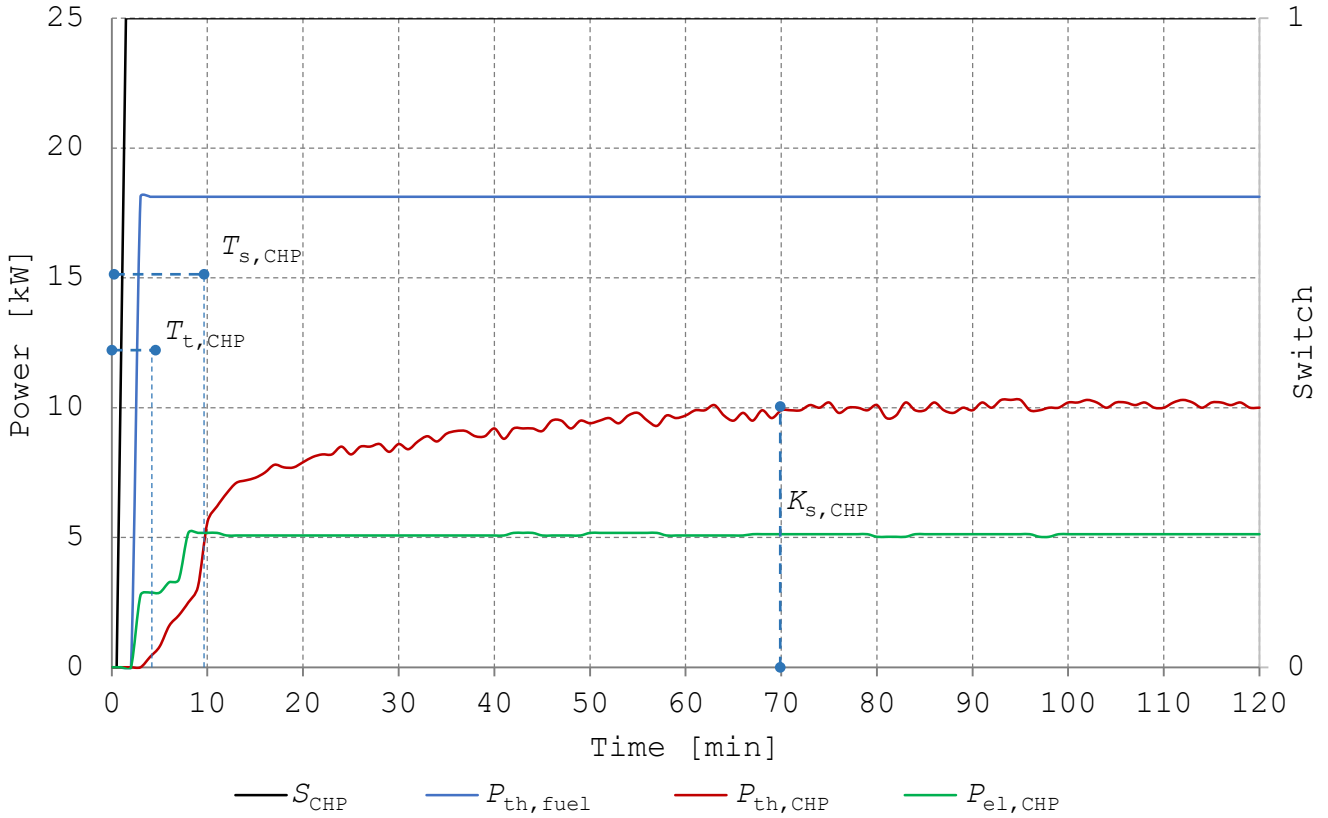
Fig. 4-23 Example of a step-response anaylsis for the CHP conducted on 09th May 2017 with delay time, time constant, and gain for the $P_{th,CHP}$ response

Using the calculated thermal power and volume flow and applying the first law of thermodynamics the feed-line temperature was calculated as in (4.16)

$$T_{f,CHP} = T_{r,CHP} + \frac{P_{th,CHP}}{\rho_w \dot{v}_{CHP} c_{p,w}} \tag{4.16}$$

The mass flow going to the HTES was calculated using (4.5) shown earlier and the electrical production of the CHP $P_{el,CHP}$ using (4.17) below:

$$P_{el,CHP} = S_{CHP} P_{el,CHP,nom} \tag{4.17}$$

Furthermore, the fuel consumed by the CHP was calculated using (4.18). This formulation aids in generalising the type of fuel that could be used in the simulation.

$$\dot{v}_{fuel} = S_{CHP} \frac{P_{el,CHP,nom} + P_{th,CHP,nom}}{HCV_{fuel}(\eta_{el,nom} + \eta_{th,nom})} \tag{4.18}$$

4.7 Outdoor coil (OC) and heat exchangers (HX)

The OC is principally a dry-cooling tower with three variable-speed fan motors consuming a total $P_{el,OC,max}$ of 0.9 kW$_{el}$ at their maximum speed $RPM_{OC,max}$ of 480 RPM (see. *Appendix B*). The actual speed of the fans RPM_{OC} can be controlled with a 0 – 10 volt signal $V_{OC,set}$. The fluid in the circuit is a 34% glycol-water mixture (brine). The OC is the heat-sink for the condenser of the chillers and the heat-source for the evaporator of the heat pump (*cf. Fig. 4-8*). Depending on the currently active operation

mode i.e. the currently connected machine, the OC volume flow $\dot{v}_{OC}$ has different but constant magnitudes.

Assuming the OC to be a cross flow air-fluid heat exchanger and assuming:

- homogeneous air flow,
- negligible effect of the instantaneous variations of air speed on the pressure,
- no pressure loss,
- constant overall heat transfer coefficient,

the OC model was derived from the *number of transfer units – effectiveness* (NTU-ε) method (Bergman et al., 2011). The NTU-ε method gives the effectiveness of a heat exchanger depending on the maximum possible heat transfer that can be hypothetically achieved. An information flow diagram for the OC model is shown in *Fig. 4-24*.
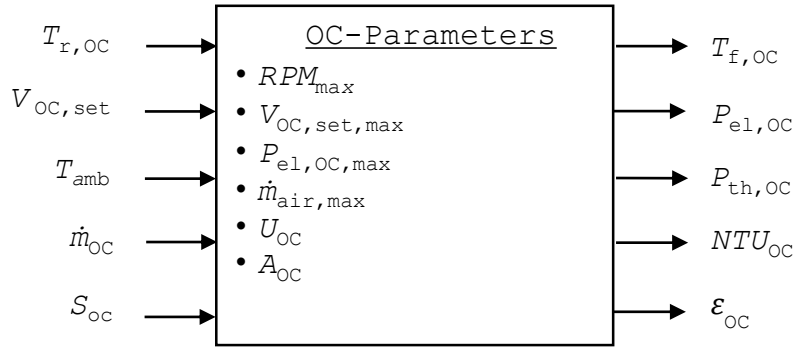
Fig. 4-24 Information flow diagram of the OC using NTU − ε method

The maximum possible thermal power of the OC $P_{th,OC,max}$ is based on the maximum possible temperature difference and was calculated using (4.19).

$$P_{th,OC,max} = C_{min}(T_{r,OC} - T_{amb}) \tag{4.19}$$

$T_{r,OC}$ is the temperature of hot fluid entering the OC and T_{amb} is the cooler ambient temperature. $C_{min}(C_{max})$ is the smaller (larger) out of the two heat capacity rates C_h and C_c. These are the heat capacity rates for the hot (brine) and cold (air) fluids respectively and were calculated as shown in equations (4.20) and (4.21).

$$C_h = \dot{m}_{OC}c_{p,b} \tag{4.20}$$

$$C_c = \dot{m}_{air}c_{p,air} \tag{4.21}$$

Where, $c_{p,air}$ and $c_{p,b}$ are the specific heat capacities of air and brine respectively. While, $\dot{m}_{air}$ and $\dot{m}_{OC}$ are their actual mass flows.

The effectiveness of the OC ε_{OC} was calculated using (4.22), where the NTU_{OC} and ratio of the heat capacity rates C_r were calculated by (4.23) and (4.24).

$$\varepsilon = \frac{1-\exp[-NTU(1-C_r)]}{1-C_r\exp[-NTU(1-C_r)]} \tag{4.22}$$

$$NTU = \frac{U_{OC}A_{OC}}{C_{min}} \tag{4.23}$$

$$C_r = \frac{C_{min}}{C_{max}} \tag{4.24}$$

The actual thermal power in the OC circuit $P_{th,OC}$ was calculated using (4.25) and an energy balance gave the two outlet temperatures from (4.26) and (4.27).

$$P_{th,OC} = \varepsilon\, P_{th,OC,max} \tag{4.25}$$

$$T_{f,OC} = T_{r,OC} - \frac{P_{th,OC}}{C_h} \tag{4.26}$$

$$T_{f,air} = T_{amb} + \frac{P_{th,OC}}{C_c} \tag{4.27}$$

Additionally, assuming a constant efficiency, a constant fan diameter, and fan speed to be linearly proportional to the volt signal, the *fan laws* were applied to simulate the relationship between the RPM_{OC}, $\dot{m}_{air}$, and electrical power consumed by the OC $P_{el,OC}$ as shown in (4.28), (4.29), and (4.30) (Mitchell and Braun, 2013).

$$RPM_{OC} = \frac{RPM_{OC,max}V_{OC,set}}{V_{OC,set,max}} \tag{4.28}$$

$$\dot{m}_{air} = \frac{RPM_{OC}\dot{m}_{air,max}}{RPM_{OC,max}} \tag{4.29}$$

$$P_{el,OC} = \frac{RPM_{OC}^3 P_{el,OC,max}}{RPM_{OC,max}^3} \tag{4.30}$$

The model for cross-flow metal plate HXs installed to separate the glycol-water and water only circuits (*Appendix B*) was developed analogous to the OC model and following assumptions were made:

- no pressure loss,
- constant overall heat transfer coefficient.

The total heat exchanger area A_{HX} and the overall heat transfer coefficient U_{HX} are the only two parameters for this model as shown in its information flow diagram in *Fig. 4-25*.
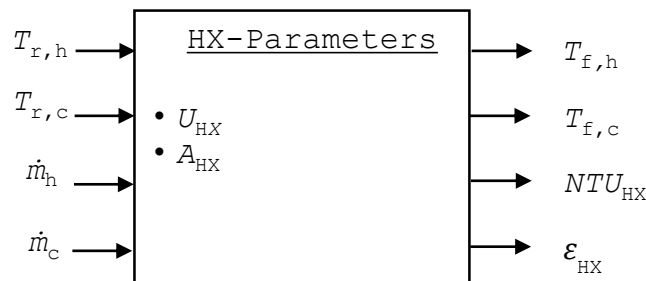
Fig. 4-25 Information flow diagram of the HX using $NTU - \varepsilon$ method

The model was developed as an object in OpenModelica and implemented once for each heat exchanger in the system.

4.8   Reversible heat pump (RHP)

The air-water-electricity RHP is of type "EWWP/014/KBW/1N" by *Daikin Air Conditioning GmbH* and operates on the principle of a vapour compression cycle (Daikin Europe, 2016). The machine can be operated as a compression chiller (CC) or as a heat pump (HP).

The major characteristic of this process is the use of refrigerants (here R407c) that extract highest possible latent heat of vaporisation from the medium (here water) to be cooled at the vaporisation temperature or transfer liquefaction heat at condensation temperature to the medium being heated. A compressor (here electric hermetic scroll compressor) provides the work input and refrigerant transport. The heat sink or source (here air over OC) is used in CC or HP modes, respectively.

Block flow diagrams for the operation of the RHP in CC mode and HP mode are shown in *Fig. 4-26* and *Fig. 4-27*. The switching of modes is achieved though external hydraulic switching valves (see *Appendix B*).
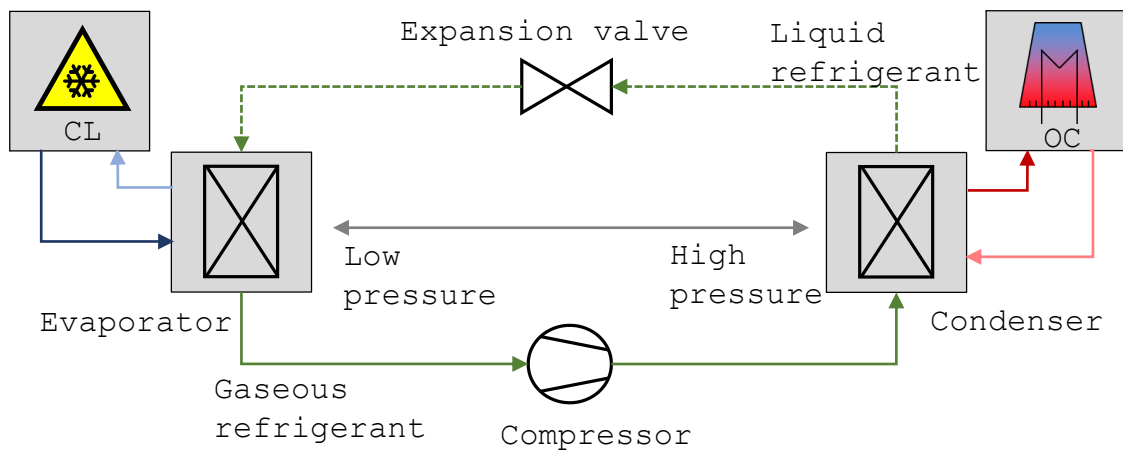
Fig. 4-26 Block flow diagram for CC operation at INES with external hydraulic switching

In the CC mode, the liquid refrigerant evaporates at low pressure and temperature in the evaporator (cross-flow plate heat exchanger) using the required heat from the cooling load. The compressor draws this refrigerant vapour out of the evaporator via a suction pipe and compresses gaseous refrigerant into the condenser at high pressure and temperature. In the condenser, the hot-gas transfers its heat to the air-cooled glycol-water mixture and condenses. The latent heat of vaporization and the compressor work that has been converted to heat is dissipated here and the liquid refrigerant is then usually routed to a liquid collector. An expansion valve reduces the high-pressure liquid refrigerant to low pressure prevailing in the evaporator and controls the charging of the evaporator under the various load conditions.
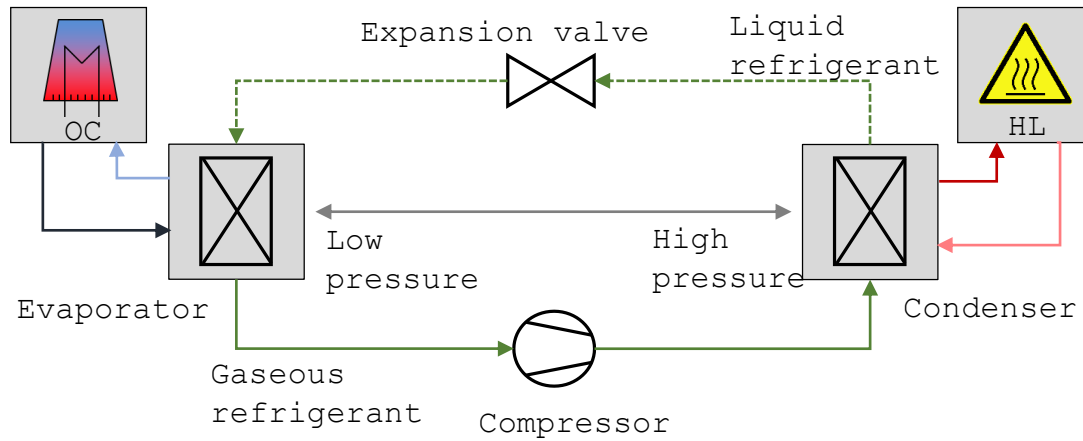
Fig. 4-27 Block flow diagram for HP operation at INES with external hydraulic switching

In the HP mode, the very low vaporisation temperature of a refrigerant is exploited by reversing the cycle and connecting the evaporator to the ambient (over OC). For instance, low temperature ambient air provides sufficient energy for vaporisation because R407c evaporates at -10 °C at 3.5 bar (Siemens Building Technologies, 2018). In the next step, refrigerant vapour is compressed for increasing its condensation point so that greater liquefaction heat can be carried away by the heating medium (water) for the heating load. Downstream from the condenser, the refrigerant is completely liquefied but still at a high pressure. The pressure is dissipated using an expansion valve, and the process cycle begins again.

The volume flows of the mediums in the evaporator and condenser circuits are maintained by external pumps and are not controlled under the scope of this work. These are kept constant for simplicity of control and to maintain the values closest-possible to the recommended nominal flows (*Table 4-1*).

Two important heat pump operating limits are defined by the minimum permissible vaporisation pressure and maximum permissible condensation pressure of the refrigerant. These limits are maintained by low-pressure and high-pressure safety pressostats in the evaporator and condenser circuits. These situations can typically arise when sufficient heat is not available to provide the vaporisation energy or the heating load is not high enough to extract the condensation heat. The minimum permissible vaporisation pressure depends on the compressor ratio and the heat source temperature. For instance, if using water in the evaporator circuit the vaporisation temperature must be above 0°C to avoid icing. The maximum permissible condensation pressure for R407c is restricted to 22 bar in practice and corresponds to a maximum heating water temperature of 50 °C (Siemens Building Technologies, 2018).

Due to the above physical restrictions, the operating limits of the HP mode at INES are lowest permissible evaporator inlet of 10 °C and highest permissible condenser outlet of 50 °C. This corresponds to an ambient temperature higher than 12 °C and HTES temperature lower than 45 °C for the HP operation.

4.8.1 CC and HP functional tests

An example of a functional test done to characterise the operation of the CC in collaboration with the CTES (homogeneous initial temperature = 31.5 °C), CL, and OC is shown in *Fig. 4-28*.

Fig. 4-28 (a) indicates four temperatures in the CTES (T_{CT1} to T_{CT4} with T_{CT1} at the bottom). The feed-line and return-line temperatures in the low-temperature evaporator circuit ($T_{f,CC,e}$ & $T_{r,CC,e}$) are also represented. The CC is switched on at Time = 04 min.

Hydraulic connection of CC to the CTES and thermal stratification: $T_{f,CC,e}$ enters the bottom of the CTES while $T_{r,CC,e}$ is extracted from the top layer. The characteristic thermal stratification behaviour is observed where the lower layer in CTES cools first. However, the stratification in CTES is not large because the temperature difference between feed-line and return-line is around 5 K.

Cooling capacity depends on inlet temperatures: The thermal powers in the two circuits are given in *Fig. 4-28 (b)*. It is observed that a steady state is reached within 10 minutes of operation. The cooling power $P_{th,CC,e}$ is significantly higher than the $P_{th,CC,e,nom}$ until Time = 110 min as the CTES temperatures are higher than nominal operation range of the machine. With cooling of the CTES the $T_{f,CC,e}$ is in its nominal range from 15 °C to 10 °C and correspondingly the $P_{th,CC,e} \approx P_{th,CC,e,nom}$. However, a reduction in $P_{th,CC,e}$ is observed as inlet temperatures in the CC reduces.

Shut-down phase has negligible effect on tank temperature: The CC is switched off at Time = 190 min, following which the circuit temperatures begin to equalise due to temporary volume flow during the machine's shut-down phase but have a negligible effect on the tank temperatures.
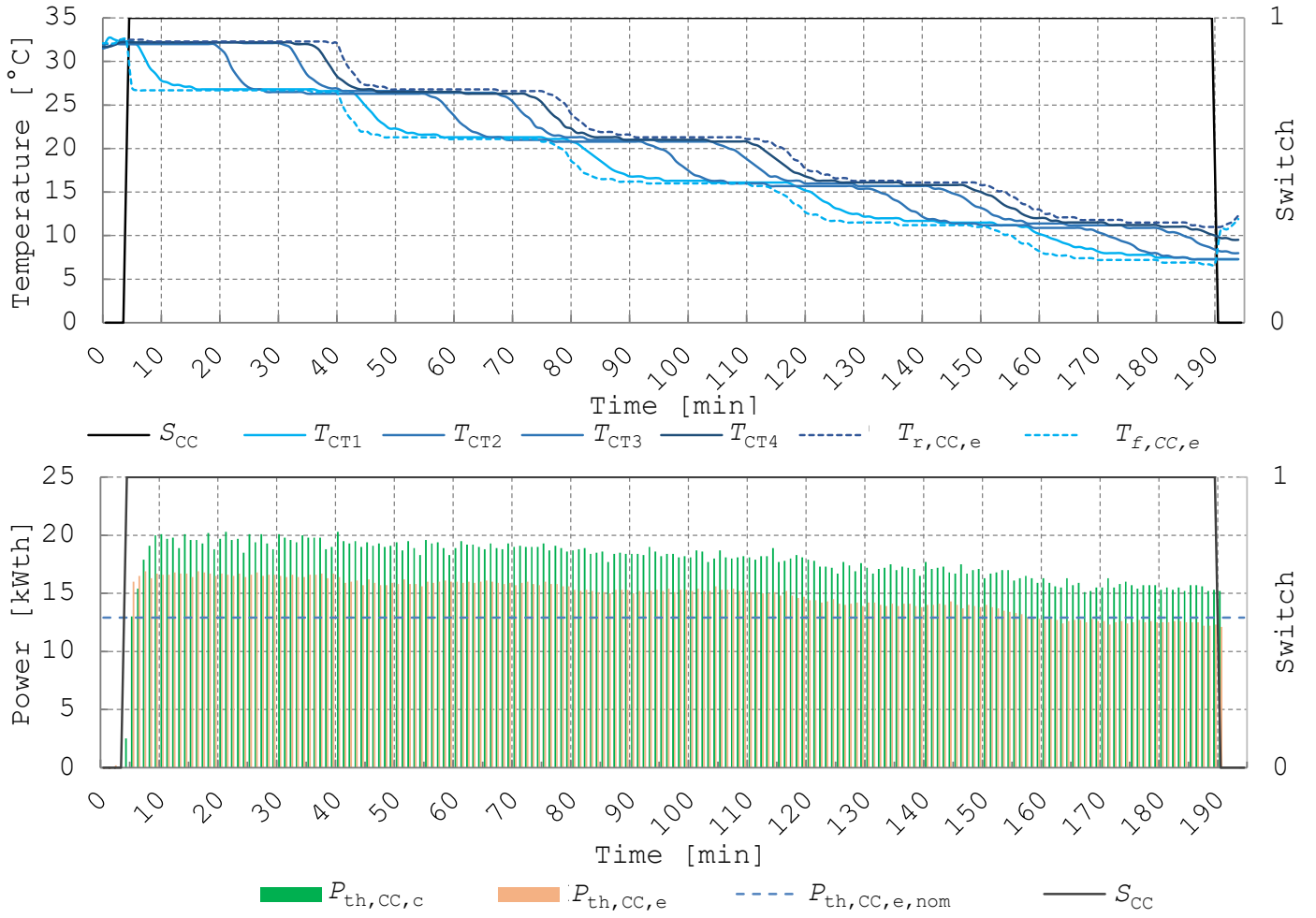
Fig. 4-28 (a) CC's low temperature (evaporator) circuit with corresponding CTES temperatures (b) Thermal powers in the medium temperature (condenser) and low temperature (evaporator) circuit of the compression chiller. Data from a standard test done on 24th Aug 2017 starting at 12:58 (Time = 0 min)

The electrical consumption and volume flows during the CC's operation are recorded in *Fig. 4-29.*

Quasi-static behaviour of electrical consumption and high energy efficiency ratio (EER): In *Fig. 4-29 (a)* the electrical consumption of the RHP $P_{el,RHP}$ reaches a steady state within 2 minutes of operation. Electrical consumption of OC $P_{el,OC}$ depends on the operation of the OC with the PID controller and is noted to be a maximum 0.3 kW_{el} during this test. The auxiliary consumption of the plant during CC operation $P_{el,aux}$ is approx. 0.2 kW_{el}. The high EER of the CC is evident from the average total electrical input of ca. 4.2 kW_{el}, to achieve an average cooling output of ca. 15.4 kW_{th} during the test.

Volume flows are constant: The constant volume flows in the two circuits are seen in *Fig. 4-29 (b),* with $\dot{v}_{CC,c} = 2.6$ m^3/h and $\dot{v}_{CC,e} = 2.4$ m^3/h. The volume flows are recorded until Time = 191 min including the CC's shut-down phase.
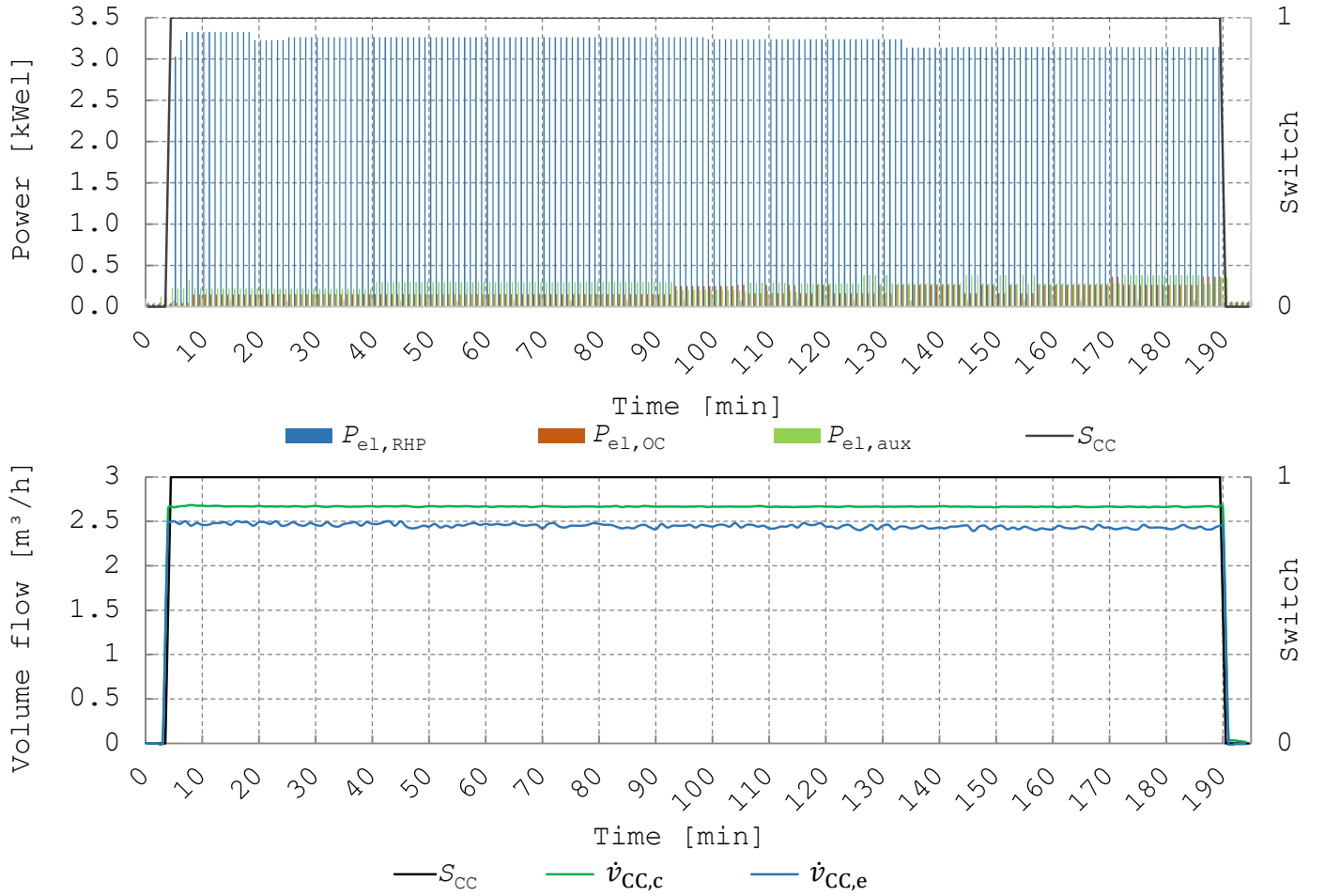
Fig. 4-29 (a) Electrical power consumption during CC operation (b) Volume flows during CC operation. Data from a standard test done on 24th Aug 2017 starting at 12:58 (Time = 0 min)

Similar to the CC functional tests the results of a functional test for the HP with a homogeneous initial temperature of 19.5 °C in the HTES are shown in *Fig. 4-30*.

Fig. 4-30 (a) indicates the nine temperatures in the hot tank (T_{HT1} to T_{HT9} with T_{HT1} at the bottom) as solid lines. The feed-line and return-line temperatures in HP-HTES primary circuit (before heat exchanger) are also represented as dashed lines. The HP is switched on at Time = 07 min.

Hydraulic connection of HP to HTES and limited thermal stratification: It is seen that the $T_{f,HP,c}$ increases rapidly after turning on the HP and enters the HX between the HP and the HTES. While $T_{r,HP,c}$ is the temperature returning from the HX and is almost equal to the temperature entering the HTES at the top. Due to technical limitations, there are no temperature sensors or volume flow meters in the secondary circuit (see *Appendix B*). A temperature difference of only 5 K is noticed in the feed-line and return-line and accordingly the thermocline is not as prominent as in CHP operation.

Heating power depends on inlet temperatures: The thermal powers in the two circuits are given in *Fig. 4-30 (b)*. A heating power $P_{th,HP,c}$ of around 16 kW$_{th}$ is measured at lower HTES temperatures. It degrades slightly as the tank becomes hotter and the $T_{r,HP,c}$ increases. However, the $P_{th,HP,c}$ is ca. 0.5 kW$_{th}$ lower than its nominal value $P_{th,HP,c,nom}$

and deviation from manufacturer's catalogue data may occur due to measurement errors or part-load behaviours.
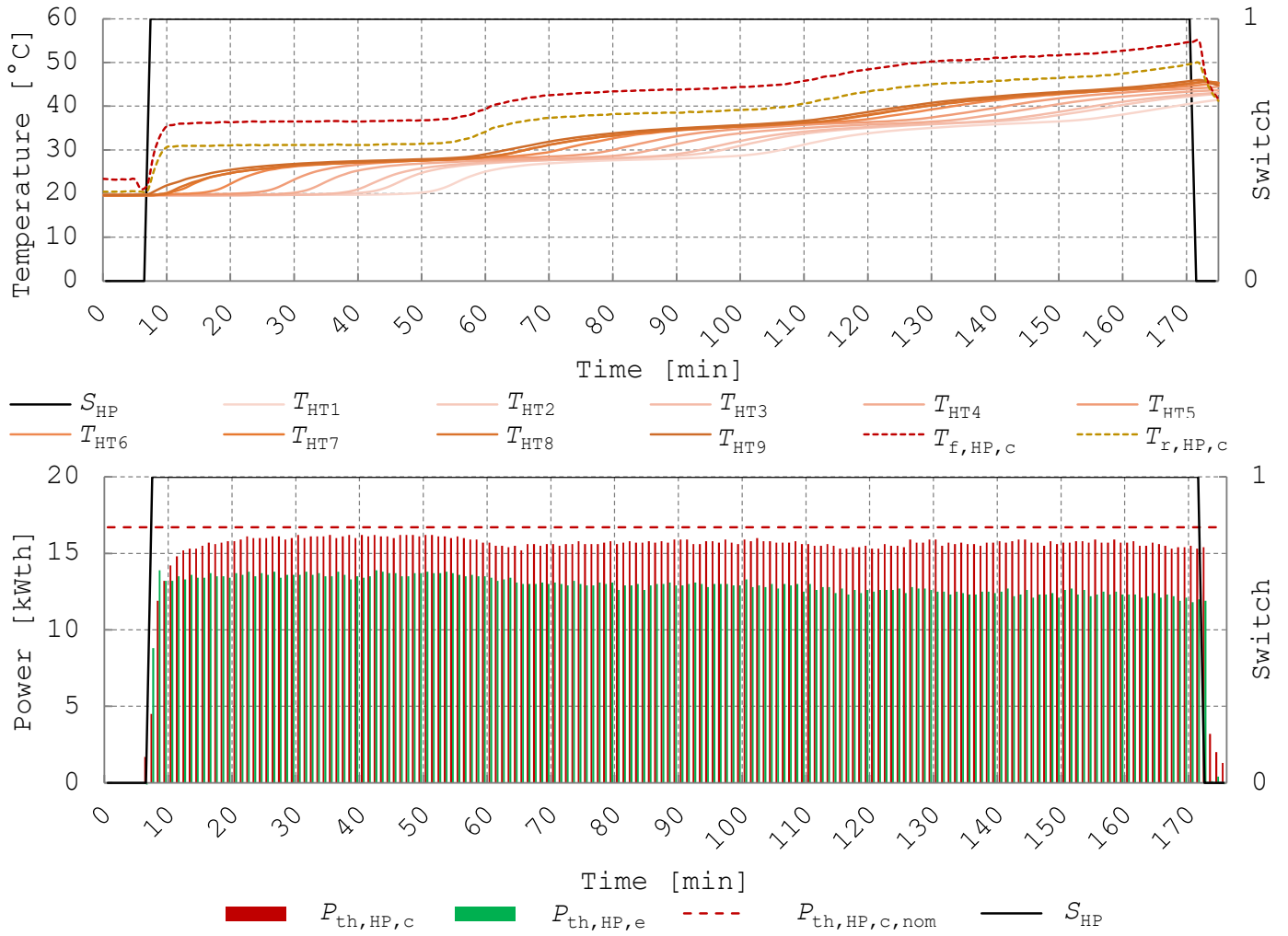
Fig. 4-30 (a) HP's high temperature (condenser) circuit with corresponding HTES temperatures (b) Thermal powers in the high temperature (condenser) and medium temperature (evaporator) circuit of the heat pump. Data from test done on 25th October 2017 starting at 14:19 (Time = 0 min)

The electrical consumption and volume flows during the HP's operation are recorded in *Fig. 4-31*.

Quasi-static response of electrical consumption and constant volume flows: The electrical powers have a quasi-static response and reach nominal values after 1 minute of operation. In the HP mode, OC runs at its maximum speed consuming maximum $P_{el,OC}$ of 1.4 kW$_{el}$[1] and $P_{el,aux}$ is approx. 0.63 kW$_{el}$. The pumps generate constant volume flows of $\dot{v}_{HP,c}$ = 2.7 m^3/h, $\dot{v}_{HP,e}$ = 2.4 m^3/h, and $\dot{v}_{OC}$ = 4.8 m^3/h as shown in *Fig. 4-31 (b)*.

---

[1] The new recooler installed in Summer 2018 consumes a maximum $P_{el,OC,max}$ of 0.9 kW$_{el}$
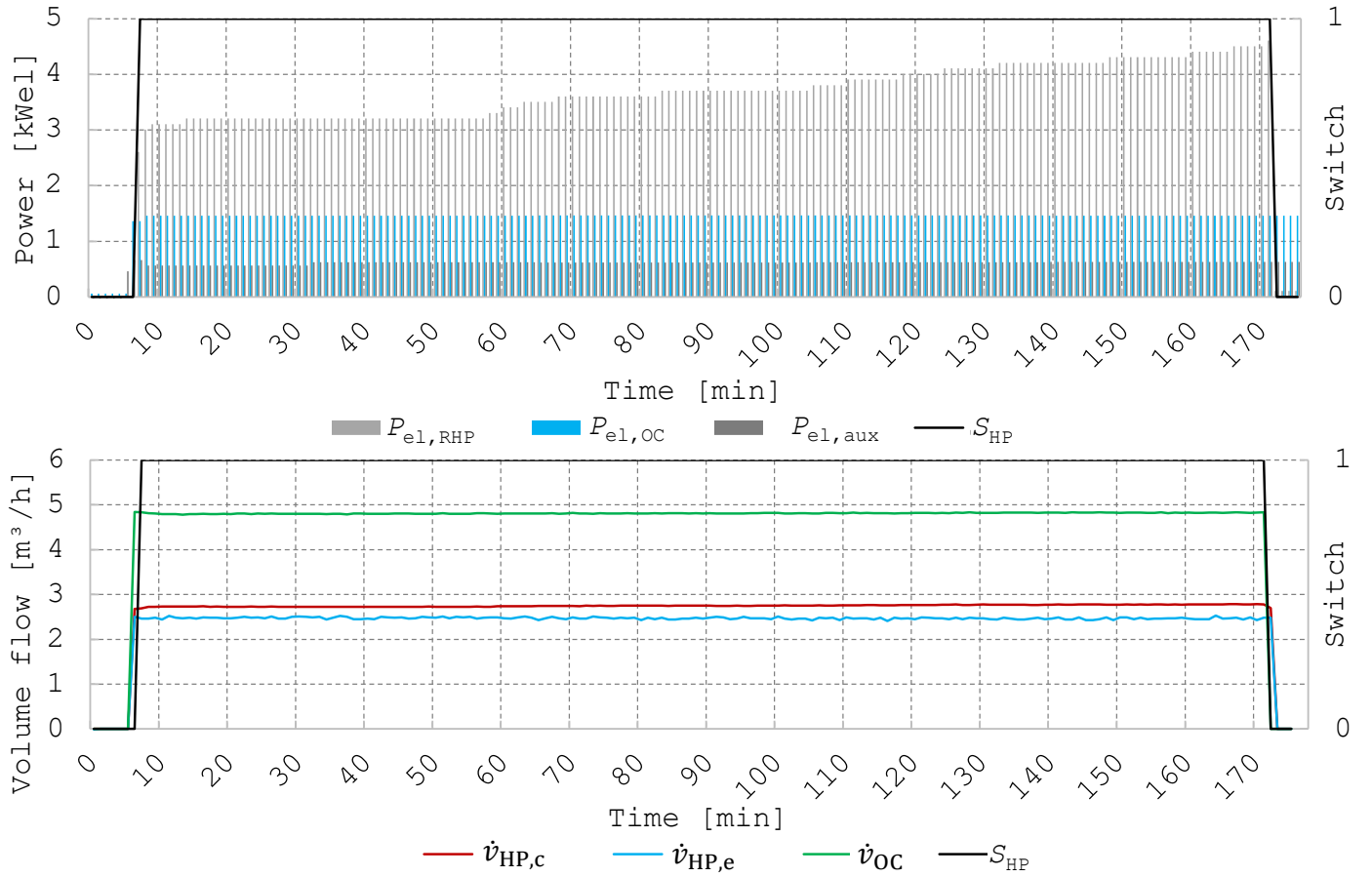
Fig. 4-31 (a) Electrical power consumption during HP operation (b) Volume flows during HP operation. Data from test done on 25th October 2017 starting at 14:19 (Time = 0 min)

Power balance over three circuits: As expected, the thermal power in the condenser circuit was almost equal to the sum of the thermal power in the evaporator circuit and the electrical consumption. This was examined in further detail to achieve possible simplification of the models.

The results of this analysis are illustrated in *Fig. 4-32*. During HP mode the evaporator circuit has medium temperature and condenser circuit has high temperature. During CC mode the evaporator circuit has low temperature and condenser circuit has medium temperature.

In *Fig. 4-32 (a),* the thermal power in the condenser circuit $P_{th,RHP,c}$ and the sum of the thermal powers in the evaporator $P_{th,RHP,e}$ and electrical power input $P_{el,RHP}$ is shown. It is noticed that $P_{th,RHP,c}$ at a given point in time is approximately equal to the sum of $P_{th,RHP,e}$ and $P_{el,RHP}$. The absolute error between them $(|P_{th,RHP,c} - P_{th,RHP,e} + P_{el,RHP})|)$ was analysed for almost 18 hours of steady state operational data and is summarised in *Fig. 4-32 (b)*. It is observed that the maximum absolute error is 2.5 kW$_{th}$ but almost 98.5% of the data has an absolute error less than 1.5 kW$_{th}$.
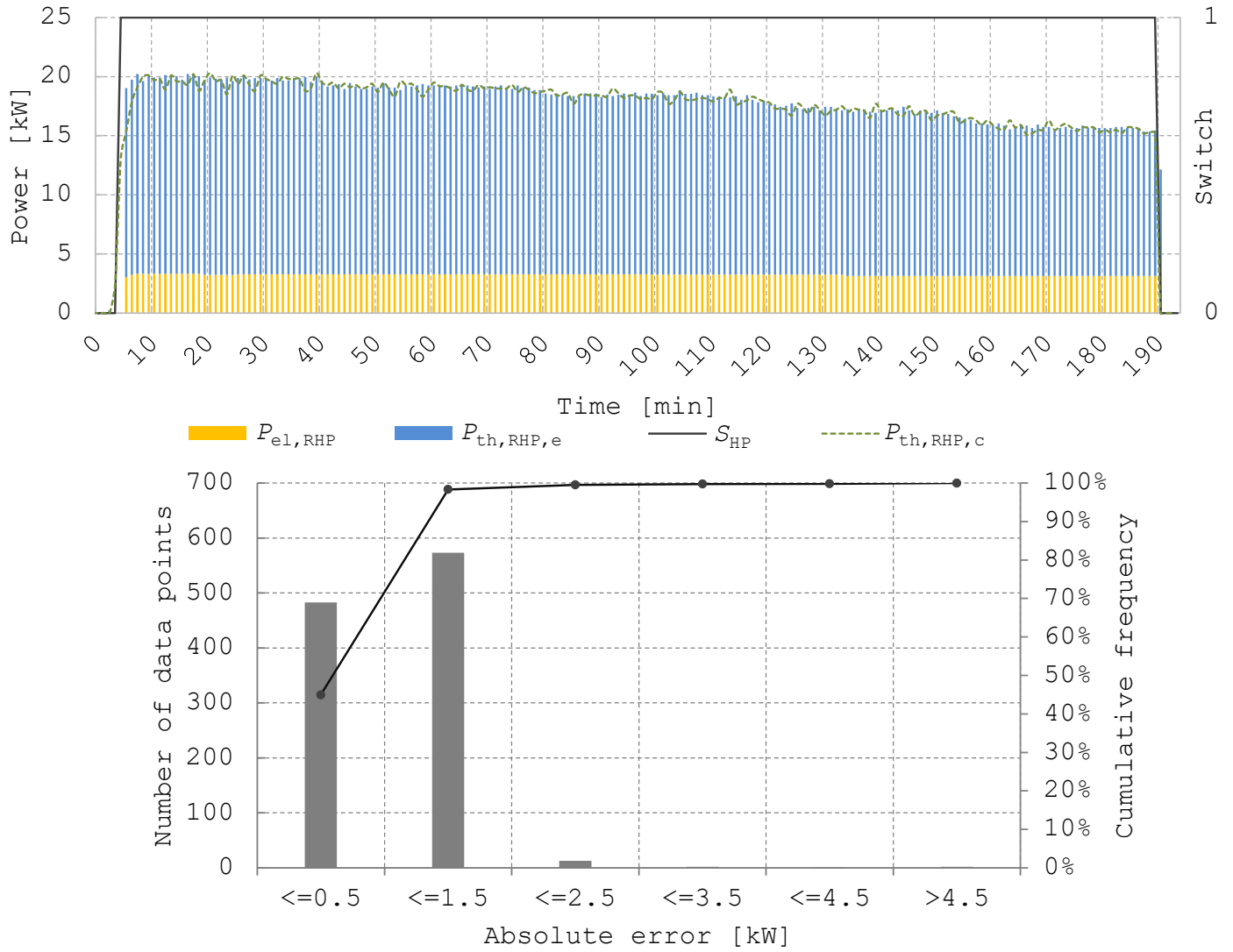
Fig. 4-32 (a) Power balance for the RHP irrespective of mode (b) Frequency and cumulative % for the absolute error between $P_{th,RHP,c}$ and the sum of $P_{th,RHP,e}$ and $P_{el,RHP}$ for 18 hours of steady state data

4.8.2 CC and HP models

In the literature study, modelling approaches were identified that use manufacturer's data tables or data that is available during the commissioning of these machines (*Table 4-6*). Operational know-how of the system gathered from the tests above was used to develop the information flow diagrams for the CC and HP models (*Fig. 4-33*).
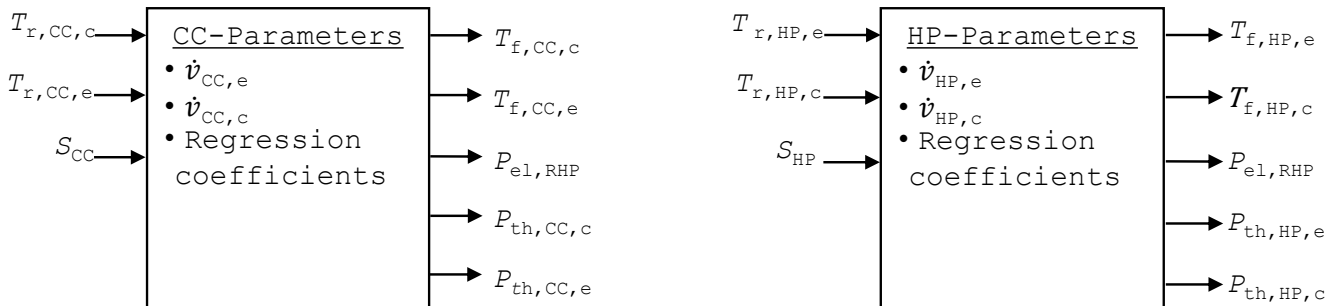
Fig. 4-33 Information flow diagram of the CC and HP models

Based on the functional tests and the literature research, the following important assumptions for the modelling of this component were established:

- the thermal power in the condenser circuit is approximately equal to the sum of thermal power in evaporator circuit and the power input (Sawant et al., 2018)
- manufacturer's catalogues of widely used industrial RHPs provide characteristic curves for cooling capacity, heating capacity and power input depending on evaporator and condenser inlet temperatures (Daikin Europe, 2016)

Using empirical data second degree equations like (4.31), (4.32), and (4.33) were fit by performing polynomial regression for calculating the heating power $P_{\text{th,HP,c}}$, cooling power $P_{\text{th,CC,e}}$ and power consumption $P_{\text{el,RHP}}$ respectively as a function of the inlet temperatures. $P_{\text{el,RHP}}$ was calculated based on the evaporator and condenser inlet temperatures of the particular mode. The equations capture the part-load behaviour of the machine as a function of the inlet temperatures.

$$P_{\text{th,HP,c}} = e_1 + e_2 T_{\text{r,HP,e}} + e_3 T_{\text{r,HP,c}} + e_4 T_{\text{r,HP,e}} T_{\text{r,HP,c}} + e_5 T_{\text{r,HP,e}}^2 + e_6 T_{\text{r,HP,c}}^2 \qquad (4.31)$$

$$P_{\text{th,CC,e}} = f_1 + f_2 T_{\text{r,CC,e}} + f_3 T_{\text{r,CC,c}} + f_4 T_{\text{r,CC,e}} T_{\text{r,CC,c}} + f_5 T_{\text{r,CC,e}}^2 + f_6 T_{\text{r,CC,c}}^2 \qquad (4.32)$$

$$P_{\text{el,RHP}} = S_{\text{RHP}}(g_1 + g_2 T_{\text{r,RHP,e}} + g_3 T_{\text{r,RHP,c}} + g_4 T_{\text{r,RHP,e}} T_{\text{r,RHP,c}} + g_5 T_{\text{r,RHP,e}}^2 + g_6 T_{\text{r,RHP,c}}^2) \qquad (4.33)$$

The coefficients of regression e_1 to e_6, f_1 to f_6, and g_1 to g_6 were found by using the data from manufacturer's data sheets as plotted in *Fig. 4-34* and their values are given in the *Appendix D*. It is noticed that the $P_{\text{th,CC,e}}$ and $P_{\text{th,HP,c}}$ tend to reduce and $P_{\text{el,RHP}}$ increases with increasing temperature in the condenser inlet and reducing temperature in the evaporator inlet. The data collected during functional tests mentioned above also represents this behaviour.
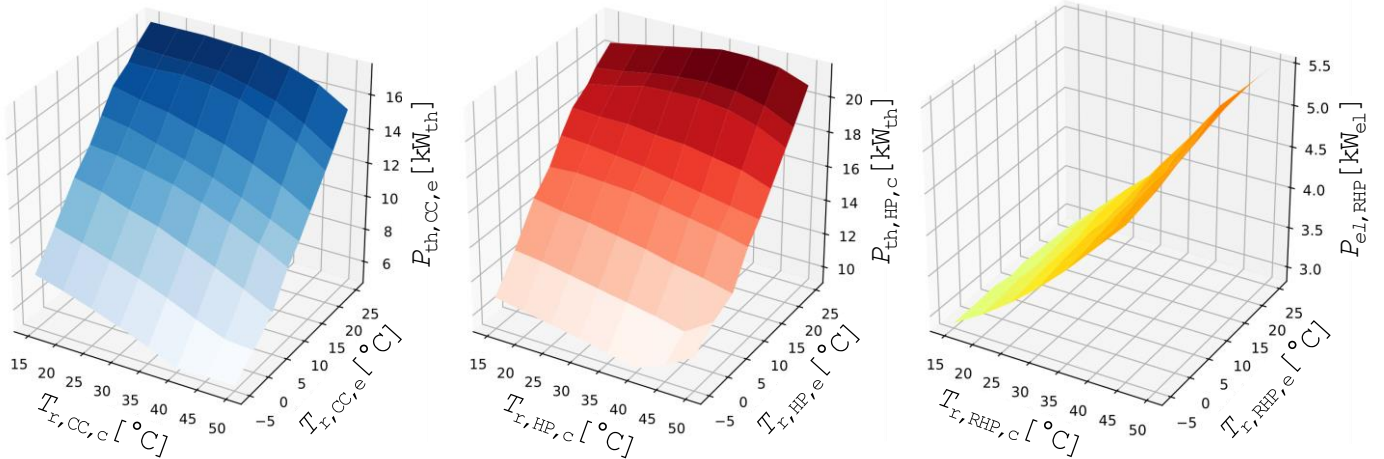
Fig. 4-34 Empirical data of RHP: (a) cooling power, (b) heating power, and (c) power input at different inlet temperatures in the two circuits

The results of the regression analysis to minimise the SNSE are summarised in *Fig. 4-35* .
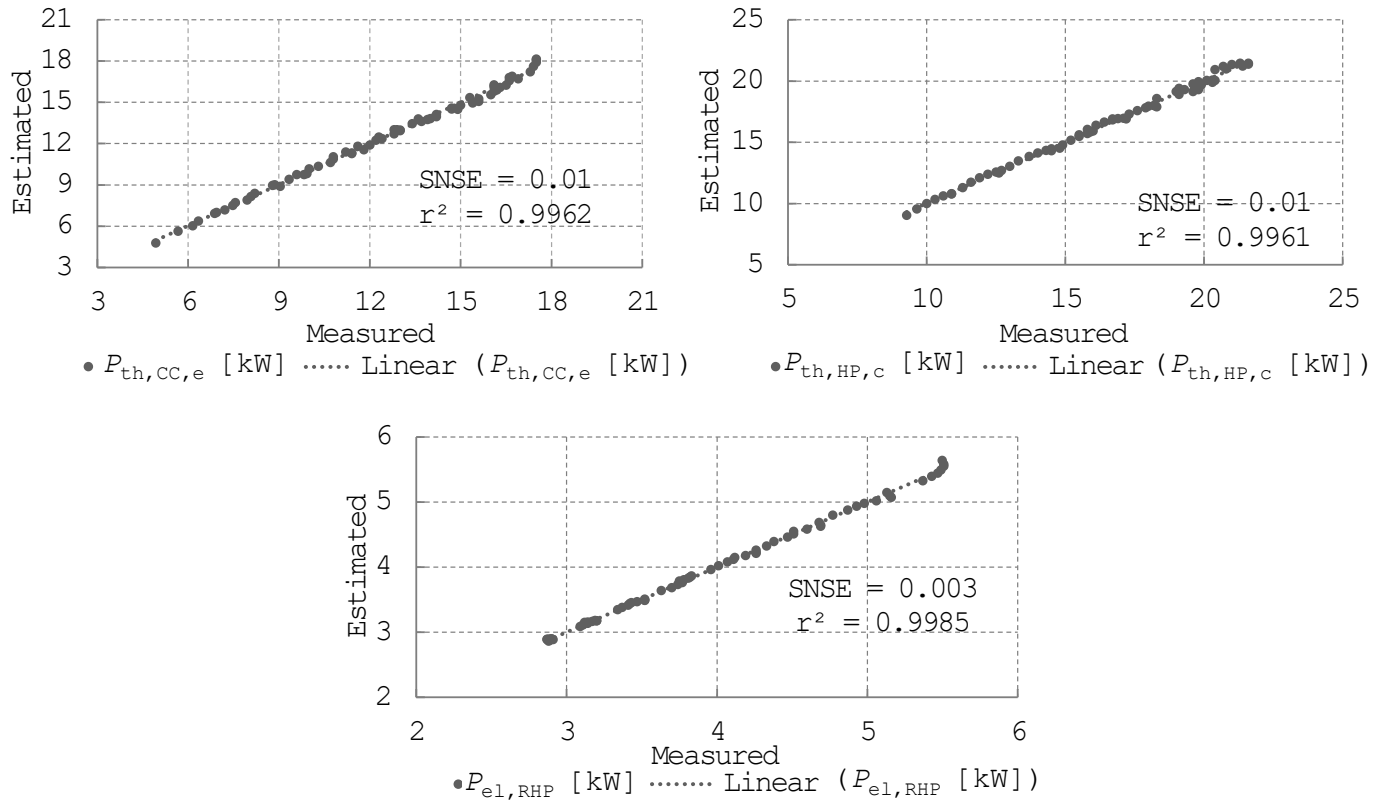
Fig. 4-35 Results of regression analysis for RHP data

Considering information from *Fig. 4-32* and assuming an ideal refrigeration cycle, the power balance for the RHP in the HP mode was calculated by (4.34) and in the CC mode by (4.35).

$$P_{th,HP,e} = P_{th,HP,c} - P_{el,RHP} \tag{4.34}$$

$$P_{th,CC,c} = P_{th,CC,e} + P_{el,RHP} \tag{4.35}$$

The first law of thermodynamics was applied in each circuit to get the feed-line temperatures as shown below for the HP condenser circuit and the CC evaporator circuit:

$$T_{f,HP,c} = T_{r,HP,c} + \frac{P_{th,HP,c}}{\frac{\rho_w}{3600}\dot{v}_{HP,c}c_{p,b}} \tag{4.36}$$

$$T_{f,CC,e} = T_{r,CC,e} - \frac{P_{th,CC,e}}{\frac{\rho_w}{3600}\dot{v}_{CC,e}c_{p,w}} \tag{4.37}$$

Where, $c_{p,b}$ and $c_{p,w}$ are the specific heat capacities of brine and water respectively. The mass flows in the two circuits were calculated using the general formulation in (4.5).

4.9   Thermal energy storages: cold thermal energy storage (CTES) and hot thermal energy storage (HTES)

The CTES and HTES are water based thermal energy storage tanks with direct heat transfer through multiple inputs and outputs at different heights. Different feed-line temperatures for various applications like domestic hot water systems or heating (cooling) circuits are possible and the exact details are available in *Appendix B.*

This design was chosen out of the standard product portfolio of a local engineering company and is widely used in small-scale energy systems (HT HelioTech GmbH, 2017). In the scope of this work, only the heating and cooling circuits of the tanks were used and domestic hot water circuits were normally closed.

Water storage tanks are the most attractive options for building HVAC systems due to the abundance, low cost and good thermal properties of water. They become more significant as the complexity of the energy plant increases. Depending on their size and application scenario, a modern storage system enables combination of irregular renewable energies and CCHP systems by buffering any time lag between production and demand. They also ensure high energy efficiency and less lime scaling due to their capability for thermal stratifications or temperature layering (Han et al., 2009). Stratifications occur due to the difference in density of cold and hot water and due to gravitational and buoyancy effects. Water entering the tank deposits at a height corresponding to its temperature. Hot water being less dense rises upwards, and cold water with heavy density falls downwards.

4.9.1 HTES and CTES model

The modelling of a stratified water storage is complex due to physical effects of thermal stratification, forced convection or laminar flows that may occur depending on the construction of the tank. Although complex, the simulation of stratification effects is important especially when performing cost-based operational optimisation (Campos Celador et al., 2011), as stratification is closely linked with the dynamic operation of the plant and its simulation increases the accuracy of the tank model. In most literature on optimisation of energy systems (*cf. Chapter 2*), mixed storage tanks or no storage tanks are used. However, it is highly recommended to apply at least a simple stratified tank model in long-term simulations like in optimal control problems with 24-hour horizons (De Césaro Oliveski et al., 2003). Information flow diagrams of the tank models are shown in *Fig. 4-36*.

The model of the thermal storages in this work was adapted from a 1-D dynamic multilayer model using the *Fourier's equation* (Eicker, 2006; Streckiene et al., 2011). This model summarises the complex convective and conductive flow using an effective vertical heat conductivity λ_{eff}. The HTES is considered as a vertically stratified cylindrical tank as shown in *Fig. 4-37* with dimensional parameters: diameter D_{HT}, height H_{HT}, thickness of tank wall d_{HT} and number of layers in the longitudinal direction N_{layers} available from the data sheet (*Table 4-1*).
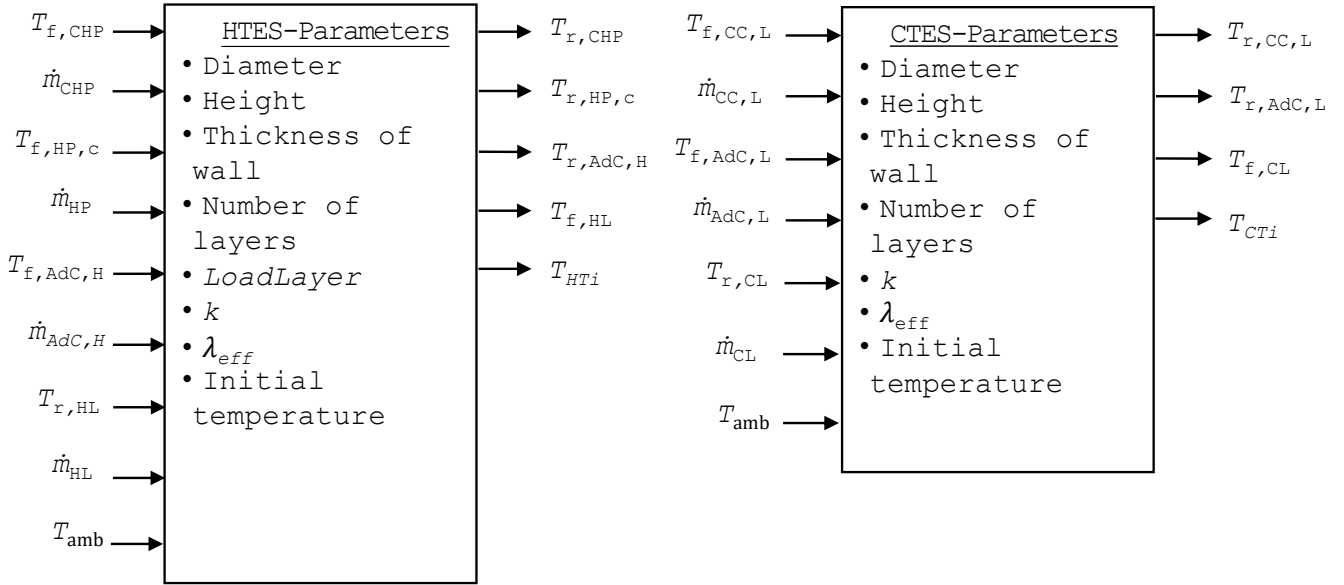
Fig. 4-36 Information flow diagrams for the HTES and CTES models

An effective mass flow $\dot{m}_i$ for each layer is calculated depending on the balance of mass flows from the *source circuit* (subscript "*s*") and *load circuit* (subscript "*l*"). If $\dot{m}_i$ is positive, then energy flows from the layer above the ith layer and is interpreted by the binary parameter $\delta_i^+ = 1$, else $\delta_i^+ = 0$. A negative $\dot{m}_i$ signifies mass flow from layer below the ith layer, i.e. $\dot{m}_l$ is greater than $\dot{m}_s$ and thus cooling of the ith layer occurs. It is considered by the parameter δ_i^-. The parameter δ_i^s is equal to 1 for the top most layer with hot water entering from the feed-line of the source circuit. Analogously, the parameter δ_i^l is equal to 1 for the bottom most layer with cooler water entering from the return-line of the load circuit. From the user-defined dimensional parameters of the tank other relevant dimensional quantities such as the exterior heat transfer surface area of a layer $A_{ext,i}$, cross-section area of a layer A_i, mass of a layer m_i and height of a layer z_i are calculated as shown in (4.38) to (4.41):

$$z_i = H_{HT}/N_{layers} \tag{4.38}$$

$$A_{ext,i} = \pi D_{HT} z_i \tag{4.39}$$

$$A_i = \pi \, (D_{HT} - 2d_{HT})^2/4 \tag{4.40}$$

$$m_i = A_i z_i \rho_w \tag{4.41}$$
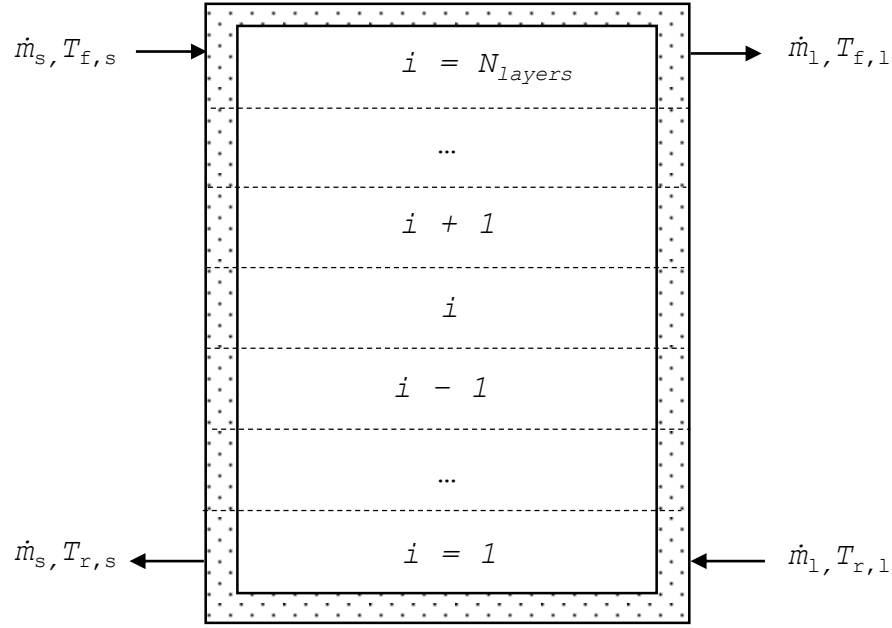
Fig. 4-37 Schematic depiction of a stratified tank with hydraulic connections and layer numbering for simple 1-D dynamic multilayer model from the literature

The general energy balance of each layer is then calculated as shown in (4.42).

$$m_i c_p \frac{dT_i}{dt} = \delta_i^s (\dot{m} c_p)_s (T_{f,s} - T_i) - \delta_i^l (\dot{m} c_p)_l (T_i - T_{r,l}) - k A_{ext,i}(T_i - T_{amb}) +$$

$$\delta_i^+ \dot{m}_i c_p (T_{i+1} - T_i) + \delta_i^- \dot{m}_i c_p (T_i - T_{i-1}) + \frac{A_i \lambda_{eff}}{z_i}(T_{i+1} - 2T_i + T_{i-1}) \qquad (4.42)$$

where,

T_i - temperature of ith layer (°C)

k - overall heat transfer coefficient of the tank envelope (W/(m²·K))

λ_{eff} - effective vertical heat conductivity (W/(m·K))

For a well-insulated steel tank k and λ_{eff} were assumed to be 0.5 W/(m²·K) and 1.5 W/(m·K) respectively (Eicker, 2006). However, the limitations of this approach with respect to the necessary characteristics for models applied in optimal control are as follows:

Differentiability: Within gradient-based optimization methods, models must be continuous and differentiable (Bürger et al., 2018). The presence of "If-Else" statements within models introduces discontinuities and must be avoided.

The formulation of the energy balance for each layer was modified to avoid the "If-Else" condition and replaced with a continuous formulation shown in (4.43) (Sawant et al., 2020a).

$$m_i c_p \frac{dT_i}{dt} = \delta_i^s (\dot{m}c_p)_s (T_{f,s} - T_i) - \delta_i^l (\dot{m}c_p)_l (T_i - T_{r,l}) - kA_{ext,i}(T_i - T_{amb}) +$$

$$\frac{\dot{m}_i c_p (\Delta T_{down,i} + \Delta T_{up,i})}{2} + \frac{\left(\sqrt{\dot{m}_i^2 + \omega}\right) c_p (\Delta T_{down,i} - \Delta T_{up,i})}{2} + \frac{A_i \lambda_{eff}}{z_i}(T_{i+1} - 2T_i + T_{i-1}) \qquad (4.43)$$

where,

$\Delta T_{down,i} = T_{i+1} - T_i$ is the temperature difference between current layer and the one above it, whereas $\Delta T_{up,i} = T_i - T_{i-1}$ is the temperature difference in the other direction. Also, $\omega \in \mathbb{R}$ and is $\ll |\dot{m}_i|$.

For $\dot{m}_i > 0$, the part "$\frac{\dot{m}_i c_p (\Delta T_{down,i} + \Delta T_{up,i})}{2} + \frac{\left(\sqrt{\dot{m}_i^2 + \omega}\right) c_p (\Delta T_{down,i} - \Delta T_{up,i})}{2}$" takes the value $\approx$ $\dot{m}_i c_p \Delta T_{down,i}$ representing charging of tank due to downward forced convection, and for $\dot{m}_i < 0$ the part "$\frac{\dot{m}_i c_p (\Delta T_{down,i} + \Delta T_{up,i})}{2} + \frac{\left(\sqrt{\dot{m}_i^2 + \omega}\right) c_p (\Delta T_{down,i} - \Delta T_{up,i})}{2}$" takes the value $\approx$ $-\dot{m}_i c_p \Delta T_{up,i}$ representing discharging of the tank due to an upward flow.

The $\dot{m}_i$ was between 0.02 kg/s and 0.69 kg/s and a value of $2\cdot10^{-4}$ was presumed for ω. With a given initial temperature distribution, the differential equation is applied to each layer and integrated over the entire forecast horizon to calculate the analytical temperature distribution over that time period.

Component design: For simplification purposes, the model in the literature assumes the hot source water enters at the top of the tank and is delivered to the load from the top of the tank. Similarly, the bottom of the tank is connected to the source and load circuits. In reality, the construction of a storage tank may have hydraulic connections at different heights of the tank and the respective layers of entry or exit of water should be defined accordingly. This enhances the accuracy of the model to simulate stratifications and also makes it adaptable to different constructions (Sawant et al., 2018).

The formulation of the energy balance over the length of the tank was modified by introducing a user-defined parameter "*LoadLayer*". It represents the layer from which water goes to the thermal loads and a differential equation is created for each section of the tank by implementing "For-loops" as shown in *Fig. 4-38*. By using this parameter, a particular hydraulic connection can be included in the model and this technique could be extended to multiple hydraulic connections at different heights of the tank.
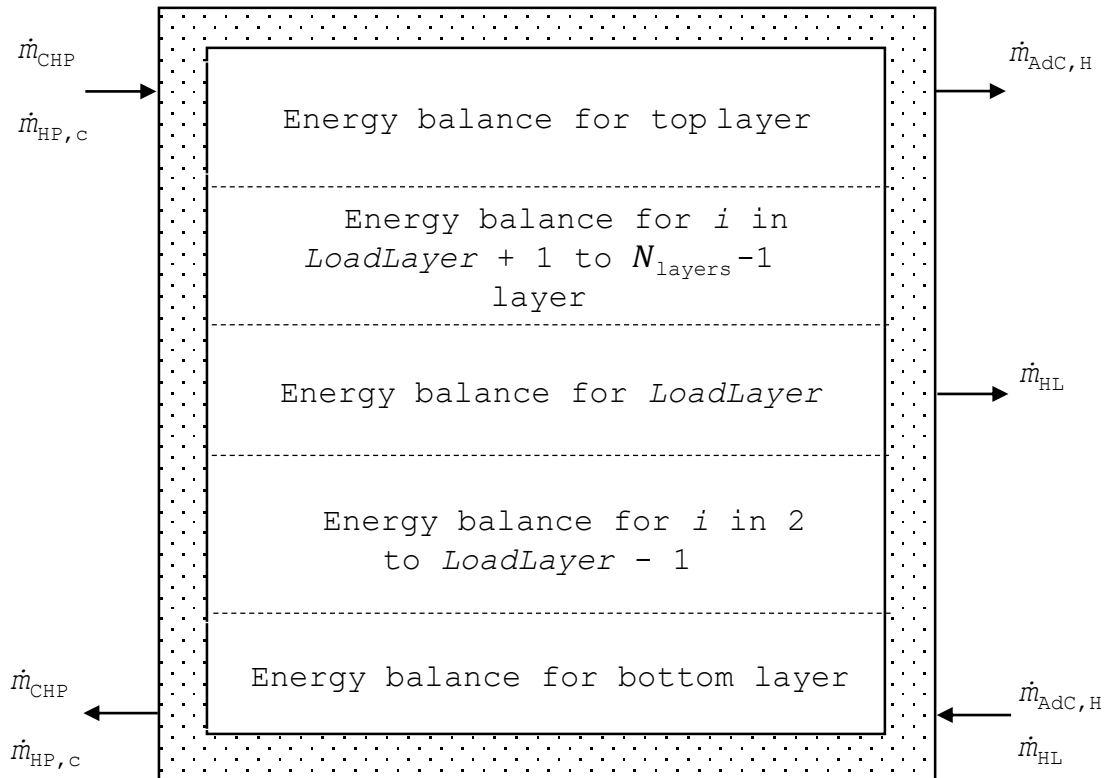
Fig. 4-38 Hydraulic inputs and output of the HTES and modification of tank model based on numerical loops to include a user-defined parameter "Loadlayer"

The model of the CTES was similarly developed but adapted to the reversal of flows between the source and load circuits. The volume flows and layering in the CTES are shown in a schematic diagram in *Fig. 4-39*.
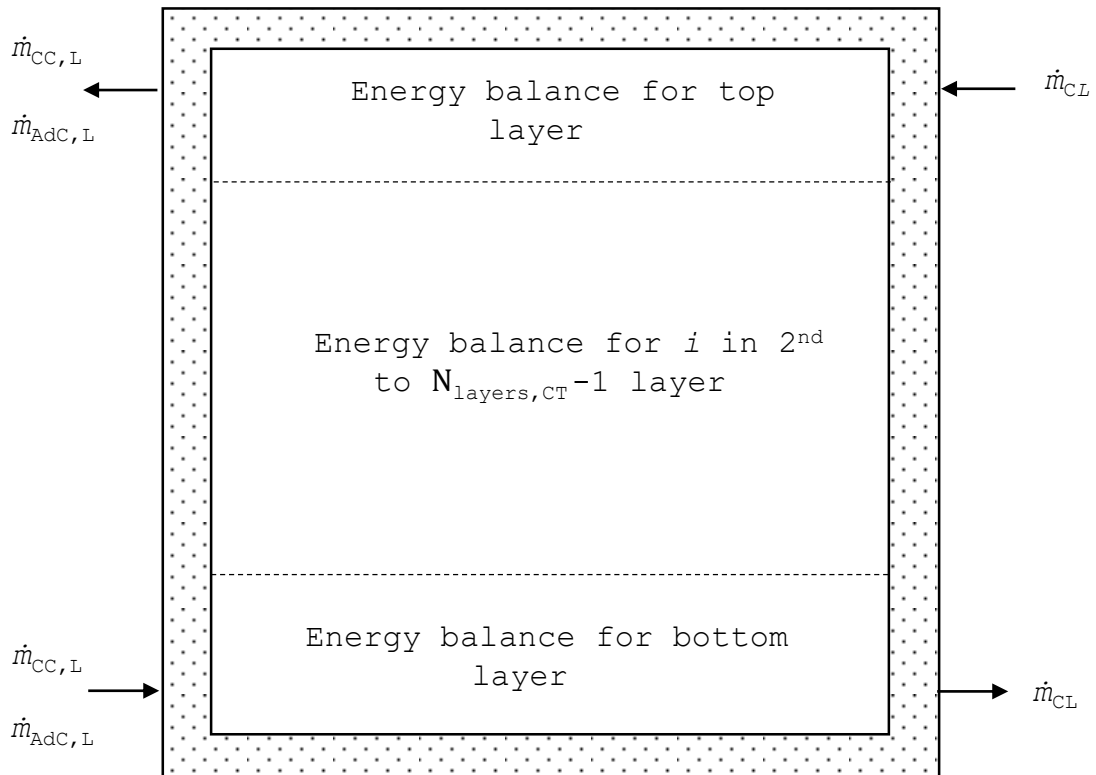
Fig. 4-39 Hydraulic inputs and output of the CTES

4.10   Thermal loads: load generator (LG) and test chamber (TC)

The heating load (HL) and cooling load (CL) are generated by circulation thermostats or load generators (LG) of type "510w" by *Huber Kältemaschinenbau AG* (Huber Kältemaschinenbau AG, 2019) and a thermally activated building system (TABS) by *Uponor GmbH* (Babiak and Vagiannis, 2015).

The LGs are high precision temperature (tolerance 0.01 K) control systems with refrigerated heating circulators. These are ideal for rapid temperature control of externally connected applications and have an internal adaptive control with an automatic switch-over between heating and cooling. The TABS in contrast are a slow heating and cooling system with pipes embedded in the structural concrete slabs or walls of two test chambers (TC) creating a thermal load of $P_{\text{th,TC}}$ (Pfafferott et al., 2016). The $P_{\text{th,TC}}$ is not controlled and reduces as the concrete slabs heated up (cooled down) in winter (summer). This load was calculated using (4.44) with constant mass flow in TC $\dot{m}_{\text{TC}}$ and the actual feed-line temperature going to TC $T_{\text{f,TC}}$.

The $T_{\text{f,TC}}$ was controlled using a three-way mixing valve and the $T_{\text{f,TC,set}}$ was characteristically set between 35 to 40 °C (low temperature heating) or 14 to 16 °C (high temperature cooling) for TABS due to its larger surface area (Pfafferott et al., 2007).

$$P_{\text{th,TC}} = \dot{m}_{\text{TC}} c_{p,\text{w}} \left(T_{\text{f,TC}} - T_{\text{r,TC}} \right) \tag{4.44}$$

The temperature returning from the TC $T_{\text{r,TC}}$ was measured every second and used for the control of the LGs.

4.10.1 LG control

The LGs were controlled over an internal controller using a set-point temperature $T_{\text{f,LG,set}}$ to generate a thermal load $P_{\text{th,LG}}$ such that the $P_{\text{th,HL}}$ or $P_{\text{th,CL}}$ in experiments were as close as possible to their forecasts created in *Section 4.2*. $P_{\text{th,LG}}$ was calculated using (4.45) and (4.46) for summer and winter respectively. In summer the heating capacity of the LGs was used,

$$P_{\text{th,LG}} = P_{\text{th,CL}} - P_{\text{th,TC}} \tag{4.45}$$

while, in winter the cooling capacity was used:

$$P_{\text{th,LG}} = P_{\text{th,HL}} - P_{\text{th,TC}} \tag{4.46}$$

$T_{\text{f,LG,set}}$ was then calculated using (4.47) or (4.48) in summer or winter respectively.

$$T_{f,LG,set} = T_{r,TC} + \frac{P_{th,LG}}{\dot{m}_{TC}c_{p,w}} \qquad (4.47)$$

$$T_{f,LG,set} = T_{r,TC} - \frac{P_{th,LG}}{\dot{m}_{TC}c_{p,w}} \qquad (4.48)$$

4.10.2 Three-way mixing valve control

Since the HL and CL were generated using the HiL set-up with a mixing valve, the models for the loads were developed by applying the first law of thermodynamics and the law of fluid mixing as shown in *Fig. 4-40*.
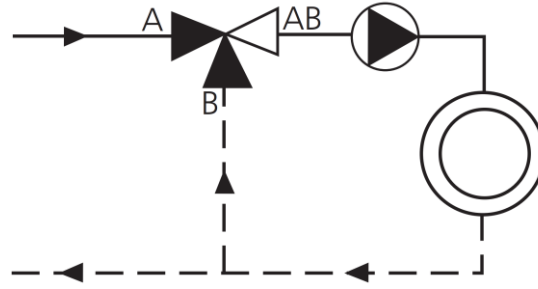
Fig. 4-40 Operation of a three-way mixing valve with fluid mixing

The temperature in mixed circuit AB is given by (4.49).

$$T_{AB} = \frac{\dot{m}_A T_A + \dot{m}_B T_B}{\dot{m}_A + \dot{m}_B} \qquad (4.49)$$

Drawing an analogy to the above figure for the INES test set-up, water was extracted from the respective tanks for heating at $T_{f,HL}$ or cooling at $T_{f,CL}$ in circuit A and mixed with water returning from the loads in circuit B to achieve the set-point temperature $T_{f,TC,set}$ in circuit AB. The information flow diagram for the mixing valve model is shown in *Fig. 4-41*.
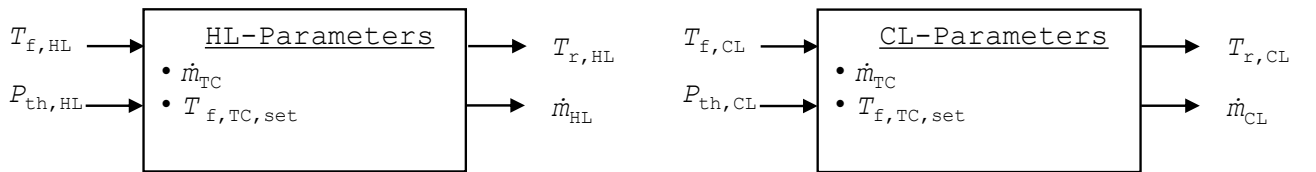
Fig. 4-41 Information flow diagrams for the HL and CL models based on a three-way mixing valve

Under following assumptions:

- the feed line temperature $T_{f,TC,set}$ and mass flow $\dot{m}_{TC}$ in the test chamber circuit is constant,
- the temperature of water returning to the tanks $T_{r,HL}$ or $T_{r,CL}$ is the same as the temperature achieved by the LG ($T_{f,LG,set}$),
- $T_{f,HL} > T_{f,TC,set}$ in winter and $T_{f,TC,set} < T_{f,CL}$ in summer,

and combining (4.45) to (4.49) the mass of water taken from the CTES or HTES for covering loads $P_{th,CL}$ or $P_{th,HL}$ was calculated using (4.50) or (4.51) respectively.

$$\dot{m}_{\text{CL}} = \frac{P_{\text{th,CL}}\dot{m}_{\text{TC}}}{\dot{m}_{\text{TC}}c_{p,\text{w}}(T_{\text{f,TC,set}} - T_{\text{f,CL}}) + P_{\text{th,CL}}} \tag{4.50}$$

$$\dot{m}_{\text{HL}} = \frac{P_{\text{th,HL}}\dot{m}_{\text{TC}}}{\dot{m}_{\text{TC}}c_{p,\text{w}}(T_{\text{f,HL}} - T_{\text{f,TC,set}}) + P_{\text{th,HL}}} \tag{4.51}$$

4.11 Model evaluation results

Examination and qualification of models can be done by using analytical tools, by comparison with other simulations or by empirical tests (Felsmann, 2002). Comprehensive qualitative and quantitative evaluation of the models' performance was done using extensive experiments (step-response tests and long-duration tests) under changing independent variables such as ambient temperatures, initial tank temperatures, load profiles, and control signals. For qualitative evaluation, time-series plots and scatter plots were examined for behaviour consistent with the expected response. For quantitative evaluation, typical model evaluation metrics in the HVAC field were calculated. However, the overall focus for the evaluation was to check if sufficient accuracy was achieved for implementing the models in an optimal scheduling problem and justified their lower complexity. To ensure homogeneity in comparison of simulation and experimental results, the measured values of ambient temperature and thermal loads were input as look-up tables for the simulations.

The Dassl integrator in OpenModelica was applied with a time-step of 60 seconds (experimental data also collected at 60 seconds interval). Conventional control of the machine was simulated and the results were saved onto a CSV file. The tank models were discretised into 10 layers for each temperature sensor. The HT with 9 temperatures sensors was discretised into 90 layers and the CT with 4 sensors was discretised into 40 layers. The load was connected to layer 6 and correspondingly the tank model parameter "*LoadLayer*" was set at 60.

4.11.1 Simulation of operation modes

Examples of time-series plots for simulation tests of the four main operational modes representing all the components are shown in *Fig. 4-42* to *Fig. 4-45*.

Test 1 (AdC operation): A summer electricity production (SEP) was simulated. In this mode, excess heat from the CHP is stored in the HTES and is used to drive the AdC and cool down the CTES. Similar to the experiment, a homogeneous temperature of 60.3 °C in the HTES and 16.6 °C in the CTES was used to initialise the simulation. The AdC model parameters $\dot{v}_{\text{AdC,L}}$, $\dot{v}_{\text{AdC,M}}$, and $\dot{v}_{\text{AdC,H}}$ were set at 1.7 m³/h, 4.3 m³/h and 1.3 m³/h respectively. These values were measured during the functional tests. A control signal of 1.5 V was applied to the OC and the volume flow in the OC circuit was 4.9 m³/h. The AdC was switched on at Time = 0 min and $T_{\text{CT4,min}}$ was set at 12 °C for conventional control of the AdC. A 7-minute average of the circuit temperatures and thermal powers was utilised to filter the noise in the measured data due to the periodic behaviour of the AdC. The results of simulation are shown in *Fig. 4-42.*

Two temperatures in the CTES ($T_{\text{CT1,meas}}$ at the bottom and $T_{\text{CT4,meas}}$ at the top) are shown in *Fig. 4-42 (a).* In addition, three temperatures in the HTES ($T_{\text{HT1,meas}}$, $T_{\text{HT5,meas}}$ & $T_{\text{HT7,meas}}$), with $T_{\text{HT1,meas}}$ being at the bottom of the tank and $T_{\text{HT7,meas}}$ corresponding to the hot feed to the AdC are shown. The stratified cooling of both tanks is observed in reality and in simulation. The simulated values of the HTES temperatures $T_{\text{HT1,sim}}$, $T_{\text{HT5,sim}}$ and $T_{\text{HT7,sim}}$ follow the pattern of the measured values with lower layer cooling first. Similar behaviour is observed for $T_{\text{CT1,sim}}$ and $T_{\text{CT4,sim}}$. A deviation in the range of 1 to 4 K is noted for the tank temperatures. The AdC ran for 110 minutes in reality compared to the 114 minutes in simulation to achieve $T_{\text{CT4,min}}$. This is also observed in the $P_{\text{th,AdC,L,meas}}$ plotted on the secondary y-axis as it becomes zero after 110 minutes whereas the simulated $P_{\text{th,AdC,L,sim}}$ is zero after 114 minutes. As in the experiment, the simulated cooling power reduces over time with the tanks cooling down and more unfavourable conditions for the AdC arise. Although this part-load operation is covered by the model, the cyclic cooling production or change in cycle times is not simulated as observed in the measured values.

The circuit temperatures corresponding to the tank temperatures are plotted in *Fig. 4-42 (b).* The periodic behaviour of the circuit temperatures is not observed in simulation results, but consistent with the assumption, this is noticed to be damped in the tank temperatures. The measured $T_{\text{f,AdC,H,meas}}$ does not follow the typical cyclic pattern after Time = 85 min since the AdC is then operating at highly unfavourable conditions of $T_{\text{r,AdC,H}} < 55°C$ and the internal controller has increased the cycle time. This behaviour is not observed in the simulated results.

The absolute error between simulated and experimental values is 2.5 kWh$_{\text{th}}$ (26% of measured value) for total cooling energy produced and 0.12 kWh$_{\text{el}}$ (37% of measured value) for electrical consumption.
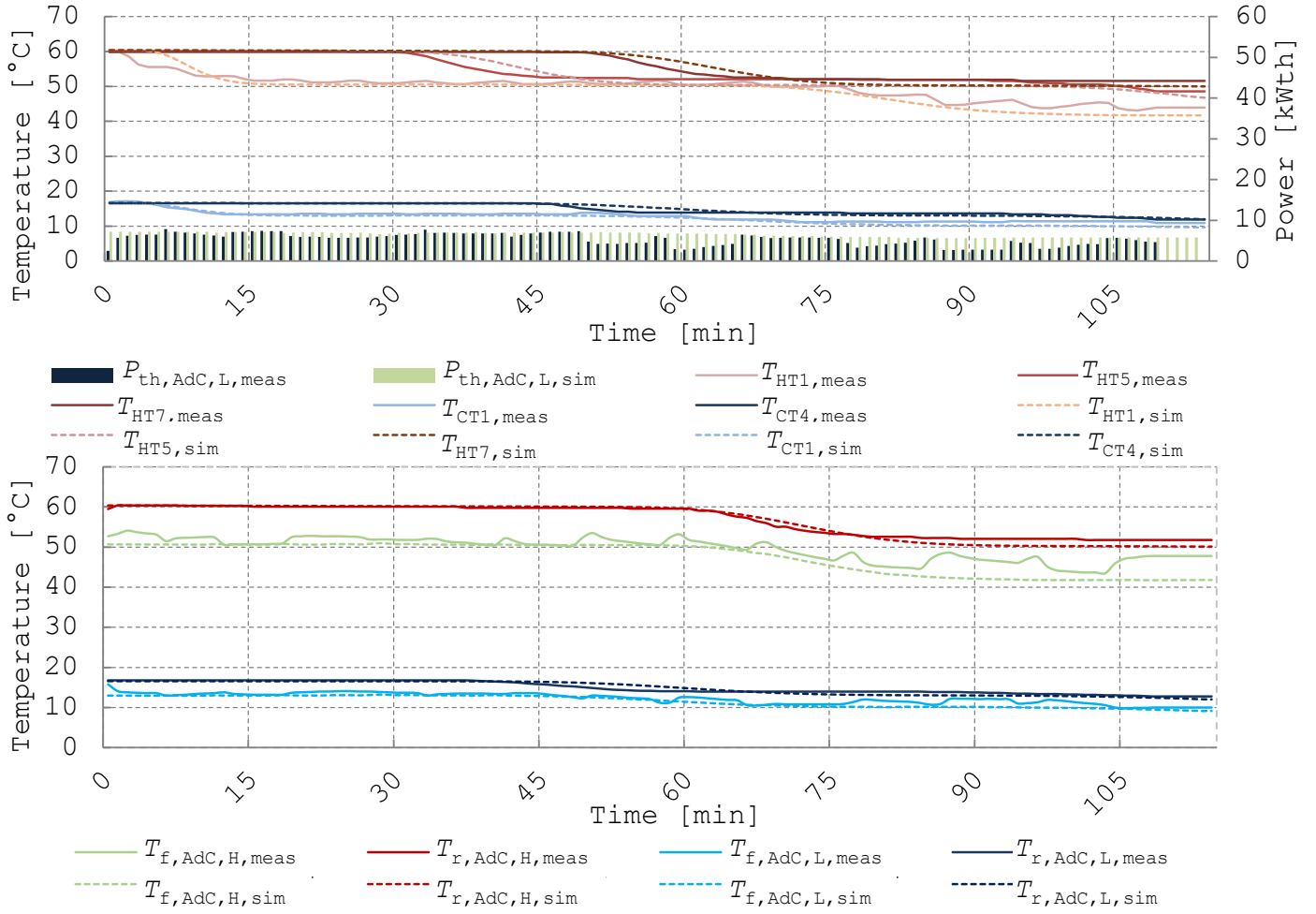
Fig. 4-42 Experimental and simulation data for the SEP mode, (a) Tank temperatures, (b) AdC circuit temperatures. Measured values (solid lines) and simulation results (dashed lines). The AdC was switched on at Time = 0 min

Test 2 (CHP operation): A winter electricity production (WEP) mode was simulated. In this mode, the heat from CHP is stored in the HTES and is used to cover the HL. Similar to the experiment, an initially mixed HTES at 43°C was used for the simulation. The CHP model parameters $P_{el,CHP,nom}$ and $P_{th,CHP,nom}$ were set to 5.3 kW$_{el}$ and 10.5 kW$_{th}$ respectively (*cf. Table 4-1*). $\eta_{el,nom}$ and $\eta_{th,nom}$ were set to 30% and 66% respectively, and the HCV_{fuel} was set as 12 kWh/m³ assuming a gas CHP (Bundesnetzagentur, 2019). The CHP was switched on at Time = 0 min and $T_{HT1,CHP,max}$ was set at 72 °C. The simulation results are shown in *Fig. 4-43*.

Three temperatures in the hot tank ($T_{HT1,meas}$, $T_{HT5,meas}$ & $T_{HT9,meas}$) with $T_{HT1,meas}$ being at the bottom of the tank are shown in *Fig. 4-43 (a)*. A visual comparison shows temperature deviation in the range 1 to 6 K in the HTES temperatures. Thermal stratification behaviour is observed both in the experimental and simulation results. The main outputs of the CHP model are the feedline temperature leaving the CHP $T_{f,CHP,sim}$, the (internally controlled) water volume flow $\dot{v}_{CHP,sim}$, and fuel consumption $\dot{v}_{fuel,sim}$ as shown in *Fig. 4-43 (b)*. Visual analysis shows good accuracy for all outputs in the steady state. The dynamic behaviour of the CHP's thermal power $P_{th,CHP,meas}$ during the start-up phase is also observed in the simulated $P_{th,CHP,sim}$. This deviates from the

measured value by ca. 1 kW$_{th}$ for the first 60 minutes and then a better fit is noticed in steady state.

The simulated electrical power $P_{el,CHP,sim}$ shows a static response whereas the measured $P_{el,CHP,meas}$ displays a quasi-static response. With the hysteresis logic the CHP turns off when $T_{HT1,meas}$ reaches $T_{HT1,CHP,max}$. This occurs after 446 minutes in the experiment and after 453 minutes in the simulation.

Although the simulated thermal power and volume flow do not turn zero due to the dynamic equations, the formulation in (4.5) ensures that no mass flow occurs when the CHP is turned off and hence the HTES is not affected.

The absolute error between simulated and experimental values is 5.5 kWh$_{th}$ (7% of measured value) for total heating energy produced, 2.1 kWh$_{el}$ (5% of measured value) for total electrical energy produced, and 0.02 m^3 (0.1% of measured value) for fuel consumption.
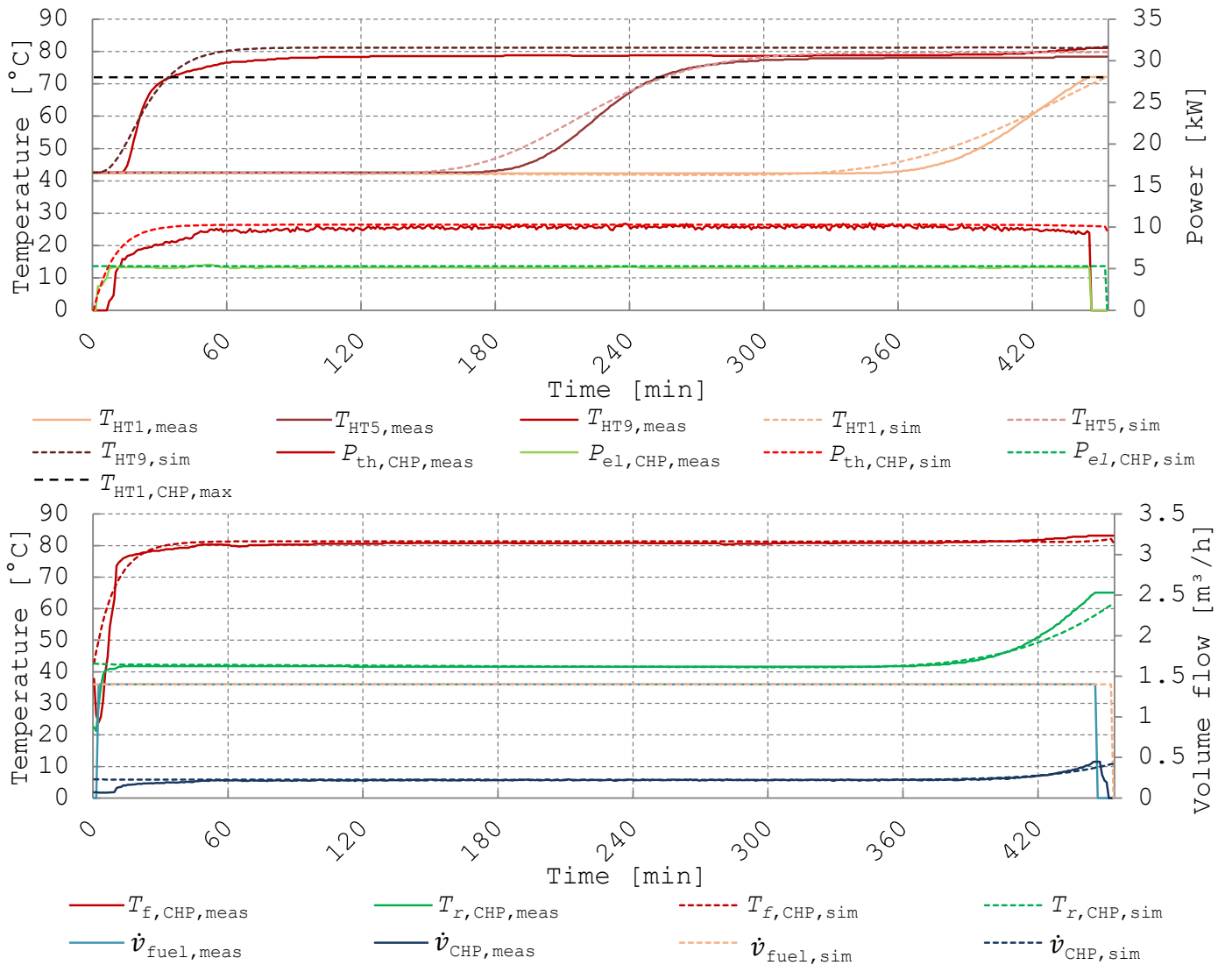
Fig. 4-43 Experimental and simulation results for the WEP mode, (a) HTES temperatures and CHP powers, (b) CHP circuit temperatures and volume flow. Measured values (solid lines) and simulation results (dashed lines). The CHP was switched on at Time = 0 min

Test 3 (CC operation): A summer electricity consumption (SEC) mode was simulated. In this mode, the cooling power of the CC $P_{th,CC,e,meas}$ charges the CTES and satisfies the CL. Similar to the experiment a homogeneous temperature of 28 °C in the CTES was used to initialise the simulation. The CC model parameters $\dot{v}_{CC,c}$ and $\dot{v}_{CC,e}$ were set at 2.6 m^3/h and 2.4 m^3/h respectively as measured during the functional tests. A control signal of 10 V was applied to the OC. The CC was switched on at Time = 0 min and $T_{CT4,min}$ was set at 8 °C.

The four temperatures in the CTES ($T_{CT1,meas}$ to $T_{CT4,meas}$ with $T_{CT1,meas}$ at bottom) are shown in *Fig. 4-44(a)*. Stratified cooling is simulated in the cold tank similar to the real case. Other outputs of the CC model are the chilled water temperature $T_{f,CC,L,sim}$ and the cooling power $P_{th,CC,L,sim}$ as shown in *Fig. 4-44 (a & b)*. Additionally, the circuit temperatures of the OC model are shown.

The OC cools down the $T_{r,OC,meas}$ in its return-line to almost the ambient temperature T_{amb} before feeding it back to the CC as $T_{f,OC,meas}$. This is in accordance to the fact that the OC is operating at its maximum speed due to the 10 V signal. A similar temperature pattern is observed in the OC model output $T_{f,OC,sim}$ shown in *Fig. 4-44 (b)*. A visual comparison shows temperature deviation of less than 2.5 K in the tank temperatures and in the circuit temperatures. The cooling power is over-estimated in the first 60 minutes, as the CTES is warmer than 25 °C. In this particular region, the temperature in the evaporator inlet is outside the range of the curve fit for $P_{th,CC,e,meas}$ (-5 °C to 25 °C) and an inaccurate extrapolation leads to the over-estimation.

$P_{th,CC,e,sim}$ displays static behaviour while $P_{th,CC,e,meas}$ displays a quasi-static behaviour with a relatively short delay time of approx. 1 minute. Another characteristic simulated is the part-load behaviour with decrease in cooling power as the CTES temperatures decrease. In the experiment, the machine ran for 158 minutes and in simulation for 163 minutes before turning off due to achieving set temperature $T_{CT4,min}$. The electrical consumption of the machine during this period $P_{el,RHP,meas}$ is simulated with high accuracy as displayed by $P_{el,RHP,sim}$.

The absolute error between simulated and experimental values is 4.9 kWh$_{th}$ (10% of measured value) for total cooling energy produced and 0.15 kWh$_{el}$ (1% of measured value) for total electrical consumption ($P_{el,RHP} + P_{el,aux} + P_{el,OC}$).
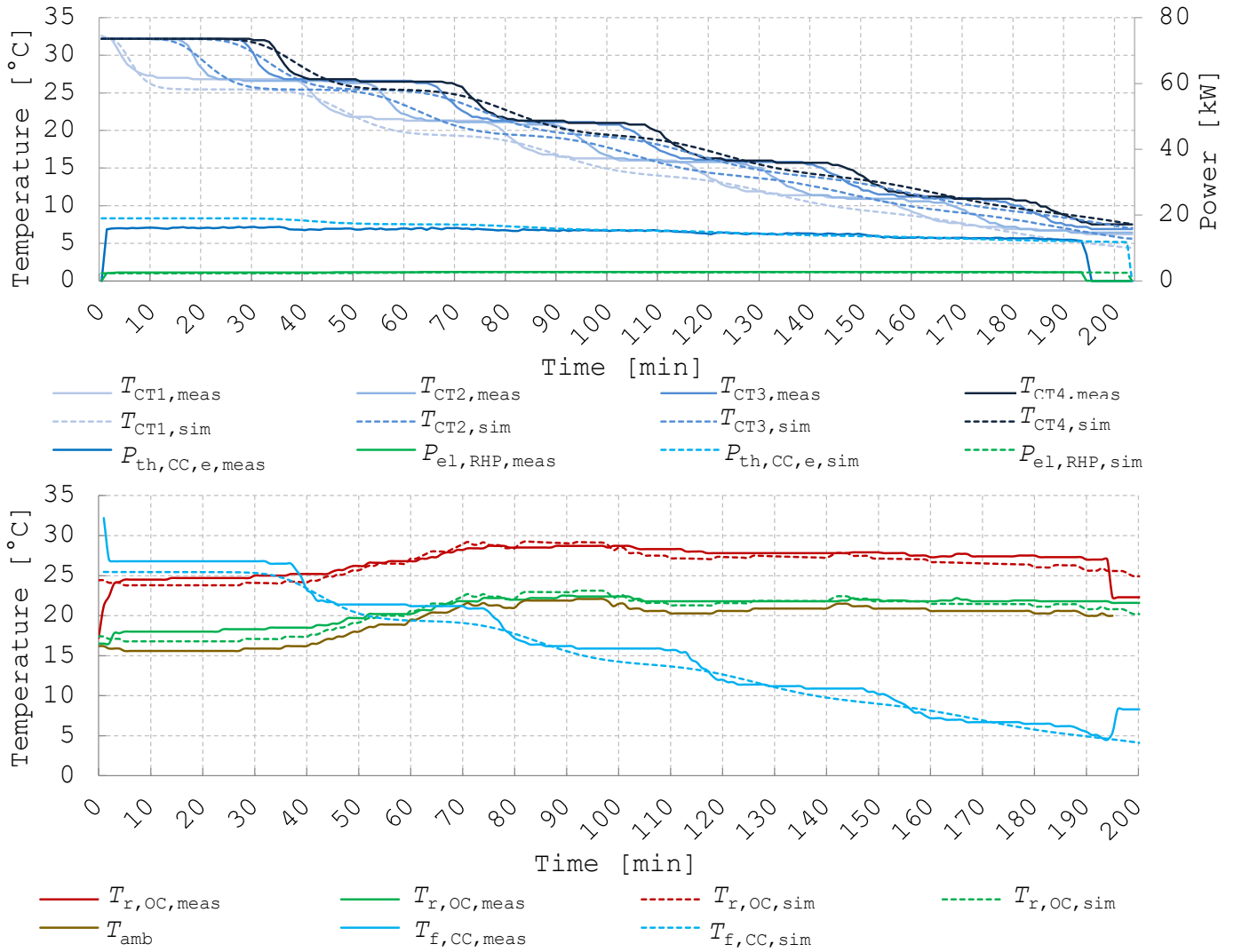
Fig. 4-44 Experimental and simulation results for the SEC mode, (a) CTES temperatures and CC power, (b) CC and OC circuit temperatures. Measured values (solid lines) and simulation results (dashed lines). The CC was switched on at Time = 0 min

Test 4 (HP operation): The winter electricity consumption (WEC) mode was simulated. In this mode, the heating power of the HP $P_{\text{th,HP,c,meas}}$ charges the HTES. In contrast to the previous tests a switching cycle was implemented for the HP, wherein it was switched on at Time = 0 min and after running for 60 minutes it was shut-down for 30 minutes and repeated twice. The switching cycle was also implemented in the simulation with an initial temperature of 20 °C in the HTES. The HP model parameters $\dot{v}_{\text{HP,c}}$ and $\dot{v}_{\text{HP,e}}$ were set to their measured values of 2.7 m³/h and 2.4 m³/h respectively. A control signal of 1.5 V was applied to the OC and the volume flow in the OC circuit $\dot{v}_{\text{OC}}$ was 4.8 m³/h. The simulation results are shown in *Fig. 4-45.*

Three temperatures in the hot tank ($T_{\text{HT1,meas}}$, $T_{\text{HT5,meas}}$ & $T_{\text{HT9,meas}}$) with $T_{\text{HT1,meas}}$ being at the bottom of the tank are shown. Thermal stratification in HTES is observed both in the experimental and simulation results. Furthermore, the quasi-static behaviour of the HP's thermal power $P_{\text{th,HP,c,meas}}$ during each start-up phase is also observed and is modelled as a static behaviour seen in $P_{\text{th,HP,c,sim}}$. The results fit better during steady state operation. The electrical consumption of the machine $P_{\text{el,RHP,meas}}$ is also simulated

with high accuracy as displayed by $P_{\mathrm{el,RHP,sim}}$. In the experiment when the HP turns off the HTES temperatures stay stable since no HL is connected and this is also seen in the simulation results.

The absolute error between simulated and experimental values is 0.34 kWh$_{\mathrm{th}}$ (0.8% of measured value) for total heating energy produced and 0.04 kWh$_{\mathrm{el}}$ (0.2% of measured value) for the total electrical consumption ($P_{\mathrm{el,RHP}} + P_{\mathrm{el,aux}} + P_{\mathrm{el,OC}}$).
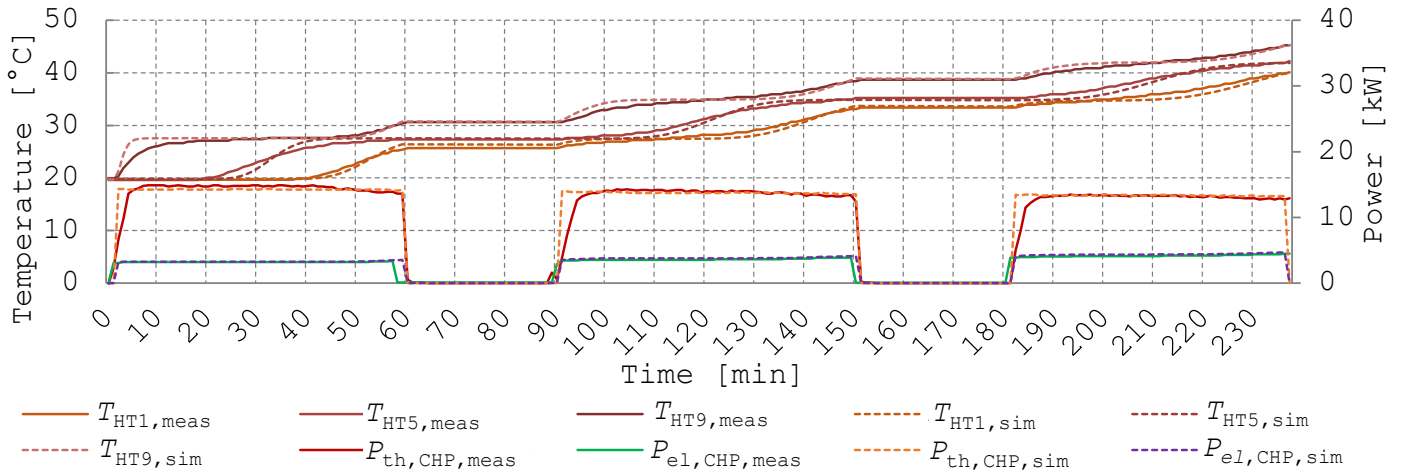
Fig. 4-45 Experimental and simulation results for the WEC mode with HTES temperatures and HP powers for a HP switching schedule(switched on at Time = 0 min, run for 60 minutes, shut-down for 30 minutes, repeat)

4.11.2 Scatter-plots

A scatter plot based analysis for circuit temperatures, tank temperatures, and volume flows was implemented by G. Salvalai to validate a heat pump model (Salvalai, 2012). This was adapted to evaluate the simulation results in this work (but for sake of simplicity only) for tank temperatures because they are the hydraulic and thermal interface between the source and load sides and capture the complex physical interactions in the energy system. Examples of scatter plots for data collected over multiple simulation tests are shown in *Fig. 4-46*. Here, T_{HT5} is analysed for operation modes with heating machines and T_{CT2} for operation modes with chillers.

Data was analysed for 6.5 hours of AdC operation, 20 hours of CHP operation, 8.5 hours of CC operation and 12 hours of HP operation. It is seen that in most cases the estimated value of tank temperatures was within +/- 10% of the measured value. This is considered as an acceptable fit in the proposed qualitative analysis. A higher deviation is observed in the CHP test (*Fig. 4-46* b) when the T_{HT5} is over-estimated and deviates 12 to 14% at temperatures between 45 to 55 °C. For the chillers, a deviation of approx. 15% is observed in the summer scenario at a lower temperature range and amounts to 1.5 K. An inaccurate extrapolation of the curve fit models was observed in this region. The formation of significant thermoclines in the tanks during CHP, CC, and HP operation is noticed in the wave-type illustration of the data points.
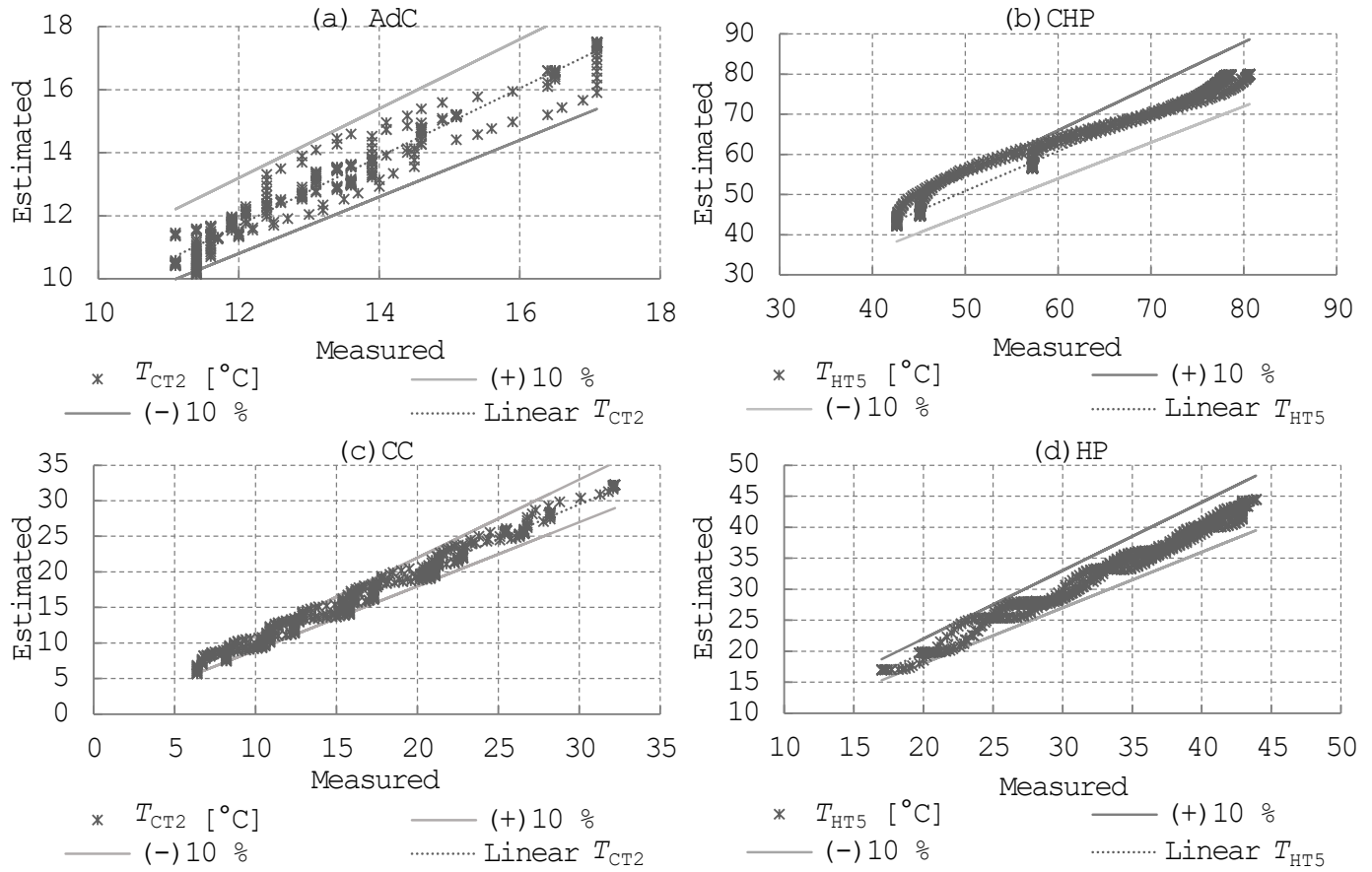
Fig. 4-46 Estimated values versus measured values for the relevant tank temperature and a range of +/- 10% of measured value for (a) AdC, (b) CHP, (c) CC, and (d) HP

4.11.3 Quantitative analysis

For the quantitative analysis, the following commonly used performance indicators or metrics in HVAC simulation were calculated (Afram and Janabi-Sharifi, 2015a):

$$NRMSRE = \sqrt{\frac{\sum_{i=1}^{N}\left(\frac{y_i - y_i^*}{y_{\max} - y_{\min}}\right)^2}{N}} \tag{4.52}$$

$$r^2 = \left(\frac{N\sum_{i=1}^{N} y_i y_i^* - (\sum_{i=1}^{N} y_i)(\sum_{i=1}^{N} y_i^*)}{\sqrt{N(\sum_{i=1}^{N} y_i^2) - (\sum_{i=1}^{N} y_i)^2}\sqrt{N(\sum_{i=1}^{N} y_i^{*2}) - (\sum_{i=1}^{N} y_i^*)^2}}\right)^2 \tag{4.53}$$

$$MAE = \frac{|y_i - y_i^*|}{N} \tag{4.54}$$

where,

$NRMSRE$ - Normalised root mean squared relative error

r^2- Coefficient of determination calculated as square of the Pearson product moment correlation coefficient

MAE- Mean absolute error

N - Number of data points

y_i - ith measured value

y_i^* - ith predicted value

$\bar{y}$ - Arithmetic mean of measured values data set

$\bar{y}^*$ - Arithmetic mean of predicted values data set

y_{max} - Maximum value of y in entire data set

y_{min} - Minimum value of y in entire data set

Experimental data used for fitting the models was not used for their evaluation. The fits are considered good when $NRMSRE$ and MAE are close to zero and r^2 is close to one. Data from 6 hours of AdC tests, 20 hours of CHP tests, 8.5 hours of CC tests and 8 hours of HP tests was accumulated and the evaluation metrics for some of the main model outputs were calculated.
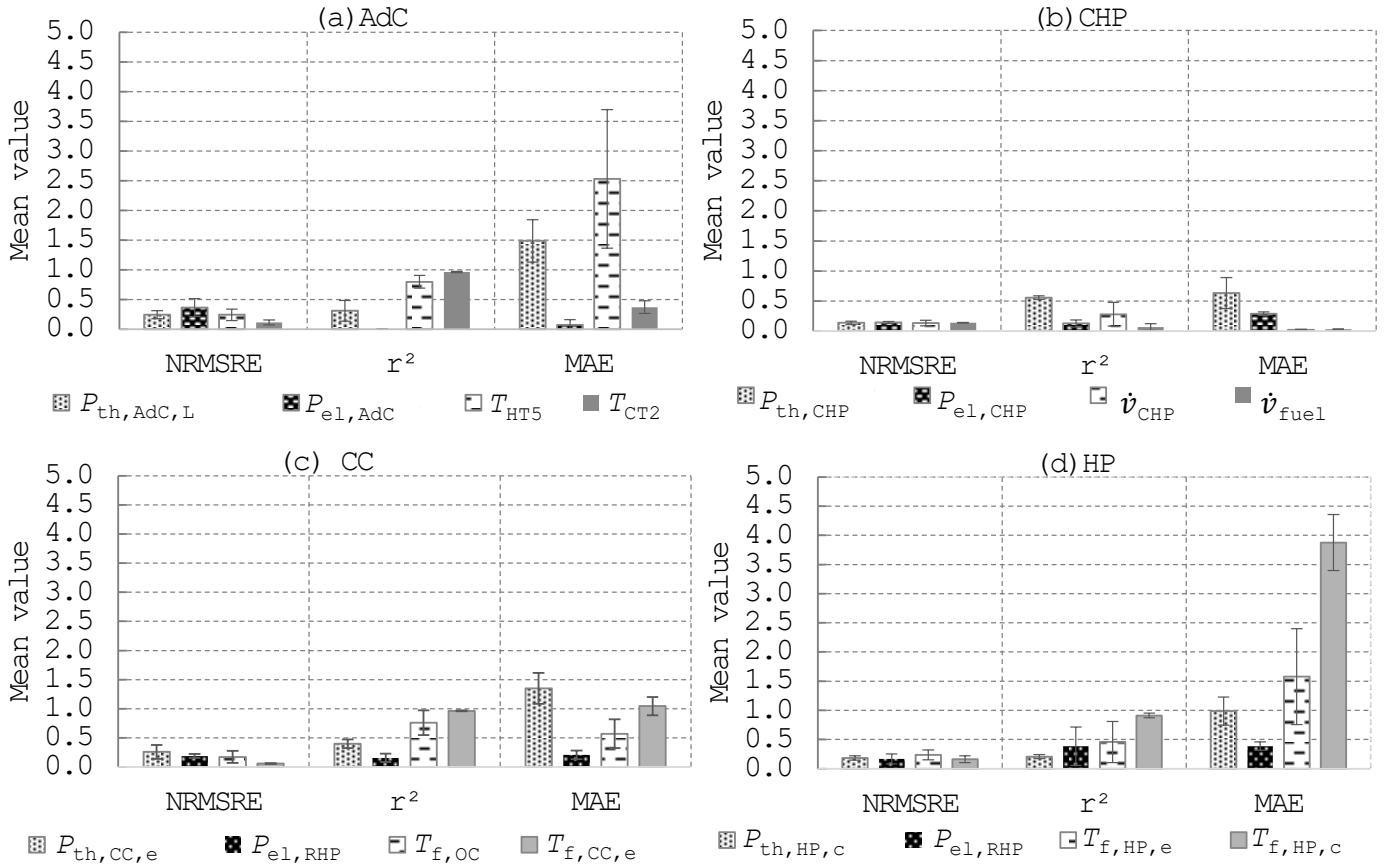
Fig. 4-47 Evaluation metrics for (a) AdC outputs, (b) CHP outputs, (c) CC outputs, and (d) HP outputs

Results of the AdC model are shown in *Fig. 4-47 (a)*. The values for T_{CT2} show best fits with $NRMSRE$ of 0.11, r^2 of 0.96, and MAE of 0.37 K. The direct model outputs, $P_{th,AdC,L}$ and $P_{el,AdC}$ have $NRMSRE$ and $r^2 < 0.4$. Their $MAEs$ are 1.5 kW$_{th}$ and 0.07 kW$_{el}$ respectively. The MAE for T_{HT5} is 2.5 K and has a higher variation in data.

In *Fig. 4-47 (b),* the results of the CHP model are shown. The values for $\dot{v}_{CHP}$ and $\dot{v}_{fuel}$ have $NRMSRE < 0.2$, $r^2 < 0.3$, and $MAE < 0.1$ m^3/h. The power outputs,

$P_{th,CHP}$ and $P_{el,CHP}$ have a *NRMSRE* < 0.2. $P_{th,CHP}$ has a better r^2 than $P_{el,CHP}$. Their *MAEs* are ca. 0.6 kW$_{th}$ and 0.3 kW$_{el}$ respectively.

In *Fig. 4-47 (c)*, the results of the CC model are shown. The chilled water temperature $T_{f,CC,e}$ shows a good fit with *NRMSRE* $= 0.06$, $r^2 = 0.96$, and *MAE* $= 1.04$ K. The $P_{th,CC,e}$ has a *NRMSRE* of 0.25, r^2 of 0.39 and *MAE* of 1.3 kW$_{th}$. One of the main outputs of the OC model ($T_{f,OC}$) working in tandem with the CC is also shown. Its *NRMSRE* is 0.17, r^2 is 0.75 and *MAE* is 0.5 K. More importantly, the electrical consumption $P_{el,RHP}$ also shows agreeable values.

Results of the HP model are shown in *Fig. 4-47 (d)*. The data for $T_{f,HP,c}$ shows a good fit with*NRMSRE* of 0.16, r^2 of 0.91 even though, its *MAE* is 3.8 K. The direct model outputs, $P_{th,HP,c}$ and $T_{f,HP,e}$ have a *NRMSRE* > 0.18 and a $r^2 < 0.5$ and their *MAEs* are 1.0 kW$_{th}$ and 1.6 K respectively. More importantly, the electrical consumption $P_{el,RHP}$ also shows agreeable values with *NRMSRE* < 0.16 and *MAE* < 0.3.

4.11.4 Discussion of simulation results

Results in the time-series plots (*Fig. 4-42* to *Fig. 4-45)* show a good fit of the tank temperatures and other main outputs of the component models in all different modes of operation. This demonstrates the ability of the individual models to work in tandem and simulate the complex hydraulic and thermodynamic interactions in the plant. However, there are certain limitations of the models and possible improvements can be summarised into the following points:

Static models for AdC and RHP: The static models for these components compromise on accuracy, especially for the AdC since the periodic behaviour and start-up cycles are not simulated. However, they benefit from lower complexity needed for application in a MPC based supervisory controller. Furthermore, the static models for AdC and RHP can be justified by the fact that the time-constants of these components are typically smaller than 5 minutes. For plant operations having two to three start-up/shut-down cycles over an entire day, it may not be necessary to model these transient dynamics.

Discretisations of tank volume: The tank model parameter N_{layers} is used to define the number of layers in the tank i.e. the number of discretisations of the tank model. The deviations above the acceptable +/- 10% range noticed in *Fig. 4-46* could be reduced by further discretising the tank volume i.e. reducing the discretisation error. For instance, simulating with 900 layers instead of 90 layers in the HTES as done in this chapter. However, in context of the MPC application, this may add to critical computation costs. On the other hand, fewer discretisations may lead to further loss of accuracy. Ultimately, a balance between model size and accuracy must be made. A separate mathematical analysis for accuracy and speed of computation will be necessary to identify the optimal number of discretisations. For sake of brevity, one layer per temperature sensor in the tanks is used for the MPC application in this work (*see Section 6.1*).

Quality of parameterisation data: The accuracy of individual outputs could be improved further by using more high-quality data for fitting the coefficients and reducing inaccurate extrapolation. Larger steady state datasets, accurate catalogue data, or data generated through optimal experimental design techniques should be used. For instance, the deviation in CC and HP models is partly due to the fitting of capacity curves as functions of the inlet temperatures although the manufacturer data sheets provide data based on outlet temperatures (*cf. Appendix B.2.4*).

Effect of neglecting thermal losses: The general assumption to neglect calculation of thermal losses over the pipes and armatures reduced the accuracy of the results. For instance, the net thermal power of CHP charging the HTES was ca. 10% lower than the nominal power due to thermal losses in the pipes and is reflected in *Fig. 4-47 (b)*. The effect of these losses is not quantified in detail and should be included in future studies either as a physics-based model or as a thermal loss parameter.

No particular metric is suitable for evaluation of all the variables: The $NRMSRE$, r^2 and MAE methods are used for quantitative analysis and the results in *Fig. 4-47* compliment the individual examples in *Fig. 4-42* to *Fig. 4-45.* However, it is seen that no particular metric is suitable for evaluation of all the variables and quantitative analysis should be performed in context of the problem formulation based on the developer's criteria. This is consistent with existing conclusions (Fumo and Rafe Biswas, 2015) that the key performance indicator for assessing quality of the model should be chosen based on the developer's criteria. During the analysis it is observed that $NRMSRE$ and r^2 are sensitive to the errors caused from mismatch of time-series or when neglecting dynamics of components and hence may not be suitable for evaluating powers or volume flows, but acceptable for evaluating tank temperatures. The MAE is easier to justify and interpret in an engineering context since it directly associates with the physical quantity and is more robust to outliers due to the averaging effect. Comparison of the different outputs indicated that a $NRMSRE$ value of less than 0.1, $r^2 > 0.95$ and $MAE < 10$ % of measured value are good fits within the scope of this work.

Sufficient accuracy of models for application in economic-MPC: The MAE for circuit temperatures are in the range of 1.2 to 3.8 K (apprx. 1% to 10% of their typical values) and the MAE for thermal capacities are in the range of 0.6 to 1.5 kW$_{th}$ (6% to 15% of their nominal values). The proposed models of AdC, CHP, and RHP are lesser accurate compared to models in the literature but also have fewer parameters and states. Indeed, they still are accurate enough for system wide simulations as can be deduced by the values for the MAE between measured and simulated values of the final energy consumption and tank temperatures for the different tests as shown in *Table 4-7*.

Table 4-7 MAE between measured and simulated values for final energy consumption and tank temperatures over different tests

Component	Quantity	MAE	Percentage of measured value
AdC	Net electrical consumption	0.08 kWh$_{el}$	36%
CHP	Total fuel consumed	0.21 m³	2%
CC	Net electrical consumption	0.16 kWh$_{el}$	2%
HP	Net electrical consumption	1 kWh$_{el}$	10%
HTES	Temperature in middle of hot tank T_{HT5}	1.29 K	2%
CTES	Temperature in middle of cold tank T_{CT2}	0.5 K	4%

The models are able to depict the consumption of final energy with high accuracy except for the AdC model due to its lower electrical consumption ($P_{el,AdC} = 0.12$ kW$_{el}$). Another important variable from the MPC point of view is the tank temperature (system-state) and this is depicted with high accuracy.

The quantitative and qualitative arguments support the application of the proposed models for system-level simulation of trigeneration plants with multiple components and thermal storages. Additionally, since the limited model errors can be alleviated within the MPC loop and the less complexity and continuous differentiability can be positively exploited, this model set can be applied in optimal scheduling with respect to the energy market. However, they are rendered unsuitable for grid voltage or frequency management based optimal scheduling problems. Furthermore, as the models use promptly available data for parameter identification and reflect internal control and part-load aspects of components, they satisfy the sought-after characteristics for real-world applications.

4.12 Technical limitations of lab and lessons learned

Technical limitations arising due to the design of the components and hydraulic connections in the lab are summarised as lessons learned in this section. Especially, the factors influencing modelling accuracy and correspondingly performance of the MPC are noted with an example. Planning and operational efficiency, model accuracy, and controller stability could be improved in future works by considering these lessons learned. The different points are organised under three main categories:

Construction of storage tanks: Storage is the hydraulic connection between the source and load sides and its external and internal features significantly influence the performance of the system. (a) Due to absence of baffle plates or porous plates at inlets and outlets of the tank, certain turbulence effects could not be hindered. For instance, the fluctuating effect of the periodic behaviour of the AdC in its chilled water circuit and high temperature driving circuit could be observed in the feed-line circuit to the TC and return-line circuit to the CHP respectively. These circuits are connected at the same heights in their corresponding storage tanks (*cf. Appendix B.2.5*). Although the

fluctuation has negligible effect on the corresponding storage tank temperature (*cf. Section 4.5.1*), it adversely affects the control of the mixing valve to maintain a set-point in the TC circuit and the control of the CHP. This behaviour is not captured by the simplified models and also causes complications in measurement of thermal powers in the load and CHP circuit (discussed in *Chapter 7* & *Chapter 8*). The fluctuations could be better mitigated if baffle plates are present instead of developing complex models to capture the AdC dynamics. (b) Due to absence of a load connection at top of hot tank, a part at the top (dead volume) is unusable. For instance, the tank connection for the AdC high temperature circuit is between T_{HT8} and T_{HT7} while T_{HT9} remains unused during most tests. This dead volume is not captured by the models. Either a connection for the demand circuit should be made at the top most part of the tank or a dead volume energy loss parameter should be included in the tank model.

Hydraulic connection for reversible heat pump: The reversible heat pump can operate both as a chiller and a heat pump and its technically defined operation range is between – 10 °C and 20 °C for evaporator inlet and 20 °C and 50 °C for condenser inlet. (a) Due to absence of an anti-freeze solution in the evaporator circuit, the operation of the heat pump at INES is restricted to a lowest permissible evaporator inlet of 10 °C (*cf. Section 4.8*). To ensure a complete range of operation both the circuits must operate with a glycol-water mixture and should be separated from water only circuits using heat exchangers. (b) Due to absence of an internal switch-over mechanism between the chiller and heat pump mode, the switch-over operation was retrofit with external valves, pumps, and heat exchangers. Prior knowledge of the switch-over mechanism for the specific machine should be collected in the functional description documents to avoid expensive, time intensive or sub-optimal retrofits.

Temperature sensors and volume flow in secondary circuit of heat exchangers: For parameterisation of the grey box models, data from commissioning tests and data sheets is used. Due to the absence of instrumentation on the secondary side of the heat exchangers accurate measurements for parameterisation and validation of their models is not facilitated. For instance, due to absence of a flow meter between the hot tank and the heat exchanger in the heat pump condenser circuit the constant volume flow in this circuit (HP model parameter) is estimated and not measured, having adverse effects on model accuracy. During the basic engineering phase, temperature sensors and volume flow meters should be planned on both, primary and secondary side of the heat exchangers.

4.13   Summary and outlook

This chapter described the experimental set-up of the INES trigeneration system and the methodology for developing its *control-oriented models*. The automation level and its communication to the field level is developed in *LabVIEW®*. A description of the plant operation with the nine main components and the *building automation and control* system was made using examples of functional tests. These tests included step-responses, commissioning routines, and long-duration operations and the data was

used to establish the operational parameters of components and interpret their complex interactions from a physical and mechanical perspective. Engineering assumptions and operational constraints were also identified during these tests. Furthermore, the synthesis of thermal load profiles and electricity price profiles to be used in the economic-MPC was illustrated with examples from the literature.

The *grey-box modelling* approach based on *regression analysis* and *step-response analysis* was chosen to model the system. It enables parameter identification using data directly available in the manufacturer's catalogues or commissioning tests and facilitates a balance between required accuracy and complexity of the models. An object-oriented, physical modelling language, *OpenModelica* was used to develop the models and they were tested against experimental data for plausibility and technical feasibility.

A thorough quantitative and qualitative evaluation of the simulation results revealed that the models are capable of capturing part-load characteristics and nonlinear behaviour of the components with sufficient accuracy without compromising on complexity or generalisation capabilities. Accordingly, a simplified form of the model set e.g. substituting the NTU-ε method for the outdoor coil model by curve fits and reduction of second degree models to first degree fits is adapted within a mixed integer optimal control problem for economic-MPC of the system (*cf. Chapter 6.1*).

However, as a proof-of-concept of the INES building automation and control system, a test case demonstration of model based control techniques using only the outdoor coil circuit is done in the next chapter.

5 Test Case with Model Based Controller for the Outdoor Coil

In this chapter, a working illustration for integrating a model based control logic in the building automation and control system is given for developing the understanding of the control architecture. A simplified application scenario with only the fan based outdoor coil or recooler for the compression chiller was selected for this illustration. A standard industrial controller, a PID controller and a model based controller were developed for the recooler and tested in the INES experimental set-up. Performance characteristics e.g. settling time, control difference, and frequency of control actions for the control loop with the three controllers were compared. The model based controller demonstrated energy savings and higher accuracy compared to the standard industrial controller and was easier to set-up than a PID controller.

5.1 The controlled system

The outdoor coil (OC) operates as the heat sink for the condenser of the CC and is the controlled system as shown in *Fig. 5-1*. It includes three variable-speed fan motors consuming a maximum electrical power $P_{el,OC,max}$ of 0.9 kW$_{el}$ when operating at a maximum speed $RPM_{OC,max}$ of 480 RPM. At $RPM_{OC,max}$ the maximum mass flow of air $\dot{m}_{air(max)}$, over a total heat exchanger area $A_{OC} = 521.8$ m^2, is 46,300 kg/h. The actual speed of the fans RPM_{OC} can be controlled with a 0 – 10 volt signal $V_{oc,set}$. The fluid in the circuit is a 34% glycol-water mixture (brine) and has a constant nominal mass flow $\dot{m}_{OC}$ of 2703 kg/h. The ambient temperature sensor T_{amb} is installed near the OC, since the OC is the system interface to the environment. The temperature entering (leaving) the OC from the CC's condenser circuit, $T_{r,OC}$ ($T_{f,OC}$) is measured with a PT-500 sensor and has a delay of approximately 1 minute.
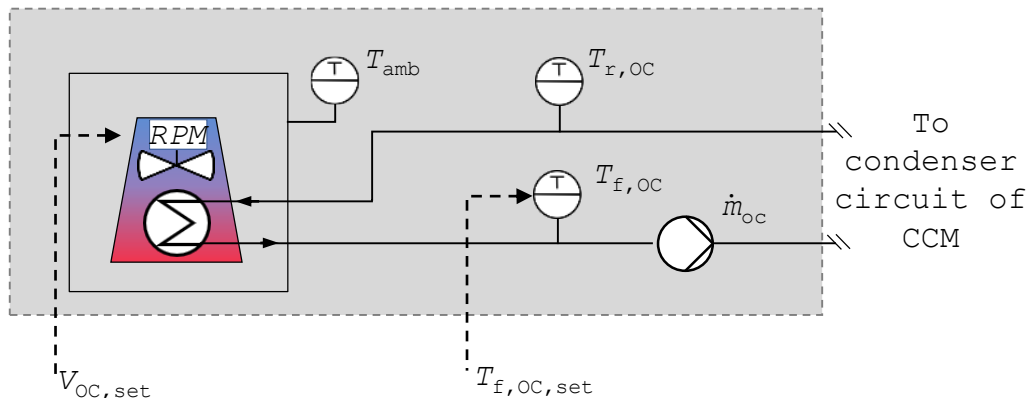
Fig. 5-1 Controlled system for the test case

For this test, the overall heat transfer coefficient U_{OC} was assumed to be constant at 26 W/(m^2·K). The control difference e between controlled variable $T_{f,OC}$ and its set-point $T_{f,OC,set}$ was calculated using (5.1).

$$e = T_{f,OC,set} - T_{f,OC} \qquad (5.1)$$

Table 5-1 shows selective research work done for controlling fan-coils and recoolers in the HVAC field.

Table 5-1 Literature on control of fan-coils and cooling towers in HVAC systems

Reference	Controlled system	Controlled variable	Controller	Research objective
(Bengea et al., 2012)	HVAC system of a medium-size office building in a field demonstration	Room temp.	MPC to optimise a variable volume, dual-duct, multi-zone HVAC unit	Demonstration of optimal control and minimise energy consumption of entire system
(Ma et al., 2009)	Cooling system for a university campus with wet cooling towers, chillers and cold water storage in a simulation	Storage temp.	MPC to decide optimal set-point temperatures and water mass flow rates for chiller and cooling tower	Minimise electricity costs of entire system and maximise COP of entire system
(Hosoz et al., 2011; Soyguder and Alli, 2009)	HVAC systems for two 0.5 m³ chambers in a lab set-up	Room temp.	PID and ANFIS to control damper-rates and fan-speed	Comparison of PID and ANFIS algorithms
(Teitel et al., 2008)	Ventilation fans with a variable-speed drive unit and an on-off unit for a greenhouse and poultry house in a field demonstration	Room temp. and humidity	On-Off and VFD to control fan-speed	Comparison of on-off and VFD algorithms
(Tianyi et al., 2011)	Fan coil units with three speeds and an electric on-off valve for a 10m² area in an experimental set-up	Room temp.	DRFCM to control fan-speed and water mass-flow rate	Minimise energy consumption of entire system
(Wemhoff, 2012)	Two-room HVAC system with a 1.5 kW$_{el}$ chiller and a variable-speed fan in a simulation	Room temp.	PID to control different equipment of the HVAC system	Minimise energy consumption and study the effect of calibration of PID coefficients on energy savings
(Yu and Chan, 2007)	Cooling system with air-cooled chiller and cooling tower with three speeds in a simulation environment	Condenser inlet temp.	MBC to control fan speed of cooling tower	Maximise COP of the chiller

ANFIS (Adaptive Network Based Fuzzy Inference System), DRFCM (Duty Ratio Fuzzy Control Method), VFD (Variable Frequency Drive)

Classical on-off controllers are most widely implemented due to their simplicity but they are unable to control moving processes with delays and can lead to energy wastage especially in transition seasons. Proportional integral derivative (PID) controllers yield promising results but their performance can degrade if the operating conditions of the systems vary from the tuning conditions. Additionally, the tuning of PID controllers can be excessively time-consuming and often requires extensive engineering knowledge of the system (Afram and Janabi-Sharifi, 2014a). There is a lack of practical implementation, evaluation, and comparison of conventional and modern controllers for HVAC recoolers.

5.2 The control loop

A reference controller, a PID controller, and a model based controller (MBC) were developed by applying their basic theoretical concepts without further tuning (Sawant et al., 2020b). A direct comparison of the methodologies was done and the controller design process was evaluated.

The controllers were programmed on the automation level of the BAC system explained in *Chapter 4* and a control loop was formed together with the plant on the field level.

5.2.1 Reference controller

The reference controller implemented in this work applied a $V_{OC,set}$ of 10 V when the OC was on or $V_{OC,set}$ of 0 V when it was off. This simple logic is meant to represent a controller in building systems where the OC is expected to operate at its maximum speed when T_{amb} is more than 25 °C.

5.2.2 PID controller

A PID controller was designed using the *Ziegler-Nicholson* method and implemented using the PID palette from the "Control and Simulation" toolbox in LabVIEW®. The following controlled system characteristics (averaged values) were calculated after performing a step-response analysis by changing the manipulated variable $V_{OC,set}$ from 0 to 10 V at different ambient temperatures ranging from ca. 24 to 28 °C.

- time-constant $T_{s,OC} = 150$ s,
- gain $K_{s,OC} = $ -2.2 K/V,
- delay time $T_{t,OC} = 60$ s.

The characteristics of the PID controller were calculated as follows:

- proportional gain $K_{p,OC} = $ -1.63 V/K,
- integral-action time $T_{n,OC} = 120$ s,
- derivative-action time $T_{v,OC} = 25.2$ s.

The control loop shown in *Fig. 5-2* was set-up in 40 person-hours with intermediate LabVIEW® skills. Most time was needed for the step-response tests and no further tuning was done. A tolerance limit for e was implemented within which the $V_{OC,set}$ did not change to avoid excessive control actions.
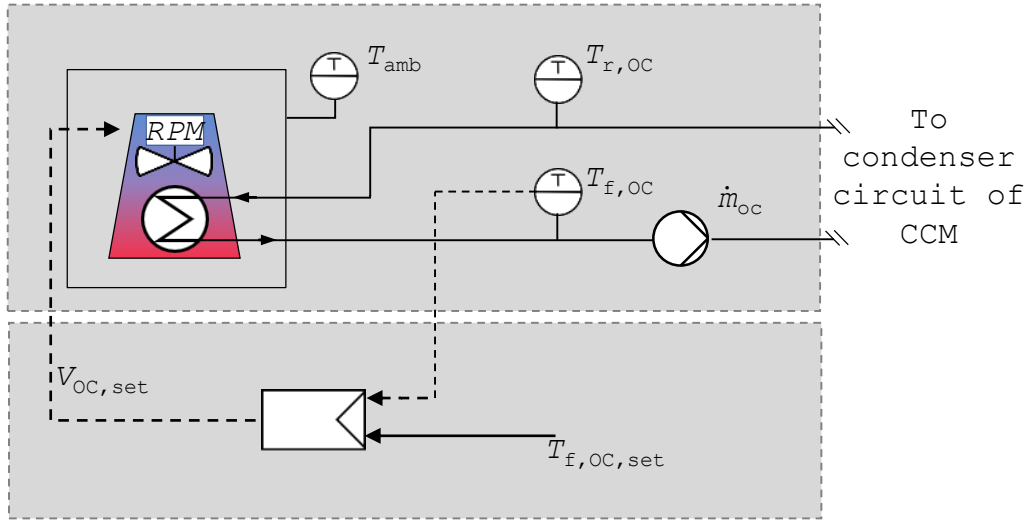
Fig. 5-2 PID control loop

5.2.3 Model based controller (MBC)

The MBC was designed as a simple open-loop controller implemented with the *Mathscript* module in an iterative loop in LabVIEW® and was based on the static NTU-ε model of the OC (*cf. Chapter 4*). The control logic is shown as a flow-chart in *Fig. 5-3*.

Step 1: At a given sampling time, if magnitude of measured error e is greater than tolerance, then the MBC logic is executed in steps 2 to 5 or else, the current $V_{OC,set}$ is repeated for the duration of the sampling time (also called the control time-step).

Step 2: On executing the MBC logic, the controller reads the current measurements of $T_{r,OC}$ and T_{amb} to be used as model inputs and the current $V_{OC,set}$ to be used as the initial control $V_{OC,set,init}$.

Step 3: The OC model is used to calculate the estimated temperature leaving the OC $T_{f,OC,sim}$ and the corresponding estimated error e_{sim} based on inputs from step 2.

Step 4: When magnitude of estimated e_{sim} is greater than tolerance limit, then Step 5 is followed, else the latest value of a virtual control signal $V_{OC,set}^+$ iteratively generated in Step 3 and Step 5 is applied as the real control signal $V_{OC,set}$.

Step 5: If the e_{sim} is negative, then $V_{OC,set}^+$ used in Step 3 is incremented by 0.01 V else, it is decremented by 0.01 V. The new $V_{OC,set}^+$ is coerced between 1 and 10 V and used in Step 2 again. Step 5 is repeated at 100 milliseconds to reduce processor utilisation.
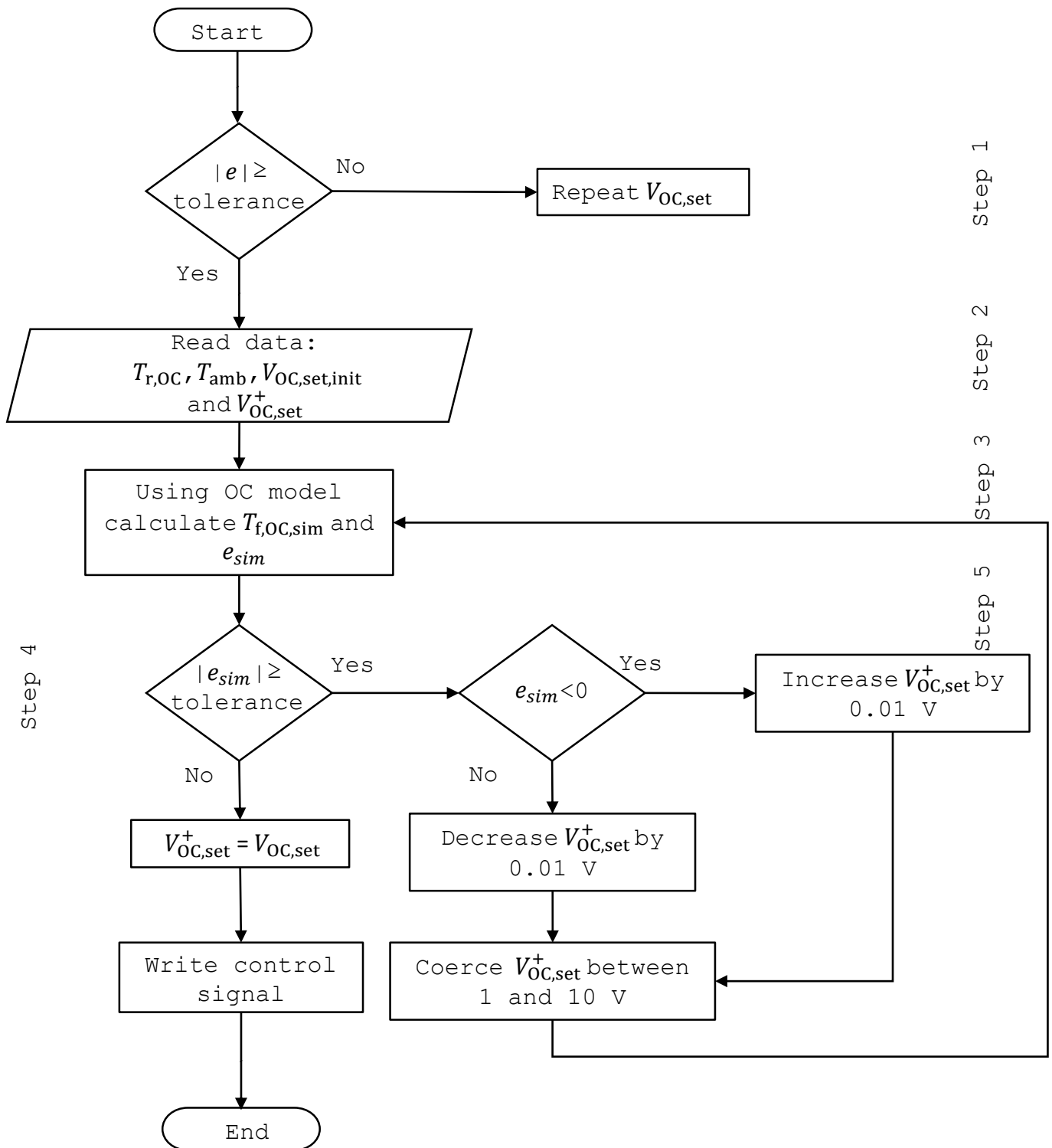
Fig. 5-3 Control logic of the MBC controller

The MBC is an open-loop controller in which the latest value of the controlled variable $T_{f,OC}$ is not fed back into the controller as shown in the control loop in *Fig. 5-4*. The controller was set-up in 0.45 person-hours with intermediate LabVIEW® skills and no further tuning was done. The parameters necessary for the model were directly available in the OC data sheet.
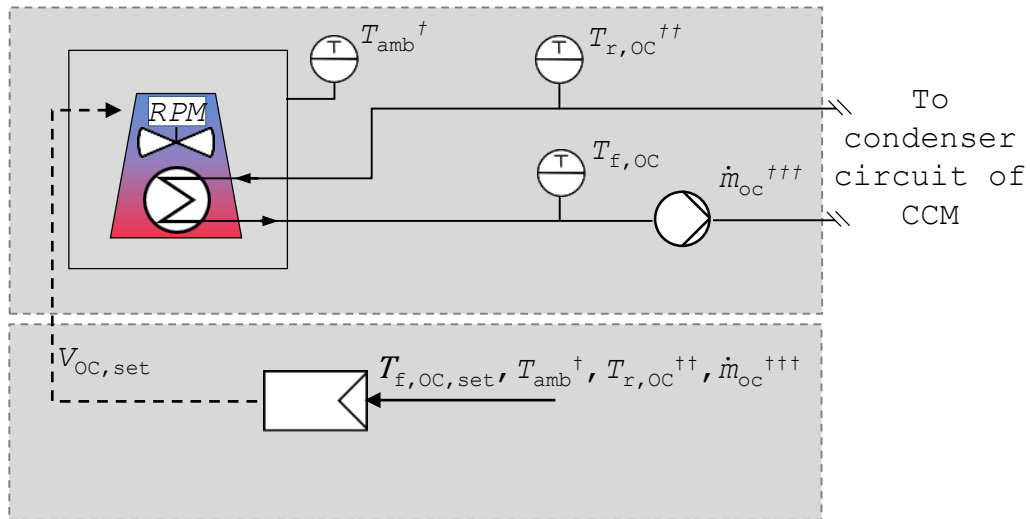
Fig. 5-4 MBC control loop based on the OC model (cf. Chapter 4) and the current measurements $T_{amb}^{\dagger}$, $T_{r,OC}^{\dagger\dagger}$, and $\dot{m}_{OC}^{\dagger\dagger\dagger}$ as its inputs

5.3   Control architecture

The MBC was implemented in a control architecture shown in *Fig. 5-5*. When the algorithm is started by the supervisory controller or manually from the management level, then it is executed in the following steps:

Step 1: The MBC loop is set up by establishing a connection to the OPC server for collecting measured data and generating an initial control value. The initial control value is used for the first iteration of the MBC loop and can be entered manually or the default value of 10 V is used.

Step 2: The MBC control logic shown previously in *Fig. 5-3* is executed to generate the appropriate control signal.

Step 3: The control signal is applied on the field level to the plant (OC) for the duration of time remaining until end of the sampling time. This is calculated by subtracting the time elapsed in Step 2 from the total sampling time.

Step 4: After waiting for time remaining until end of sampling time, the next sampling instance occurs and the measurements of the process variables relevant to the MBC are updated.

Step 5: The updated measurements and the previous control signal are collected as variables and parameters for the MBC loop. These are needed as the initial model inputs and control value.
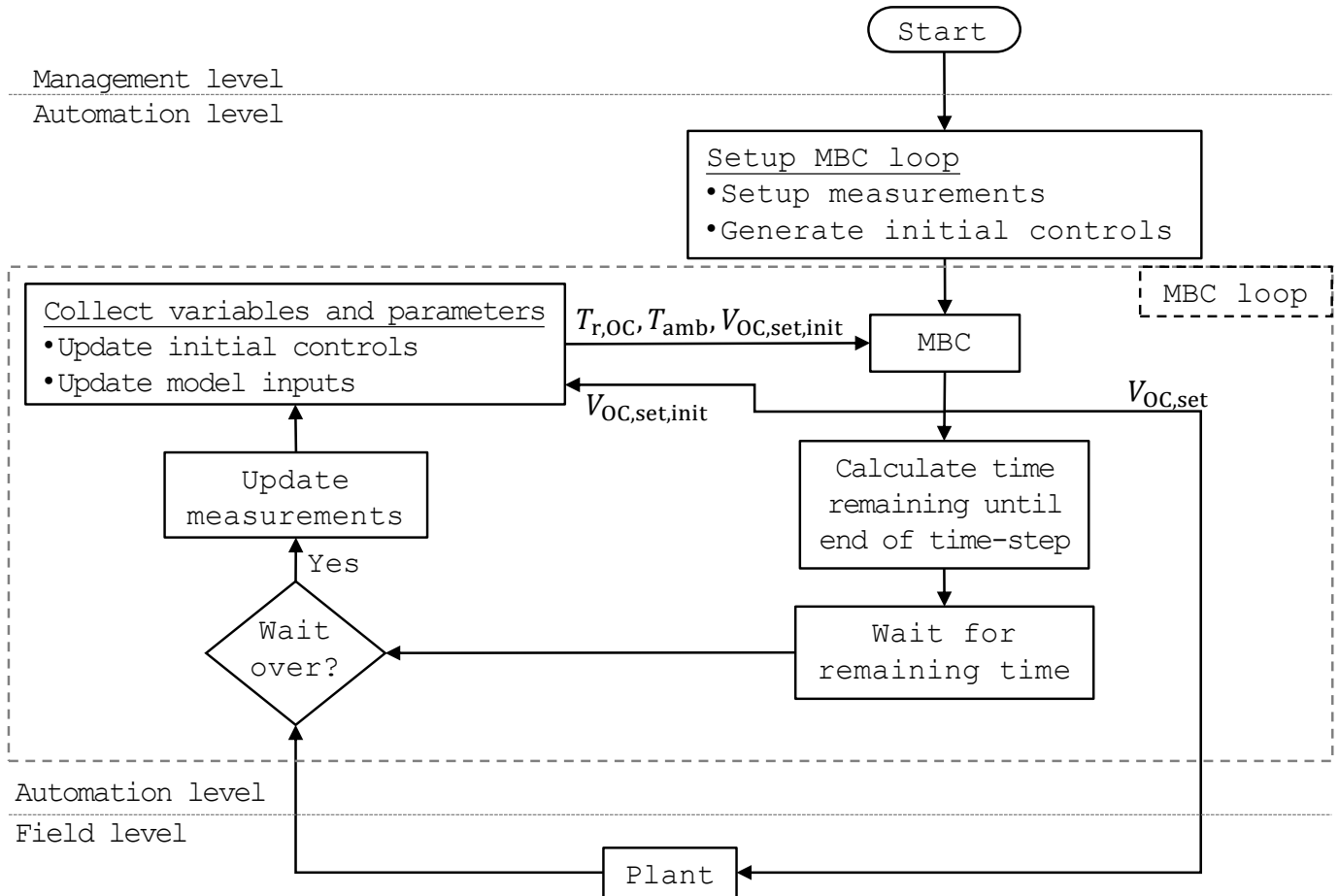
Fig. 5-5 Control architecture to implement the MBC loop in the INES building automation and control system

5.4   Experimental results

Two methods were used to compare the performance and efficiency of the controllers: (a) steady state operation using fixed set-point control, (b) step-response analysis at varying ambient temperatures.

For the first method, a set-point $T_{f,OC,set}$ of 30°C was applied. This value was used in accordance to the datasheet of the CC (Daikin Europe, 2016). A tolerance limit of +/- 0.3 K was implemented for the e in both PID and MBC. The sampling time for the MBC was set at 3 seconds.

The results of a test with approx. 5 hours of steady state operation with the reference controller, PID, and MBC individually is shown in *Fig. 5-6*. The ambient temperature varies between 21 °C and 32 °C and cold tank temperatures are maintained between 25 °C and 26 °C. The reference controller cooled the $T_{f,OC}$ to the ambient temperature regardless of the $T_{f,OC,set}$ whereas, the PID and MBC reasonably maintain the set-point. The $T_{f,OC}$ controlled by PID oscillates at lower ambient temperature and is more stable after T_{amb} is higher than 26 °C while the MBC output stays relatively smooth and continuous throughout.

The electrical consumption of the CC and OC together was 20.03 kWh$_{el}$ for the reference controller, 17.20 kWh$_{el}$ for PID, and 17.29 kWh$_{el}$ for MBC over the 5 hours.
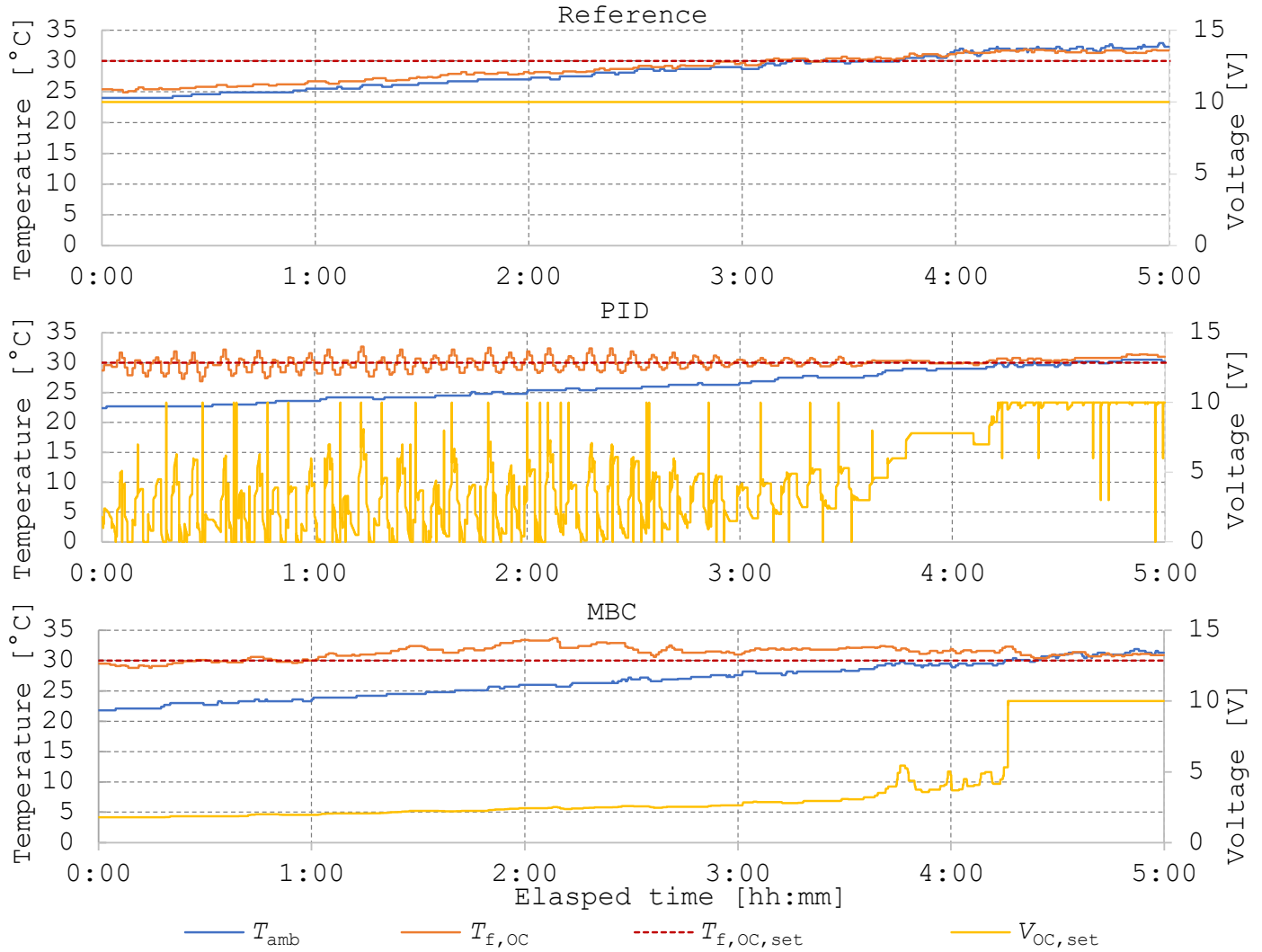
Fig. 5-6 Sample data set for steady state operation with the three controllers

Data from multiple tests was analysed to establish the relationship between the manipulated variable or control signal $V_{OC,set}$ and the interference variable T_{amb} for the three controllers. The average $V_{OC,set}$ was calculated using data points at +/- 0.5 K of the measured T_{amb}.

The results are shown in Fig. 5-7 with error bars representing the standard deviation of $V_{OC,set}$. A larger standard deviation indicates higher fluctuation or change-of-value in the control signal. The PID controller shows steady increase in the control signal with T_{amb} but a larger standard deviation especially at lower ambient temperatures. This is in accordance with behaviour of the PID controller from Fig. 5-6. The MBC volt signal for the OC also increases steadily with the ambient temperature but its magnitude tends to be lesser than the equivalent PID signal. Comparatively, the MBC has lower fluctuation of control actions except at 30 °C since this includes data from 29.5 °C to 30.5 °C. At T_{amb} below 30°C the MBC significantly tries to control the OC to achieve the $T_{f,OC,set}$, however, at T_{amb} above 30 °C the MBC generates a steady 10 V signal. In contrast, the PID takes

inessential control actions at higher ambient temperatures as seen in the standard deviation of the control signal.
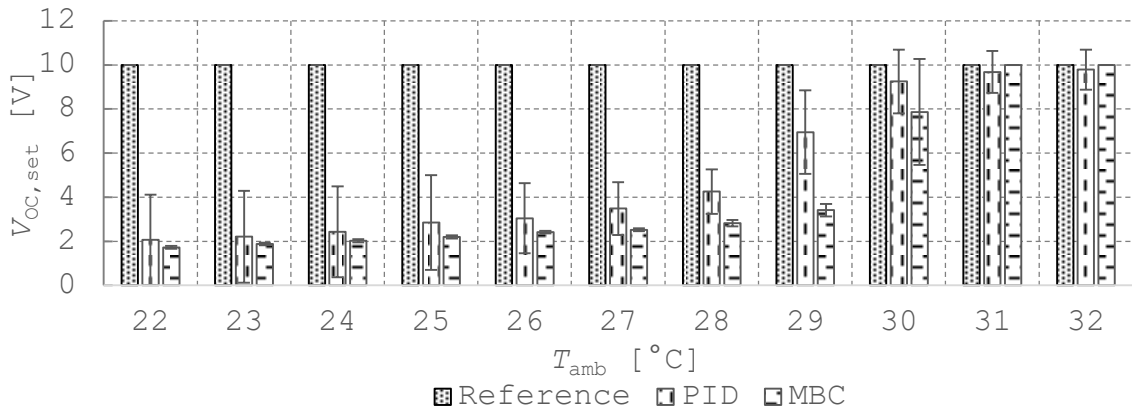
Fig. 5-7 Average control signal values of the three controllers at different ambient temperatures

Additionally, the relationship between the average control difference and the T_{amb} is plotted in *Fig. 5-8*. The reference controller has the highest error at lower ambient temperatures and it decreases as T_{amb} approaches 30 °C. The PID controller has a larger standard deviation but lower average error compared to MBC. The PID is most accurate when T_{amb} lies between 27 °C and 29 °C. The error for MBC is positive at lower T_{amb} when slight overcooling occurs and becomes negative as T_{amb} rises when undercooling occurs.
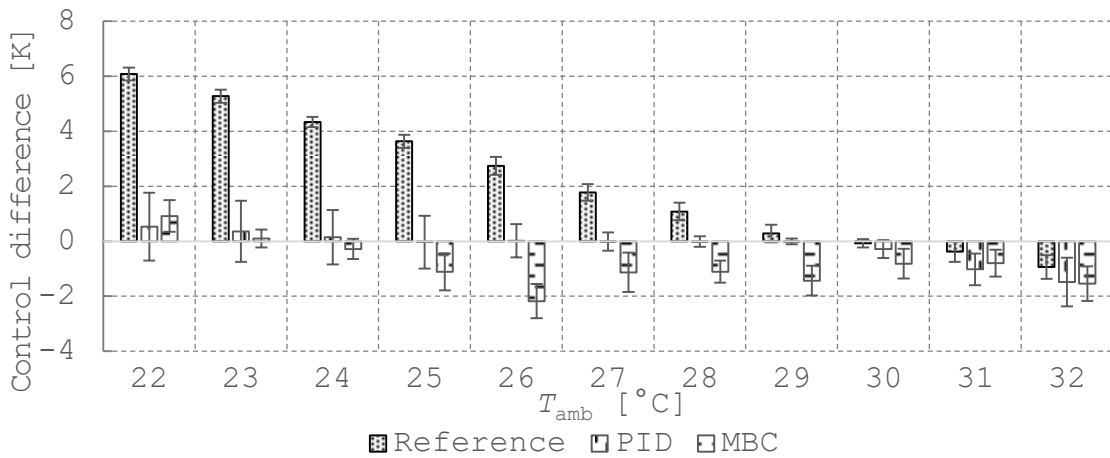
Fig. 5-8 Average control difference with the three controllers at different ambient temperatures

As T_{amb} is greater than 30 °C a negative error is noticed for all controllers, since the dry-cooling OC cannot cool the working fluid below the T_{amb}.

For the second method, a step-response analysis was done to examine the average time-constant of the controllers. In Case-1, a disturbance was introduced by turning off the OC until $T_{f,OC}$ reached 40 °C and then turning it on with $T_{f,OC,set} = 35$ °C. In Case-2, the OC was operated with $V_{OC,set} = 10$ V without a controller until $T_{f,OC}$ reached 25 °C and then a controller was turned on with $T_{f,OC,set} = 30$ °C. *Table 5-2* shows the average results collected for multiple tests of the two cases. In both the cases, the PID was able to respond faster than the MBC by approximately one minute.

Table 5-2 Average time-constant (in seconds) for different step-responses of the respective controlled loop

Case type	PID	MBC
Case-1	131 s	219 s
Case-2	187 s	244 s

5.5   Discussions

The reference conventional controller used in this work was easy to implement and is the standard practice in building HVAC. It is appropriate for the OC to run at maximum speed in summer months with higher ambient temperatures to achieve a set-point close to the ambient temperature. However, during transition seasons, energy is wasted as the medium is over cooled when the set-point is above the cooler ambient temperature as shown in *Fig. 5-6*.

The accuracy of the PID controller was highest for ambient temperatures between 24 °C to 29 °C since it was set-up in this region. Outside this zone, the controller deteriorated but was within acceptable limits of 30 °C +/- 2 K as recommended by the manufacturer of the CC.

The accuracy of MBC was comparable to the PID and stayed within the acceptable limits, while using less fluctuating controller outputs (benefitting the OC hardware). However, the MBC was slower than the PID, which is acceptable only in systems with less fluctuations and more thermal inertia. The speed could be improved by reducing the loop time of 100 ms in Step 5 or increasing the magnitude of correction for $V_{OC,set}^+$, e.g. from 0.01 V to 0.1 V. The $V_{OC,set}$ for the MBC stays constant even when error increases as deduced by the smaller standard deviation of data in *Fig. 5-7*. This occurs since it is an open-loop controller and the assumptions in the OC model lead to inaccuracies.

5.6   Summary and outlook

Three different controllers for the outdoor coil (OC) were programmed on the automation level of the BAC system explained in *Chapter 4* and the resulting control loops were compared in a real-world environment. A conventional controller was compared against a PID and a model based controller (MBC). Following information was collected during the set-up and testing phase:

- Due to absence of a storage element (in this test case) that could be predictively controlled, extension of the MBC to predictive control was considered unnecessary,
- The PID control loop was set-up in 40 person-hours with intermediate LabVIEW® skills whereas the MBC was set-up in 0.45 person hours,
- Multiple step-response tests were necessary for parameterising the PID controller whereas the parameters for the MBC controller were promptly available in the datasheet of the OC,

- The PID and MBC were not only more accurate but also saved 14.5% and 14.1% respectively in electricity consumption,
- A further saving in energy can be expected in transition seasons when the ambient temperature is lower than the set-point of the CC condenser inlet.

Other strengths and weaknesses of the controllers are summarised in *Table 5-3*.

Table 5-3 Summary of strengths and weaknesses of the three controllers

Control	Efforts for set-up	Self-learning capabilities	Accuracy	Fluctuation	Settling time	Energy consumption
Ref.	++	--	--	++	++	--
PID	--	+	++	-	++	+
MBC	+	++	+	+	+	+

"+" = strength, "-" = weakness. Efforts for set-up: time required and practical parameterisation. Fluctuation: Change-of-value of control signal.

MBC shows potential improvement over PID controllers as they are easier to set-up and generalise. These advantages have been reported in the literature and are now experimentally recognised. MBC's accuracy could be improved further by better parameterisation of the model, dynamic modelling of the system, or extending it into a closed-loop controller. These measures should be less complicated and more time-efficient as they are only software related corrections compared to hardware related issues of tuning the PID for different operational ranges and for different conditions or systems. The PID and MBC controllers should be used instead of conventional on-off methods either in green-field or retrofit scenarios to save operating costs and hardware degradation. The experience with setting up the MBC loop using the BAC system and extending the model based approach to use predictive nature of thermal storages is investigated in the next chapter for applying MPC to the entire system.

6   Development of the Optimal Control Framework for the Trigeneration System

The application of a conventional on-off controller, PID controller, and a model based controller for the outdoor coil was shown in the previous chapter. In the test case, the control architecture for implementing a component's model to control its output was demonstrated and basic requirements to apply predictive control were identified. In this chapter, the control architecture is extended to control the entire trigeneration system predictively by including forecasts, an optimisation problem, and physically motivated system constraints. A mixed integer optimal control problem using implicit economic-MPC is developed in a receding horizon scheme. All constraints are relaxed using slack variables to ensure feasibility of the problem and yet have a hardware-friendly operation (*cf. Chapter 3*). The control logic and the architecture are explained in a flow chart while the complex MPC model with system states, constraints, parameters, and controls is also summarised.

6.1   Models and constraints for the MPC problem

The nonlinear grey-box models developed in *Chapter 4* were used to form the *economic-MPC* problem for optimal scheduling of the trigeneration system. Although the models fulfilled necessary characteristics in terms of straightforward parameterisation capabilities and continuous differentiability (*cf. Chapter 3*), they were simplified further before applying in the optimisation routine.

Remark on nonlinearity of models in MPC: The quantification of increasing complexity with increasing nonlinearity of models is possible through certain methods e.g. parametric bootstrap and generalised degrees of freedom (Diehl, 2014b; Steyerberg et al., 2001). However, a common consensus in the research community regarding increasing model nonlinearity (exponential functions or higher degree polynomials) is: (a) the computation efforts for finding global optimums increase, (b) the reliability of nonlinear programming solvers reduces, and (c) the nonlinear systems identification techniques are less effective (Serale et al., 2018; Wang and Ma, 2008).

Model simplification: The models were simplified primarily to reduce their nonlinearity and computation efforts.

- First degree polynomials for curve fits of RHP

The second degree polynomials to calculate the heating power $P_{\text{th,HP,c}}$, cooling power $P_{\text{th,CC,e}}$ and power consumption $P_{\text{el,RHP}}$ of the RHP in (4.31), (4.32), and (4.33) were replaced by first degree polynomials in (6.1), (6.2), and (6.3) respectively:

$$P_{\text{th,HP,c}} = e_1^* + e_2^* T_{\text{r,HP,e}} + e_3^* T_{\text{r,HP,c}} \tag{6.1}$$

$$P_{\text{th,CC,e}} = f_1^* + f_2^* T_{\text{r,CC,e}} + f_3^* T_{\text{r,CC,c}} \tag{6.2}$$

$$P_{\text{el,RHP}} = S_{\text{RHP}}(g_1^* + g_2^* T_{\text{r,RHP,e}} + g_3^* T_{\text{r,RHP,c}}) \tag{6.3}$$

The coefficients of regression e_1^* to e_3^*, f_1^* to f_3^*, and g_1^* to g_3^* were found similarly as in *Chapter 4* and are provided in *Appendix D*. The inaccuracy of the models increased due to the simplification as the sum of normalised squared error for the fits increased from 0.01 for the thermal powers and 0.003 for the electrical input to 0.06 and 0.04 respectively. However, these were assumed acceptable in return for reduction of the model order for the MPC application.

- Curve fits or thermal losses instead of OC and HX models

To avoid the highly nonlinear NTU-ε method for modelling the OC and HX, their models were replaced by curve fits or parameters. The CC evaporator inlet $T_{\text{r,CC,e}}$, which was calculated as an output of the OC model $T_{\text{f,OC}}$ in *Chapter 4*, was replaced by a parameter $T_{\text{f,OC,set}}$ in the CC model. It is in fact the set-point temperature for the PID controller of the OC (*cf. Chapter 5*). Similarly, the OC and HX models were replaced with (6.4) to calculate the inlet in the medium temperature circuit of the AdC, which returns from the OC over the system-separating HX.

$$T_{\text{r,AdC,M}} = h_1 + h_2 T_{\text{amb}} \tag{6.4}$$

The coefficients h_1 and h_2 were included as parameters of the AdC model and were found by regression analysis with data from ca. 130 hours of steady state summer operation (*Appendix D*). The HP evaporator inlet $T_{\text{r,HP,e}}$ coming from the OC was calculated using (6.5) and helped avoid the OC and HX model.

$$T_{\text{r,HP,e}} = T_{\text{amb}} - T_{\text{HX,loss}} \tag{6.5}$$

$T_{\text{HX,loss}}$ was included as a parameter of the HP model and represents a temperature loss over the HP-OC heat exchanger.

The HX on the secondary side of the HP condenser circuit to HTES was replaced by a thermal loss parameter $P_{\text{th,HX,loss}}$ in the HP model. The effective heating power $P_{\text{th,HP,c,eff}}$ was calculated using (6.6).

$$P_{\text{th,HP,c,eff}} = P_{\text{th,HP,c}} - P_{\text{th,HX,loss}} \tag{6.6}$$

Since the OC and HX models were replaced by curve fits the need to evaluate the mass and energy balance in the AdC and RHP medium temperature circuits was not necessary.

- Maximum electrical power consumption of OC $P_{\text{el,OC}}$ in all operation modes

To avoid using the highly nonlinear fan laws for calculating the OC's power consumption $P_{\text{el,OC}}$ it was assumed that the OC operates at its maximum speed $RPM_{\text{OC,max}}$ during all operation modes. This is indeed a reasonable assumption considering the operation of chillers in summer usually requires a greatest possible heat sink and the operation of HP in winter requires a greatest possible heat source.

Additionally, this assumption facilitated for the economic optimisation to solely consider the electrical consumption of the two machines ($P_\text{el,RHP}$ and $P_\text{el,AdC}$) with the OC's consumption being same for both. The $P_\text{el,OC}$ was calculated using (6.7).

$$P_\text{el,OC} = P_\text{el,OC,max}(S_\text{CC} + S_\text{AdC} + S_\text{HP}) \tag{6.7}$$

- Reduced number of layers (discretisations) in HTES and CTES

Since each layer in the tank model is a system state, it would be impractical to implement the HTES and CTES models with 90 and 40 layers respectively (as in *Chapter 4*) in the MPC formulation. Instead, the tanks were simulated with one layer for each temperature sensor installed in the tank (9 for HTES and 4 for CTES) and it was assumed that the sensors are equidistantly placed. This was in accordance to the literature that a simplified stratified tank model suffices for control related applications and gives better results than a completely mixed tank (*cf. Chapter 4*).

- Auxiliary consumption of the plant $P_\text{el,aux}$ during different operational modes

$P_\text{el,aux}$ was calculated as a function of the switches of the components and their corresponding auxiliary consumption, as shown in (6.8).

$$P_\text{el,aux} = P_\text{el,aux,HP}S_\text{HP} + P_\text{el,aux,CC}S_\text{CC} + P_\text{el,aux,AdC}S_\text{AdC} \tag{6.8}$$

The individual auxiliary consumptions were measured during the functional tests of the different operation modes (*cf. Chapter 4*).

Operational constraints: Application oriented constraints were used to avoid running the system under unfavourable conditions such as beyond safety limits or outside the data-range used to fit the models. The constraints were classified as *critical constraints* or *not-critical constraints* for simplification of the optimisation problem.

Critical constraints were defined as constraints whose violation leads to a solution which is not physically implementable on the plant or which leads to a system shut-down requiring a complete manual restart. Critical constraints, e.g. electricity balance or simultaneous operation of two *contradicting machines* were programmed as *hard constraints*. Whereas, the not-critical constraints were defined as constraints whose violation leads to a shut-down by the individual component's internal controller but no manual restart is necessary. They were included as *soft constraints* (Lefort et al., 2013) and *smoothened vanishing constraints* (Jung et al., 2018) using slack variables for numerical stability of the algorithm and also a hardware-friendly operation.

Examples of critical constraints are:

- Constraint on simultaneous operation of two contradicting machines

When the simultaneous operation of two or more machines was not desired, then they were designated as contradicting machines and hydraulically separated. For instance, the simultaneous operation of both chillers, CC and AdC, is restricted. In this case, the binary switches of contradicting machines were used in a hard inequality constraint as shown in (6.9), (6.10), and (6.11).

$$0 \leq S_{CHP} + S_{HP} \leq 1 \tag{6.9}$$

$$0 \leq S_{HP} + S_{CC} \leq 1 \tag{6.10}$$

$$0 \leq S_{CC} + S_{AdC} \leq 1 \tag{6.11}$$

where, $S_{CHP}, S_{HP}, S_{CC},$ and $S_{AdC} \in \{0,1\}$.

The solution provides only physically permissible combinations of the different switches i.e. a permissible operating mode (*see Appendix B.3*)

- Electrical balance

The electrical power balance in the system, irrespective of the operation mode, was framed as an equality constraint shown in (6.12) using two continuous control variables $P_{el,grid,buy}$ and $P_{el,grid,sell}$. They represent the amount of electricity bought from the grid or sold to the grid respectively. The other terms are calculated in the respective component models or are time-varying parameters.

$$P_{el,CHP} + P_{el,grid,buy} = P_{el,EL} + P_{el,RHP} + P_{el,AdC} + P_{el,OC} + P_{el,aux} + P_{el,grid,sell} \tag{6.12}$$

Examples of not-critical constraints are:

- Constraints on HP operation limits

The operation of a HP was limited within the minimum permissible vaporisation pressure and the maximum permissible condensation pressure of the refrigerant (*cf. Chapter 4*). The corresponding temperatures for the evaporator inlet and condenser inlet were used to formulate a smoothened vanishing constraint to restrict the HP's operation outside these temperatures.

$$S_{HP}(T_{r,HP,e,min} - T_{amb} - s_{T_{r,HP,e,min}}) \leq \varepsilon_{T_{r,HP,e,min}} \tag{6.13}$$

$$S_{HP}(T_{r,HP,c} - T_{r,HP,c,max} - s_{T_{r,HP,c,max}}) \leq \varepsilon_{T_{r,HP,c,max}} \tag{6.14}$$

where, $\varepsilon_{T_{r,HP,e,min}} \ll T_{r,HP,e,min}$ and $\varepsilon_{T_{r,HP,c,max}} \ll T_{r,HP,c,max}$. The application of (6.13) ensures that HP operation at ambient temperatures below a user-defined temperature limit $T_{r,HP,e,min}$ is penalised via the slack variable $s_{T_{r,HP,e,min}} \geq 0$ in the cost function. Similarly, the constraint (6.14) ensures that HP operation at condenser inlet temperatures $T_{r,HP,c}$ (corresponding to T_{HT1}) higher than a user-defined temperature limit $T_{r,HP,c,max}$ is penalised via the slack variable $s_{T_{r,HP,c,max}} \geq 0$.

- Constraint on maximum CHP return-line temperature $T_{r,CHP}$

Using a slack variable $s_{T_{r,CHP,max}}$, the formulation in (6.15) ensures that CHP operation is penalised at return-line temperatures $T_{r,CHP}$ (corresponding to $HT1$) higher than a user-defined temperature limit $T_{r,CHP,max}$.

$$S_{CHP}(T_{r,CHP} - T_{r,CHP,max} - s_{T_{r,CHP,max}}) \leq \varepsilon_{T_{r,CHP,max}} \tag{6.15}$$

The violation of this constraint leads to a safety shut-down of the CHP and an automatic restart occurs after the temperature cools down below a pre-set value.

No critical danger is posed to the operation of the MPC architecture but multiple automatic restarts may lead to component failure.

- Constraint on minimum HTES temperature for AdC operation

Using slack variable $s_{T_{r,AdC,H,min}}$, the constraint (6.16) ensures that an AdC operation at driving temperatures (corresponding to T_{HT8}) below a user-defined temperature limit $T_{r,AdC,H,min}$ is penalised in the cost function.

$$S_{AdC}(T_{r,AdC,H,min} - T_{r,AdC,H} - s_{T_{r,AdC,H,min}}) \leq \varepsilon_{T_{r,AdC,H,min}} \tag{6.16}$$

The violation of this constraint leads to low efficiency operation of AdC but no critical shut-down.

- Constraint on system states

The tank temperatures and the dynamic thermal power of CHP were limited within a range by formulating soft constraints (6.17) to (6.22).

$$T_{HT_i} \leq T_{HT_{i,max}} + s_{T_{HT_i}} , \text{for } i \text{ in } 1,\dots,N_{layers,HT} \tag{6.17}$$

$$T_{HT_i} \geq T_{HT_{i,min}} - s_{T_{HT_i}} , \text{for } i \text{ in } 1,\dots,N_{layers,HT} \tag{6.18}$$

$$T_{CT_i} \leq T_{CT_{i,max}} + s_{T_{CT_i}}, \text{for } i \text{ in } 1,\dots,N_{layers,CT} \tag{6.19}$$

$$T_{CT_i} \geq T_{CT_{i,min}} - s_{T_{CT_i}} , \text{for } i \text{ in } 1,\dots,N_{layers,CT} \tag{6.20}$$

$$P_{th,CHP} \leq P_{th,CHP,nom} + s_{P_{th,CHP}} \tag{6.21}$$

$$P_{th,CHP} \geq 0 \tag{6.22}$$

The minimum and maximum permissible temperatures for each layer are time-constant general parameters in the MPC model and $s_{T_{HT_i}}$ and $s_{T_{CT_i}} \in \mathbb{R}, \geq 0$ are their corresponding slacks. Similarly, the non-negative slack $s_{P_{th,CHP}}$ corresponds to the system state $P_{th,CHP}$.

- Constraint on tank temperatures to ensure adequate heating or cooling feed-line temperature

The CTES and HTES temperatures connected to the feed-line in the TC circuit were constrained using slack variables. Inadequate temperature in tanks were penalised using (6.23) and (6.24) respectively.

$$T_{CT1} \leq T_{f,TC,set} + s_{T_{f,TC,set}} \tag{6.23}$$

$$T_{HT,LoadLayer} \geq T_{f,TC,set} - s_{T_{f,TC,set}} \tag{6.24}$$

- Minimum runtime or maximum switching cycles of a machine

Manufacturers of the CHP and RHP recommended maximum switching cycles or minimum runtimes to maintain a longer operational life of the mechanical components. The minimum up-times and down-times of the machines were constrained using

minimum dwell time constraints (Jung et al., 2018) formulated within the *combinatorial integral approximation problem* (*cf. Chapter 3*).

With the setting of minimum runtime constraints typically in the range of 30 to 60 minutes the switching over of modes requiring 140 seconds is assumed irrelevant to be included in the simulation models or the NLP formulation. This is in reference to the assumption made in *Section 4.4.*

The slack variable vector $\boldsymbol{s}$ resulting from the above constraint formulations is summarised in (6.25):

$$\boldsymbol{s}^{\mathrm{T}} =$$
$$[\boldsymbol{s}_{\mathrm{HT}_{\{1,\dots,\mathrm{HT}_N\}}}, \boldsymbol{s}_{\mathrm{CT}_{\{1,\dots,\mathrm{CT}_N\}}}, s_{P_{\mathrm{th,CHP}}}, s_{T_{\mathrm{r,HP,e,min}}}, s_{T_{\mathrm{r,HP,c,max}}}, s_{T_{\mathrm{r,CHP,max}}}, s_{T_{\mathrm{r,AdC,H,min}}}, s_{T_{\mathrm{f,TC,set}}}] \quad (6.25)$$

Summary of models, parameters, constraints, and controls:

The model set from *Chapter 4* and the above simplifications formed an explicit ODE system of type $\dot{x}(t) = f(x(t), u(t), b(t), c(t), p)$. The system states $\boldsymbol{x}$ are thermal power of the CHP and HTES and CTES layer temperatures. The continuous controls $\boldsymbol{u}$ are the electrical power bought from and sold to the grid. The binary controls $\boldsymbol{b}$ are the switches for the four components. The parameter set $\boldsymbol{p}$ comprises of various component model parameters, such as nominal capacities and efficiencies, and also MPC tuning parameters such as maximum tank temperatures used for constraining the optimisation problem. The time-varying parameters $\boldsymbol{c}$ are forecasts for ambient temperature, loads and electricity prices as shown in (6.26) to (6.30).

$$\boldsymbol{x}^{\mathrm{T}} = [P_{\mathrm{th,CHP}}, T_{\mathrm{HT1}}, \dots, T_{\mathrm{HT9}}, T_{\mathrm{CT1}}, \dots, T_{\mathrm{CT4}}], \tag{6.26}$$

$$\boldsymbol{u}^{\mathrm{T}} = [P_{\mathrm{el,grid,buy}}, P_{\mathrm{el,grid,sell}}], \tag{6.27}$$

$$\boldsymbol{b}^{\mathrm{T}} = [S_{\mathrm{CHP}}, S_{\mathrm{HP}}, S_{\mathrm{AdC}}, S_{\mathrm{CC}}], \tag{6.28}$$

$$\boldsymbol{p}^{\mathrm{T}} =$$
$$[c_{p,\mathrm{w}}, \rho_{\mathrm{w}}, \dot{v}_{\mathrm{AdC,L}}, \dot{v}_{\mathrm{AdC,H}}, P_{\mathrm{el,AdC,nom}}, P_{\mathrm{el,CHP,nom}}, P_{\mathrm{th,CHP,nom}}, \eta_{\mathrm{el,nom}}, \eta_{\mathrm{th,nom}}, HCV_{\mathrm{fuel}}, \dot{v}_{\mathrm{HP,c}},$$
$$T_{\mathrm{HX,loss}}, P_{\mathrm{th,HX,loss}}, \dot{v}_{\mathrm{CC,e}}, T_{\mathrm{f,OC,set}}, P_{\mathrm{el,OC,max}}, P_{\mathrm{el,aux}}, D_{\mathrm{HT}}, H_{\mathrm{HT}}, d_{\mathrm{HT}}, N_{\mathrm{layers,HT}}, LoadLayer,$$
$$D_{\mathrm{CT}}, H_{\mathrm{CT}}, d_{\mathrm{CT}}, N_{\mathrm{layers,CT}}, k, \lambda_{\mathrm{eff}}, r_{\mathrm{fuel}}, \dot{m}_{\mathrm{TC}}, T_{\mathrm{f,TC,set}}, T_{\mathrm{r,HP,e,min}}, T_{\mathrm{r,HP,c,max}}, T_{\mathrm{r,CHP,max}},$$
$$T_{\mathrm{r,AdC,H,min}}, \boldsymbol{T}_{\mathrm{HT}i,\mathrm{min}}, \boldsymbol{T}_{\mathrm{HT}i,\mathrm{max}}, \boldsymbol{T}_{\mathrm{CT}i,\mathrm{min}}, \boldsymbol{T}_{\mathrm{CT}i,\mathrm{max}}, \boldsymbol{\varepsilon}, \boldsymbol{W}_{\mathrm{s}}],$$
$$\tag{6.29}$$

$$\boldsymbol{c}^{\mathrm{T}} = [T_{\mathrm{amb}}, P_{\mathrm{th,HL}}, P_{\mathrm{th,CL}}, P_{\mathrm{el,EL}}, r_{\mathrm{el,buy}}, r_{\mathrm{el,sell}}], \tag{6.30}$$

6.2   Economic-MPC problem formulation

The economic-MPC was formulated as a MIOCP with an economic objective and constraints on the operation limits. The following assumptions were made regarding the terms used in the cost function:

- for the operational optimisation of a plant, its investment costs are not of significance especially in a retrofit scenario,

- the consumption related costs for final energies are of more significance in an economic optimisation than the operation and maintenance costs and if necessary the latter can be included in the cost function of an existing framework with relative ease,
- if the minimum up/down time requirements are included as constraints in the MPC problem, then it is redundant to include start-up and shut-down costs in the cost function,
- the tariff for final energies represents an ideal market situation where the complex interactions between energy markets, economic and regulatory frameworks, and status of grid are all captured in the tariff structure.

Although some of the points above are a highly contested field of research, these assumptions lead to a clear simplification of certain highly complex issues with less significance to the end user of such control algorithms, e.g. the logic behind electricity price signals generated by grid operators or the different primary energy factors. Additionally, under the above assumptions the cost-efficient operation of a plant could be considered analogous to its energy efficient operation.

The controller's objective is shown in (6.31a). It is used to find an optimal control sequence that minimises the demand-related costs for final energy as described in *VDI 2067* and penalises violations of the operational constraints. The total demand-related cost is calculated as the integrated CHP fuel costs and the electricity bill over the entire time horizon $t \in [t_0, t_\mathrm{f}]$. The electricity bill comprises of the cost of electricity bought from the grid less the revenues generated by selling electricity to the grid. $\boldsymbol{W}_s$ is an appropriate diagonal weighting matrix $\in \mathbb{R}^{n_s \times n_s}$ reflecting the relative penalisation of slack variables $\boldsymbol{s} \in \mathbb{R}^{n_s}$.

For $t \in [t_0, t_\mathrm{f}]$:

$$\min_{\substack{\mathbf{x}(\cdot),\mathbf{u}(\cdot),\\ \mathbf{b}(\cdot),\mathbf{s}(\cdot)}} \int_{t_0}^{t_\mathrm{f}} (S_{\mathrm{CHP}}(t)\dot{v}_{\mathrm{fuel}}(t)r_{\mathrm{fuel}}(t) + P_{\mathrm{el,grid(buy)}}(t)r_{\mathrm{el,buy}}(t) - P_{\mathrm{el,grid(sell)}}(t)r_{\mathrm{el,sell}}(t)$$
$$+ \boldsymbol{s}(t)^{\mathrm{T}}\boldsymbol{W}_{\mathrm{s}}\boldsymbol{s}(t))\mathrm{d}t$$

$$\text{(6.31a)}$$

subject to:
$$\dot{\boldsymbol{x}}(t) - f(\boldsymbol{x}(t),\boldsymbol{u}(t),\boldsymbol{b}(t),\boldsymbol{c}(t),\boldsymbol{p}) = 0, \tag{6.31b}$$

$$h(\boldsymbol{x}(t),\boldsymbol{u}(t),\boldsymbol{b}(t),\boldsymbol{c}(t),\boldsymbol{s}(t),\boldsymbol{p}) \leq 0, \tag{6.31c}$$

$$\boldsymbol{x}(t_0) - \boldsymbol{x_0} = 0, \tag{6.31d}$$

$$\boldsymbol{u}_{\mathrm{lb}} \leq \boldsymbol{u}(t) \leq \boldsymbol{u}_{\mathrm{ub}}, \tag{6.31e}$$

$$\boldsymbol{s}(t) \geq 0, \tag{6.31f}$$

$$\boldsymbol{b}(t) \in \{0,1\}^{n_b}. \tag{6.31g}$$

The nonlinear system dynamics and nonlinear path constraints are considered in (6.31b) and (6.31c) respectively while the initial state constraint for $\boldsymbol{x_0} \in \mathbb{R}^{n_x}$ is shown in (6.31d). The magnitude of the continuous controls $\boldsymbol{u}(t)$ is bounded by a set of upper

bound values $\mathbf{u}_{ub} \in \mathbb{R}^{n_u}$ and a set of lower bound values $\mathbf{u}_{lb} \in \mathbb{R}^{n_u}$. The switches of the components are the binary controls $\boldsymbol{b}(t)$ that are constrained to take a value either 0 or 1 in (6.31g).

A simplified MPC schematic is shown in *Fig. 6-1* and the entire control architecture is discussed in the next section.
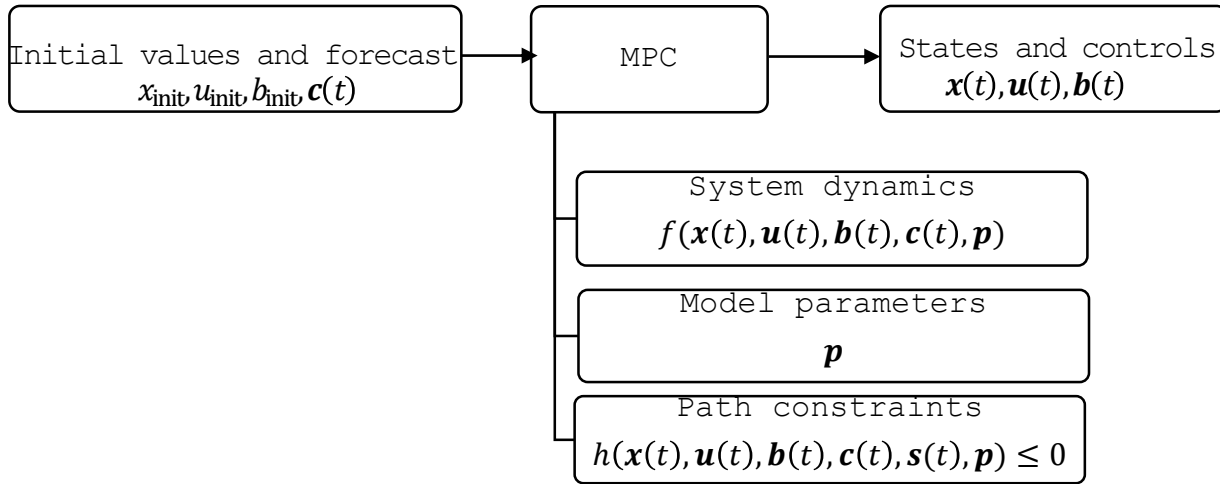
Fig. 6-1 A simplified MPC schematic with inputs and outputs

6.3 Control logic and control architecture

The control logic of the MPC was implemented in the BAC system using the architecture shown in *Fig. 6-2* and the steps involved in its execution are explained below:

Step 1: The MPC loop is built by setting up the time grid (corresponding to prediction horizon and sampling time), the forecast reader, the NLP (formulation in (6.31)), and the NLP solver. Practical initial guesses for states and controls are generated for the entire prediction horizon using the conventional control logic within a simulation.

Step 2: As part of the combinatorial integral approximation method (*cf. Chapter 3*), the NLP is first solved to create an optimal control vector with relaxed binary control variables. The optimal solution comprises of $\boldsymbol{b}_{relx} \in [0,1]$, optimal continuous controls $\boldsymbol{u}_{opt}$, and the states corresponding to that solution $\boldsymbol{x}_{opt}$.

Step 3: If the relaxed solution is feasible then, it is approximated to a strictly binary solution
$\boldsymbol{b}_{aprx} \in \{0,1\}$.

Step 4: Only if both steps 2 and 3 lead to a feasible solution then, the actual $\boldsymbol{b}_{aprx}$ is used as $\boldsymbol{b}_{opt}$ to generate the control signal. However, if an infeasibility or error is reported in the previous steps then, the previous optimal solution is used to generate the control signal. This fall-back mechanism ensures that useful control signals are always provided to the field level even if the solutions of the optimisation problems are not successful.

Step 5: If the actual $\boldsymbol{b}_{\text{opt}}$ is used then, the first element for each component switch from the entire optimal solution vector is identified. Or else, if the previous optimal solution is used then, the component switches corresponding to the current time stamp is identified. The relevant combination of switches is used to generate the corresponding operation mode number (*cf. Appendix B.3*). The time remaining until end of time-step is calculated considering the time needed from Step 2 through Step 5.

Step 6: The operation mode number generated in step 5 is applied as the control signal for the duration of time remaining until end of sampling time. The operation of the plant is realised through the communication structure between the automation level and the field level (*cf. Chapter 4*).

Step 7: After waiting for time remaining until end of sampling time, measurements of the process variables relevant to the MPC are updated and a new prediction horizon shifted by sampling time length is generated.

Step 8: At the next sampling instance, the updated measurements, new forecast, and the previous control signal are collected as variables and parameters for the MPC loop. These are needed as the initial states, initial controls, and time-varying parameters for the NLP. The new NLP is solved again in Step 2 and the process is repeated.

6.4 Programming execution and computation hardware

At the management level of the BAC, all necessary algorithms and data sources were programmed in the *Python 3.7 64-bit* environment using the Scientific Python Development Environment (Spyder 3.3.5). The simulation of system dynamics was done using grey-box models of the components from *Section 4.4* and their further simplifications from *Section 6.1* adapted into the Python environment from OpenModelica. *CasADi* (Andersson et al., 2019) was used via its Python interface for implementation of the system model and the discretized MIOCP. The numerical integration of the models within simulations was done using the *IDAS* solver from the *SUNDIALS* suite (Hindmarsh et al., 2005). The relaxed NLPs were solved by employing *IPOPT* (Wächter and Biegler, 2006) with the linear solver *MUMPS* (Amestoy et al., 2001) in the CasADi environment. The combinatorial integral approximation problem with minimum up/down-time constraint was solved using the tailored branch-and-bound method implemented in *pycombina* (Bürger, 2020). For inputs to the MPC, Python modules such as *Dark Sky API* (Kubis, 2018) for ambient temperature and *epex-scraper* for electricity prices (Roche, 2018) were used. Load profiles were saved as CSV files and input in the MPC framework using *Python Pandas* (McKinney, 2010).

All necessary software, database, and communication protocols were installed on the same workstation computer with an *Intel® Xeon 3.07 GHz* CPU and 8 GB RAM and running a *Windows 10 64-bit* system.

6.5   Summary and outlook

The theory of mixed integer optimal control problems (MIOCP) from *Chapter 3* and results of control-oriented models, forecast values, and the experimental set-up from *Chapter 4* were brought together in the development of an optimisation algorithm for the INES trigeneration system.

Engineering know-how gained during experiments for system analysis and model evaluation was used for simplification of the models making the MIOCP more computationally robust and fast. *Soft constraints* and *smoothened vanishing constraints* were programmed using *slack variables* to increase feasibility of the optimisation problem. Similarly, the *combinatorial integral approximation method* along with *direct collocation* was implemented for faster solutions of the MIOCP problems and acquiring binary control signals for the machines. The optimisation problem was summarised into system states, parameters, binary controls, continuous controls, and slack variables by combining the models, forecast data and component catalogues. These were integrated into the control architecture for implementation of MPC. The setting up of time loops, collecting forecast data, initialisation of the problem, its execution after every sampling time, and application of the optimal control vector was explained in a flowchart.

With the individual blocks for MPC application now in place a full-scale demonstration is given in coming chapters to test the algorithm for its real-time capabilities and industry-oriented application. Examples of individual tests with different types of load and electricity price profiles or different component combinations are shown and discussed.

Start

Step 1

Setup MPC loop:
- Setup time grid
- Setup forecast
- Setup NLP
- Setup NLP solver
- Generate initial controls

Models:
- Parameters
- Equations

$p, f(x(t), u(t), b(t), c(t), p)$

MPC loop

Collect variables and parameters
- Update initial states to time grid
- Update initial controls to time grid
- Update forecast to time grid

Forecasts
- Weather
- Load
- Electricity price

c

$x_{init}, u_{init}, b_{init}, c(t)$

Solve NLP

Step 2

Feasible solution?

No

Yes b_{relx}

Binary approximation

Step 3

b_{aprx}

Apply previous feasible solution

Feasible solution?

No

Step 4

b_{opt}

Yes b_{opt}

x

b_{prev}

Shift time horizon
- Update measurements

Step 8

Generate control signal

Step 5

Calculate time remaining until end of time-step

Control signal (Operation mode)

Yes

Wait over?

Wait for remaining time

Step 7

Management level

Automation level
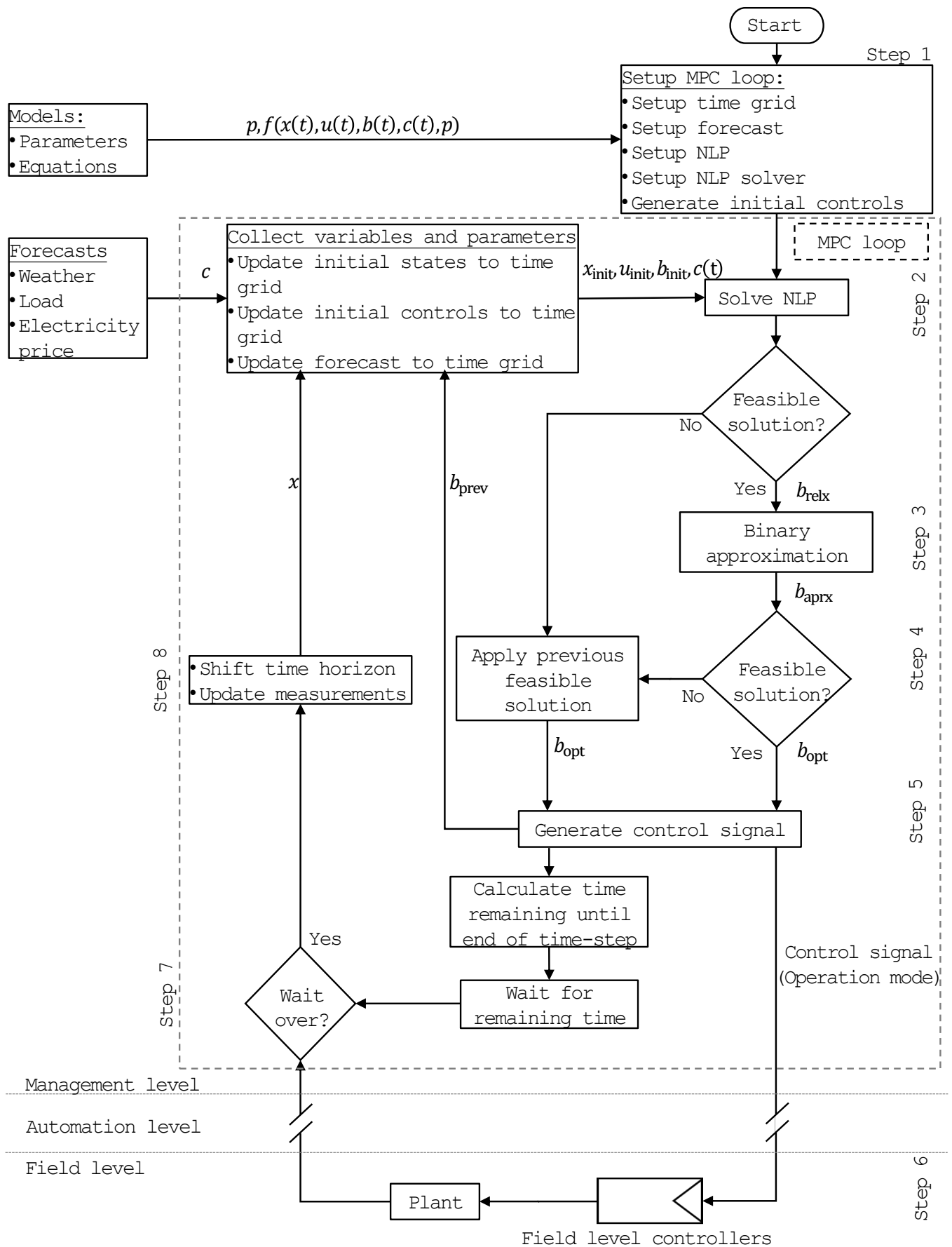
Field level

Plant

Field level controllers

Step 6

Fig. 6-2 Control logic of MPC and control architecture to implement the MPC loop in the INES building automation and control system

7 Experimental Results: Economic-MPC for the Trigeneration System

The energy plant management system for the INES trigeneration system implements an implicit economic-MPC in a receding horizon scheme. At each sampling instance or time-step, the MPC algorithm uses a 24-hour horizon to calculate an optimal solution and simulate the corresponding system response for the entire horizon. It then applies but only the first element of the control signal vector before repeating in loop. A complete demonstration of this scheme is given in this chapter and the MPC's plausibility is evaluated by illustrating and discussing the results of a single MPC iteration, multiple MPC iterations, and the measured values for one example of a long-duration test per season. The shortcomings and potential improvement for application of MPC in optimal scheduling of trigeneration systems are also discussed in this chapter.

7.1 Results of one MPC iteration

The control signal vector or optimal schedule and corresponding results for the 24-hour horizon from one MPC iteration are discussed in this section. One example with a summer scenario and one example with a winter scenario representing typical applications of microscale trigeneration systems and the MPC tuning process are evaluated. Here, the interdependence of different aspects e.g. model output, initial states, constraints, and electricity prices, relevant to control of an energy system is discussed and the plausibility of MPC to provide a solution within this interdependency is demonstrated.

7.1.1 Summer scenario

Table 7-1 summarises the parameters used to implement the summer scenario and to set-up the MPC. These parameters are selected using data sheets of the components and horizon lengths are selected based on standard MPC practices recommended in the literature (*cf. Chapter 3.3 and Chapter 4.1*).

The control signal vector from one MPC iteration comprises of the switching sequence for the four machines (i.e. CHP, HP, AdC, and CC) over the entire horizon and is shown in *Fig. 7-1 (a)*. Additionally, the results of the thermal balance, electrical balance, and tank temperatures corresponding to this binary control signal are shown in *Fig. 7-1(b–c)*.

The computation time for this iteration was 15 seconds and the significant results of a plausibility check in each subplot are explained in the following:

Optimal solution maintains minimum up/down time and simultaneous switching constraints: The relaxed solution for the CHP $S_{CHP,relx}$, CC $S_{CC,relx}$, and AdC $S_{AdC,relx}$ is between 0.3 to 0.6 and it is 0.0 for the HP's relaxed solution $S_{HP,relx}$. These relaxed solutions respect the hard constraint (e.g. $0 \leq S_{CC,relx} + S_{AdC,relx} \leq 1$) programmed in *Chapter 6* to avoid simultaneous switching of two contradicting machines. The binary

solutions also respect this constraint due to the optimisation routine within pycombina. Additionally, the minimum up/down times are maintained as the CHP and AdC remain on or off for at least 1 hour while the CC remains on or off for at least 0.5 hours. As expected, the HP is not activated in summer.

CC and AdC's operation is reactive to electricity price and cold tank is charged predictively to support peak cooling load: For lower electricity buying price $r_{el,buy}$, the CC's operation is induced (increasing $S_{CC,relx}$) and AdC's is reduced (reducing $S_{AdC,relx}$) and the cold tank is charged. Between 20 to 24 hours on the predicted horizon the CC's operation is reduced (reducing $S_{CC,relx}$) and AdC is induced (increasing $S_{AdC,relx}$) as the $r_{el,buy}$ is higher. Energy from the previously charged cold tank is used to satisfy higher cooling load during the peak hours.

Table 7-1[1] Data for the time-varying parameters and constant parameters used to define a sample summer scenario for one MPC iteration

Parameter	Data		Parameter	Data
For implementing the scenario:			$T_{r,CHP,max}$	73 °C
Forecast T_{amb}	Historical data		$T_{r,AdC,H,min}$	55 °C
Load forecast	Hospital load, scaling between 12 kW$_{th}$ and 2.7 kW$_{th}$		**For MPC set-up:**	
Elec. price forecast	Two-price tariff, $r_{el,buy,EWERK}$		Forecast horizon	24 hours
For model set-up:			Time grid	Varying length
HCV_{fuel}	12 kWh/m³ (Bundesnetzagentur, 2019)		NLP solver	IPOPT, MUMPS, adaptive strategy
r_{fuel}	0.72 €/m³ (Bundesnetzagentur, 2019)		IPOPT acceptable tolerance	0.01
$T_{f,OC,set}$	30°C		IPOPT max. CPU time	30 s
$T_{HX,loss}$	2 K		$\varepsilon_{T_{r,HP,e,min}}$, $\varepsilon_{T_{r,HP,c,max}}$, $\varepsilon_{T_{r,CHP,max}}$, $\varepsilon_{T_{r,AdC,H,min}}$	0.1
$P_{th,HX,loss}$	1 kW$_{th}$		W_s	1
$\dot{v}_{TC}$	1.2 m³/h		Pycombina max. CPU time	30 s
$T_{f,TC,set}$	14 °C		Min. up/down time	1 h for CHP and AdC 0.5 h for HP and CC
For operational constraints:			Initial tank temp. [°C]	$[T_{HT1}...T_{HT9}]$ = [65...80] $[T_{CT1}...T_{CT4}]$ = [10...12]
$T_{HTi,max}$	95 °C		Initial controls	CHP and AdC = On CC and HP = Off
$T_{HTi,min}$	5 °C		Initial state vector	Conventional control simulation
$T_{CTi,max}$	30 °C			
$T_{CTi,min}$	5 °C			

Varying time-steps: The varying time-grid or time-steps of 5 minutes for the first 15 minutes and then 15 minutes for the remaining 23 hours and 45 minutes is observed in

---

[1] Parameters defined in Chapter 4 to 6 are not included

Fig. 7-1 (b-d). For the first 15 minutes, three 5-minute discretisations are calculated and for the remaining time, ninety-five 15-minute discretisations are calculated.

Dynamic behaviour of CHP's thermal output and part-load behaviour of AdC's cooling power is observed in thermal (heating) balance: The dynamic behaviour of $P_{th,CHP}$ is simulated as it takes two to three 15-minute discretisations for reaching its nominal value of ca. 10.5 kW$_{th}$ after the CHP is switched on. The $P_{th,AdC,H}$ is higher when the AdC is switched on and then reduces with decreasing HTES temperature due to part-load operation. Additionally, there is no heating load $P_{th,HL}$ or thermal power of the HP $P_{th,HP,H}$, as expected during this summer test. The discharge of HTES occurs due to $P_{th,AdC,H}$ and is balanced by the thermal power of the CHP $P_{th,CHP}$ and the power consumed from the hot tank $P_{th,HT}$ at a particular instant. Negative $P_{th,CHP}$ indicates the power stored in the HTES and results in increase of the tank temperature.

Static behaviour and part-load behaviour of CC's and AdC's cooling power is observed in thermal (cooling) balance: The CC's cooling power $P_{th,CC,e}$ and AdC's cooling power $P_{th,AdC,L}$ display static behaviour as they reach their maximum output immediately after starting the machine. Their part-load operation depending on inlet temperatures (tank temperatures) is also simulated. For instance, $P_{th,AdC,L}$ is greater when the machine begins operation under favourable conditions of higher HTES and CTES temperatures and reduces when driving temperature reduces in HTES and CTES also cools down.

Lower cooling load during the night and higher cooling load during the day is forecasted in accordance to hospital operations: The cooling load forecast $P_{th,CL}$ is input from a database and is predicted to be lower during the night (Time = 4 to 15 h) and increase during the day (Time = 15 h) with a peak of ca. 12 kW$_{th}$ during the afternoon at 14:00 (Time = 22 h). This load is balanced by $P_{th,CC,e}$ or $P_{th,AdC,L}$ in combination with the power from the cold tank at a particular instant $P_{th,CT}$. A negative cooling power indicates the power stored in the CTES and results in decrease of the tank temperature.

CHP operation is reactive to electricity price and long peak electrical loads are avoided: The total electrical load $P_{el,EL,total}$ comprises of the reference (imaginary) load from a database and actual requirements of the machines. The $P_{el,EL,total}$ is satisfied by the electrical power of the CHP $P_{el,CHP}$ and electricity bought from grid $P_{el,grid,buy}$. Negative $P_{el,CHP}$ represents the electricity sold to the grid $P_{el,grid,sell}$. The generation of peaks is avoided and operation of CHP is favoured especially during times of high $r_{el,buy}$.
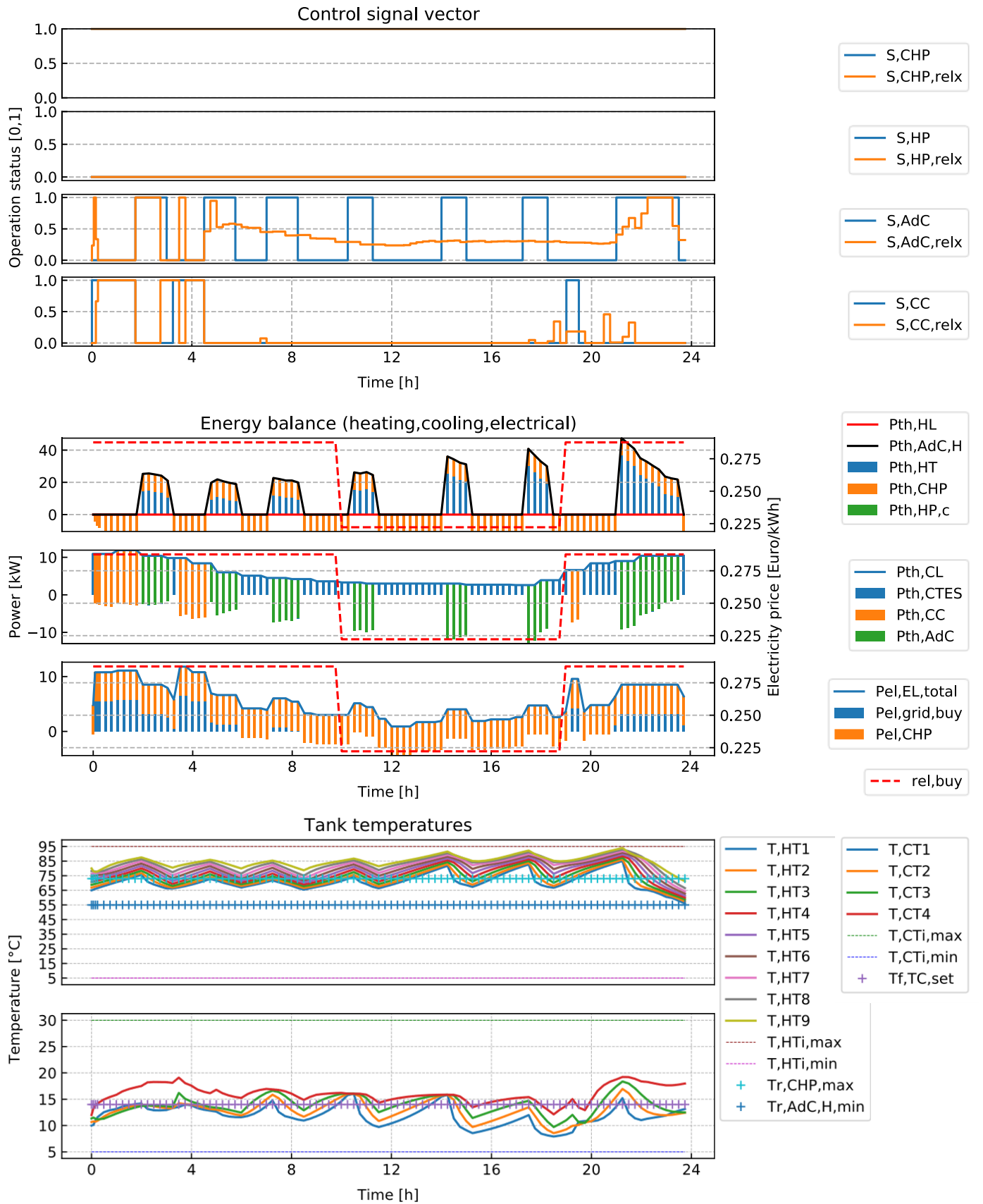
Fig. 7-1 Graphical representation and plausibility check of the MPC's solution at 11:00 (Time = 0 h) for a 24-hour forecast horizon for a test in summer. (a) Relaxed solution and resulting control signal with binary switches, (b) Thermal (heating and cooling) and electrical balance, and (c) tank temperatures corresponding to the binary switches. Negative $P_{th,CHP}$ and $P_{el,CHP}$ represent charging of HTES and electricity sold to grid respectively

MPC finds an optimal state vector while respecting operational constraints: The simulated tank temperatures are system states in the optimisation problem and are constrained using soft constraints (*cf. Chapter 6*). The optimal solution maintains these states within the maximum and minimum temperatures specified for the two tanks $T_{HTi,max}$, T_{min}, $T_{CTi,max}$, and T_{min} in *Table 7-1* and respects operational constraints such as maximum CHP return-line temperature $T_{r,CHP,max}$, minimum return-line temperature for driving the AdC $T_{r,AdC,H,min}$, and feed-line temperature for the TC $T_{f,TC,set}$. Any charging of the HTES (CTES) as shown in the thermal balance plots leads to increase (decrease) of the temperatures. Discharging has the reverse effect. The formation of thermoclines is more prominent in the HTES due to the higher temperature difference in feed-line and return-line during CHP operation. The stratification in CTES is not prominent due to the smaller (ca. 5 K) temperature differential for the chillers.

7.1.2 Winter scenario

Table 7-2 summarises the parameters used to implement the winter scenario and to set-up the MPC. These parameters are selected using data sheets of the components and are based on standard MPC practices recommended in the literature (*cf. Chapter 3.3 and Chapter 4.1*). The optimal control vector and corresponding results for energy balances and tank temperatures of one MPC iteration for this winter scenario are shown in *Fig. 7-2 (a-d)* and the significant observations regarding MPC's plausibility are:

Table 7-2[1] *Data for the time-varying parameters and constant parameters used to define the winter scenario for one MPC iteration*

Parameter	Data	Parameter	Data
For implementing the scenario:		**For MPC set-up:**	
Forecast T_{amb}	Historical data	Min. up/down time	1 h for CHP 0.5 h for HP
Load forecast	Hospital load, scaling between 16 kW$_{th}$ and HL 4.6 kW$_{th}$	Initial tank temp. [°C]	$[T_{HT1}...T_{HT9}] = [65...80]$
Elec. price forecast	EPEX SPOT SE day-ahead price, $r_{el,buy,EPEX}$	Initial controls	CHP = On HP = Off
For model set-up:		Initial state vector	Conventional control simulation
$T_{f,TC,set}$	40 °C		
For operational constraints:			
$T_{HTi,max}$	95 °C		
$T_{HTi,min}$	10 °C		
$T_{r,CHP,max}$	70 °C		
$T_{r,HP,c,max}$	45 °C		

---

[1] Parameters from previous table are not repeated

Heating load and electricity price forecast is in accordance to hospital operations and EPEX day-ahead auction prices respectively: The heating load forecast $P_{th,HL}$ is input from a database and is predicted to be lower during the night (Time = 5 to 11h) and increase during dawn (Time = 11h) with a peak of ca. 16 kW$_{th}$ in the afternoon from 14:00 and 16:00 (Time = 21 to 23 hours). The load shows variation as expected in the operation of a hospital with multiple peaks in the morning and afternoon. This is balanced by the thermal power of the CHP $P_{th,CHP}$ and the power consumed from the hot tank $P_{th,HT}$ at a particular instant. Negative $P_{th,CHP}$ indicates the power stored in the HTES and results in increase of the tank temperature. The electricity forecast $r_{el,buy}$ corresponds to the $r_{el,buy,EPEX}$ (*cf. Chapter 4.1.6*) and varies over the 24-hour horizon. The price is in the lower range during the evening hours and higher during the daytime operation.

Heat pump operation is completely avoided: The HP is meant to cover peak loads (between 10 kW$_{th}$ and 16 kW$_{th}$) with its nominal capacity of 16.7 kW$_{th}$. However, the MPC solution covers the peak thermal loads (e.g. from Time = 16h to 24h) with the CHP and HTES combination. It provides a solution where HP is not operated over the entire period ($P_{th,HP,c}$ = 0 kW$_{th}$) and the CHP's operation is prioritised.

CHP operation is reactive to electricity price and hot tank is charged predictively to support peak heating loads: Similar to the summer scenario, the total electrical load $P_{el,EL,total}$ comprises of a reference load from a database and requirements of the machines. The $P_{el,EL,total}$ is satisfied by the electrical power of the CHP $P_{el,CHP}$ and electricity bought from grid $P_{el,grid,buy}$. Negative electrical balance represents the electricity sold to the grid. The peaks during the day are supported by full-load operation of CHP at higher $r_{el,buy}$. It is observed that the CHP is switched off for approximately 1.5 hours (more than minimum down time) during night-time at lower $r_{el,buy}$ and saving HTES capacity for daytime operation of the CHP.

MPC finds an optimal state vector while respecting operational constraints: The simulated results of the temperatures in the HTES illustrate the formation of thermoclines and the initial temperatures as summarised in *Table 7-2*. The MPC maintains tank temperatures T_{HTi} within the maximum and minimum limits $T_{HTi,max}$ and $T_{HTi,min}$ set at 95 °C and 10 °C respectively. Additionally, T_{HT1} does not violate the $T_{r,CHP,max}$ set at 70 °C and $T_{r,HP,c,max}$ set at 45 °C. The temperature of T_{HT6} is above the $T_{f,TC,set}$ set at 40°C ensuring adequate temperature is available in the tank for heating.

7.1.3 Conclusion from one MPC iteration in summer and winter scenario

The analysis of the results from one MPC iteration in each scenario has shown a plausible control schedule for the plant that considers both thermal and electrical load forecasts while also maintaining operational constraints. The data needed to set-up the MPC was available in the data sheets of the components, facilitating the adaptability or tuning of the MPC to similar plants. Two different types of price signals and load profiles were

used. The simulated response of the system to the calculated control signal was of reasonable accuracy and the usefulness of the simplified models was established.

The computation time for one iteration was between 10 to 15 seconds. This was within 3% of the shortest control time-step and facilitated for the 140 seconds of valve positioning before a new iteration started. The maximum solution time was limited with the parameters: maximum CPU time in IPOPT (30 seconds) and in pycombina (30 seconds). An improvement in solution quality could be expected by permitting more time for these solvers. However, the permitted time should be set in the context of the length of a time-step. For instance, computation times of more than 1 minute on a sampling interval of 5 minutes especially in processes that change dramatically over the 5 minutes could compromise the efficacy of the solution.

With sensitivity analysis and long-duration tests on the real system the plausibility and availability of the complete MPC framework is evaluated in the next sections of this chapter.
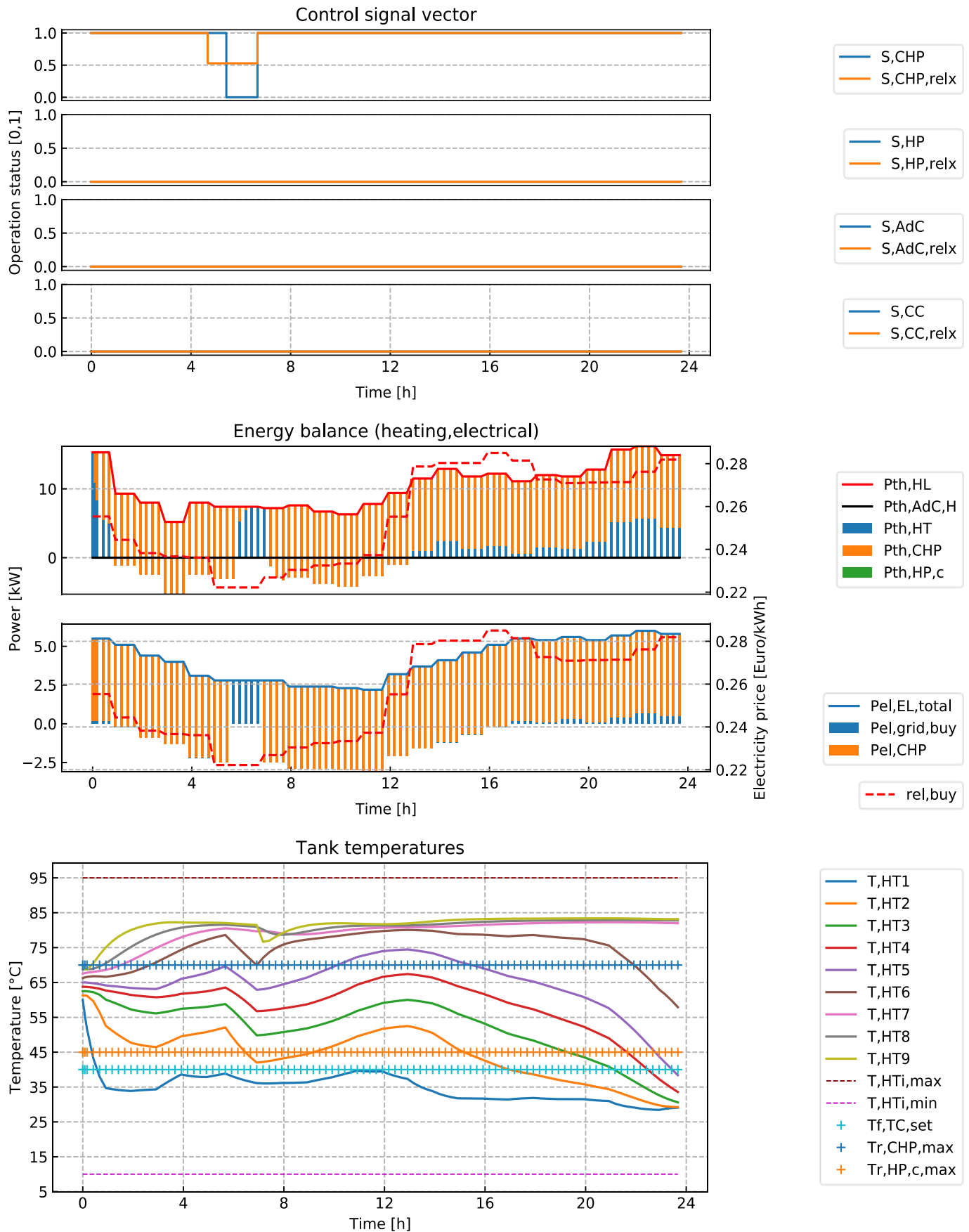
Fig. 7-2 Graphical represenation and plausibility check of the MPC's solution at ca. 17:00 (Time = 0 h) for a 24-hour forecast horizon for a test in winter. (a) Relaxed solution and resulting control signal with binary switches, (b) thermal (heating) balance, (c) electrical balance, and (d) tank temperatures corresponding to the binary switches

7.2   Parameter analysis

A basic parameter analysis or what-if analysis was done to understand the effect of varying input parameters and initial values on the MPC solution. With the previously defined summer scenario as reference, a single iteration was solved with the following parameter variations:

- increased minimum up/down time for all components to 4 hours,
- reduced cooling load forecast by a factor of 0.75,
- reduced initial temperature in hot tank, $[T_{HT1} \dots T_{HT9}] = [40\dots50]$.

The results are presented in *Fig 7-3*. The reference scenario was discussed in *Section 7.1.1* and the variations are discussed below:

(a) Increasing the minimum up/down time leads to a solution with fewer switches: It is noticed that the binary approximation routine maintains this constraint and calculates solutions with lesser frequent switching than the reference scenario. Although this may benefit the hardware, it may lead to violation of the tank temperature constraints, higher electricity consumption or other sub-optimal solutions. A careful tuning of the controller based on switching characteristics of the individual machines should be done and if minimum up/down time constraints are already formulated in the MPC problem, then it may be unnecessary to included switching costs in the objective function.

(b) Reducing the cooling load leads to lower AdC and CC operation: As expected, the lower cooling load requires less operation of the chillers. The MPC adjusts its solution to cover majority of the load with AdC and reduce CC operation compared to the reference scenario. However, the lower requirement of AdC leads to lower CHP operation hours even though the electrical load is same as the reference scenario.

(c) Lower initial HTES temperatures leads to higher CC operation and lower AdC operation: Due to the initially discharged HTES providing lower driving energy for the AdC, a lower AdC operation (lower $S_{AdC,relx}$) and a higher CC operation (higher $S_{CC,relx}$) is observed. This is indeed during peak hours especially in the first 4 hours of the test leading to higher consumption-related costs.

The comparison of different cases not only demonstrates the plausibility of the MPC to adapt to various conditions but also highlights the effect of the binary approximation method on the final solution. The switching sequence of the AdC and CC are different in all the cases even though in some cases their relaxed solutions are similar with the difference arising due to solution of the MILP by pycombina (cf. *Chapter 6*). The quality of the binary approximation could be improved by increasing the maximum permissible CPU time for the pycombina routine or improving the mathematical formulation of the binary approximation problem.

Only one MPC iteration per case is discussed to identify changes in the relaxed and binary solution. Variation of entire MPC solution for different scenarios is discussed in measured data of long-duration tests in *Chapter 8*.
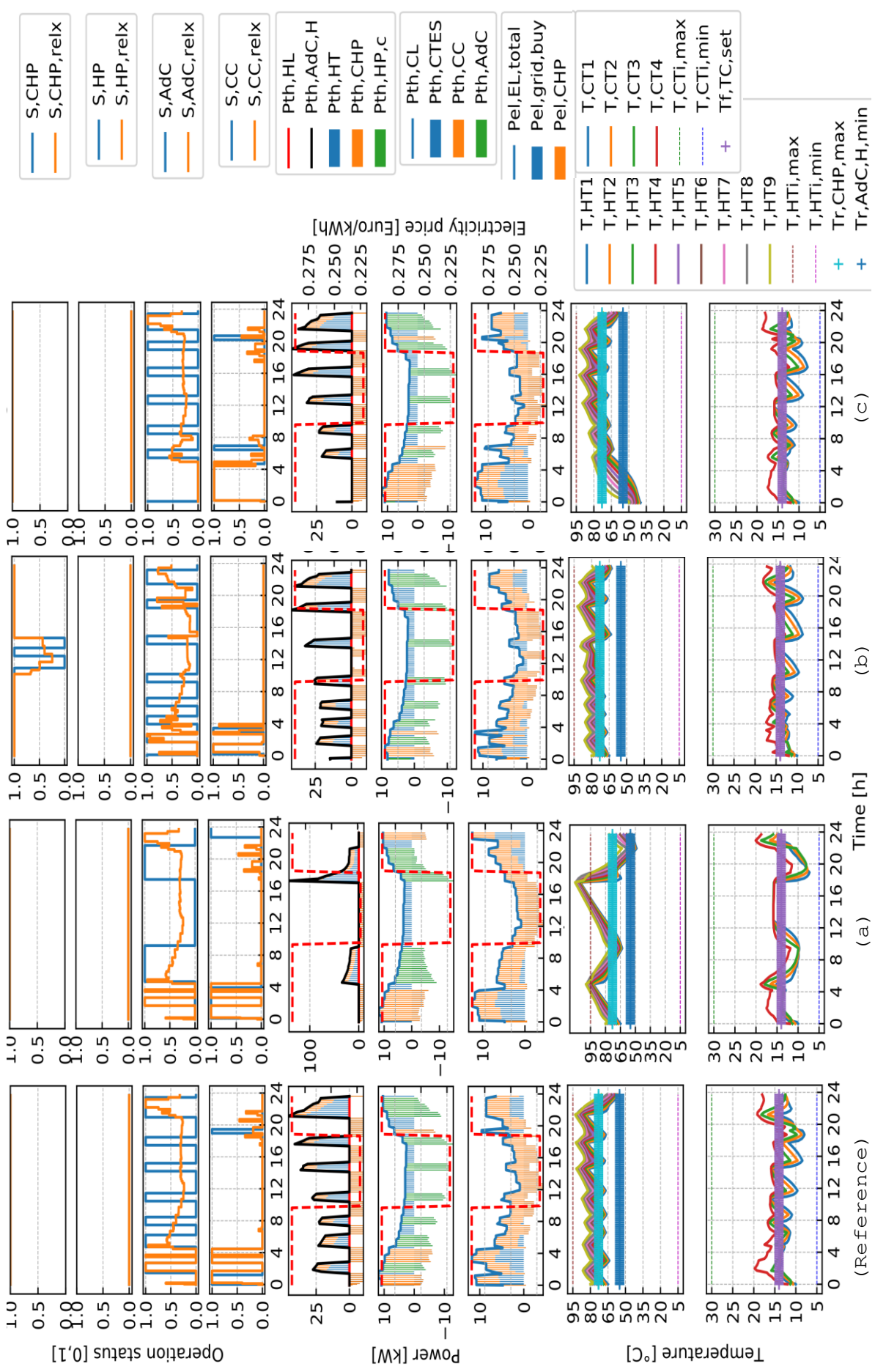
Fig. 7-3 MPC solutions for the reference summer scenario with parameter variation: (a) increased minimum up/down time, (b) reduced cooling load, and (c) lower initial HTES temperature.

7.3   Solution of binary problem versus relaxed problem

The reason for applying strictly binary (integer value) controls instead of the relaxed (real value) controls to the components is the technical limitation of hardware. For the hardware implementation of a non-binary solution, the components should include a 0-100% capacity control and the hydraulic connections should facilitate their simultaneous operation. For instance, a variable fuel input for CHP or variable speed compressor for RHP and multiple storage tanks permitting simultaneous operation of both chillers should be planned. Conversely, even in modern microscale systems such an output modulation is not standard practice while the modulation is often possible only between a minimum power output (e.g. 25%) and the 100% power output due to technical limitations or other efficiency related issues. However, for evaluating the efficacy of the relaxed solution, highlighting the effect of its approximation to a binary signal, and for identifying any potential benefits (economic, operational or optimisation process), the MPC was simulated with relaxed binary controls by assuming to operate the components at a percentage of their maximum capacities.

7.3.1   Summer scenario

In *Fig. 7-4,* the optimal control variables and corresponding results for the reference summer scenario from *Section 7.1* are shown on the left-hand side. As a comparison, the reference scenario was solved with relaxed switches and the results are shown on the right-hand side of the figure. In contrast to the frequent binary switching, the relaxed solution implements the solution of the NLP to (theoretically) operate the components continuously at a percentage of their maximum capacities. The AdC and CC are operated simultaneously. Correspondingly, in the energy balances, fewer peaks are observed and continuous (but lower) charging of CTES and purchase from grid is noticed. This is also noticed in the tank temperatures as the saw-tooth behaviour of binary switching is replaced by a smoother solution. An improvement is also noticed in the tank temperatures as their terminal values match the operational limits. For instance, the terminal value of T_{CT1} is ca. 14 °C and is interpreted as optimal usage of the CTES's capacity over the 24-hour horizon.

7.3.2   Winter scenario

A similar comparison is made to the reference winter scenario from *Section 7.1.* The CHP operates continuously in the relaxed solution and is turned off for 1 hour. However, there is no significant difference in the two solutions since the CHP operates at full-load in both cases for most of the horizon. A mixing of the top layers is noticed in tank temperatures of the relaxed solution between Time = 6 to 8 h. The CHP operates at part-load during this period and temperature difference between feed-line (T_{HT9}) and return-line (T_{HT1}) is low. This results in colder water entering the already hot tank and causing deterioration of the thermal stratification.

Fig. 7-4 Comparison of MPC output with strictly binary switches (MINLP) and MPC output with relaxed switches (NLP) for the previously shown reference summer scenario. (a) Solution with binary switches and (b) solution with relaxed switches

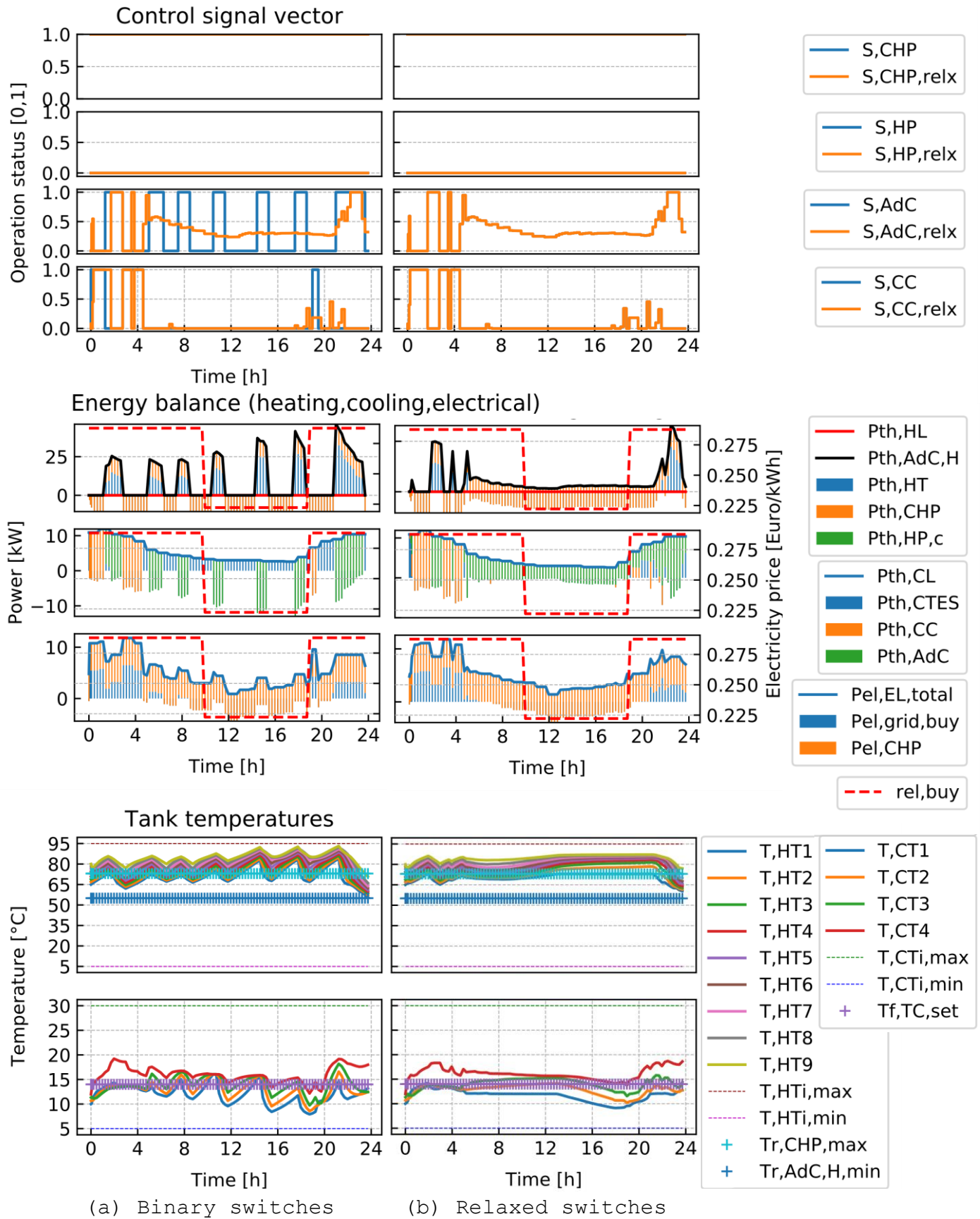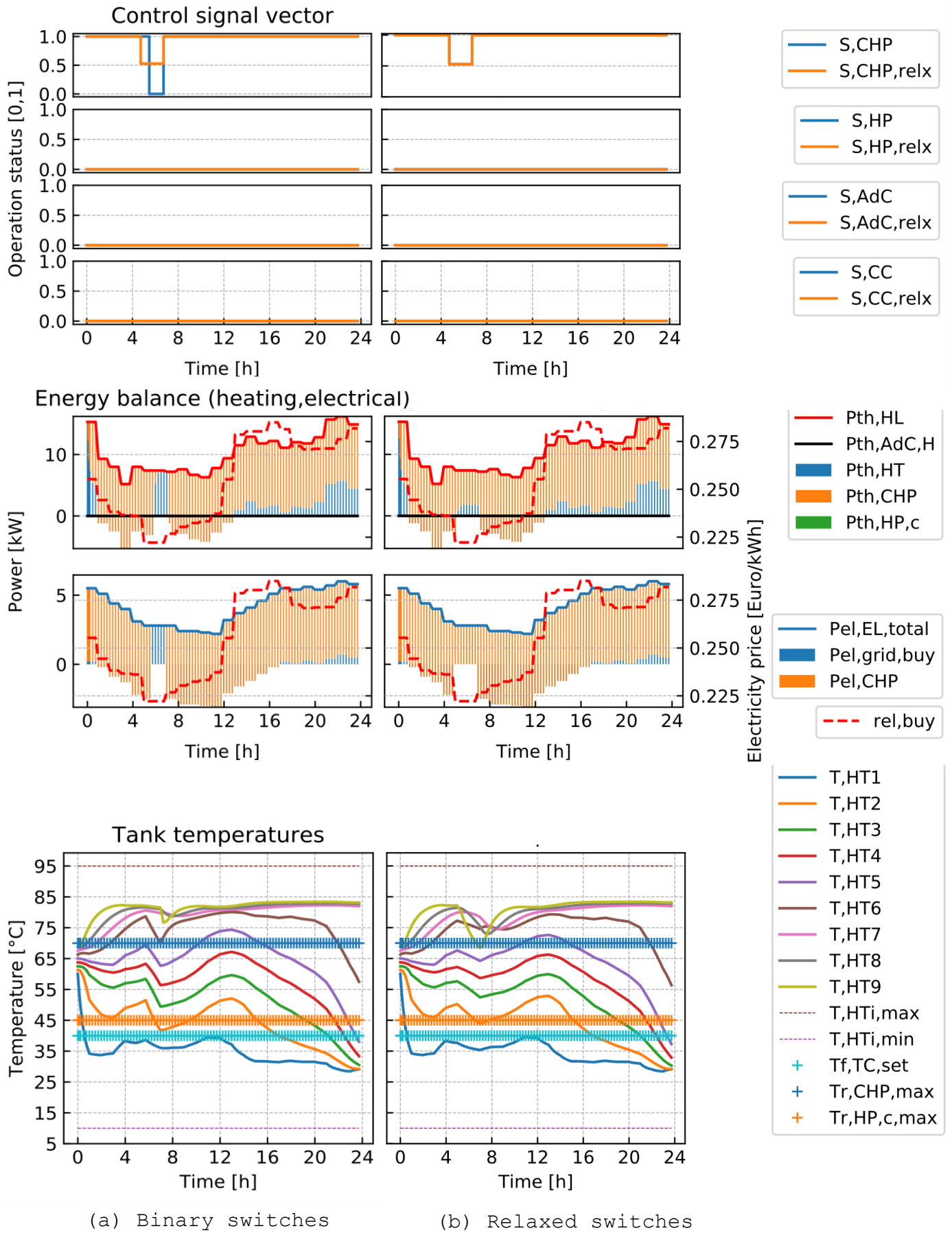(a) Binary switches (b) Relaxed switches

Fig. 7-5 Comparison of MPC output with strictly binary switches (MINLP) and MPC output with relaxed switches (NLP) for the previously shown reference winter scenario. (a) Solution with binary switches and (b) solution with relaxed switches

7.4   Results of multiple MPC iterations

The receding horizon scheme for MPC is applied in this work. As an example of this scheme, MPC iterations for a winter scenario with weekday loads of a non-residential building and electricity prices corresponding to the $r_{\text{el,buy,IMG}}$ from *Section 4.3*, are collected at a 4-hour interval over a 24-hour period. The results of this test are illustrated in *Fig. 7-6* with the thermal (heating) balance calculated at the particular sampling time (specified as title of subplot). As the forecast horizon recedes or shifts, the heating load forecast $P_{\text{th,HL}}$ and electricity price $r_{\text{el,buy}}$ for the next 24 hours are updated and a new optimal schedule is calculated. For instance, in the second subplot (2020-02-25 15:45) the electricity price at Time = 0 h is higher (> 0.26 €/kWh$_{\text{el}}$) than the expected price (< 0.24 €/kWh$_{\text{el}}$) as per the forecast at Time = 4 h in the first subplot (2020-02-25 11:45).

Another change in the optimal schedule is noticed within the last four subplots as the MPC uses more $P_{\text{th,HP}}$ during lower electricity prices with increasing $P_{\text{th,HL}}$ in the updated forecast. Since the $P_{\text{th,HL}}$ profile is based on a weekday (no significant intra-day changes in thermal loads), the forecast at 11:45 on both days is similar.
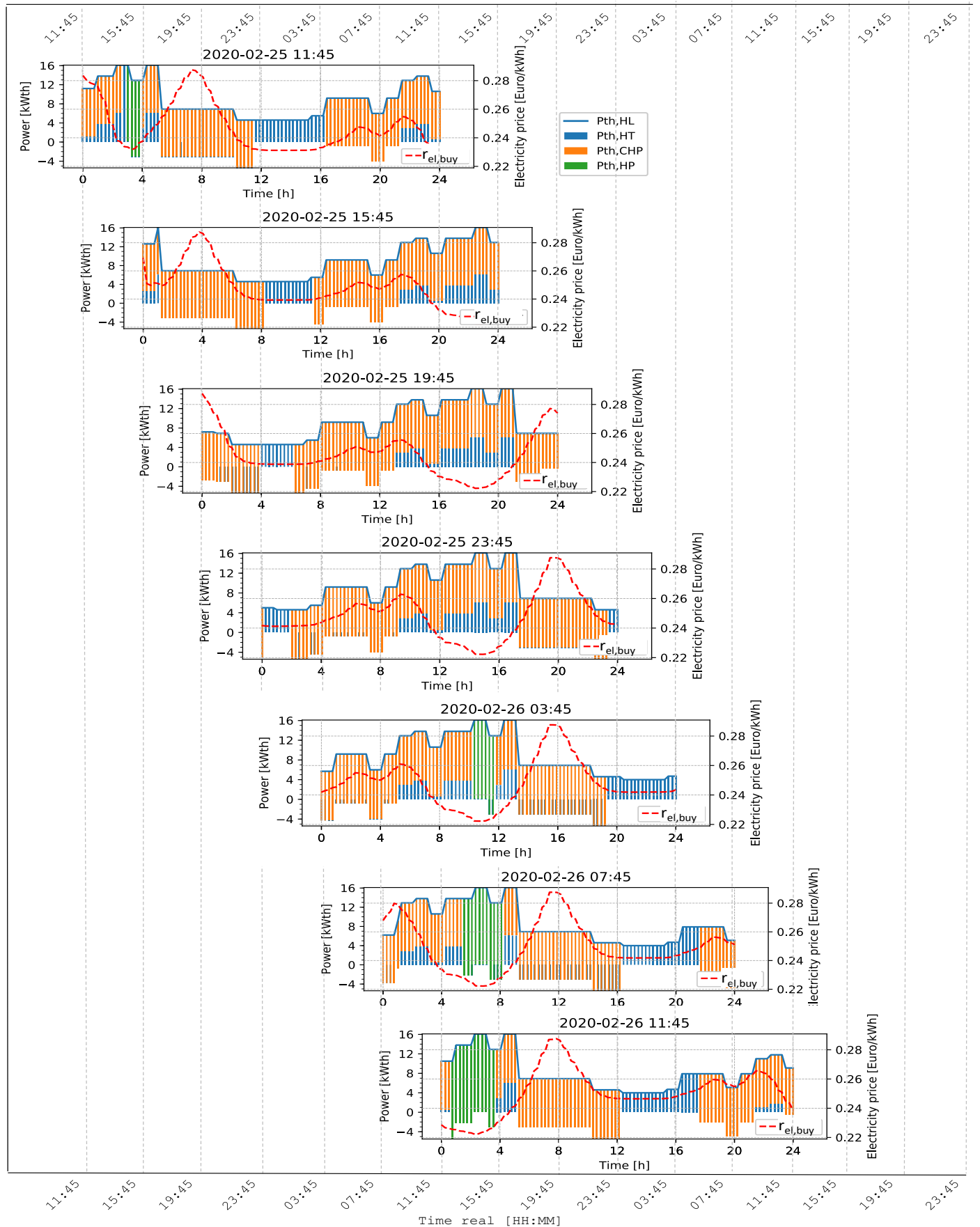
Fig. 7-6 Multiple MPC iterations in 4-hour intervals representing a 24-hour test. Shifting of horizon and update of forecast, electricity rate and optimal schedule is noticed in each sub-plot. For instance, inclusion of more HP operation during cheaper electricity rate as higher heating load is forecasted on the horizon

7.5 Long-duration tests with economic-MPC

For the full-scale demonstration of cost-efficient and grid-supportive scheduling of the plant with MPC, long-duration tests with varying initial conditions, load forecasts or MPC settings were performed. The aim of these tests was to exhibit a stable, integrated, and practical operation of the MPC as part of the building automation and control system. The results for one summer and one winter scenario are illustrated. The detailed operation of the machines and the resulting changes in tank temperatures and interaction of the hydraulic circuits are explained in *Chapter 4*.

7.5.1 Summer scenario

A scenario with a small hospital having 12 kW$_{th}$ peak cooling load and adjusted to start on a Thursday was selected for the summer test. The hot and cold tanks (HTES and CTES) were mixed and had an initial homogeneous temperature of ca. 56 °C and 15 °C respectively. The initial control guess for the machines was based on the initial tank temperatures. For example, the initial values of the HTES temperatures were closer to minimum temperature for operating the AdC ($T_{r,AdC,H,min} = 55\,°C$), so the initial controls for AdC was set to off. The initial values for CTES temperatures were higher than the set feed-line temperature in the TC circuit ($T_{f,TC,set} = 14\,°C$), i.e. the CTES was warmer than constraint, so the initial control for peak load compression chiller CC was set to on. Other parameters for the summer scenario are summarised in *Table 7-3*.

Table 7-3[1] Data for the time-varying parameters and constant parameters used to define the summer scenario for a long-duration test

Parameter	Data
For implementing the scenario:	
Forecast T_{amb}	For Offenburg with the Dark Sky API
Load forecast	Hospital load, scaling between 12 kW$_{th}$ and 2.7 kW$_{th}$
Elec. price forecast	Two-price tariff, $r_{el,buy,EWERK}$
Assumed start day	Thursday
For model set-up:	
$T_{f,OC,set}$	14 °C
For operational constraints:	
$T_{HTi,max}$	95 °C
$T_{HTi,min}$	5 °C
$T_{r,CHP,max}$	73 °C
$T_{r,AdC,H,min}$	55 °C

Parameter	Data
For MPC set-up:	
Min. up/down time	1 h for CHP and AdC 0.25 h for HP and CC
Initial tank temp. [°C]	$[T_{HT1}...T_{HT9}] = [53...56]$ $[T_{CT1}...T_{CT4}] = [14...15]$
Initial controls	CHP and CC = On AdC and HP = Off
Initial state vector	Conventional control simulation

---

[1] Parameters from previous tables are not repeated

The data measured during 4 days (approx.) of testing is illustrated in *Fig. 7-7 (a-c)* and the important points are summarised below:

MPC utilises the CHP-AdC combination for prolonging CHP operation: $P_{th,CHP}$ and $P_{th,HT}$ satisfy the thermal load generated by the AdC $P_{th,AdC,H}$. Negative $P_{th,HT}$ represents charging of the HTES and is observed in the corresponding rise of its temperature. Four temperatures in HTES are shown, T_{HT1} to T_{HT8}, with T_{HT1} being at the bottom and corresponding to the return-line for CHP and T_{HT8} corresponding to the driving temperature for the AdC. In most cases, the AdC operates as high temperature heat accumulates in the HTES and thereby the CHP operation is prolonged due to available HTES capacity.

Tank temperature constraints are not violated: The temperature of all layers in the HTES or CTES are within their maximum or minimum safety constraints, namely $T_{HTi,max}$, T_{min}, $T_{CTi,max}$, and T_{min}.

Non-critical temperature constraint violations are noted: $T_{r,AdC,H,min}$ and $T_{r,CHP,max}$ are both violated. The AdC is on while the T_{HT8} is below $T_{r,AdC,H,min}$ from ca. 20:45 to 21:45 on the second day of operation (marked with "+" in *Fig. 7-7 a*). The CHP is on while T_{HT1} is higher than $T_{r,CHP,max}$ and is shut-down by its internal controller, e.g. at ca. 05:00 on the second day, at ca. 04:00 on the third day, and at ca. 06:30 on the third day (marked with "×" in *Fig. 7-7 a*)[1]. The minimum up/down times are respected for the AdC and CC. However, the CHP operation violates this constraint at ca. 09:45 on the third day. Additionally, for some hours of the test T_{CT1} is above the set $T_{f,TC,set}$ of 14 °C e.g. from ca. 12:45 to 19:45 of second day. This leads to inadequate temperature for the three-way mixing vales to achieve the $T_{f,TC,set}$.

Cooling load profile depicts a typical hospital operation and predictive charging of CTES is observed: $P_{th,CC,e}$, $P_{th,AdC,L}$, and $P_{th,CT}$ satisfy the cooling load $P_{th,CL}$. The load follows the forecast for a hospital with higher demand during the day and lowers during night. Considering the start of the test adjusted to start the load profile on a Thursday, the demand is higher on first two days and only slightly less over third and fourth day (weekend). Cooling demand in a hospital does not significantly reduce on weekends. The variations in $P_{th,CL}$ due to the periodic operation of AdC are also observed (*cf. Section 4.12*). Negative $P_{th,CT}$ represents excess cooling produced by the chillers and charging of the CTES. Correspondingly, the CTES temperature reduces. Two temperatures in CTES are shown, T_{CT1} and T_{CT4}, with T_{CT1} being at the bottom and matching to the feed-line of the TC and T_{CT4} matching to the return-line of the chillers. A night-time cooling of the CTES is observed especially on the second night for predictively charging the CTES to support daytime peak thermal loads.

MPC operates the plant reactive to electricity price and energy requirements: The electricity price $r_{el,buy,EWERK}$ follows the two-tariff structure with a high tariff and

---

[1]The violation of this limit and shutting down of CHP was partly observed due to the AdC's fluctuating behaviour (*cf. Section 4.12*)

low tariff at certain times of the day. The total electrical load $P_{el,EL,total}$ is satisfied by the electricity produced by the CHP $P_{el,CHP}$ and electricity purchased from the gird $P_{el,grid}$. Negative $P_{el,grid}$ represents excess electricity produced by the CHP and sold to the grid. The peaks in $P_{el,EL,total}$ arise when CC is turned on. The MPC enables coupling of thermal and electrical loads and reduction of peaks during high $r_{el,buy,EWERK}$ by:

- utilising minimum runtime operation of the CC,
- predictive charging of CTES at low $P_{th,CL}$, and
- planning CHP operation during high $r_{el,buy,EWERK}$ by combining CHP with AdC.

However, there are a few instances where the MPC operation is not (intuitively) grid-supportive. For instance, the CC operates for ca. 5 hours in the beginning of the test (marked with "×"in *Fig. 7-7 c*) at high tariff. Another example is when the AdC-CHP combination is not running during high $r_{el,buy,EWERK}$ on the third day of the test (marked with "+" in *Fig. 7-7 c*) even though the HTES is completely charged.

(a) Thermal (heating) balance

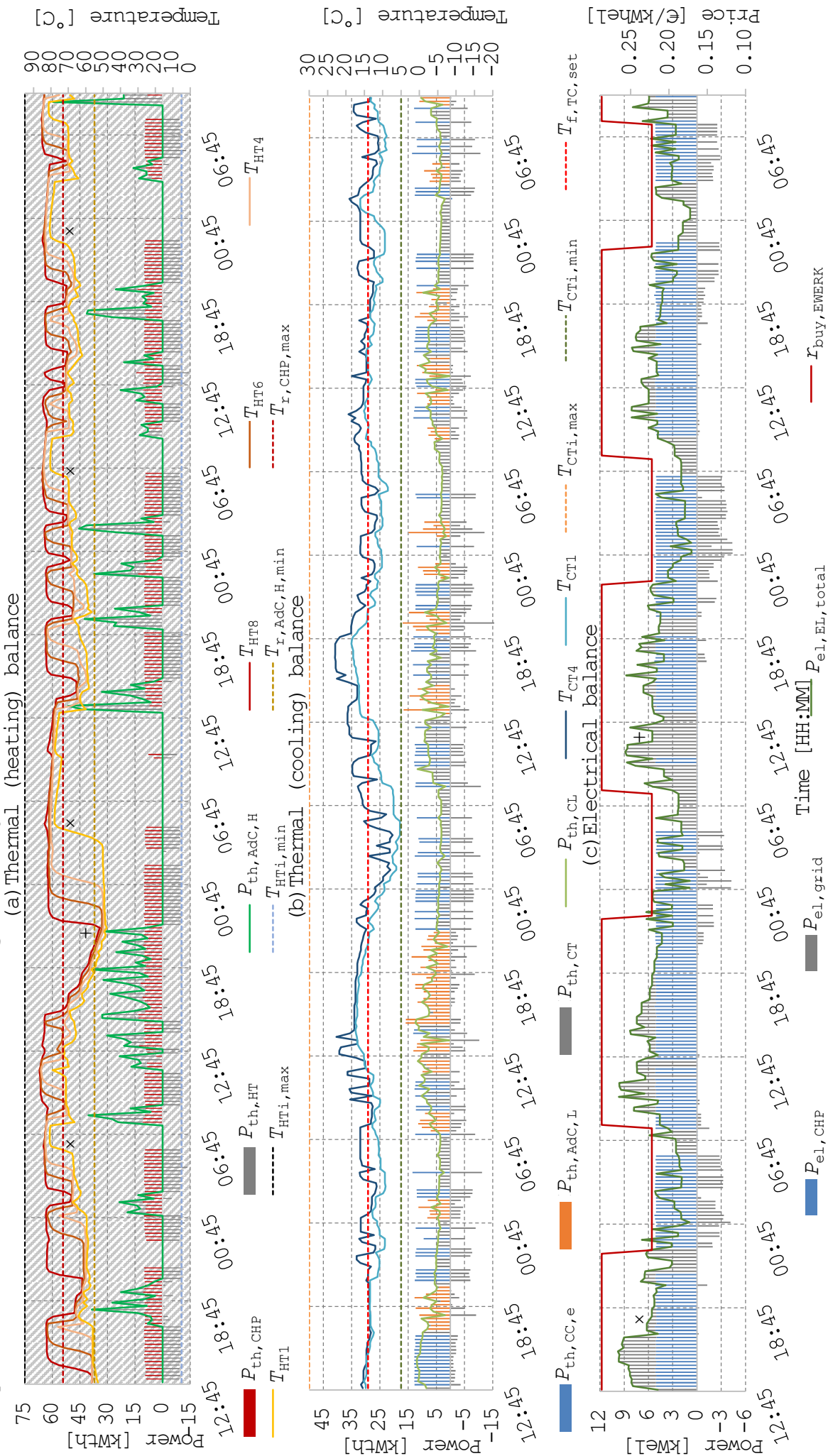(b) Thermal (cooling) balance

(c) Electrical balance

Fig. 7-7 Measurement data in 15-minute intervals for 92.75 hours of a long-duration test of a summer scenario started on 01.09.2019 at 12:45. (a) Heating balance with hot tank temperatures and contraints, (b) Cooling balance with cold tank temperatures and contraints, and (c) electrical balance

7.5.2 Winter scenario

A scenario with a small hospital having 16 kW$_{th}$ peak heating load and adjusted to start on a Thursday, was selected for the winter test. The HTES had a homogeneous initial temperature of ca. 49.7 °C and accordingly the initial control for the CHP was set to on and for the HP was off. Other parameters for the winter scenario are summarised in *Table 7-4*.

Table 7-4 Data for the time-varying parameters and constant parameters used to define the winter scenario for a long-duration test

Parameter	Data		Parameter	Data
For implementing the scenario:			**For MPC set-up:**	
Forecast T_{amb}	For Offenburg with the Dark Sky API		Min. up/down time	1 hour for CHP 0.5 hour for HP
Load forecast	Hospital load, scaling between 16 kW$_{th}$ and 4.6 kW$_{th}$		Initial tank temp. [°C]	$[T_{HT1}...T_{HT9}] = [35...53]$
Elec. price forecast	EPEX SPOT SE day-ahead price, $r_{el,buy,EPEX}$		Initial controls	CHP = On HP = Off
Assumed start day	Thursday		Initial state vector	Conventional control simulation
For model set-up:				
$T_{f,OC,set}$	40 °C			
For operational constraints:				
$T_{HTi,max}$	95 °C			
$T_{HTi,min}$	10 °C			
$T_{r,CHP,max}$	73 °C			
$T_{r,HP,c,max}$	45 °C			

The data measured during approx. 4 days of testing is illustrated in *Fig. 7-8 (a & b)* with the following observations:

Heating load profile is consistent to a typical hospital operation and lower change-of-value in heating load is observed: $P_{th,CHP}$ and $P_{th,HT}$ satisfy the thermal load $P_{th,HL}$ while $P_{th,HP,c}$ is not used. The heating load follows the forecast for a hospital with higher demand during the day and lowers during night. Considering the start of the test adjusted to start the load profile on a Thursday, the demand is higher on first two days and only slightly less over third and fourth day (weekend). It increases again on the final day representing a Monday. Heating demand in a hospital does not significantly reduce on weekends. Unlike the variations in measured thermal load during summer $P_{th,CL}$, the thermal load in winter $P_{th,HL}$ has lower change-of-value since AdC is not used (*cf. Section 4.12*). Negative $P_{th,HT}$ represents excess heating produced by the CHP and charging of the HTES. Congruently the HTES temperature increases and a thermocline is formed. Four temperatures in HTES are shown, T_{HT1} to T_{HT8}, with T_{HT1} being at the bottom and corresponding to the return-line for CHP, T_{HT6} corresponding to the feed-line temperature for the TC ($T_{HT,LoadLayer}$) and T_{HT8} at the top of the tank.

No significant violation of constraints is observed: The layer-temperatures in the HTES do not violate their maximum or minimum safety constraint $T_{\mathrm{HT}i,\mathrm{max}}$ or $T_{\mathrm{HT}i,\mathrm{min}}$. Additionally, T_{HT1} does not violate the $T_{\mathrm{r,CHP,max}}$ set at 73 °C while CHP is on or $T_{\mathrm{r,HP,c,max}}$ set at 45 °C when HP is on. The minimum up/down time is mostly respected for the CHP with an exception at ca. 01:00 during the third night when it is switched off for 0.75 hours (marked with an 'x' in *Fig. 7-8 a*) before turning on again. T_{HT6} is only shortly below the set $T_{\mathrm{f,TC,set}}$ of 40 °C e.g. from ca. 17:00 to 19:30 of second day. This leads to inadequate temperature for the three-way mixing vales to achieve the $T_{\mathrm{f,TC,set}}$.

MPC operates the plant reactive to electricity price and energy requirements: The electricity price $r_{\mathrm{el,buy,EPEX}}$ follows the EPEX day-ahead tariff and $P_{\mathrm{el,EL,total}}$ is covered by $P_{\mathrm{el,CHP}}$ and $P_{\mathrm{el,grid}}$. Negative $P_{\mathrm{el,grid}}$ represents excess electricity produced by the CHP and sold to the grid. Consistent with user behaviour in a hospital the $P_{\mathrm{el,EL,total}}$ is higher during the morning hours and a second peak is in the afternoon. As calculated in the previous section with one MPC iteration, the MPC manages to operate the CHP supporting the grid also in this long-duration test. It predictively turns off the CHP at low $r_{\mathrm{el,buy,EPEX}}$ and low $P_{\mathrm{el,EL,total}}$ to avoid overheating the HTES and ensure continuous operation of the CHP during the daytime. Another observation is the avoidance of HP usage and consequently no electrical peaks are generated during high $r_{\mathrm{el,buy,EPEX}}$.

(a) Thermal (heating) balance
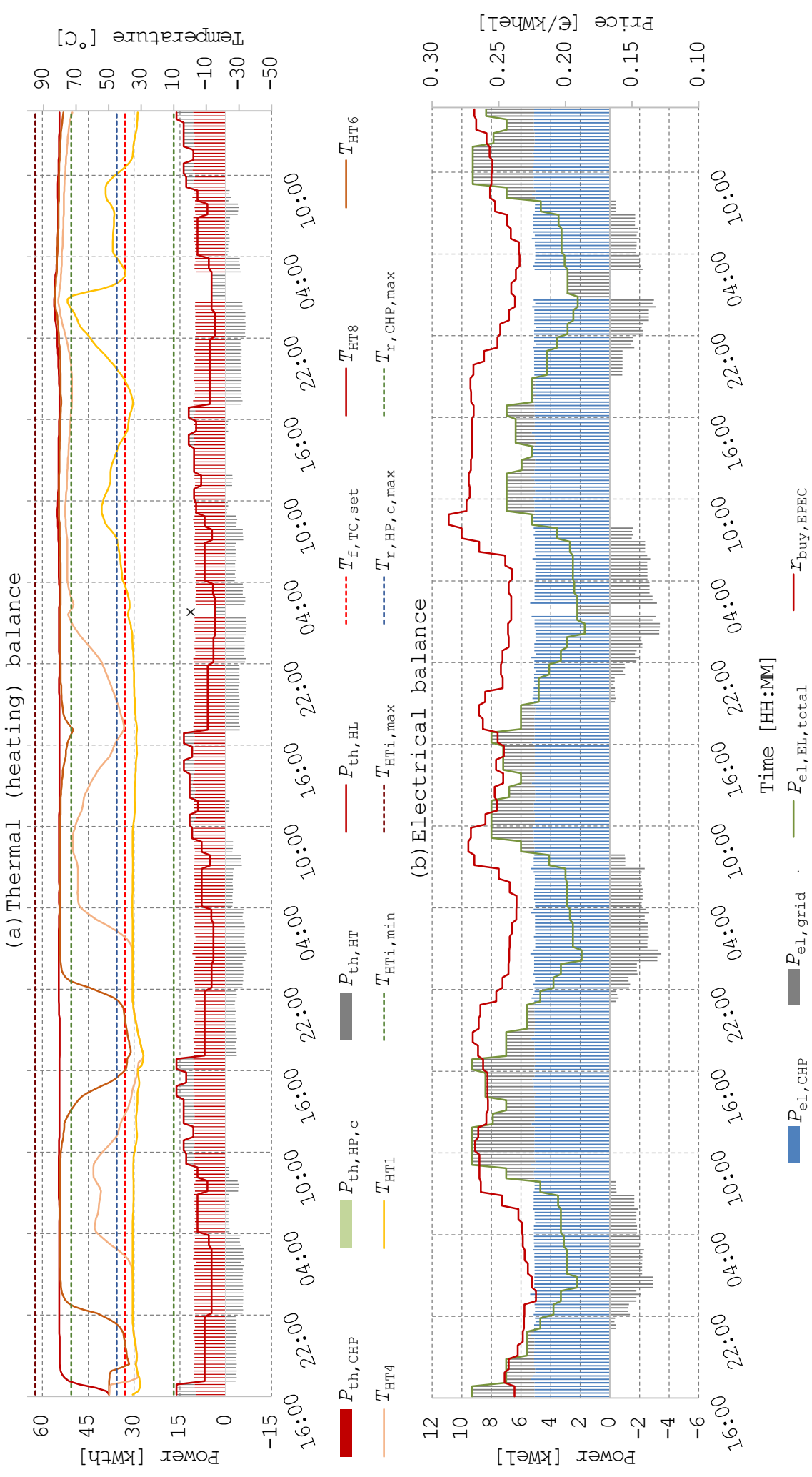

(b) Electrical balance

Fig. 7-8 Measurement data in 15-minute intervals for 94.5 hours of a long-duration test of a summer scenario started on 16.12.2019 at 16:00. (a) Thermal (heating) balance with hot tank temperatures and contraints and (b) electrical balance

7.5.3 Conclusion of long-duration tests

The results of the two long-duration tests over multiple days demonstrated the plausibility of the MPC loop for a stable optimal scheduling of the plant. The average computation time for one iteration was 10.4 seconds. The machines and the storage capacities were used to satisfy the thermal and electrical loads in consistence with the electricity price and weather forecasts. However, global optimality was not always guaranteed and the output of the binary approximation algorithm strongly affected the optimal schedule. Additionally, the choice of MPC parameters e.g. maximum permissible CPU time, tolerance of solvers, initial tank temperatures, and the load patterns also affected the performance of the solvers. A quantification of their effects through sensitivity analysis is an important research point for follow-up studies and the current lab set-up facilitates it.

7.6   Fall-back solution and availability of the MPC framework

Since a mathematical evaluation of the controller's stability, e.g. *Lyapunov stability* is limited for economic-MPC problems, an alternative approach was used to evaluate the availability of the MPC. Considering availability to be a representative metric for the probability that the controller framework provides a practical schedule for the plant, the solver status provided by NLP solver IPOPT and time taken by pycombina was recorded to calculate the availability of the MPC framework. More precisely, a counter recorded the number of times an optimal solution, an acceptable solution (considering the tolerance of the NLP solver), or an infeasible solution was found, and if solution in pycombina exceeded the permitted time.

The results for 378 hours of operational data are summarised in *Fig. 7-9.* An optimal solution was found for 80% of the total iterations and an acceptable solution was found for 12% of the total iterations. For 8% of the time an infeasible solution was recorded by the NLP solver. No particular correlation could be identified as cause of this infeasibility since many factors e.g. mathematical stability of solver, current tank temperature, predicted load, and minimum runtime are interdependent even in a single MPC iteration.

As mentioned in *Chapter 6*, in case of an infeasible solution, the control signal corresponding to the current time-step from the previous optimal solution was applied. This fall-back solution increased the availability of the MPC framework as it did not fail to apply a practical control signal and ensured a reliable operation of the plant irrespective of numerical errors or mechanical errors during the MPC loop.
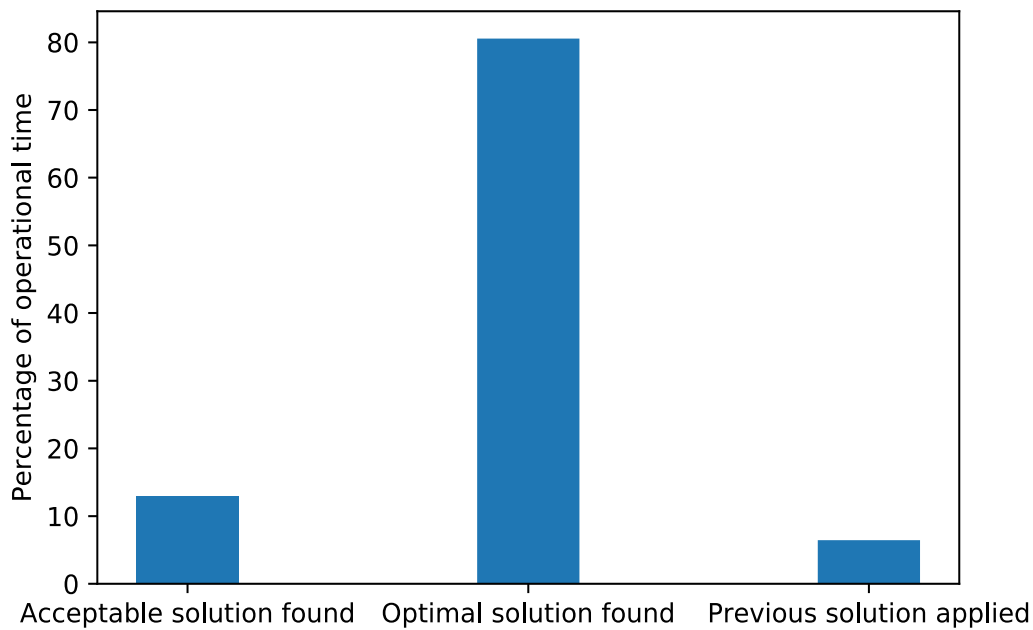
Fig. 7-9 High availability of the MPC framework due to the application of a fall-back solution as represented in terms of solution quality over 378 hours of operation time. In most iterations an optimal solution or an acceptable solution was found. In < 10% an infeasible solution was found and due to fall-back solution in the MPC framework the previous optimal solution was applied. No particular correlation could be identified as cause of this infeasibility since many factors e.g. mathematical stability of solver, current tank temperature, predicted load, and minimum runtime are interconnected even in a single MPC iteration

7.7   Summary and outlook

Theoretical concepts of *mixed integer optimal control problems* and the practical framework of a *building automation and control* system were integrated together to demonstrate the application of an *economic-MPC* for optimal scheduling of the INES trigeneration lab. The analysis of MPC solutions for one iteration or multiple iterations established the plausibility of MPC to provide a predictive switching schedule capable of minimising *consumption-related costs* by considering multiple input forecasts, hardware constraints, and storage capacities simultaneously. The process of a *receding horizon scheme* was displayed and the complex interdependence of the various factors affecting the MPC solution was highlighted.

The fall-back solution programmed in the control architecture of MPC resulted in high availability of the controller and was quantified by recording the output of the nonlinear problem solver and time taken for the binary approximation.

The good fit of simulated system states and measured data established the efficacy of the models developed in *Chapter 4* (and simplifications in *Chapter 6*) to be used in MPC of trigeneration systems. The recommendation that models need to be only of sufficient accuracy for MPC of thermal systems was successfully applied in this work as noticed in the MPC results and measured data of long-duration tests.

Although the constraint violations e.g. CHP safety return-line temperature or minimum runtime did not lead to failure of the algorithm or hardware damage, avoiding all constraint violations is of significant importance for widespread acceptance of MPC. For evaluating the violation of temperature constraints and minimum runtime constraints by MPC, the data from multiple tests was analysed. The details of this analysis and possible improvements are discussed in *Chapter 8*.

7.7.1 Challenges and research potential

Multiple challenges and research potential were identified for the implementation of MPC to industrial systems in the future.

Application of machine learning algorithms: The application of *grey-box models* makes it possible to integrate machine learning algorithms for parameterisation of the component models when developing MPC for green-field and retrofit systems. This is a highly relevant field of research and gives the possibility to include different component technologies and provide customised solutions for sector coupling and optimal control of decentralised energy systems.

Cascading with rule-based controller: The possibility to cascade a MPC with a rule-based controller could be realised by applying *explicit-MPC* techniques. The optimal schedule of the MPC is forwarded as a look-up table for a rule-based controller in the form of the set-point values for tank temperatures or switching point between the primary and back-up systems. The rule-based controller then operates the plant as per these optimally set parameters but overrides the control in case any constraint violations occur. This type of cascaded control may facilitate a safer operation due to the hard constraints of the rule-based controller and simultaneously exploit the features of optimal control.

Implementation of relaxed solution: The potential benefits of implementing a relaxed solution in this study were based on an elementary comparison and further analysis is necessary for their quantification. Such an analysis is possible through detailed long-duration simulations or a test set-up with components capable of output modulation. However, based on the practical experience gathered during this study, it is highly recommended that the economic benefits of a relaxed solution in retrofit scenarios will not overcome the investments (monetary and time) for modifying any internal controllers or hydraulic connections to ensure its hardware implementation.

Mathematical scrutiny of optimisation algorithm and problem formulation: To improve the quality of the relaxed solution i.e. solution of the original nonlinear problem a thorough mathematical scrutiny of the optimisation algorithm and the problem formulation should be done. Further simplification of the models and reducing number of algebraic constraints should be attempted. Additionally, advanced solvers e.g. MA27 and MA57 within the IPOPT package and sensitivity analysis with the IPOPT setting parameters should be attempted.

Quality of binary approximation solution: The effectiveness of the binary approximation algorithm to find binary solutions that closely capture the dynamics of a relaxed solution and respect all constraints is of crucial importance. The evaluation of single MPC iterations revealed that the binary approximation is more effective if the relaxed solution for a component is closer to 0 or 1 (bang-bang form). Further improvement of the binary approximation method is necessary in order to find a best possible solution corresponding to the relaxed solution and is a valuable field of research in terms of MINLP solvers. The binary approximation methods must be critically evaluated for their mathematical formulation and further tests e.g. with higher permissible times should be done for their development.

Uncertainty in forecast data, price predictions, and model mismatch: A deterministic forecast was used in this work because the focal point was to demonstrate and compare MPC against a reference controller under almost-identical conditions. Additionally, with the assumption that the slow dynamics of a thermal system are handled adequately with a receding horizon scheme a practical and simple approach was possible. However, when the effect of uncertainties in the input data (disturbances and measurement noise) or model output (numerical errors or mismatch) are a matter of concern then explicit techniques to formulate robust MPC or stochastic MPC should be applied (*cf. Section 3.3*). This is a highly relevant field of research and many theoretical studies have developed these approaches. A practical application of these approaches and quantitative analysis to evaluate their benefits for systems highly sensible to uncertainties and model mismatch is also a valuable research topic.

8 Experimental Results: Comparison of a Reference Controller and MPC

A demonstration of the MPC's performance in comparison to a rule-based conventional controller is given in this chapter. In addition to a detailed experimental analysis of one test per season, an economic calculation and operational analysis using data from 6 experiments in summer and 8 experiments in winter for a total operational time of 391 hours and 577 hours respectively is presented. An economic benefit in final energy costs of 6% to 15% was realised using MPC and further qualitative benefits from an engineering perspective were identified.

8.1 Experimental analysis

The performance of the MPC was compared to a reference controller under scenarios with almost-identical parameters: e.g. thermal load profile, electricity prices, and initial tank temperatures. The duration of a test was 1 to 5 days for each controller whereby the ambient temperature did not vary significantly. The details for each test are available in the list of tests in *Appendix E*. The results for one comparison in a summer scenario and one comparison in a winter scenario are illustrated in the following sections.

8.1.1 Summer

The summer scenario for a long-duration MPC test described in *Chapter 7* was also used for the reference controller. The reference controller followed a conventional *base load matching – following thermal load strategy* (BLM-FTL) as described in *Section 2.3* and *Section 4.1*. *Table 8-1* summarises the parameterisation of the conventional controller.

Table 8-1 Parameters for implementing the reference controller for summer with switching point

Parameter	Value
$T_{CT1,max}$	12 °C
$T_{CT4,min}$	12 °C
Switching point	6.5 kW$_{th}$
$T_{HT6,min}$	70 °C
$T_{HT1,CHP,max}$	70 °C

The values were selected after multiple tuning experiments and discussions with the component manufacturers to design a conventional controller specifically for the INES laboratory set-up. A hysteresis over the top and bottom tank temperatures was introduced to avoid frequent switching of the components and utilise the entire tank volume. $T_{f,TC,set}$ was set at 14 °C and during the test with a reference controller $T_{f,TC,ref}$ was achieved and during the test with the MPC $T_{f,TC,MPC}$ was achieved. Further description of the parameter selection is given in *Appendix B.4*.

The profiles of input parameters for both the controllers over the entire monitoring campaign are illustrated in *Fig. 8-1*. The ambient temperature for the reference controller $T_{amb,ref}$ and the MPC $T_{amb,MPC}$ are similar over the 8 days of tests. The cooling load forecast $P_{th,CL,fc}$ is same for both the tests and is based on a hospital load profile. The actual cooling load covered by the reference controller $P_{th,CL,ref}$ and by the MPC $P_{th,CL,MPC}$ are also shown in the figure.
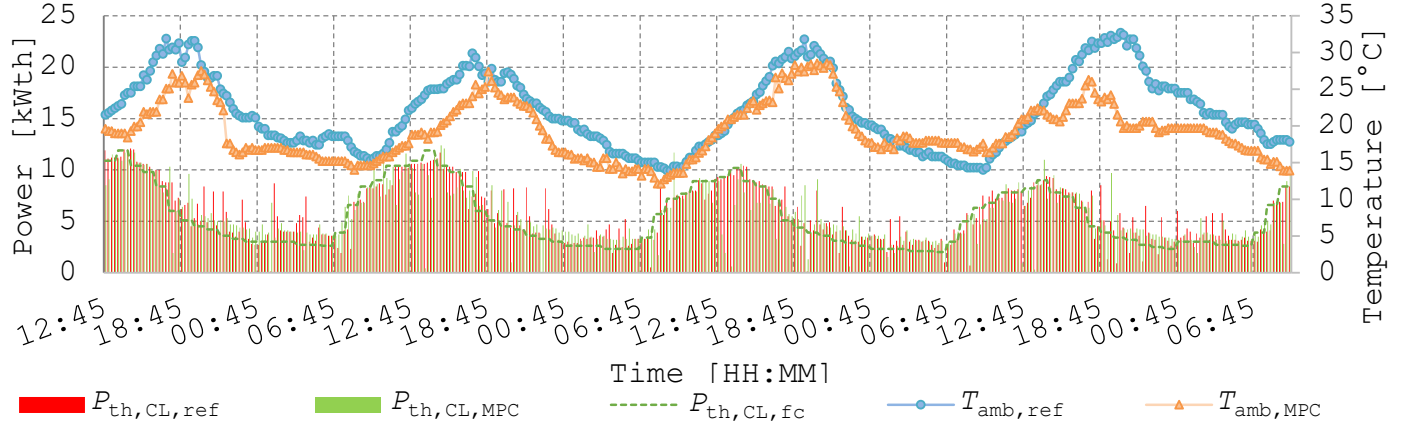

Fig. 8-1 Input data for a long-duration test of a summer scenario with reference controller started on 28.08.2019 at 12:45 and MPC controller started on 01.09.2019 at 12:45

In *Fig. 8-2*, the measured data for feed-line temperature to the TC achieved by the three-way mixing valve during the two tests is illustrated. During both tests the $T_{f,TC,set}$ set at 14 °C is closely tracked, with the exception of $T_{f,TC,MPC}$ during 12:45 to 18:45 on the second and third day of operation, which are referred later in this section.
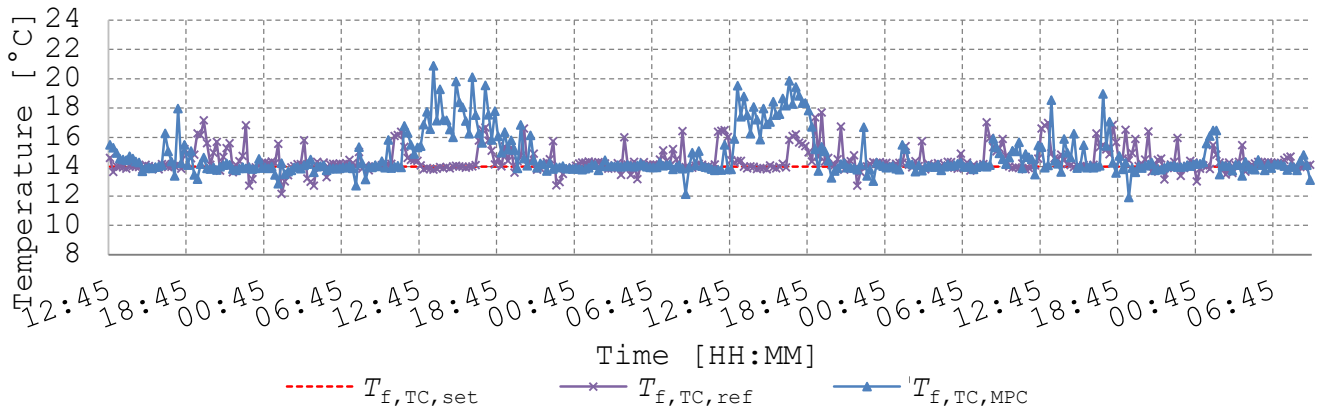
Fig. 8-2 Measurement data for the feed-line temperature to the cooling circuit in test chambers with reference controller and MPC starting at 12:45. Deviations from set-point occuring during times of inadequate cooling feed-line temperature in CTES are noticed

To understand fundamental differences in the actions of the two controllers, the thermal and electrical balances with tank temperatures and electricity price are plotted in *Fig. 8-3*.

The results of the test with reference controller are plotted on the left side of the figure and results with MPC are plotted on the right side. Both tests are of the same duration

(92.75 hours) and started with similar initial temperatures in the tanks. The significant observations are summarised below:

Simpler tuning of MPC: The tuning of the MPC is done by defining the permissible operation range in the HTES and CTES using the parameters $T_{\text{HT}i,\text{max}}, T_{\text{min}}, T_{\text{CT}i,\text{max}}$, and T_{min}. The operation is bounded with temperature limits $T_{\text{r,AdC,H,min}}$, $T_{\text{r,CHP,max}}$, and $T_{\text{f,TC,set}}$, which are promptly defined in datasheets of the components.

These constraints specify a wide range of possible operation within which the MPC automatically finds an optimal solution whereas the tuning of the reference controller is through the nontrivial process of commissioning routines, simulation studies, or guesswork based on recommendation of individual component manufacturers (often not directly suitable for multicomponent systems).

Base load matching-following thermal load strategy and hysteresis is noticed in reference controller's operation: In *Fig. 8-3 (a)* of the reference controller, the following thermal load operation of the CHP is observed. The CHP turns on when T_{HT6} is cooler than $T_{\text{HT6,min}}$ and remains on till T_{HT1} is hotter than $T_{\text{HT1,CHP,max}}$. Similarly, the hysteresis control operation of the AdC and CC is seen in *Fig. 8-3(b)* of the reference controller. The chillers operate until T_{CT4} is cooler than $T_{\text{CT4,min}}$ and turn on when T_{CT1} is warmer than $T_{\text{CT1,max}}$. This operation gives the hysteresis controller its distinct saw-tooth pattern. As defined in the conventional controller's base load matching configuration, it operates the AdC if $P_{\text{th,CL}} \leq 6.5 \text{ kW}_{\text{th}}$, else it operates the CC.

In the thermal (heating) balance, $P_{\text{th,CHP}}$ and $P_{\text{th,HT}}$ satisfy $P_{\text{th,AdC,H}}$ and charging of the HTES leads to stratified tank temperatures. Four temperatures in HTES are shown, with T_{HT1} being at the bottom and corresponding to the return-line for CHP and T_{HT8} corresponding to the driving temperature for the AdC. In the thermal (cooling) balance, $P_{\text{th,CC,e}}, P_{\text{th,AdC,L}}$, and $P_{\text{th,CT}}$ satisfy $P_{\text{th,CL}}$. Two temperatures in CTES are shown, with T_{CT1} being at the bottom (feeding the load) and T_{CT4} (going to the chillers).

MPC does not violate minimum runtime constraint: As discussed in *Section 6.1* the minimum runtime constraint is implemented in the controllers to consider the maintenance and lifetime of mechanical components in *switch-critical machines* such as CHP or RHP. It is implemented using the hysteresis logic in the reference controller and as a mathematical constraint in the MPC.

In this particular scenario, a less switching or a more continuous operation of the components is observed in the reference controller due to the hysteresis dead-band logic over tank temperatures. The switching of components in MPC is more frequent because it does not depend only on the current tank temperatures but also on the forecast data, economic costs over the entire horizon, and the minimum up/down time setting as discussed in *Chapter 7*. The MPC maintains a higher average temperature in the HTES (73 °C compared to 66 °C by reference controller) and the switching of components does not violate minimum runtime constraint.

A more detailed analysis of this point is done in *Section 8.3.2* with data collected over multiple tests.

Inadequate cooling feed-line temperature in CTES: Even though a 2 K buffer was planned for the reference controller by setting the $T_{\text{CT1,min}} = 12\,°C$ for the $T_{\text{f,TC,set}} = 14\,°C$, the tank temperature is inadequate at certain points during the operation. The MPC also violates this constraint especially from 12:45 to 18:45 on the second and third day of operation. Referring to *Fig. 8-2* earlier, it is in these regions of inadequate tank temperatures that $T_{\text{f,TC,MPC}}$ and $T_{\text{f,TC,ref}}$ deviate from $T_{\text{f,TC,set}}$.

Predictive charging of CTES by MPC: Higher night-time charging of the CTES with MPC is observed as it operates the CC even at lower cooling loads to predictively charge the CTES (almost till minimum permissible temperatures) for using the energy during daytime.

Grid-adverse operation of reference controller and grid-supportive operation of MPC: Interpreting the thermal balances with respect to the electrical balances and electricity price $r_{\text{el,buy,EWERK}}$ in *Fig. 8-3 (c),* it is observed that the reference controller often operates the CC i.e. generates electrical peaks during times of high $r_{\text{el,buy,EWERK}}$. This behaviour is more frequent when high thermal and electrical loads occur simultaneously and is significantly grid-adverse since electricity is purchased during peak hours. Additionally, it is observed that the reference controller produces excess electricity and adversely feeds it to the grid during night-time.

On the other hand, the MPC minimises peaks (in most cases) during times of high $r_{\text{el,buy,EWERK}}$. However, under certain circumstances e.g. lack of sufficient energy in CTES and peak cooling loads, the MPC also operates the CC during times of high $r_{\text{el,buy,EWERK}}$. It then exploits the minimum up/down time of the CC and switches the machine frequently to avoid longer peaks.

8-Experimental Results: Comparison of a Reference Controller and MPC
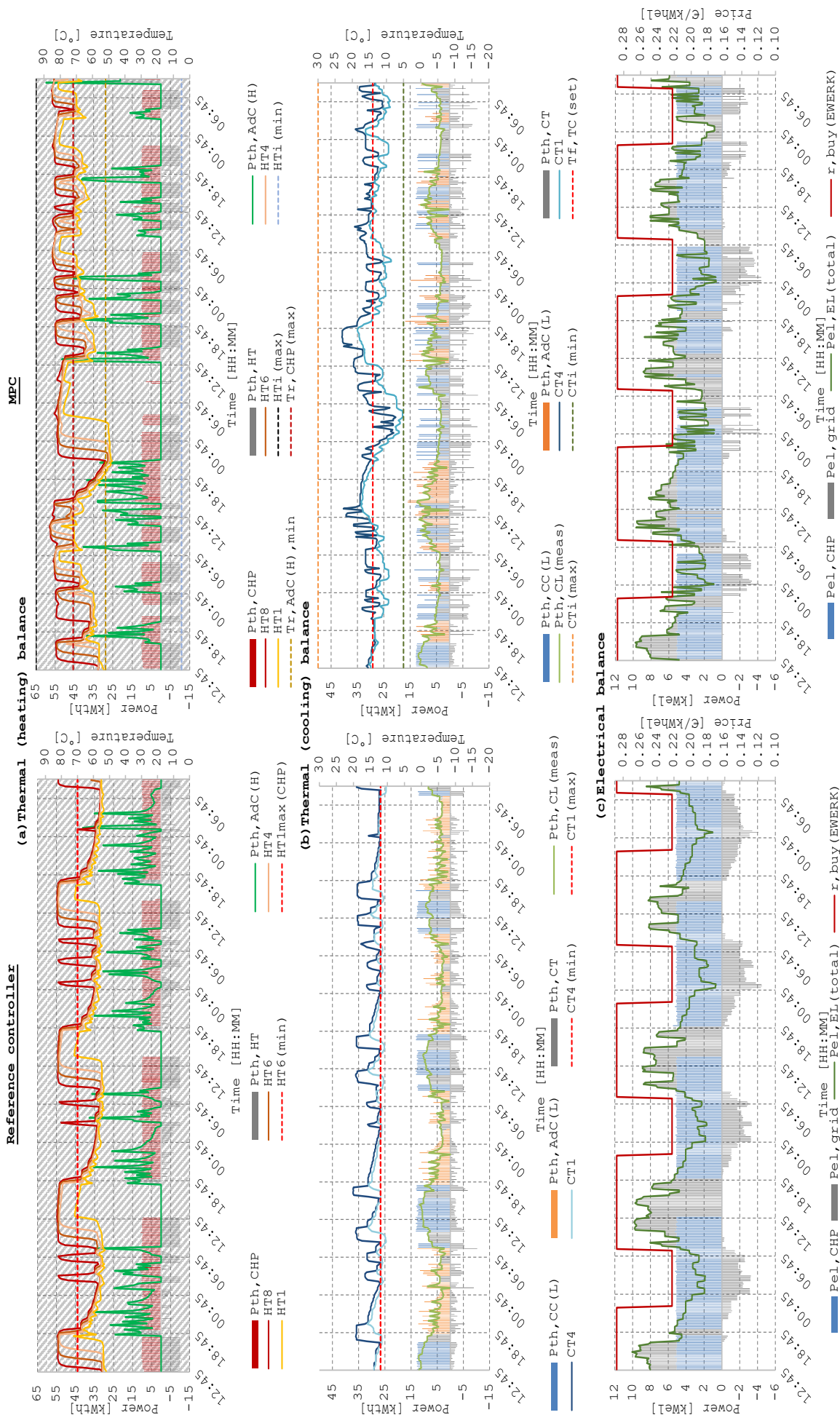

Fig. 8-3 Measurement data in 15-minute intervals for 92.75 hours of a long-duration test of a summer scenario with reference controller started on 28.08.2019 at 12:45 and MPC controller started on 01.09.2019 at 12:45

8.1.2 Winter

The winter scenario for a long-duration MPC test described in *Chapter 7* was also used for the reference controller. The reference controller followed a conventional BLM-FTL strategy. *Table 8-2* summarises the parametrisation of the reference controller with hysteresis and a description of the parameter selection is given in *Appendix B*.

Table 8-2 Parameters for implementing the reference controller for winter scenario with switching point

Parameter	Value
$T_{HT1,max,CHP}$	70 °C
$T_{HT1,max,HP}$	43 °C
$T_{HT6,min}$	70 °C
Switching point	10.5 kW$_{th}$

The profiles of input parameters for both the controllers over the entire monitoring campaign are illustrated in *Fig. 8-4.* Although the profiles of the ambient temperature are different during the two tests, the average ambient temperature is similar and the daily temperature differential is lower compared to summer tests. The heating load forecast $P_{th,HL,fc}$ is same for both the tests and is based on a hospital load profile used in *Chapter 7*. The actual heating load covered by the reference controller $P_{th,HL,ref}$ and by the MPC $P_{th,HL,MPC}$ are also shown in the figure. Both the controllers follow the forecast more closely in winter compared to the summer test.
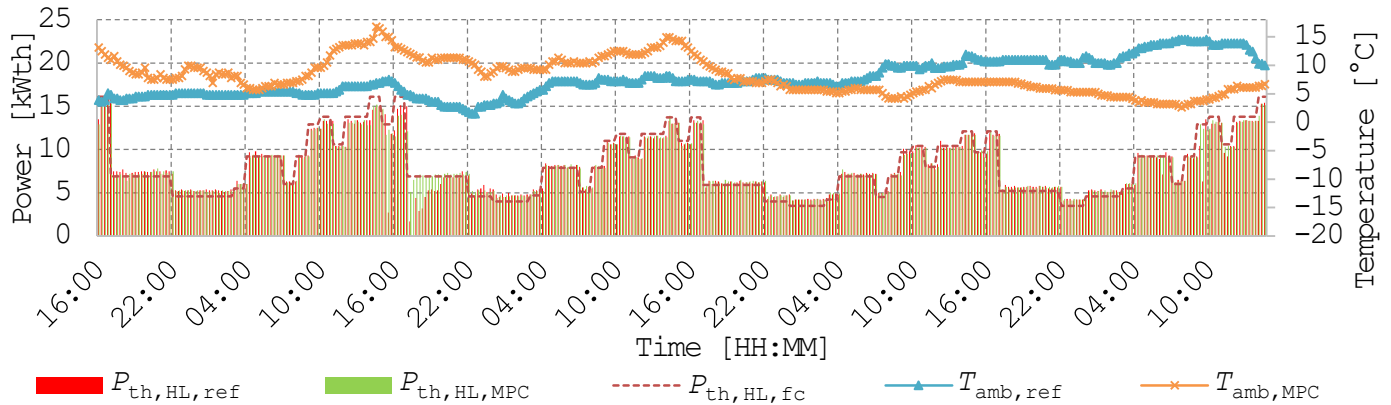

Fig. 8-4 Input data for a long-duration test of a winter scenario with reference controller started on 11.12.2019 at 16:00 and MPC controller started on 16.12.2019 at 16:00

In *Fig. 8-5,* the measured data for feed-line temperature to the TC achieved by the three-way mixing valve during the two tests is illustrated. During both tests the $T_{f,TC,set}$ set at 40 °C is closely tracked with the exception at Time = ca. 16:00 to 22:00 on the second day of operation and the two distinct peaks for the $T_{f,TC,ref}$ at Time = ca. 16:00 on the second day and Time = ca. 09:45 on the last day, which are referred to later in this section.
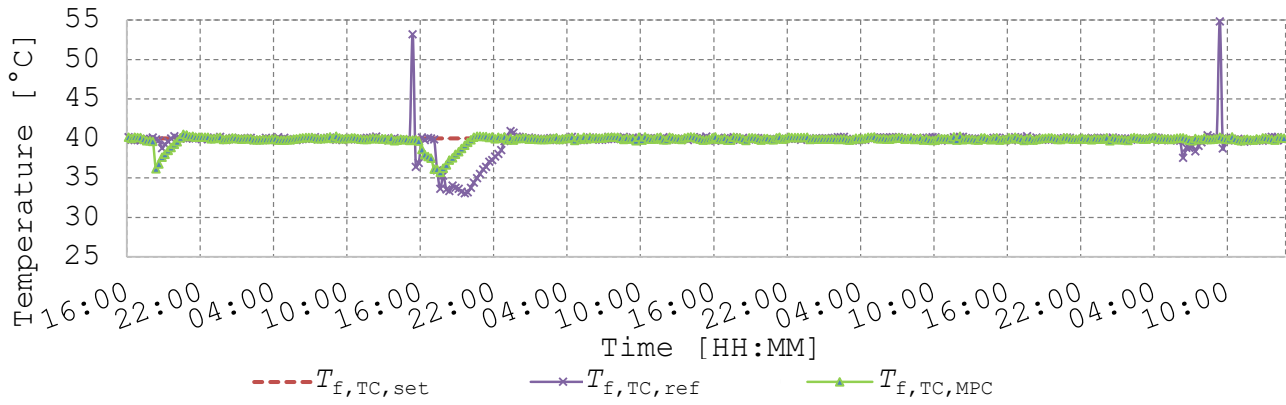
Fig. 8-5 Measurement data for the feed-line temperature to the heating circuit in test chambers with reference controller and MPC starting at 16:00. Deviations from set-point occuring during times of inadequate heating feed-line temperature and peaks due to rapid mixing in HTES are noticed

To understand fundamental differences in the actions of the two controllers, the thermal and electrical balances with tank temperatures and electricity price are plotted in *Fig. 8-6.* Both tests are of the same duration (94.5 hours) and start with a homogeneous HTES initial temperature of ca. 50 °C. The significant observations are summarised below:

Simpler tuning of MPC: Similar to the summer scenario, the tuning of MPC is done by defining an operation in the HTES using the two parameters $T_{HTi,max}$ and $T_{HTi,min}$. The operation is bounded with temperature limits $T_{r,HP,c,max}$, $T_{r,CHP,max}$, and $T_{f,TC,set}$, which are promptly defined in datasheets of the components.

Base load matching-following thermal load strategy and hysteresis is noticed in reference controller's operation: The BLM-FTL strategy of the CHP and HP is observed in the thermal balance of the reference controller. The CHP is on if $P_{th,HL} \leq 10.5$ kW$_{th}$, else the HP is on. In addition to this switching logic, the hysteresis over the HTES temperatures is also observed. The CHP or HP goes on if T_{HT6} is cooler than $T_{HT6,min}$ and the CHP goes off when T_{HT1} is warmer than $T_{HT1,CHP,max}$. and HP goes off when T_{HT1} is warmer than $T_{HT1,HP,max}$.

The $P_{th,CHP}$, $P_{th,HP,c}$, and $P_{th,HT}$ satisfy $P_{th,HL}$ and charging of the HTES leads to stratified tank temperatures. Four temperatures in HTES are shown, with T_{HT1} being at the bottom and corresponding to the return-line for CHP and HP, while T_{HT8} is at the top.

Mixing of tank temperatures due to HP operation: The noticeable mixing of tank layers due to smaller temperature differential and high volume flow of HP is also observed in the reference controller operation. Referring to *Fig. 8-5* above, it is in these regions of rapid mixing that the peaks in deviation of $T_{f,TC,ref}$ from $T_{f,TC,set}$ occur as the three-way mixing valve cannot react fast enough.

MPC minimises HP operation: The MPC solution has a higher average temperature in the HTES (64 °C compared to 60 °C by reference controller) and the heating load is satisfied only with $P_{th,CHP}$ and $P_{th,HT}$ as discussed in *Section 7.1.2.*

Inadequate heating feed-line temperature in HTES: Although the MPC does not operate the HP over the entire test period, it is counter-intuitive in cases when adequate tank temperature is not available during peak load requirements. Referring to *Fig. 8-5* earlier, it is in these regions of inadequate tank temperature that $T_{f,TC,MPC}$ deviates from $T_{f,TC,set}$. A discussion on this behaviour arising from the goal of economic optimisation or model inaccuracies is done in *Section 8.3.2*.

In case of the reference controller inadequate temperatures arise when the CHP is turned on as per its hysteresis logic and the load layer reaches adequate temperature much later due to the thermal inertia of stratification. Referring to *Fig. 8-5* above, it is in these regions of inadequate tank temperature that the $T_{f,TC,ref}$ deviates from $T_{f,TC,set}$.

Grid-adverse operation of reference controller and grid-supportive operation of MPC: Interpreting the thermal balances with respect to the electrical balances and electricity price in *Fig. 8-6 (b)*, it is observed that the reference controller operates the HP i.e. generates electrical peaks irrespective of the forecasted electrical load or price of electricity $r_{el,buy,EPEX}$. This operation leads to grid-adverse switching of the HP especially when peak $P_{th,HL}$ occurs simultaneously with peak electrical loads and high $r_{el,buy,EPEX}$.

In contrast, the MPC provides a grid-supportive schedule with respect to the $r_{el,buy,EPEX}$ e.g. by switching off the CHP in times of lower $P_{th,HL}$ and $P_{el,EL,total}$, thereby avoiding HTES overheating and switching on the CHP at higher $P_{th,HL}$ and $P_{el,EL,total}$ as seen on last two days of the MPC test.
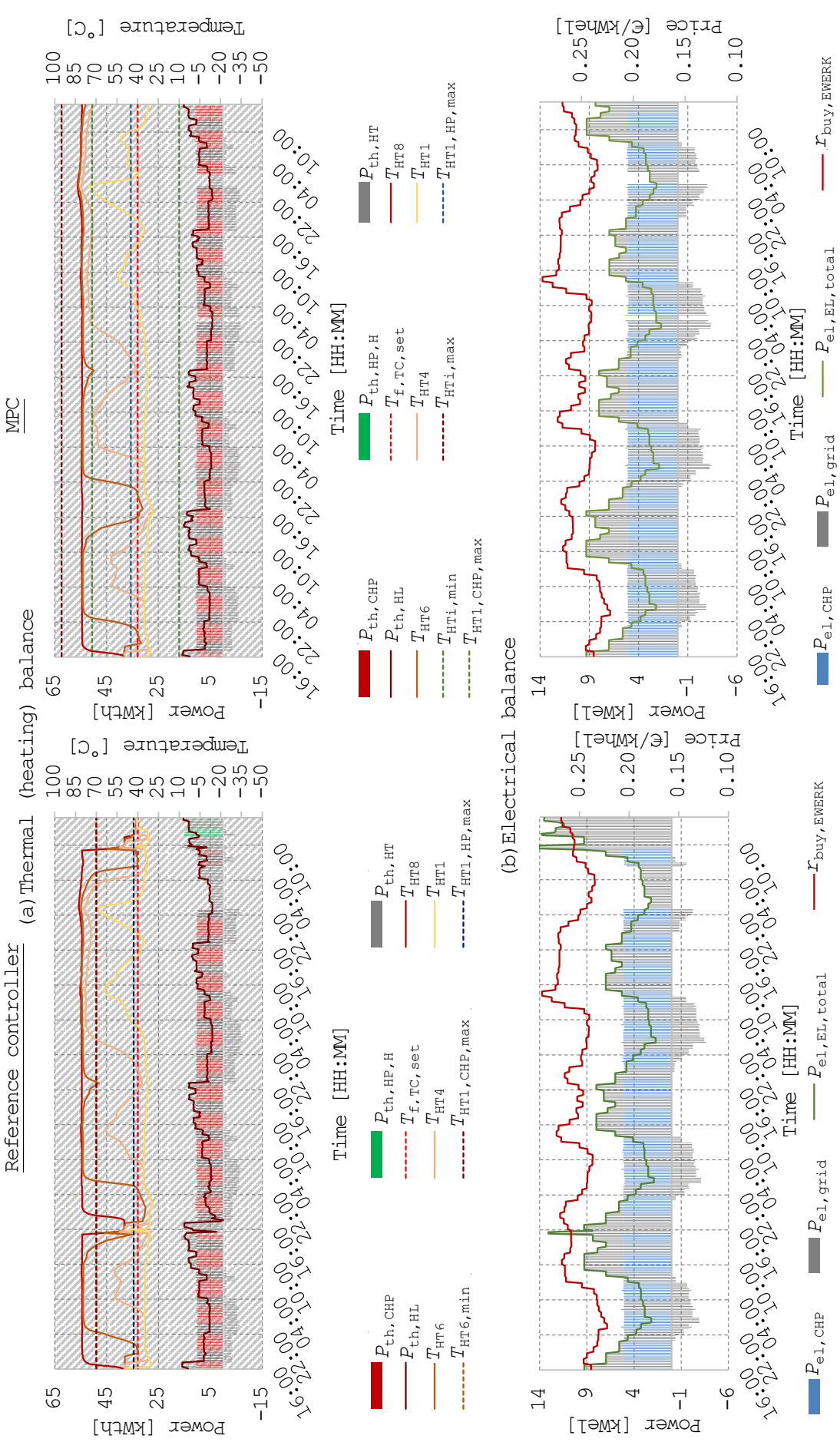
Fig. 8-6 *Measurement data in 15-minute intervals for 94.5 hours of a long-duration test of a winter scenario with reference controller started on 11.12.2019 at 16:00 and MPC controller started on 16.12.2019 at 16:00*

8.1.3 Conclusion of experimental analysis

The reference controller and MPC were available throughout the test duration and the building automation and control framework did not fail. Since the reference controller was set-up with extensive operational knowledge of this exact system, its performance was not significantly lower than the MPC. For instance, it also facilitated high CHP operation, usage of the AdC and usage of storage capacity. However, the major differences in MPC operation were observed in the predictive charging of tanks, reduced usage of RHP, and more operation of the CHP-AdC combination.

It is challenging to interpret the advantage of the optimal solution only by graphical analysis of measured data. The measured data captures the effect of the actually applied control signal out of the complete predictive solution calculated by the MPC over the entire horizon. For a detailed comprehension of the MPC's solution quality, the 24-hour solution from each iteration must be recorded and analysed. Such an analysis was out of scope of this work and the advantage of MPC is quantified using economic and operational analysis of entire measured data.

8.2 Economic analysis

An economic analysis of the experimental data from reference controller and MPC was done using total *consumption-related costs* and *simple levelised cost of energy* calculations considering the cost function defined in *Section 6.2*. Results from multiple tests under various scenarios producing 968 hours of monitoring data were analysed to balance out the effects of uncontrollable operational fluctuations and achieve reproducibility of results when comparing both controllers.

For calculating the electricity bought $P_{\text{el,grid,buy}}$ or sold to grid $P_{\text{el,grid,sell}}$, the electrical power balance in (8.1) was used.

$$P_{\text{el,grid}}(t) = \left(P_{\text{el,EL}}(t) + P_{\text{el,HP}}(t) + P_{\text{el,CC}}(t) + P_{\text{el,AdC}}(t) + P_{\text{el,OC}}(t) + P_{\text{el,aux}}(t) \right) - P_{\text{el,CHP}}(t)$$
(8.1 a)

If,

$$P_{\text{el,grid}}(t) > 0, P_{\text{el,grid,buy}}(t) = P_{\text{el,grid}}(t) \text{ and } P_{\text{el,grid,sell}}(t) = 0$$
(8.1 b)

Else,

$$P_{\text{el,grid,sell}}(t) = P_{\text{el,grid}}(t) \text{ and } P_{\text{el,grid,buy}}(t) = 0$$
(8.1 c)

Since the electricity prices are in 15-minute time intervals, the total cost of electricity $Cost_{\text{el}}$ for $t \in [t_0, t_f]$ was calculated using an integration interval $\mathrm{d}t = 0.25$ hours as in (8.2).

$$Cost_{el} = \int_{t_0}^{t_f} (P_{el,grid,buy}(t) r_{el,buy}(t) - |P_{el,grid,sell}(t)| r_{el,sell}(t)) \mathrm{d}t \tag{8.2}$$

The total cost of fuel $Cost_{fuel}$ was also calculated using an integration interval $\mathrm{d}t = 0.25$ hours as in (8.3).

$$Cost_{fuel} = \int_{t_0}^{t_f} (\dot{v}_{fuel}(t) r_{fuel}(t)) \mathrm{d}t \tag{8.3}$$

The total consumption-related costs for final energy $Cost_{fe}$ was calculated using (8.4) and was the focus of comparison between the reference and MPC controller since it was the target function of the economic-MPC.

$$Cost_{fe} = Cost_{el} + Cost_{fuel} \tag{8.4}$$

However, for getting a more practically relevant metric to compare economic performance of the controllers, the simple levelised cost of energy $sLCOE$[1] was also calculated. The thermal simple levelised cost of energy $sLCOE_{th}$ was calculated based on the total useful energy required for the thermal load and the electrical simple levelised cost of energy $sLCOE_{el}$ was calculated using the total useful energy required for electrical load. The system boundary for energy and cost balance is shown in *Fig. 8-7*.
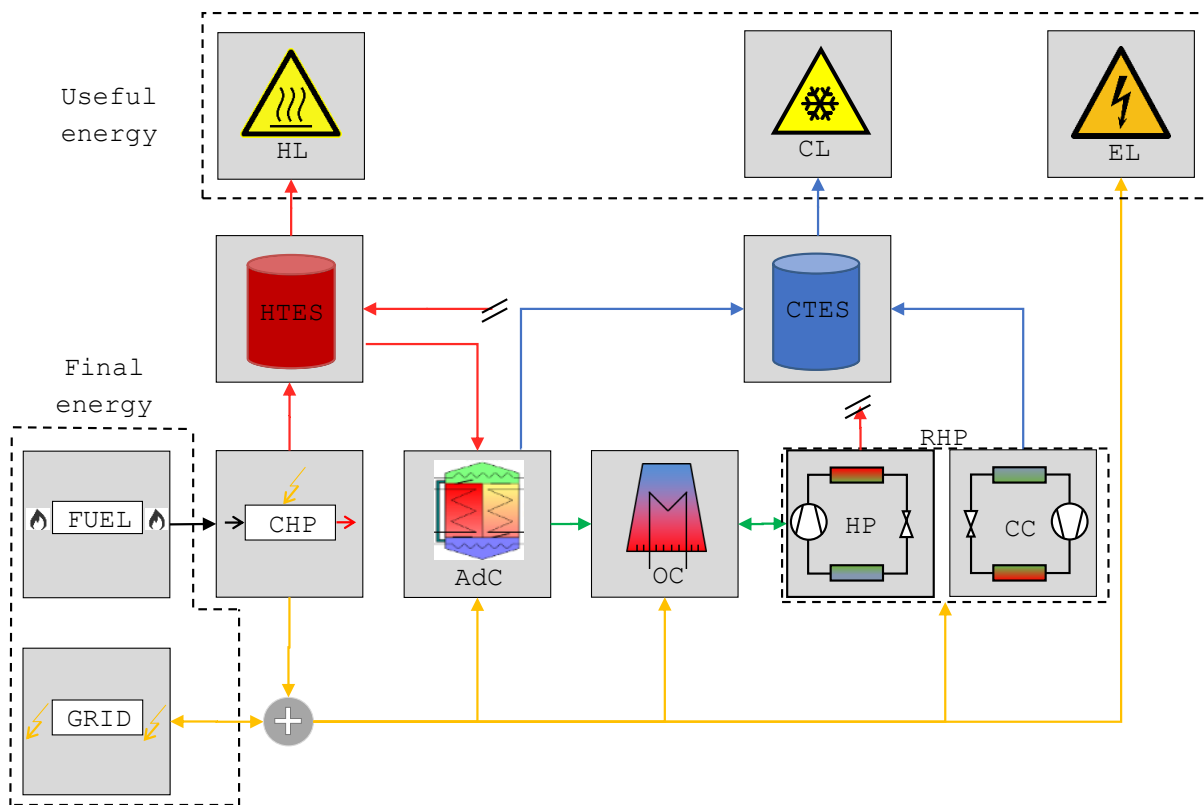
Fig. 8-7 System boundary for calculating the simple levelised cost of energy considering the useful energies required for thermal and electrical load

The electrical load satisfied $W_{el,EL}$ was calculated using (8.5).

---

[1] The *sLCOE* used in this work is related to final energy demand-related costs over the monitoring campaign only and does not include investment costs or operation-related costs over life of plant as used in complex LCOE calculations (definition in glossary of terms).

$$W_{\text{el,EL}} = \int_{t_0}^{t_\text{f}} P_{\text{el,EL}}(t)\, \mathrm{d}t \tag{8.5}$$

Whereas, the total cooling load covered $Q_{\text{th,cool}}$ and total heating load covered $Q_{\text{th,heat}}$ were calculated using (8.6) and (8.7) respectively.

$$Q_{\text{th,cool}} = \int_{t_0}^{t_\text{f}} P_{\text{th,CL}}(t)\, \mathrm{d}t \tag{8.6}$$

$$Q_{\text{th,heat}} = \int_{t_0}^{t_\text{f}} P_{\text{th,HL}}(t)\, \mathrm{d}t \tag{8.7}$$

The $sLCOE_{\text{el}}$, $sLCOE_{\text{th,cool}}$, and $sLCOE_{\text{th,heat}}$ were calculated using their respective energy balances and are summarised in (8.8), (8.9), and (8.10) below.

$$sLCOE_{\text{el}} = \frac{Cost_{\text{fe}}}{W_{\text{el,EL}}} \tag{8.8}$$

$$sLCOE_{\text{th,cool}} = \frac{Cost_{\text{fe}}}{Q_{\text{th,cool}}} \tag{8.9}$$

$$sLCOE_{\text{th,heat}} = \frac{Cost_{\text{fe}}}{Q_{\text{th,heat}}} \tag{8.10}$$

The following indicators or coefficients were calculated for characterising the different load profiles, identifying their effects on the consumption-related costs, and quantifying the usage of storage capacity:

- *Load ratio* is the ratio of the electrical load to thermal load ($W_{\text{el,EL}}/Q_{\text{th,CL}}$ or $W_{\text{el,EL}}/Q_{\text{th,HL}}$) satisfied over the test duration. A higher load ratio signifies a load profile with greater electrical load requirements than thermal load requirements e.g. transition season in non-residential buildings.
- *Energy stored in the tank* (thermal energy produced – thermal load covered), assuming all thermal losses during test duration are represented in the thermal loss over the tanks.
- *Self-consumption ratio* is the ratio of the total electricity produced by the CHP to the total electrical load satisfied[1] ($W_{\text{el,CHP}}/W_{\text{el,EL,total}}$), and the total cooling (heating) produced by the CC (HP) to the cooling (heating) load satisfied ($Q_{\text{th,CC(L)}}/Q_{\text{th,CL}}$ or $Q_{\text{th,HP(H)}}/Q_{\text{th,HL}}$). An electrical self-consumption ratio greater than 1 signifies complete coverage of electric load with CHP's generation and possible feed-in to the grid. A higher thermal self-consumption ratio signifies coverage of thermal load predominantly with the RHP.

The results of the economic analysis are summarised in *Table 8-3* for summer tests and in

Table 8-4 for winter tests. The date of the test and duration of the test in number of days of operation with each controller are noted.

In the summer scenario, the $Cost_{\text{fe}}$ is 6% lower (average of different tests) with MPC, ranging between 1.5% to 9% savings. For all the tests, $sLCOE_{\text{el}}$ is lower with MPC and an

---

[1] Including the electrical energy requirements of components.

average 6% saving is noticed. For most tests, $sLCOE_{th,cool}$ is lower with MPC and an average saving of 1.4% is noticed. With an increasing load ratio, the magnitude of $sLCOE_{th,cool}$ increases as the total $Cost_{fe}$ is higher due to higher electrical loads. Accordingly, the magnitude of electrical self-consumption ratio reduces for both controllers. In most cases, the MPC has a higher electrical self-consumption ratio and a lower thermal (cooling) self-consumption ratio compared to the reference controller. This indicates the higher usage of CHP and lower usage of the CC by the MPC controller. Additionally, the $sLCOE_{th,cool}$ with MPC is higher in two tests when more energy in the CTES is stored.

In the winter scenario, a higher saving in $Cost_{fe}$ and $sLCOE$ is noticed compared to the summer scenario. This is because, in winter, electricity can be strictly either consumed (RHP) or produced (CHP) to provide heating unlike the possibility to provide cooling along with electricity production in all modes for summer. The final energy costs are 15% lower (average of different tests) with the MPC, ranging between 3.4% to 35% savings. The $sLCOE_{el}$ is also lower with MPC and an average 15% saving is noticed. An average 14.6% saving in $sLCOE_{th,heat}$ is noticed with MPC compared to the reference controller. Similar to the summer scenario, increasing load ratio leads to increasing $sLCOE_{th,heat}$ and lower electrical self-consumption ratio with both controllers. It is observed that MPC stored more energy in HTES and covered all the HL profiles with a lower thermal self-consumption ratio i.e. lower HP operation.

Table 8-3 Economic analysis of multiple <u>summer scenario</u> tests using different varying load profiles, electricity tariffs, and test duration (chronological order). Only CTES energy analysed for summer to keep table concise

Test date & duration	Load ratio	$Cost_{fe}$ [€]		$sLCOE_{el}$ [€/kWh$_{el}$]		$sLCOE_{th,cool}$ [€/kWh$_{th}$]		Energy stored in CTES [kWh$_{th}$]		Electrical self-consumption ratio		Thermal self-consumption ratio	
	Both	Ref	MPC	Ref	MPC	Ref	MPC	Ref	MPC	Ref	MPC	Ref	MPC
21.10.19 (3 days)	0.90	74.7	70.6	0.296	0.280	0.235	0.239	44.80	63.65	0.66	0.84	0.74	0.66
16.10.19 (3 days)	1.79	137	127	0.266	0.247	0.420	0.421	44.25	61.37	0.37	0.52	0.75	0.42
11.10.19 (1.5 days)	1.71	73.5	68.8	0.271	0.254	0.411	0.399	31.95	23.13	0.34	0.52	0.84	0.62
01.10.19 (4 days)	0.61	106	99.2	0.346	0.323	0.195	0.188	54	48	0.89	0.82	0.51	0.60
23.09.19 (1.5 days)	0.59	41.9	38.1	0.371	0.338	0.208	0.205	14.13	8.45	0.69	0.74	0.65	0.54
10.09.19 (5 days)	1.02	94.5	93.1	0.306	0.301	0.258	0.252	56.20	23.27	0.90	0.75	0.40	0.51

Table 8-4 Economic analysis of multiple <u>winter scenario</u> tests using different load profiles, electricity tariffs, and test duration (chronological order). Higher saving observed in winter

Test date & duration	Load ratio	$Cost_{fe}$ [€]		$sLCOE_{el}$ [€/kWh$_{el}$]		$sLCOE_{th,heat}$ [€/kWh$_{th}$]		Energy stored in HTES [kWh$_{th}$]		Electrical self-consumption ratio		Thermal self-consumption ratio	
	Both	Ref	MPC	Ref	MPC	Ref	MPC	Ref	MPC	Ref	MPC	Ref	MPC
08.04.20 (3 days)	0.39	86.1	58.3	0.314	0.213	0.126	0.085	69.58	84.5	0.68	1.23	0.36	0.05
31.03.20 (0.9 days)	0.39	29.2	24	0.313	0.258	0.117	0.096	-20	-4.5	0.69	1.0	0.28	0.12
07.02.20 (4.7 days)	0.75	193	158	0.265	0.217	0.200	0.160	64.9	195.8	0.53	0.80	0.18	0
22.01.20[1] (3.8 days)	0.39	58.2	58	0.204	0.203	0.079	0.079	197	209.6	1.64	1.64	0	0
03.01.20 (3.8 days)	0.75	71.5	69.1	0.240	0.232	0.150	0.150	99.5	161.2	0.94	1.02	0	0
11.12.19 (3.9 days)	0.63	110	101	0.229	0.210	0.144	0.132	118	172.6	0.79	0.95	0.08	0
02.12.19 (2.6 days)	0.76	103	97.8	0.234	0.222	0.179	0.171	63.8	71.28	0.66	0.72	0.05	0
13.11.19 (1 day)	0.39	32.3	21.0	0.358	0.233	0.141	0.094	-62	5.10	0.48	1.25	0.27	0

The primary energy consumption for both controllers was calculated assuming a factor of 1.1 for fuel and 1.8 for electricity (EnEV-online, 2016). An energy-economy mismatch was noticed in a few control sequences where the MPC consumed 8% to 10% more primary energy but was also a more economical variant.

8.3   Operational analysis

Two methods were used to compare the performance and efficiency of the controllers through operational analysis: (a) Analysis of operational runtime of machines with respect to electricity price and load profiles (b) violation of constraints.

8.3.1 Operational runtime of machines based on electricity price and load

The operational data collected for the different machines in the summer and winter scenarios was grouped into nine categories (low, medium, and high) according to magnitude of the electricity price and forecasted thermal or electrical load. The total number of data points in each category was same for the reference and MPC controller. Therefore, it was possible to compare the percentage of time a machine(s) was operated by each controller in that category. The operational time of a machine or combination of

---

[1] In the test on 22.01.2020, the control actions of the reference controllers and the MPC were very similar, emphasising the point that the reference controller was already very well planned for this particular plant and any added economic benefits with MPC are highly valuable.

machines in a particular category was calculated as a percentage of the plant's total operational time in that category by counting the number of data points when the relevant machine(s) was on.

The results for operational analysis of the experimental data in summer scenario with respect to electricity price and the thermal load are shown in *Fig. 8-8*. For instance, out of 484 data points or 121 hours of operational time in the category low price – low load, the "CHP+AdC" combination is used for 51% of the time (61.5 hours) by the reference controller and for 21% of the time (25.25 hours) by MPC. Operation of the machines is dependent on multiple factors such as tank temperatures, load forecast, and ambient temperature simultaneously and therefore a direct correlation is not possible in all cases. However, the significant differences that were in accord with the measured data and operational experience are highlighted below:

MPC operates the CHP for a longer duration: In most tests, the MPC operates the CHP or a combination of CHP (larger blue and yellow pies) with other machines for a longer duration compared to the reference controller. This is even more significant when electricity prices are higher and the grid is supported. An exception however is the category high price – low load and low price – low load, where the reference controller operates the CHP for a longer duration. This is due to the higher operation of AdC (leading to higher CHP operation) by the reference controller in low thermal load category.

No data points exist in categories high load and low or medium electricity price: The synthesised load profiles and electricity profiles complement (unintentionally) in such a manner that the electricity price is in the higher category whenever the load is in the higher category. For instance, on a working day during peak office hours in a non-residential building, the thermal load and electricity price are both in the higher category.

Switching point control logic of reference controller is identified: Irrespective of electricity price, the reference controller operates the CC (larger yellow and orange pies) significantly during medium and high cooling loads and the AdC during low cooling loads. This corresponds to the switching point logic defined for the reference controller.

Grid-supportive operation of MPC: The MPC uses the AdC and CC flexibly considering the electricity price. For instance, in low price – low load region the CC is operated to benefit from the low electricity price and charging the cold tank. During high price – high load the CC operation with MPC is considerably lesser (38%) than the reference controller (100%) to avoid consumption of electricity in peak hours.
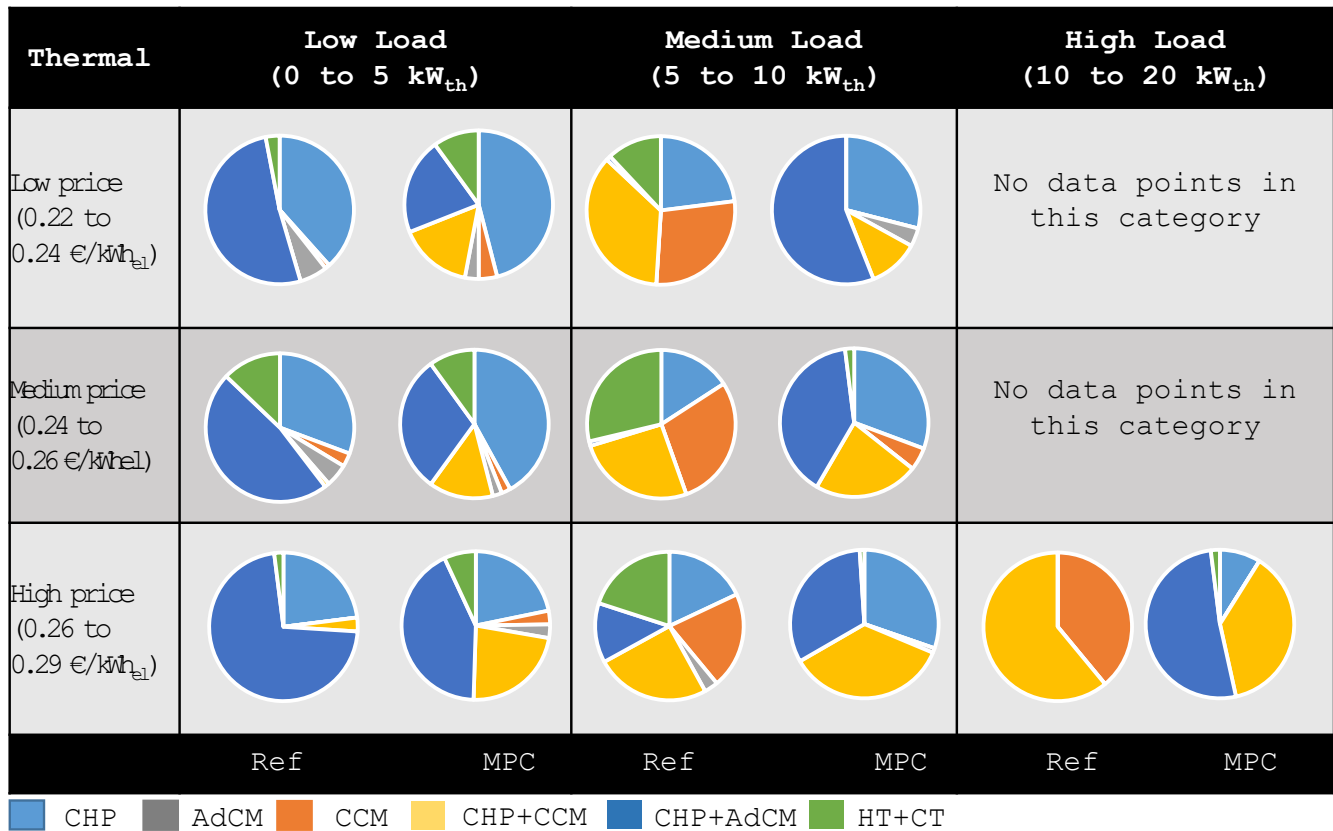
Fig. 8-8 Operational analysis of 391 hours of _summer_ experimental data for operating hours of a machine in a particular _electricity price – thermal load (cooling) category_. 100% of a pie represents the total number of data points in that price - load category. The number of data points in a category is same for both controllers. The different operational times of machines run by the controller is shown. _Note:_ Only a few relations could be established based on the measured data and not every pie-chart represents a reliable correlation or comparison
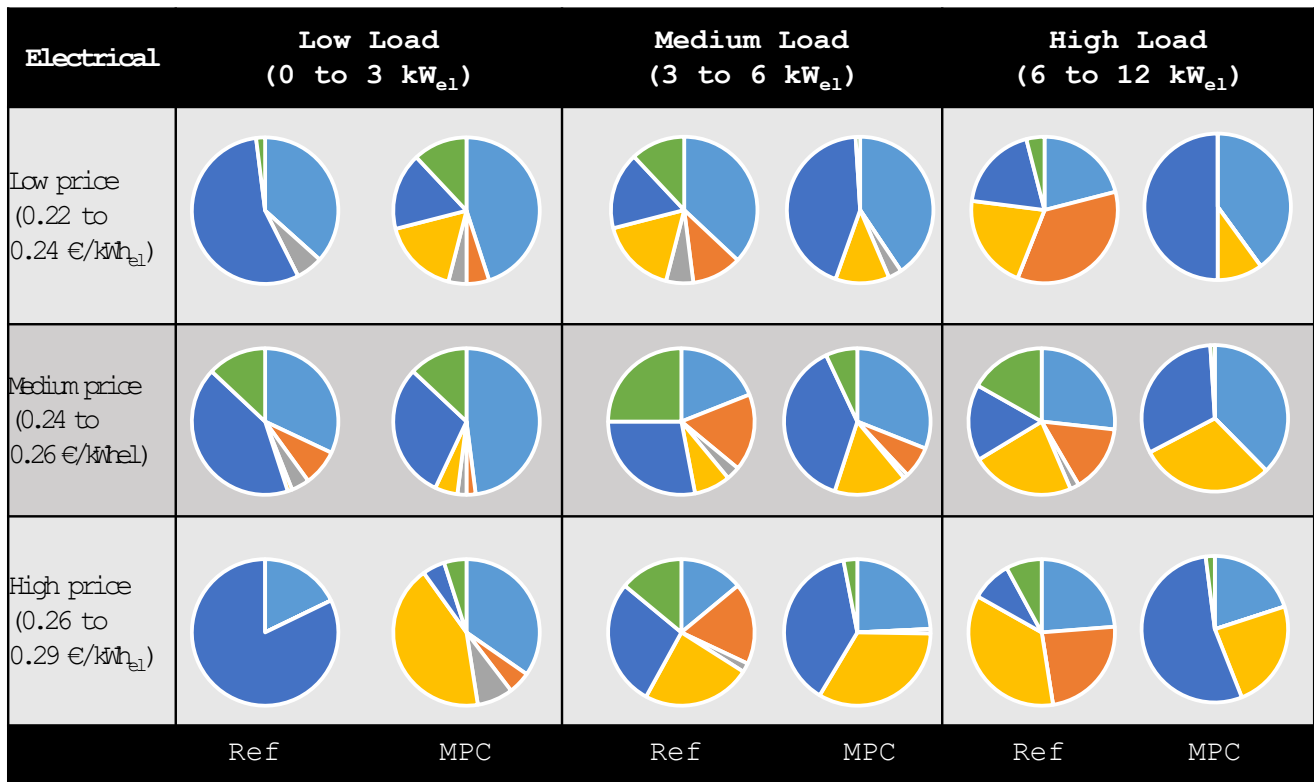
The results for operational analysis of the experimental data in summer scenario with respect to electricity price and the electrical load are shown in _Fig. 8-9._

MPC operates the CHP for a longer duration only during medium and high load categories: The MPC operates the CHP for a longer duration in these significant categories when electrical loads and prices are higher and the grid is supported. However, during the low electrical load categories the CHP is operated lesser compared to the reference controller. This is linked to the reduced AdC operation (reduced heat sink for CHP in summer) and increased CC operation by the MPC in low load categories for predictively charging the CTES.

Grid-supportive operation of MPC: Under the assumption that the electricity price directly represents the production and demand situation in the grid, it is detected that the MPC operates the CHP and CC complementary to the electrical load profile. For instance, the CC is operated lesser during times of medium and high load to minimise net purchase from the grid and consecutively relieve load on grid especially in the high price category.

Similar operation of MPC and reference controller: Unlike the distinct differences in the magnitude of operational times of the different machines in _Fig. 8-8_ (thermal load

analysis) the analysis with respect to electrical load reveals a similar operation of the controllers with a mix of all three machines being used in the different categories.

Fig. 8-9 Operational analysis of 391 hours of <u>summer</u> experimental data for operating hours of a machine in a particular <u>electricity price – electrical load</u> category. MPC operates CHP more often (larger blue and yellow pies) in most categories. In high price – high load category MPC minimises CC operation and still uses AdC

The results for operational analysis of the experimental data in winter scenario with respect to electricity price and the heating load are shown in *Fig. 8-10.* Operation of the machines is dependent on multiple factors such as tank temperatures, load forecast, and ambient temperature simultaneously. A direct correlation is not possible in all cases. However, the significant differences that were in accord with the measured data and operational experience are highlighted below:

MPC operates the CHP for a longer duration: Based on the type of optimal schedules calculated by MPC (*cf. Chapter 7*) it is seen in the summarised data that the operational time of the CHP is much longer in MPC compared to the reference controller. It is noted that the HTES is charged and discharged predictively and the stratification model is used optimally to ensure the long operation hours of the CHP.

HP operation is minimised in MPC: Another advantage of the optimal control strategy is the satisfaction of heating load without applying the HP (peak load component) as noticed in its smaller pie area for MPC. The peak load hours are covered by the MPC by using the storage capacity of the HTES optimally. The implication of this result is that greater load demands could be satisfied with the same size equipment using MPC.
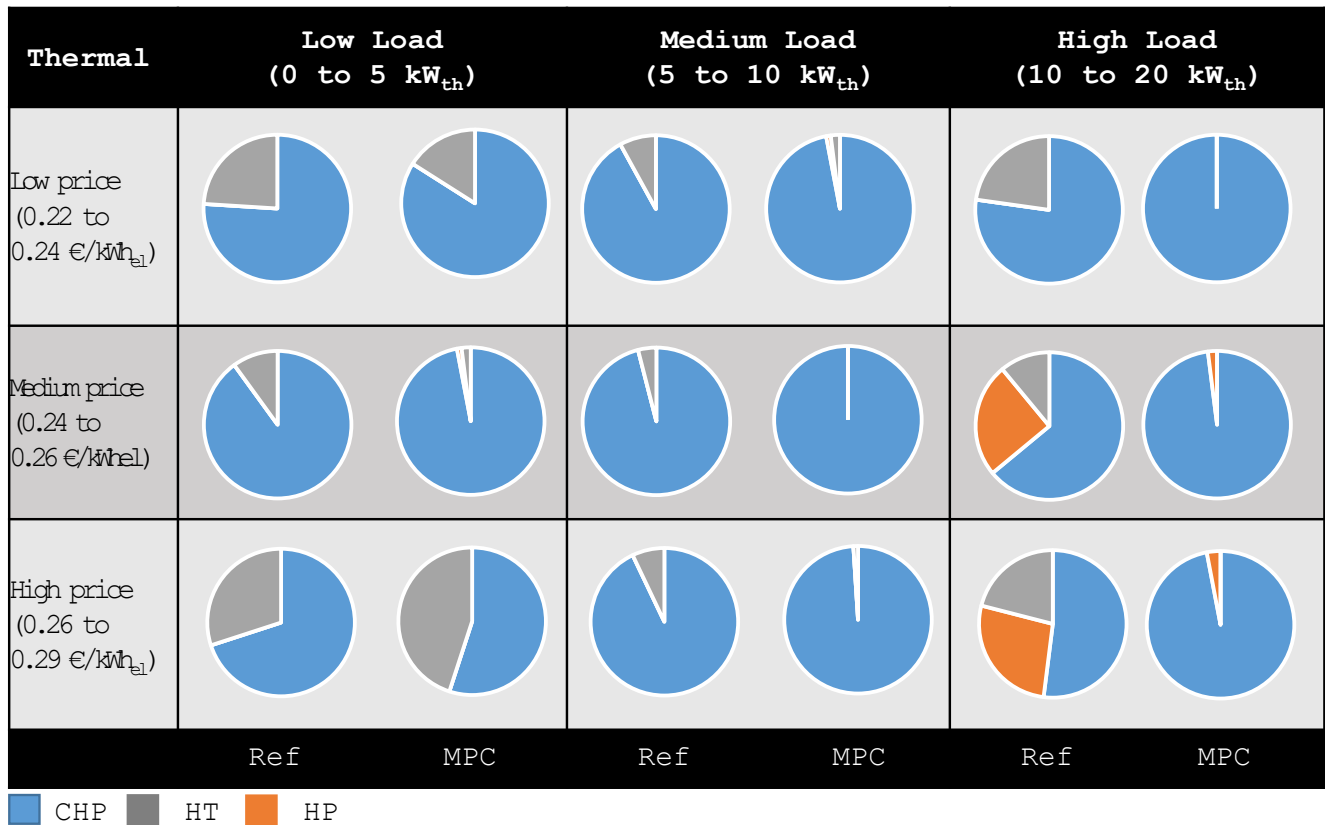
Thermal	Low Load (0 to 5 kW$_{th}$)		Medium Load (5 to 10 kW$_{th}$)		High Load (10 to 20 kW$_{th}$)	
Low price (0.22 to 0.24 €/kWh$_{el}$)						
Medium price (0.24 to 0.26 €/kWhel)						
High price (0.26 to 0.29 €/kWh$_{el}$)						
	Ref	MPC	Ref	MPC	Ref	MPC

■ CHP ■ HT ■ HP

Fig. 8-10 Operational analysis of 577 hours of <u>winter</u> experimental data for operating hours of a machine in a particular <u>electricity price – thermal load (heating)</u> category. MPC minimises HP operation and is able to cover greater thermal loads with same equipment capacity by using storage optimally

The results for operational analysis of the experimental data in winter scenario with respect to electricity price and the electrical load are summarised in *Fig. 8-11.*

Grid-supportive operation of MPC: The longer duration of CHP operation and minimal application of HP especially in high load and high price categories translates to a grid supportive operation of MPC assuming the electricity price represents variability in the grid. A grid supportive behaviour would be enhanced if HP is operated in low price categories. The reference controller applies the HP during high load hours as described in its "switching point" control logic. This is of significant disadvantage when high load hours correspond with high electricity price hours as seen in the summarised data.
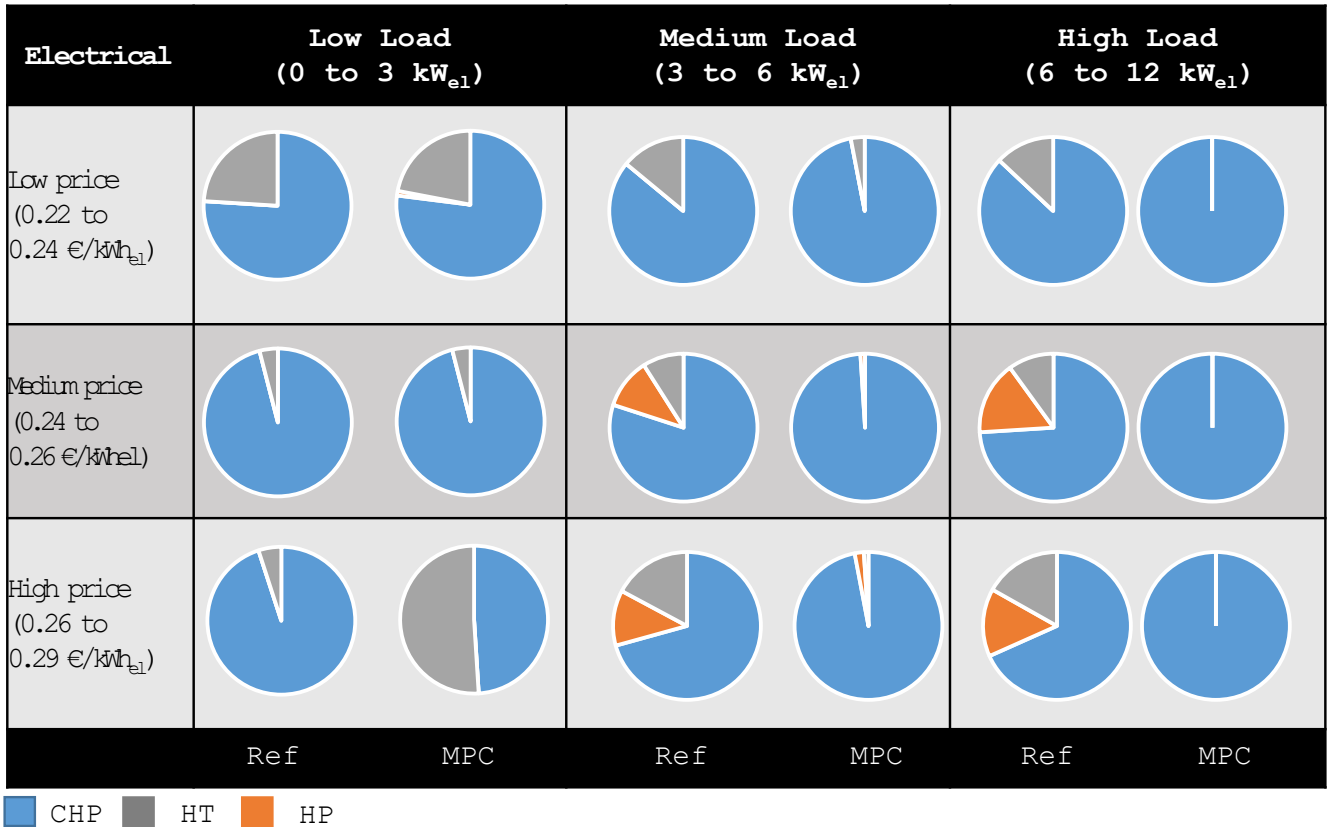
Electrical	Low Load (0 to 3 kW$_{el}$)		Medium Load (3 to 6 kW$_{el}$)		High Load (6 to 12 kW$_{el}$)	
Low price (0.22 to 0.24 €/kWh$_{el}$)						
Medium price (0.24 to 0.26 €/kWh el)						
High price (0.26 to 0.29 €/kWh$_{el}$)						
	Ref	MPC	Ref	MPC	Ref	MPC

CHP ■ HT ■ HP

Fig. 8-11 Operational analysis of 577 hours of <u>winter</u> experimental data for operating hours of a machine in a particular <u>electricity price – electrical load</u> category. Grid adverse operation of reference controller due to HP application in medium and high price-load categories is noticed

8.3.2 Constraint violations

In the second method for operational analysis, measured data for both seasons amounting to 758 hours of operation per controller was evaluated to identify violation of operational constraints as formulated in *Chapter 6*: (a) temperature limits, (b) minimum up/down time, and (c) adequate tank temperature for heating or cooling.

(a) Violation of temperature limits: If the controller operated a machine even when the applicable operational temperature limit was exceeded, the data point was recorded as a violation. The number of violations out of the total data points was counted to calculate the percentage of total time a machine operated under unacceptable conditions.

The results of the analysis for the violation of temperature limits are summarised in *Fig. 8-12*. It is observed that the MPC operated the CHP beyond its temperature limit $T_{r,CHP,max}$ for ca. 2.5% of its total operation time while the reference controller did not violate this constraint. The reference controller operated the HP for 20% of the total operational time in an unacceptable region because of both the constraints whereas the MPC did not violate these constraints. Both, reference and MPC controller operated the AdC for less than 1.5% of its total operational time at temperatures lower than $T_{r,AdC,H,min}$.

The rule-based reference controller uses the $T_{HT1,max}$ as a hard constraint and shuts down the CHP immediately as this temperature is exceeded thereby avoiding violation of $T_{r,CHP,max}$. On the other hand, the HP and AdC constraints are violated since they are not programmed as a hard constraint in the controller's algorithm (reduced control accuracy) but are avoided by setting the $T_{HT1,HP,max}$ and $T_{HT6,min}$ parameters. The tuning of these parameters is scenario dependent requiring previous knowledge of the system and basic energy balance calculations. These violations could be avoided by programming hard constraints or adding further rules to the reference controller, making the tuning process more complex and prone to error in judgement.

In case of MPC, a preliminary evaluation of the measured data showed that the temperature violations occur when it used slack variables in the soft constraint to achieve a more economical solution, when it used a sub-optimal binary approximation solution, or when the models inaccurately predicted the circuit temperatures. For example, at certain data points it was more economical for the MPC to keep the CHP running even at higher return-line temperatures and paying the penalty for slacks instead of shutting down the CHP completely. In other cases, the binary approximation did not shut down the CHP even though the relaxed solution was close to zero. An example of such behaviour was demonstrated in the long-duration summer test in *Section 7.5.1*.
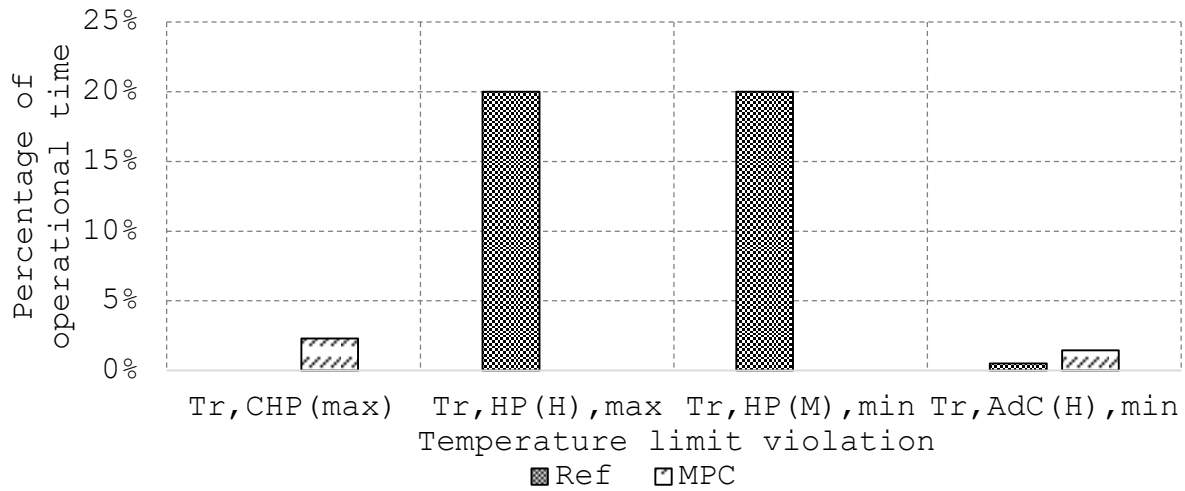

Fig. 8-12 Violation of temperature limits over total operational time of the corresponding machine. CHP constraint programmed as hard constraint in reference controller leading to no violation whereas HP constraints not programmed as hard constraints leading to more violations. MPC's violation of CHP constraint due to slack variable usage or sub-optimal binary approximation solutions is observed

(b) Violation of minimum up/down time: The supervisory controller, MPC or reference, both overwrite the internal restrictions of the components such that the final on-off signal is received only from the supervisory controller. Hence, the minimum runtime logic is programmed in these controllers as either mathematical constraints or using the hysteresis logic.

Similar to temperature violations an analysis of the minimum up/down time violations was done for the four machines. The total number of flanks for a machine was

calculated based on the number of times it was switched on or off. A violation was recorded if the machine was not operated for the predefined minimum runtime before a flank occurred. The number of flank violations as a percentage of the total flanks was calculated to compare the performance of the two controllers. The results are shown in *Fig. 8-13*.
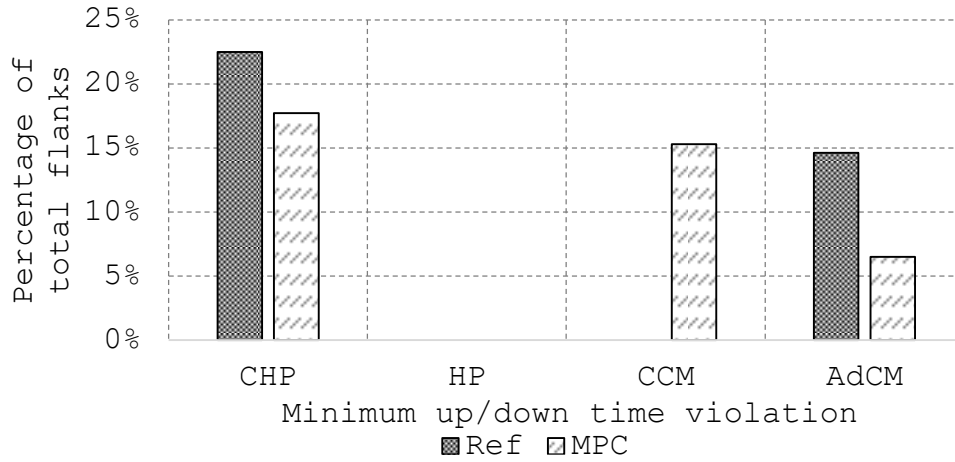

Fig. 8-13 Violation of minimum up/down time for total flanks over total operational time

The reference controller violated the minimum up/down time constraint in case of CHP for 22.5% of the total flanks and in case of AdC for 14.6% of the total flanks. For both these machines, the MPC violated the constraint a fewer times with 17.7% in case of CHP and 6.5% in case of AdC. However, the MPC violated the constraint a greater number of times in case of CC with 15.3% whereas the reference controller did not violate the CC constraint due to its hysteresis dead-band logic.

The numerical complexities of solving a MINLP do not always lead to global optimum and further improvements of the NLP solver and the binary approximation routine should be made for stricter implementation of the minimum up/down time constraint. A mathematical evaluation of the binary approximation algorithm in pycombina for improving the quality of binary solutions is necessary. Such an evaluation was not in the scope of this study and is recommended as future research work. In any case, the setting of a minimum runtime constraint in MPC is more intuitive and practical than estimating the tank temperatures for the hysteresis logic to achieve the minimum runtime in the reference controller.

(c) Adequate heating or cooling feed-line temperature in tanks: Finally, an analysis for adequacy of tank temperature to achieve the set feed-line temperature in the TC circuit $T_{f,TC,set}$ was done. The adequacy was calculated as an absolute temperature difference between the temperature of the tank-layer supplying the load (T_{HT6} or T_{CT1}) and $T_{f,TC,set}$. If T_{HT6} (T_{CT1}) was lower (higher) than the $T_{f,TC,set}$ for the heating (cooling) scenario, then the temperature in the tank was considered inadequate. The inadequacy increases with increasing magnitude of temperature difference. The results for this operational analysis are summarised in *Fig. 8-14*.
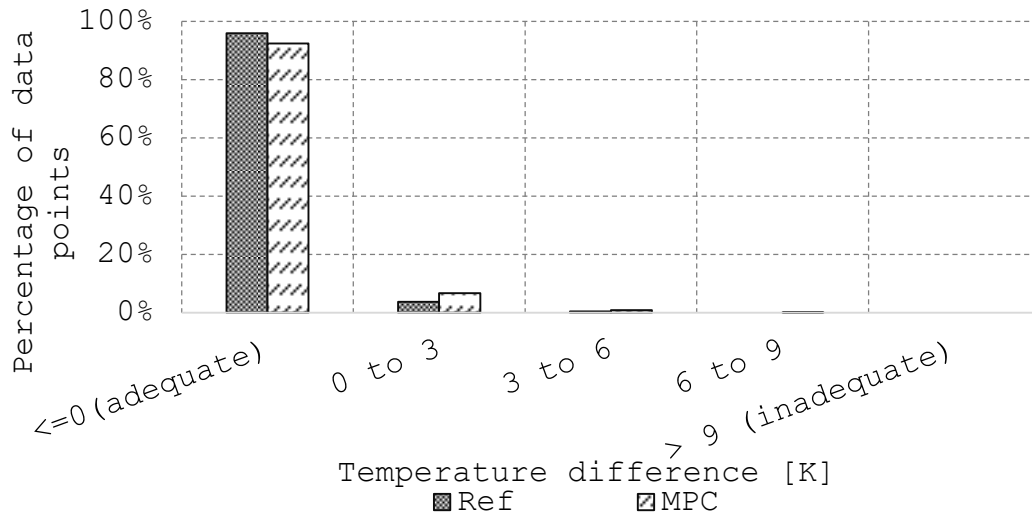
Fig. 8-14 Frequency for the adequacy of tank temperature over 758 hours of experimental data

Both the controllers were able to maintain adequate temperatures in the tank for more than 90% of the experimental data. However, the MPC controller violated the soft constraint to maintain adequate tank temperature by a maximum of 3 K for 6.6% of the total time. The number of violations greater than 3 K are negligible and in certain cases the measured data shows deviation due to the periodic behaviour of the AdC and the limitations of the three-way mixing valve controller. A detailed evaluation of this deviation was not in the scope of this work.

8.3.3 Conclusion of operational analysis

The MPC violated certain *not-critical constraints* for temperature and minimum runtime more than the reference controller, but followed its main aim of economic improvement (*cf. Section 8.1.3*) and operated stably without posing a risk to the hardware or reducing system efficiency significantly. In the cases, when hard constraints were programmed in the reference controller (exactly for this set-up in a nontrivial process) the violations were smaller than the MPC.

The preliminary analysis of measured data revealed following primary reasons or combinations of them for the constraint violations: (a) usage of slack variables for violating the soft constraints when the total economic cost was still minimum, (b) sub-optimal solutions for the binary approximation problem, (c) impractically scaled thermal loads, (d) model-mismatch including technical limitations(*cf. Chapter 4.13*).

To minimise constraint violations further tuning of the controllers is necessary. For the reference controller, more time-consuming tests and calculations or simulations with the system are needed to adapt the control logic. Moreover, such a tuning may be effective only for the target system and scenario and the performance of the reference controller may deteriorate when the system operates outside the range used for tuning the controller.

On the other hand, as discussed in *Section 8.1,* the MPC is easily tuned and is more flexible to choose the optimal solution within the entire operational range. It can be

adapted to other plants and scenarios without excessive tuning efforts as it automatically calculates the control signal.

8.4 Summary and outlook

The results from multiple long-duration tests in summer and winter with ca. 950 hours of MPC operation and implementing different types of loads, electricity tariff structures, and initialisation parameters was analysed and a stable operation of the control loop was demonstrated. The MPC was compared under almost-identical circumstances to a reference controller based on a conventional *following thermal load- base load matching* strategy. The thermal and electrical energy balances of both controllers were assessed and the measured data was evaluated for economic and operational analysis. The MPC controller showed an average saving of 5.9% to 11.7% in *simple levelised cost of energy* over the reference controller. In addition to the economic benefits, the MPC also showed operational benefits in terms of grid-supportive scheduling of the components and following hardware constraints. For instance, lower switching of *switch-critical machines* like CHP and AdC and higher switching of less critical components like RHP. It was noted that the reference controller was specifically developed for the INES trigeneration lab after multiple tests and recommendations of the component manufacturers. Thus, economic and operational benefits of an MPC controller would be even greater over a standard reference controller.

In addition to the quantifiable gains, the following qualitative advantages for MPC from an engineering perspective were identified:

Commissioning of controller: After developing the initial mathematical framework of the MPC in an extensive effort, it was tuned using basic engineering knowledge and component data sheets. The commissioning and adaption of this MPC in a green-field or retrofit scenario for different set-ups can be time and resource efficient considering: (a) marginal modelling effort to integrate new machines and their constraints or cost function terms and (b) easier tuning of the controller

Extension of existing framework: It was clear through the tests that developing a control logic considering multiple factors such as tank temperatures, operational constraints, electricity price, and load forecasts is extremely complex in a conventional controller. Even if successfully tested for a particular scenario, the extension of the framework to another scenario would require new analysis and planning. On the other hand, the existing framework of the MPC controller could be adapted for any season of year and further components and their constraints or cost function terms could be added without high programming effort.

The above-mentioned qualitative advantages of MPC were reported in the literature and are experimentally verified. A detailed sensitivity analysis of the slack stage-cost penalties, mathematical evaluation of the *pycombina* solver, and experiments for more load scenarios are necessary for improving the overall MPC quality.

9   Summary and Outlook

Applying optimal control to a decentralised trigeneration system facilitates the minimisation of its consumption related final-energy costs, enhances sector-coupling, and grid-supportive scheduling. For achieving these benefits, the effort primarily lies in a system-wide operation optimisation that utilises the flexibility provided by combining the different components and not in optimising the operation of individual components. Accordingly, the common consensus in the engineering and research community regarding gaps for implementing optimal control is the lack of demonstration projects using experimentally validated models, off-the-shelf components, and an optimisation algorithm integrated into state-of-art *building automation and control* hardware. The challenge lies in including their nonlinear characteristics and providing practically applicable control signals within solution times relevant for real-time operations.

In the scope of this work, theoretical concepts and recommendations from existing literature were successfully combined with practical approaches in building technologies, common modelling software, and optimisation algorithms to develop an *economic model predictive control* based *energy plant management system*. The MPC controller was applied to a nontrivial process, namely the micro-scale trigeneration system at the *Institute for Energy Systems Technology, Offenburg*. The performance of this controller was qualitatively and quantitatively compared to a conventional controller under almost-identical operating conditions.

Technical background (Chapters 2 – 4a)

Trigeneration systems can be classified into multiple categories and are often conventionally controlled using *following thermal load* or *following electrical load* strategies. However, in recent years the focus of the research community is on channelling the potential of optimal control for scheduling these systems. One possibility is to integrate an MPC based supervisory controller in the *hierarchical and centralised architecture* of a typical building automation and control system. Between the different types of MPC formulations and modelling techniques presented in the reviewed works, the *economic-MPC* framework with *grey-box models* is considered most practical for thermal energy plants with slow-dynamics and was implemented in this thesis. The models developed in this work satisfy the necessary characteristics for application in real-world MPC, namely: (a) capturing dynamic characteristics and part-load behaviour, (b) capturing internal control logic, (c) practical parameterisation capabilities, (d) adaptability to component design, (e) lower complexity, (f) sufficient accuracy, and (g) continuous differentiability.

Programming with nonlinear models to accurately predict the nonlinear dynamics of the system and usage of binary controls resulted in a *mixed integer optimal control nonlinear problem*. For achieving solutions in real-time (reducing the computation costs) and keeping the problem feasible, a few techniques such as *slack variable - soft*

constraints, *direct collocation,* and *combinatorial integral approximation* were implemented. A *receding forecast horizon* of 24 hours was chosen and was split into *variable length time-steps* of 5 minutes for the first 0.25 hours and 15 minutes for the remaining time 23.75 hours. This helped to reduce the number of discretisations (96 to 98 discretisation steps) and thus the size of the problem whilst maintaining higher accuracy of the solution for near future and acceptable lower accuracy for distant future.

The experimental set-up of the micro-scale trigeneration system comprised of common HVAC components, namely a *cogeneration unit*, an *adsorption chiller*, a *reversible heat pump*, and *stratified water thermal storages* and was capable of multiple operation modes as a prosumer over different seasons. A conventional building automation and control system based on the *OPC-UA* protocols in *LabVIEW®* and using standard PLC hardware was used for data acquisition, monitoring, and control.

Commissioning and performance tests revealed that components often have an internal control logic suited to their operation and safety. In some cases, this logic leads to part-load behaviour or in others it may directly affect the physical parameters of the system e.g. volume flows. These characteristics were included as continuously differentiable first or second degree functions using manufacturer's catalogue data or data directly available during commissioning of the plant. If neither approach was possible, then engineering assumptions relevant to the particular component that capture a majority of the operational scenarios were made. On the other hand, the technical constraints of the components such as safety temperatures, were formulated as soft constraints in the MPC algorithm to increase its robustness.

MPC development (Chapters 4b - 6)

As the solution of the scheduling problem strongly depends on the accuracy of the mathematical models used for simulations, the proposal in literature to develop simple component models, which connected together will predict relevant system-states for MPC of the entire plant with sufficient accuracy was successfully applied in this work. Solving a system of implicit equations e.g. stratified storages and intuitively connecting hydraulic components of the trigeneration system was considered impractical in a signal-oriented modelling approach. The models were programmed and tested in the object-oriented, and equation-based approach of *OpenModelica* against experimental data for plausibility and technical feasibility. The results of a thorough qualitative and quantitative analysis showed a good fit of the simulation data to the measured data. A component-wise detailed explanation of applying the grey-box methodology by combining basic physical principles with curve fits or simplifying assumptions for complex processes was given. In addition to facilitating development of MPC-suitable models (that include the sought-after characteristics), it was recognised that the grey-box methodology is especially effective when working with real systems because it allows the model developer or user to implement their knowledge of the system to better effect. Additionally, machine-learning algorithms could be applied for developing these models.

A generalizable mixed integer optimal control problem was developed using system states from differential equations, parameters from component data sheets, binary controls of the components, continuous controls, and slack variables related to the plant and an objective to minimise the consumption-related costs of the plant. All necessary algorithms and data sources were programmed in the *Python 3.7 64-bit* environment. *CasADi* was used via its Python interface for implementation of the system model and the discretized MIOCP. The IDAS solver from the *SUNDIALS* suite was used for numerical integration of the models within simulations. The NLPs were solved by employing *IPOPT* in the CasADi environment. The combinatorial integral approximation problem with minimum up/down-time constraint was solved using the tailored branch-and-bound method implemented in *pycombina*. The complete software on management and automation level was installed on a HP desktop PC with an Intel® Xeon 3.07 GHz CPU and 8 GB RAM and running a Windows 10 64-bit system. Execution of the MPC framework on this low specification computer ensures the execution of the MPC framework on a standard industrial computer, which has typically higher specifications.

Application test of the MPC framework (Chapter 7)

The feasibility and usefulness of MPC for complex energy systems had been expressed in previous theoretical studies and this work demonstrated it in a practical environment. The demonstration with standard industrial components and protocols supports the retrofit deployment of MPC in existing energy systems and the ease of setting up and tuning the controller supports its deployment to green-field scenarios. Compared to a well-tuned conventional controller, savings in final energy costs and hardware-friendly operation were noticed in numerous tests. The closed-loop behaviour in these tests also showed good performance, especially for deviations in ambient temperatures or forecasted loads. Additionally, it was observed that MPC is better suited for operating the plant under the influence of simultaneous input factors, as will be the case in a future energy system with multiple decentralised prosumers. Although an all-inclusive approach for developing an optimal controller is not possible due to the specific properties inherent to every problem, it is safe to assume that adapting an existing MPC framework is easier compared to adapting a conventional controller for other operational conditions or systems. However, the stability of the MPC controller and availability of reliable forecast data are the prerequisites for tapping into these advantages and studies focusing specially on these topics should be performed.

Outlook

The MPC framework designed in this work is primarily based on knowledge of open-source modelling and optimisation software tools. A thorough mathematical scrutiny of the optimisation problem and the solvers for improving the quality of the solution (e.g. reducing constraint violation or reducing solution time) should be done. The benefits of improving such MINLP solvers are manifold since most real-world systems operate nonlinearly and in any case with integer (if not binary) controls. The field experience and know-how gained through preliminary trial-and-error testing e.g. improvement of the solution with reinitialization of problem, effect of solver tolerance or engineering

assumptions to simplify problem formulations, could be useful for advancing such a mathematical study and further research for their quantification and documentation should be performed.

A sensitivity analysis of multiple factors directly influencing the plant operation for example, characteristics of the MPC formulation, forecast uncertainty, initialisation problems, solver attributes, or increasing capacity of components, has significant practical value. Practice oriented relationships (functions) could be derived from such an analysis and implemented to either improve existing conventional controllers or simplify future MPC formulations. The most feasible way to proceed in this field would be to implement a plant model that is a virtual, possibly high-accuracy representation of the controlled system needed to close the control loop in simulation. Unlike experiments with real systems the digital-twin of the plant can be used for simulating the performance of the MPC algorithm for longer durations (weeks to months) or for a faster analysis.

Finally, in light of the research trend on future of energy systems comprising of components like micro-CHPs, heat pumps, batteries, photovoltaic, wind energy etc., it is of significant importance to facilitate their operation as interconnected prosumer cells in real-time. Such an energy system network will support the utility service provider with possibility of sector-coupling technologies like Power-to-Heat or Fuel-to-Power. For the large-scale realisation of interdependent energy systems, it will be necessary to establish a data analysis and communication architecture, implement machine-learning algorithms for model development and fault-finding, and aim for direct application of optimal control on the plant PLC hardware.

Bibliography

Afram, A., Janabi-Sharifi, F., 2015a. Gray-box modeling and validation of residential HVAC system for control system design. Appl. Energy 137, 134–150. https://doi.org/10.1016/j.apenergy.2014.10.026

Afram, A., Janabi-Sharifi, F., 2015b. Black-box modeling of residential HVAC system and comparison of gray-box and black-box modeling methods. Energy Build. 94, 121–149. https://doi.org/10.1016/J.ENBUILD.2015.02.045

Afram, A., Janabi-Sharifi, F., 2014a. Theory and applications of HVAC control systems – A review of model predictive control (MPC). Build. Environ. 72, 343–355. https://doi.org/10.1016/j.buildenv.2013.11.016

Afram, A., Janabi-Sharifi, F., 2014b. Review of modeling methods for HVAC systems. Appl. Therm. Eng. 67, 507–519. https://doi.org/10.1016/J.APPLTHERMALENG.2014.03.055

Al Moussawi, H., Fardoun, F., Louahlia-Gualous, H., 2016. Review of tri-generation technologies: Design evaluation, optimization, decision-making, and selection approach. Energy Convers. Manag. 120, 157–196. https://doi.org/10.1016/j.enconman.2016.04.085

Amestoy, P.R., Duff, I.S., Koster, J., L'Excellent, J.-Y., 2001. A Fully Asynchronous Multifrontal Solver Using Distributed Dynamic Scheduling. SIAM J. Matrix Anal. Appl. 23, 15–41.

Andersson, J.A.E., Gillis, J., Horn, G., Rawlings, J.B., Diehl, M., 2019. CasADi: a software framework for nonlinear optimization and optimal control. Math. Program. Comput. 11, 1–36. https://doi.org/10.1007/s12532-018-0139-4

Andiappan, V., 2017. State-Of-The-Art Review of Mathematical Optimisation Approaches for Synthesis of Energy Systems. Process Integr. Optim. Sustain. 1, 165–188. https://doi.org/10.1007/s41660-017-0013-2

Angrisani, G., Akisawa, A., Marrasso, E., Roselli, C., Sasso, M., 2016. Performance assessment of cogeneration and trigeneration systems for small scale applications. Energy Convers. Manag. 125, 194–208. https://doi.org/10.1016/j.enconman.2016.03.092

Angrisani, G., Rosato, A., Roselli, C., Sasso, M., Sibilio, S., 2012. Experimental results of a micro-trigeneration installation. Appl. Therm. Eng. 38, 78–90. https://doi.org/10.1016/j.applthermaleng.2012.01.018

Asghar, S.A., Tariq, S., 2010. Design and Implementation of a User Friendly OpenModelica Graphical Connection Editor. Linköping University.

Babiak, J., Vagiannis, G., 2015. Thermally Activated Building System (TABS): Efficient cooling and heating of commercial buildings. Climamed 2015.

Badea, N., 2014. Design for Micro-Combined Cooling , Heating and Power Systems: Stirling Engines and Renewable Power Systems. Springer.

Beck, T., Fischer, H., 1994. The if-problem in automatic differentiation. J. Comput. Appl. Math. 50, 119–131. https://doi.org/10.1016/0377-0427(94)90294-1

Bengea, S.C., Kelman, A.D., Borrelli, F., Taylor, R., 2012. Model Predictive Control for Mid-Size Commercial Building HVAC : Implementation , Results and Energy Savings, in: The Second International Conference on Building Energy and Environment. pp. 979–986.

Bergman, T.L., Incropera, F.P., DeWitt, D.P., Lavine, A.S., 2011. Fundamentals of heat and mass transfer. John Wiley & Sons.

Biegler, L.T., 2010. Nonlinear programming: concepts, algorithms, and applications to chemical processes. Siam.

BMWi, 2018. The Energy of the Future – Reporting Year 2016 - Summary.

BMWi, 2016. Kraft-Wärme-Kopplungsgesetz Gesetz für die Erhaltung, die Modernisierung und den Ausbau der Kraft-Wärme-Kopplung. Germany.

Bohlin, T., 1994. A case study of grey box identification. Automatica 30, 307–318. https://doi.org/10.1016/0005-1098(94)90032-9

Bracco, S., Delfino, F., Pampararo, F., Robba, M., Rossi, M., 2014. A mathematical model for the optimal

operation of the University of Genoa Smart Polygeneration Microgrid: Evaluation of technical, economic and environmental performance indicators. Energy 64, 912–922. https://doi.org/10.1016/j.energy.2013.10.039

Bracco, S., Dentici, G., Siri, S., 2013. Economic and environmental optimization model for the design and the operation of a combined heat and power distributed generation system in an urban area. Energy 55, 1014–1024. https://doi.org/10.1016/j.energy.2013.04.004

Bruni, G., Cordiner, S., Mulone, V., Rocco, V., Spagnolo, F., 2015. A study on the energy management in domestic micro-grids based on Model Predictive Control strategies. Energy Convers. Manag. 102, 50–58. https://doi.org/10.1016/j.enconman.2015.01.067

Bundesnetzagentur, 2019. Informationen zu Strom- und Gaspreisen für Haushaltskunden [WWW Document]. URL https://www.bundesnetzagentur.de/DE/Sachgebiete/ElektrizitaetundGas/Verbraucher/PreiseRechnTarife/preiseundRechnungen-node.html (accessed 8.7.20).

Bürger, A., 2020. Nonlinear mixed-integer model predictive control of renewable energy systems: methods, software, and experiments. University of Freiburg. https://doi.org/10.6094/UNIFR/175441

Bürger, A., Sawant, P., Bohlayer, M., Altmann-Dieses, A., Braun, M., Diehl, M., 2017. Efficient operation scheduling for adsorption chillers using predictive optimization-based control methods, in: IOP Conference Series: Materials Science and Engineering. https://doi.org/10.1088/1757-899X/257/1/012007

Bürger, A., Zeile, C., Altmann-Dieses, A., Sager, S., Diehl, M., 2018. An Algorithm for Mixed-Integer Optimal Control of Solar Thermal Climate Systems with MPC-Capable Runtime. 2018 Eur. Control Conf. ECC 2018 1379–1385. https://doi.org/10.23919/ECC.2018.8550424

Bussieck, M.R., Pruessner, A., 2003. Mixed-Integer Nonlinear Programming [WWW Document]. gamsworld. URL http://www.gamsworld.org/minlp/siagopt.pdf (accessed 1.29.21).

Camacho, E.F., Bordons, C., 2007. Model Predictive control, Advanced Textbooks in Control and Signal Processing. Springer London, London. https://doi.org/10.1007/978-0-85729-398-5

Campos Celador, a., Odriozola, M., Sala, J.M., 2011. Implications of the modelling of stratified hot water storage tanks in the simulation of CHP plants. Energy Convers. Manag. 52, 3018–3026. https://doi.org/10.1016/j.enconman.2011.04.015

Chandan, V., Do, A., Jin, B., Jabbari, F., Brouwer, J., Akrotirianakis, I., 2012. Modeling and Optimization of a Combined Cooling , Heating and Power Plant System, in: American Control Conference. Montreal, pp. 3069–3074.

Chicco, G., Mancarella, P., 2009. Matrix modelling of small-scale trigeneration systems and application to operational optimization. Energy 34, 261–273. https://doi.org/10.1016/j.energy.2008.09.011

Chicco, G., Mancarella, P., 2007. Trigeneration primary energy saving evaluation for energy planning and policy development. Energy Policy 35, 6132–6144. https://doi.org/10.1016/j.enpol.2007.07.016

Cho, H., Luck, R., Eksioglu, S.D., Chamra, L.M., 2009a. Cost-optimized real-time operation of CHP systems. Energy Build. 41, 445–451. https://doi.org/10.1016/j.enbuild.2008.11.011

Cho, H., Mago, P.J., Luck, R., Chamra, L.M., 2009b. Evaluation of CCHP systems performance based on operational cost, primary energy consumption, and carbon dioxide emission by utilizing an optimal operation scheme. Appl. Energy 86, 2540–2549. https://doi.org/10.1016/j.apenergy.2009.04.012

Cho, H., Smith, A.D., Mago, P., 2014. Combined cooling, heating and power: A review of performance improvement and optimization. Appl. Energy 136, 168–185. https://doi.org/10.1016/j.apenergy.2014.08.107

Chua, H.T., Ng, K.C., Malek, A., Kashiwagi, T., Akisawa, A., Saha, B.B., 1999. Modeling the performance of two-bed, sillica gel-water adsorption chillers. Int. J. Refrig. 22, 194–204. https://doi.org/10.1016/S0140-7007(98)00063-2

Chua, K.J., Chou, S.K., Yang, W.M., Yan, J., 2013. Achieving better energy-efficient air conditioning - A review of technologies and strategies. Appl. Energy 104, 87–104.

https://doi.org/10.1016/j.apenergy.2012.10.037

Cole, W.J., Powell, K.M., Edgar, T.F., 2012. Optimization and advanced control of thermal energy storage systems. Rev. Chem. Eng. 28, 81–99. https://doi.org/10.1515/revce-2011-0018

Collazos, A., Maréchal, F., Gähler, C., 2009. Predictive optimal management method for the control of polygeneration systems. Comput. Chem. Eng. 33, 1584–1592. https://doi.org/10.1016/j.compchemeng.2009.05.009

Dagdougui, H., Minciardi, R., Ouammi, A., Robba, M., Sacile, R., 2012. Modeling and optimization of a hybrid system for the energy supply of a "Green" building. Energy Convers. Manag. 64, 351–363. https://doi.org/10.1016/j.enconman.2012.05.017

Daikin Europe, 2016. Daikin HydroCube [WWW Document]. URL https://www.daikin.de/de_de/produkte/EWWP-KBW1N.html (accessed 8.7.20).

De Césaro Oliveski, R., Krenzinger, A., Vielmo, H. a., 2003. Comparison between models for the simulation of hot water storage tanks. Sol. Energy 75, 121–134. https://doi.org/10.1016/j.solener.2003.07.009

Di Somma, M., Yan, B., Bianco, N., Graditi, G., Luh, P.B., Mongibello, L., Naso, V., 2015. Operation optimization of a distributed energy system considering energy costs and exergy efficiency. Energy Convers. Manag. 103, 739–751. https://doi.org/10.1016/j.enconman.2015.07.009

Diehl, M., 2019. Skript zur Vorlesung "Systemtheorie und Regelungstechnik 1" [WWW Document]. Lehrstuhl für Syst. Regelungstechnik und Optimierung. URL https://www.syscop.de/files/users/jochem.deschutter/systemtheorie.pdf (accessed 12.29.20).

Diehl, M., 2016. Lecture Notes on Numerical Optimization. Freiburg.

Diehl, M., 2014a. Lecture Notes on Optimal Control and Estimation [WWW Document]. Lehrstuhl für Syst. Regelungstechnik und Optimierung. URL http://www.syscop.de/files/2015ss/optcont/oce_script.pdf (accessed 12.29.20).

Diehl, M., 2014b. Lecture Notes on Modelling and System Identification [WWW Document]. Lehrstuhl für Syst. Regelungstechnik und Optimierung. URL https://www.syscop.de/files/2014ws/teaching/msi/msi3.pdf (accessed 12.29.20).

Dongol, D., Feldmann, T., Schmidt, M., Bollin, E., 2018. A model predictive control based peak shaving application of battery for a household with photovoltaic system in a rural distribution grid. Sustain. Energy, Grids Networks 16, 1–13. https://doi.org/https://doi.org/10.1016/j.segan.2018.05.001

Dwivedi, V., 2009. Thermal Modelling and Control of Domestic Hot Water Tank. University of Strathclyde.

E-Werk Mittelbaden AG, 2019. E>strom//Wärme (Grundversorgung) [WWW Document]. URL https://www.e-werk-mittelbaden.de/strom-waermepumpe (accessed 1.26.21).

EBC-IEA, 2016. IEA/ECBCS Annex 54: Integration of Micro-Generation and Related Energy Technologies in Buildings.

Eicker, U., 2006. Storage Modelling, in: Solar Technologies for Buildings. John Wiley & Sons, Stuttgart, pp. 97–103.

Elliott, M.S., 2008. Decentralized Model Predictive Control of a Multiple Evaporator HVAC System. Texas A&M University.

Ellis, M., Durand, H., Christofides, P.D., 2014. A tutorial review of economic model predictive control methods. J. Process Control 24, 1156–1178. https://doi.org/10.1016/j.jprocont.2014.03.010

EnEV-online, 2016. EnEV ab 2016 [WWW Document]. URL https://enev-online.de/index.htm (accessed 8.7.20).

EPEX SPOT SE, 2008. Market Data: Day-Ahead Auction [WWW Document]. URL http://www.epexspot.com/en/market-data/dayaheadauction (accessed 1.26.21).

Facci, A.L., Andreassi, L., Ubertini, S., 2014. Optimization of CHCP (combined heat power and cooling) systems operation strategy using dynamic programming. Energy 66, 387–400. https://doi.org/10.1016/j.energy.2013.12.069

Fahrenheit GmbH, 2014. FAHRENHEIT eCoo Operating Manual [WWW Document]. URL https://fahrenheit.cool/en/products/ (accessed 8.7.20).

Bibliography

Felsmann, C., 2002. Ein Beitrag zur Optimierung der Betriebsweise heizungs- und raumlufttechnischer Anlagen. Technischen Universität Dresden.

Figueiredo, J., Martins, J., 2010. Energy Production System Management – Renewable energy power supply integration with Building Automation System. Energy Convers. Manag. 51, 1120–1126. https://doi.org/10.1016/j.enconman.2009.12.020

Flores, R.J., Shaffer, B.P., Brouwer, J., 2014. Dynamic distributed generation dispatch strategy for lowering the cost of building energy. Appl. Energy 123, 196–208. https://doi.org/10.1016/j.apenergy.2014.02.028

Fritzson, P., 2014. Principles of object-oriented modeling and simulation with Modelica 3.3: a cyber-physical approach. John Wiley & Sons.

Fuentes-Cortés, L.F., Dowling, A.W., Rubio-Maya, C., Zavala, V.M., Ponce-Ortega, J.M., 2016. Integrated design and control of multigeneration systems for building complexes. Energy 116, 1403–1416. https://doi.org/10.1016/j.energy.2016.05.093

Fumo, N., Rafe Biswas, M.A., 2015. Regression analysis for prediction of residential energy consumption. Renew. Sustain. Energy Rev. 47, 332–343. https://doi.org/10.1016/J.RSER.2015.03.035

Gräber, M., Kirches, C., Bock, H.G., Schlöder, J.P., Tegethoff, W., Köhler, J., 2011. Determining the optimum cyclic operation of adsorption chillers by a direct method for periodic optimal control. Int. J. Refrig. 34, 902–913. https://doi.org/10.1016/j.ijrefrig.2010.12.021

Gu, W., Wang, Z., Wu, Z., Luo, Z., Tang, Y., Wang, J., 2017. An Online Optimal Dispatch Schedule for CCHP Microgrids Based on Model Predictive Control. IEEE Trans. Smart Grid 8, 2332–2342. https://doi.org/10.1109/TSG.2016.2523504

Gu, W., Wu, Zhi, Bo, R., Liu, W., Zhou, G., Chen, W., Wu, Zaijun, 2014. Modeling, planning and optimal energy management of combined cooling, heating and power microgrid: A review. Int. J. Electr. Power Energy Syst. 54, 26–37. https://doi.org/10.1016/j.ijepes.2013.06.028

Han, Y.M., Wang, R.Z., Dai, Y.J., 2009. Thermal stratification within the water tank. Renew. Sustain. Energy Rev. 13, 1014–1026. https://doi.org/10.1016/j.rser.2008.03.001

Heinrich, C., Wittig, S., Albring, P., Lutz Richter, M., Safarik, Böhm, U., Hantsch, A., 2014. Nachhaltige Kälteversorgung in Deutschland an den Beispielen Gebäudeklimatisierung und Industrie, CLIMATE CHANGE 25/2014. Dresden.

Henze, G.P., Biffar, B., Kohn, D., Becker, M.P., 2008. Optimal design and operation of a thermal storage system for a chilled water plant serving pharmaceutical buildings. Energy Build. 40, 1004–1019. https://doi.org/10.1016/j.enbuild.2007.08.006

Henze, G.P., Kalz, D.E., Simeng, L., Felsmann, C., 2005. Experimental Analysis of Model-Based Predictive Optimal Control for Active and Passive Building Thermal Storage Inventory. HVAC&R Res. 11, 189–213. https://doi.org/10.1080/10789669.2005.10391134

Hidalgo Rodriguez, D.I., Spitalny, L., Myrzik, J., Braun, M., 2012. Development of a control strategy for mini CHP plants for an active voltage management in low voltage networks, in: 3rd IEEE PES Conference. Berlin, pp. 1–8. https://doi.org/10.1109/ISGTEurope.2012.6465797

Hindmarsh, A.C., Brown, P.N., Grant, K.E., Lee, S.L., Serban, R., Shumaker, D.E., Woodward, C.S., 2005. SUNDIALS. ACM Trans. Math. Softw. 31, 363–396. https://doi.org/10.1145/1089014.1089020

Hosoz, M., Ertunc, H.M., Bulgurcu, H., 2011. An adaptive neuro-fuzzy inference system model for predicting the performance of a refrigeration system with a cooling tower. Expert Syst. Appl. 38, 14148–14155. https://doi.org/https://doi.org/10.1016/j.eswa.2011.04.225

HT HelioTech GmbH, 2017. Operating Strategies Stratified Tank [WWW Document]. URL www.ht-heliotech.de (accessed 8.7.20).

Huang, G., 2011. Model predictive control of VAV zone thermal systems concerning bi-linearity and gain nonlinearity. Control Eng. Pract. 19, 700–710. https://doi.org/10.1016/J.CONENGPRAC.2011.03.005

Huber Kältemaschinenbau AG, 2019. Datasheet Huber-Unistat 510w [WWW Document]. URL https://www.huber-online.com/de/imprint.aspx (accessed 8.7.20).

IET Labs Inc., 2016. PT 100 Resistance Table [WWW Document]. URL

http://www.ietlabs.com/pdf/Datasheets/Pt100Temperature_Resistance4digits.pdf (accessed 8.7.20).

Imsland, L., Kittilsen, P., Schei, T.S., 2010. Model-Based Optimizing Control and Estimation Using Modelica Model. Model. Identif. Control A Nor. Res. Bull. 31, 107–121. https://doi.org/10.4173/mic.2010.3.3

Invensor GmbH, 2019. Invensor Product Data Sheets [WWW Document]. URL https://invensor.com/en/products/ (accessed 8.7.20).

Jin, G.Y., Cai, W.J., Lu, L., Lee, E.L., Chiang, A., 2007. A simplified modeling of mechanical cooling tower for control and optimization of HVAC systems. Energy Convers. Manag. 48, 355–365. https://doi.org/10.1016/j.enconman.2006.07.010

Jin, G.Y., Tan, P.Y., Ding, X.D., Koh, T.M., 2011. A hybrid water-cooled centrifugal chiller model. Proc. 2011 6th IEEE Conf. Ind. Electron. Appl. ICIEA 2011 2298–2303. https://doi.org/10.1109/ICIEA.2011.5975975

Jin, H., Spitler, J.D., 2002. A parameter estimation based model of water-to-water heat pumps for use in energy calculation programs, in: ASHRAE Transactions. pp. 3–17.

Jradi, M., Riffat, S., 2014. Tri-generation systems: Energy policies, prime movers, cooling technologies, configurations and operation strategies. Renew. Sustain. Energy Rev. 32, 396–415. https://doi.org/10.1016/j.rser.2014.01.039

Jung, M.N., Kirches, C., Sager, S., Sass, S., 2018. Computational Approaches for Mixed Integer Optimal Control Problems with Indicator Constraints. Vietnam J. Math. 46, 1023–1051. https://doi.org/10.1007/s10013-018-0313-z

Kalz, D., Klein, K., Palzer, A., Schlösser, T., Schumacher, P., Sterchele, P., Stinner, S., Yu, Y.J., Kallert, A.M., 2018. Grid-supportive buildings and districts: Buildings relieve power grids. BINE Inf. Serv. Themeninfo I /2018 A Compact Guid. to energy Res. 24.

Kavvadias, K.C., Maroulis, Z.B., 2010. Multi-objective optimization of a trigeneration plant. Energy Policy 38, 945–954. https://doi.org/10.1016/j.enpol.2009.10.046

Kim, J.S., Edgar, T.F., 2014. Optimal scheduling of combined heat and power plants using mixed-integer nonlinear programming. Energy 77, 675–690. https://doi.org/10.1016/j.energy.2014.09.062

Klein, K., Langner, R., Kalz, D., Herkel, S., Henning, H.M., 2016. Grid support coefficients for electricity-based heating and cooling and field data analysis of present-day installations in Germany. Appl. Energy 162. https://doi.org/10.1016/j.apenergy.2015.10.107

Kneiske, T.M., Braun, M., Hidalgo-Rodriguez, D.I., 2018. A new combined control algorithm for PV-CHP hybrid systems. Appl. Energy 210, 964–973. https://doi.org/10.1016/j.apenergy.2017.06.047

Kofránek, J., Mateják, M., Privitzer, P., Tribula, M., 2008. Causal or acausal modeling: labour for humans or labour for machines, in: Technical Computing Prague 2008. pp. 1–16.

Kubis, L., 2018. Darksky API for Python: darskylib. GitHub Repos.

Lasdon, L.S., Waren, A.D., Jain, A., Ratner, M., 1976. Design and Testing of a Generalized Reduced Gradient Code for Nonlinear Programming. ACM Trans. Math. Softw. 4, 51.

Lefort, A., Bourdais, R., Ansanay-Alex, G., Guéguen, H., 2013. Hierarchical control method applied to energy management of a residential house. Energy Build. 64, 53–61. https://doi.org/10.1016/j.enbuild.2013.04.010

Lemort, V., Lebrun, J., Felsmann, C., 2009. Testing and validation of simulation tools of HVAC mechanical equipment including their control strategies part III: validation of an air-cooled chiller model, in: IBPSA Building Simulation. pp. 1121–1128.

Li, C.Z., Shi, Y.M., Huang, X.H., 2008. Sensitivity analysis of energy demands on performance of CCHP system. Energy Convers. Manag. 49, 3491–3497. https://doi.org/10.1016/j.enconman.2008.08.006

Li, L., Mu, H., Gao, W., Li, M., 2014. Optimization and analysis of CCHP system based on energy loads coupling of residential and office buildings. Appl. Energy 136, 206–216. https://doi.org/10.1016/j.apenergy.2014.09.020

Li, S., Wu, J.Y., 2009. Theoretical research of a silica gel-water adsorption chiller in a micro combined cooling, heating and power (CCHP) system. Appl. Energy 86, 958–967. https://doi.org/10.1016/j.apenergy.2008.09.016

Bibliography

Liu, M., Shi, Y., Fang, F., 2014. Combined cooling, heating and power systems: A survey. Renew. Sustain. Energy Rev. 35, 1–22. https://doi.org/10.1016/j.rser.2014.03.054

Liu, M., Shi, Y., Fang, F., 2013. Optimal power flow and PGU capacity of CCHP systems using a matrix modeling approach. Appl. Energy 102, 794–802. https://doi.org/10.1016/j.apenergy.2012.08.041

Liu, P., Georgiadis, M.C., Pistikopoulos, E.N., 2013. An energy systems engineering approach for the design and operation of microgrids in residential applications. Chem. Eng. Res. Des. 91, 2054–2069. https://doi.org/10.1016/j.cherd.2013.08.016

Lozano, M.A., Carvalho, M., Serra, L.M., 2009. Operational strategy and marginal costs in simple trigeneration systems. Energy 34, 2001–2008. https://doi.org/10.1016/j.energy.2009.08.015

Ma, Y., Borrelli, F., Hencey, B., Packard, A., Bortoff, S., 2009. Model Predictive Control of thermal energy storage in building cooling systems, in: 48th IEEE Conference on Decision and Control (CDC). pp. 392–397. https://doi.org/10.1109/CDC.2009.5400677

McKinney, W. et al., 2010. Data structures for statistical computing in python, in: Proceedings of the 9th Python in Science Conference. pp. 51–56.

Menon, R.P., Maréchal, F., Paolone, M., 2016. Intra-day electro-thermal model predictive control for polygeneration systems in microgrids. Energy 104, 308–319. https://doi.org/10.1016/j.energy.2016.03.081

Mitchell, J.W., Braun, J.E., 2013. Principles of Heating, Ventilation and Air Conditioning in Buildings, ISBN: 978-0-470-62457-9. Wiley.

Murugan, S., Horák, B., 2016. Tri and polygeneration systems-A review. Renew. Sustain. Energy Rev. 60, 1032–1051. https://doi.org/10.1016/j.rser.2016.01.127

Núñez, T., 2010. Thermally Driven Cooling: Technologies, Developments and Applications. J. Sustain. Energy 1, 16–24.

Oldewurtel, F., Ulbig, A., Parisio, A., Andersson, G., Morari, M., 2010. Reducing peak electricity demand in building climate control using real-time pricing and model predictive control, in: 49th IEEE Conference on Decision and Control. Atlanta, pp. 1927–1932. https://doi.org/10.1109/CDC.2010.5717458

Ommen, T., Markussen, W.B., Elmegaard, B., 2014. Comparison of linear, mixed integer and non-linear programming methods in energy system dispatch modelling. Energy 74, 109–118. https://doi.org/10.1016/j.energy.2014.04.023

Ortiga, J., Bruno, J.C., Coronas, A., 2013. Operational optimisation of a complex trigeneration system connected to a district heating and cooling network. Appl. Therm. Eng. 50, 1536–1542. https://doi.org/10.1016/j.applthermaleng.2011.10.041

Parisio, A., Wiezorek, C., Kyntaja, T., Elo, J., Johansson, K.H., 2015. An MPC-based Energy Management System for multiple residential microgrids. IEEE Int. Conf. Autom. Sci. Eng. 2015-Octob, 7–14. https://doi.org/10.1109/CoASE.2015.7294033

Pfafferott, J., Himmelsbach, S., Lang, T., Frietsch, M., 2016. Messtechnische Bestimmung von Aufwandszahlen unterschiedlicher Flächentemperiersysteme. Bauphysik 38, 389–399. https://doi.org/10.1002/bapi.201610039

Pfafferott, J.Ü., Herkel, S., Kalz, D.E., Zeuschner, A., 2007. Comparison of low-energy office buildings in summer using different thermal comfort criteria. Energy Build. 39, 750–757. https://doi.org/10.1016/J.ENBUILD.2007.02.005

Rawlings;, J.B., Mayne, D.Q., Diehl, M.M., 2019. Model Predictive Control: Theory, Computation, and Design, 2nd ed. Nob HIll Publishing, Santa Barbara.

Ren, H., Gao, W., Ruan, Y., 2008. Optimal sizing for residential CHP system. Appl. Therm. Eng. 28, 514–523. https://doi.org/10.1016/j.applthermaleng.2007.05.001

Roche, R., 2018. Market data from EPEX-SPOT: epex-scraper for Python. GitHub Repos.

Romero, J.A., Navarro-Esbrí, J., Belman-Flores, J.M., 2011. A simplified black-box model oriented to chilled water temperature control in a variable speed vapour compression system. Appl. Therm. Eng. 31, 329–335. https://doi.org/10.1016/J.APPLTHERMALENG.2010.09.013

Rong, A., Lahdelma, R., 2005. An efficient linear programming model and optimization algorithm for trigeneration. Appl. Energy 82, 40–63. https://doi.org/10.1016/j.apenergy.2004.07.013

Rong, A., Su, Y., 2017. Polygeneration systems in buildings: A survey on optimization approaches. Energy Build. 151, 439–454. https://doi.org/10.1016/j.enbuild.2017.06.077

Sager, S., 2009. Reformulations and algorithms for the optimization of switching decisions in nonlinear optimal control. J. Process Control 19, 1238–1247. https://doi.org/10.1016/j.jprocont.2009.03.008

Sager, S., Jung, M., Kirches, C., 2011. Combinatorial integral approximation. Math. Methods Oper. Res. 73, 363–380. https://doi.org/10.1007/s00186-011-0355-4

Saha, B.B., Boelman, E.C., Kashiwagi, T., 1995. Computational analysis of an advanced adsorption-refrigeration cycle. Energy 20, 983–994. https://doi.org/10.1016/0360-5442(95)00047-K

Sakoda, A., Suzuki, M., 1984. Fundamental study on solar powered adsorption cooling system. J. Chem. Eng. Japan 17, 52–57. https://doi.org/10.1252/jcej.17.52

Salvalai, G., 2012. Implementation and validation of simplified heat pump model in IDA-ICE energy simulation environment. Energy Build. 49, 132–141. https://doi.org/10.1016/j.enbuild.2012.01.038

Sawant, P., Bürger, A., Doan, M.D., Felsmann, C., Pfafferott, J., 2020a. Development and experimental evaluation of grey-box models of a microscale polygeneration system for application in optimal control. Energy Build. 215, 109725. https://doi.org/10.1016/j.enbuild.2019.109725

Sawant, P., Feldmann, T., Elmar, B., Pfafferott, J., 2019. ISG plus KWKK Vernetzung eines hybriden Smart Grids mit einer Anlage zur Kraft-Wärme-Kältekopplung zur Verbesserung der Netzdienlichkeit. Offenburg.

Sawant, P., Ho, E., Pfafferott, J., 2020b. Application and analysis of a model based controller for cooling towers in compression chiller plants. Heliyon 6, e03249. https://doi.org/10.1016/j.heliyon.2020.e03249

Sawant, P., Pfafferott, J., 2017. Experimental Investigation of a Real-Life Microscale Trigeneration System Using Adsorption Cooling , Reversible Heat-Pump and a Cogeneration Unit, in: 7th IC- EPSMSO. Learning Foundation in Mechantronics, Greece, pp. 155–165.

Sawant, P., Pfafferott, J., Felsmann, C., 2018. Quasi-First-Principle Based Grey-Box Modelling of Microscale Trigeneration Systems for Application in Automatic Control. IFAC-PapersOnLine 51, 690–695. https://doi.org/10.1016/j.ifacol.2018.11.785

Schicktanz, M., Núñez, T., 2009. Modelling of an adsorption chiller for dynamic system simulation. Int. J. Refrig. 32, 588–595. https://doi.org/10.1016/j.ijrefrig.2009.02.011

Schicktanz, M.D., Wapler, J., Henning, H.M., 2011. Primary energy and economic analysis of combined heating, cooling and power systems. Energy 36, 575–585. https://doi.org/10.1016/j.energy.2010.10.002

Seifert, J., 2013. Mikro-BHKW-Systeme für den Gebäudebereich. VDE Verlag GmbH, Berlin.

Seifert, J., Schegner, P., Meinzenbach, A., Haupt, J., Seidel, P., Schinke, L., Heß, T., Werner, J., 2015. Regionales Virtuelles Kraftwerk auf Basis der Mini- und Mikro-KWK Technologie. Dresden.

SenerTech GmbH, 2014. Planungshandbuch Dachs Gen1.1 [WWW Document]. URL http://senertec-center.com/wordpress/index.php/unterlagen/ (accessed 8.7.20).

Serale, G., Fiorentini, M., Capozzoli, A., Bernardini, D., Bemporad, A., 2018. Model Predictive Control (MPC) for Enhancing Building and HVAC System Energy Efficiency: Problem Formulation, Applications and Opportunities. Energies 11, 631. https://doi.org/10.3390/en11030631

Siemens Building Technologies, 2018. Control of Heating Plants [WWW Document]. URL https://www.downloads.siemens.com/download-center/Download.aspx?pos=download&fct=getasset&id1=A6V11498465 (accessed 12.7.20).

Široký, J., Oldewurtel, F., Cigler, J., Prívara, S., 2011. Experimental analysis of model predictive control for an energy efficient building heating system. Appl. Energy 88, 3079–3087. https://doi.org/10.1016/j.apenergy.2011.03.009

Sohlberg, B., 2003. Grey box modelling for model predictive control of a heating process. J. Process Control 13, 225–238.

Soyguder, S., Alli, H., 2009. Predicting of fan speed for energy saving in HVAC system based on adaptive network based fuzzy inference system. Expert Syst. Appl. 36, 8631–8638.

https://doi.org/10.1016/j.eswa.2008.10.033

Steyerberg, E.W., Harrell, F.E., Borsboom, G.J.J.M., Eijkemans, M.J.C.R., Vergouwe, Y., Habbema, J.D.F., 2001. Internal validation of predictive models : Efficiency of some procedures for logistic regression analysis. J. Clin. Epidemiol. 54, 774–781.

Stoecker, W.F., 1989. Design of thermal systems. McGraw Hill Book Company, New York.

Streckiene, G., Martinaitis, V., Vaitiekunas, P., 2011. Simulation of Thermal Stratification in the Heat Storage for CHP Plant, in: 8th IC- Env. Engg. Vilnius, pp. 812–819.

Teitel, M., Levi, A., Zhao, Y., Barak, M., Bar-lev, E., Shmuel, D., 2008. Energy saving in agricultural buildings through fan motor control by variable frequency drives. Energy Build. 40, 953–960. https://doi.org/10.1016/J.ENBUILD.2007.07.010

Tianyi, Z., Jili, Z., Dexing, S., 2011. Experimental study on a duty ratio fuzzy control method for fan-coil units. Build. Environ. 46, 527–534. https://doi.org/10.1016/j.buildenv.2010.09.002

Tichi, S.G., Ardehali, M.M., Nazari, M.E., 2010. Examination of energy price policies in Iran for optimal configuration of CHP and CCHP systems based on particle swarm optimization algorithm. Energy Policy 38, 6240–6250. https://doi.org/10.1016/j.enpol.2010.06.012

Trčka, M., Hensen, J.L.M., 2010. Overview of HVAC system simulation. Autom. Constr. 19, 93–99. https://doi.org/10.1016/j.autcon.2009.11.019

Tveit, T.M., Savola, T., Gebremedhin, A., Fogelholm, C.J., 2009. Multi-period MINLP model for optimising operation and structural changes to CHP plants in district heating networks with long-term thermal storage. Energy Convers. Manag. 50, 639–647. https://doi.org/10.1016/j.enconman.2008.10.010

Ünal, A.N., Ersöz, İ., Kayakutlu, G., 2016. Operational optimization in simple tri-generation systems. Appl. Therm. Eng. 107, 175–183. https://doi.org/10.1016/j.applthermaleng.2016.06.059

Urbanucci, L., 2018. Limits and potentials of Mixed Integer Linear Programming methods for optimization of polygeneration energy systems. Energy Procedia 148, 1199–1205. https://doi.org/10.1016/j.egypro.2018.08.021

Wächter, A., Biegler, L.T., 2006. On the implementation of an interior-point filter line-search algorithm for large-scale nonlinear programming. Math. Program. 106, 25–57. https://doi.org/10.1007/s10107-004-0559-y

Wagner, M.J., Gilman, P., 2011. System Advisor Model Documentation. Technical Manual for the Physical Trough Model.

Wang, D.C., Li, Y.H., Li, D., Xia, Y.Z., Zhang, J.P., 2010. A review on adsorption refrigeration technology and adsorption deterioration in physical adsorption systems. Renew. Sustain. Energy Rev. 14, 344–353. https://doi.org/10.1016/j.rser.2009.08.001

Wang, L., Singh, C., 2008. Stochastic combined heat and power dispatch based on multi-objective particle swarm optimization. Int. J. Electr. Power Energy Syst. 30, 226–234. https://doi.org/10.1016/j.ijepes.2007.08.002

Wang, S., Ma, Z., 2008. Supervisory and optimal control of building HVAC systems: A review. HVAC R Res. 14, 3–32. https://doi.org/10.1080/10789669.2008.10390991

Wemhoff, A.P., 2012. Calibration of HVAC equipment PID coefficients for energy conservation. Energy Build. 45, 60–66. https://doi.org/10.1016/J.ENBUILD.2011.10.021

Wetter, M., 2009. Modelica Library for Building Heating, Ventilation and Air-Conditioning Systems, in: Proceedings of the 7 International Modelica Conference Como, Italy. pp. 393–402. https://doi.org/10.3384/ecp09430042

Whiten, B., 2013. Model completion and validation using inversion of grey box models. ANZIAM J. 54, 187–199. https://doi.org/http://dx.doi.org/10.21914/anziamj.v54i0.6125

Wu, D.W., Wang, R.Z., 2006. Combined cooling, heating and power: A review. Prog. Energy Combust. Sci. 32, 459–495. https://doi.org/10.1016/j.pecs.2006.02.001

Wu, J.Y., Wang, J.L., Li, S., 2012. Multi-objective optimal operation strategy study of micro-CCHP system. Energy 48, 472–483. https://doi.org/10.1016/j.energy.2012.10.013

Yao, Y., Huang, M., Chen, J., 2013. State-space model for dynamic behavior of vapor compression liquid chiller ´ tat du comportement dynamique d ' une Mode ` compression de vapeur refroidisseur de liquide a. Int. J. Refrig. 36, 2128–2147. https://doi.org/10.1016/j.ijrefrig.2013.05.006

Yu, F.W., Chan, K.T., 2007. Modelling of a condenser-fan control for an air-cooled centrifugal chiller. Appl. Energy 84, 1117–1135. https://doi.org/10.1016/J.APENERGY.2007.05.004

Zhai, X.Q., Wang, R.Z., 2009. A review for absorbtion and adsorbtion solar cooling systems in China. Renew. Sustain. Energy Rev. 13, 1523–1531. https://doi.org/10.1016/j.rser.2008.09.022

Zhang, D., Shah, N., Papageorgiou, L.G., 2013. Efficient energy consumption and operation management in a smart building with microgrid. Energy Convers. Manag. 74, 209–222. https://doi.org/10.1016/j.enconman.2013.04.038

Zhang, Y., Zhang, F., Wu, X., Zhang, J., Sun, L., Shen, J., 2017. Supervisory optimization of the MGT-CCHP system using model predictive control, in: 2017 17th International Conference on Control, Automation and Systems (ICCAS). IEEE, pp. 836–841. https://doi.org/10.23919/ICCAS.2017.8204341

Zhao, Y., Lu, Y., Yan, C., Wang, S., 2015. MPC-based optimal scheduling of grid-connected low energy buildings with thermal energy storages. Energy Build. 86, 415–426. https://doi.org/10.1016/j.enbuild.2014.10.019

Zhou, Z., Liu, P., Li, Z., Pistikopoulos, E.N., Georgiadis, M.C., 2013. Impacts of equipment off-design characteristics on the optimal design and operation of combined cooling, heating and power systems. Comput. Chem. Eng. 48, 40–47. https://doi.org/10.1016/j.compchemeng.2012.08.007

A. Literature analysis on optimisation for operation of trigeneration systems

Table. 1 summarises the literature analysed to identify and evaluate the state-of-art with respect to application of optimisation tools for operation of trigeneration systems. The key online search was done on *Mendeley, Science Direct,* and *Google Scholar* using keywords such as "optimal supervisory controllers", "optimisation of trigeneration systems", and "optimal scheduling for polygeneration systems" amongst others. A period of 2009 to 2019 was chosen to establish the state-of-art.

Journal papers and conference proceedings were directly analysed. However, review articles covering multiple publications were scanned for contributions falling within scope of this analysis. The papers filtered out of the review articles are identified in the table using the first author's last name.

Due to the large number of articles, a filtering of target papers was done to identify papers that included an electric or thermal chiller and focussed on optimisation for operation or scheduling of a trigeneration system. Additionally, contributions from same research groups were not counted more than once. After the filtering, 133 publications were reduced to 33 publications for a more detailed analysis.

Appendix

Table. 1 Tabular analysis of scientific literature published from 2009 to 2019 with a focus on optimisation of a trigeneration system's operation

Reference (Years ascending)	Experimental / simulation	System configuration	Chiller	Thermal storage	Objective of optimisation
(Rong and Lahdelma, 2005)	Simulation	•Large-scale power plant •Gas turbine, back-up boiler	None	None	LP to minimise simultaneously the production and purchase costs of three energy components, as well as CO_2 emissions costs
(Ren et al., 2008)	Simulation in *LINGO*	•Micro-scale system for a two-floor residential building having a total floor area of 250 m² •Gas CHP, back-up boiler	Electric air conditioner	Mixed water storage tank	MINLP determining component sizes and operational strategies throughout the year
(Wang and Singh, 2008)	Simulation	•4 Power generation units and 2 CHPs •Scale: NA	None	None	Particle swarm optimisation for economic dispatch
(Collazos et al., 2009)	Simulation in the *AMPL-CPLEX* framework	•Micro-scale for a single family house •Stirling engine CHP and back-up boiler	None	Mixed water storage tank	MILP for operation cost reduction
(Chicco and Mancarella, 2009)	Simulation	•Medium-scale CCHP for hospital site •3 micro-turbine CHPs and 6 back-up boilers	Electric and absorption	None	LP for optimal operation strategy to reduce costs
(Lozano et al., 2009)	Simulation in *LINGO*	•Medium-scale CCHP •Gas engine CHP, back-up boiler	Electric and absorption	None	LP for optimal operation strategy to reduce costs
(Cho et al., 2009b)	Simulation in *TRNSYS*	•Micro-scale CCHP •Gas CHP, back-up boiler	Absorption	None	LP for optimal design and operation to reduce costs, energy consumption and CO_2 emissions
(Kavvadias and Maroulis, 2010)	Simulation	•Medium-scale CCHP for 300 bed hospital •Gas engine CHP, back-up boiler	Electric and absorption	None	Genetic algorithms for multi-objective design optimisation
(Chandan et al., 2012)	Simulation in *MATLAB*	•Large-scale CCHP •Gas turbine CHP, steam turbine, back-up boilers	Electric	Stratified water storage tank	NLP look-ahead optimisation problem to minimise the operating cost of the plant

Appendix

Reference	Method	System	Cooling	Storage	Optimisation
(Cole et al., 2012), 5 papers were of interest in this review article. Only 1 met the scope of this tabular analysis	Simulation: 3 papers (Sancho-Bastos, Dotzauer, Caldon)	●Large-scale gas and steam turbine CCHP: 2 papers (Sancho-Bastos, Dotzauer) ●Virtual power plant: 1 paper (Caldon)	●Absorption: 1 paper (Sancho-Bastos) ●None: 2 papers (Dotzauer, Caldon)	●General storage: 2 papers (Dotzauer, Caldon) ●None: 1 paper (Sancho-Bastos)	LP for optimal control: 1 paper (Sancho-Bastos) Dynamic problem for economic dispatch: 1 paper (Dotzauer) NLP for optimal operation: 1 paper (Caldon)
(P. Liu et al., 2013), 8 papers were of interest in this review article. Only 1 met the scope of this tabular analysis	Simulation: 8 papers (Tetsuya, Shaneb, Bosman, Naraharisetti, Kwok, Ren, Morais, Mehleri)	●Micro-scale residential micro-grid: 7 papers (Tetsuya, Shaneb, Bosman, Naraharisetti, Kwok, Mehleri, Morais) ●Medium-scale CCHP: 1 paper (Ren)	●Electric: 1 paper (Ren) ●None: 7 papers (Tetsuya, Shaneb, Bosman, Naraharisetti, Kwok, Mehleri, Morais)	●General storage: 4 papers (Shaneb, Bosman, Ren, Mehleri) ●None: 4 papers (Tetsuya, Naraharisetti, Kwok, Morais)	Optimal scheduling with: ●LP: 1 paper (Shaneb) ●MILP: 7 papers (Tetsuya, Bosman, Naraharisetti, Kwok, Mehleri, Morais, Ren)
(Ortiga et al., 2013)	Simulation in *GAMS*	●Large-scale CCHP for urban district ●Gas engine CHP, back-up boiler	Absorption	None	LP for optimal operation strategy to reduce costs
(Bracco et al., 2013)	Simulation	Medium-scale to large-scale with multiple gas turbines and engine CHPs	None	None	MILP for system selection, sizing and configuration
(Zhang et al., 2013)	Simulation in the *GAMS-CPLEX* framework	●Small-scale CHP for smart building with multiple homes and smart appliances ●Back-up boilers	None	General storage unit	MILP for adjusting smart building production and consumption patterns
(M. Liu et al., 2013)	Simulation in *MATLAB* (*fmincon*)	●Small-scale CHP for hotel ●Gas engine CHP, back-up boilers	Electric and absorption	None	Sequential quadratic problem for cost reduced operation
(Li et al., 2014)	Simulation	●CCHP for residential building ●Gas CHP and back-up boilers	Electric and absorption	Mixed water storage tank	NLP for capacity and configuration optimisation
(Flores et al., 2014)	Simulation	●Medium-scale for buildings ●CHP, back-up boilers	None	None	Economic dispatch
(Facci et al., 2014)	Simulation	●Large-scale system for hospital ●Gas engine CHP, back-up boiler	Mechanical and absorption	None	Backward dynamic programing for operation optimisation to reduce costs
(Kim and Edgar, 2014)	Simulation	●Large-scale CCHP for university campus ●Gas turbine CHP, steam turbine, back-up boilers	Electric	None	MINLP for economic dispatch

Reference / Notes	Simulation	System	Cooling	Storage	Optimisation
(Cho et al., 2014), 20 papers were of interest in this review article. Only 2 met the scope of this tabular analysis	Simulation: 2 papers (Sakawa, Guo)	●Scale: NA for 1 paper (Sakawa) ●Boilers: 1 paper (Sakawa) ●Gas engine and micro-turbine CCHP: 1 paper (Guo) ●Medium-scale CCHP micro-grid: 1 paper (Guo)	●Absorption: 1 paper (Sakawa) ●Absorption and electric: 1 paper (Guo)	●None: 1 paper (Sakawa) ●Mixed thermal storage: 1 paper (Guo)	MILP for operational planning: 2 papers (Sakawa, Guo)
(Iradi and Riffat, 2014), 5 papers were of interest in this review article. Only 1 met the scope of this tabular analysis	Simulation: 1 paper (Wu)	●Gas engine and back-up boiler CCHP: 1 paper (Wu)	Adsorption and electric: 1 paper (Wu)	None: 1 paper (Wu)	MINLP for operational optimisation: 1 paper
(Gu et al., 2014), ca. 5 papers were of interest in this review article. But none met the scope of this tabular analysis as they were already referenced					
(Liu et al., 2014), 10 papers were of interest in this review article. Only 2 met the scope of this tabular analysis	Simulation: 3 papers (Zafra, Nusrat, Hashemi)	●CHP: 1 paper (Zafra) ●Micro-scale PV-CCHP: 1 paper (Nusrat) ●Medium-scale CCHP: 1 paper (Hashemi)	None: 1 paper (Zafra) Absorption:2 papers (Nusrat, Hashemi)	●None: 1 paper (Zafra) ●General storage:2 papers (Nusrat, Hashemi)	●MPC: 1 paper (Zafra) ●Rule-based dispatch: 1 paper (Nusrat) ●Offline NLP: 1 paper(Hashemi)
(Di Somma et al., 2015)	Simulation in *MATLAB-CPLEX* framework	●Medium-scale building ●Gas turbine CHP and reversible heat pump	Electric reversible heat pump and absorption	Mixed water storage tank	MILP for operation optimisation
(Parisio et al., 2015)	Simulation in *Virtual MicroGrid Lab* and *CPLEX* framework	●Small-scale residential micro-grid ●CHPs and reversible heat pumps	Electric	None	MILP for minimising overall cost
(Zhao et al., 2015)	Simulation in *MATLAB*	●Medium-scale for building ●CHP, back-up boiler, Photovoltaic	Electric and adsorption	Mixed water storage tank	NLP for cost reduced optimisation
(Ünal et al., 2016)	Simulation in *Visual-Basic using*	●Large-scale CCHP for food industry ●4 Gas CHPs, back-up boiler	Mechanical and absorption	None	LP for optimal operation strategy to reduce costs

Appendix

Reference	Simplex in Microsoft Excel Data Solver				
(Menon et al., 2016)	Simulation	• Micro-scale CHP in a micro-grid • CHP and heat pumps	Electric	Mixed thermal storage	MILP for electricity price based optimised operation
(Fuentes-Cortés et al., 2016)	Simulation in *BARON-GAMS* framework	• Medium-scale for building with 420 households • Engines, fuel cells, micro-turbines, Stirling engines, solar water heaters as technology options	Absorption	None	MINLP multi-objective for design optimisation and control optimisation
(Murugan and Horák, 2016), ca. 5 papers were of interest in this review article. But none met the scope of this tabular analysis as they were already referenced					
(Al Moussawi et al., 2016), ca. 5 papers were of interest in this review article. But none met the scope of this tabular analysis as they were already referenced					
(Rong and Su, 2017), 40 papers were of interest in this review article. Only 2 met the scope of this tabular analysis	• Simulation in *EES*: 1 paper (Ghaebi) • Simulation in *AIMMS-CPLEX* framework: 1 paper (Ameri) • Simulation in *GAMS-BnB* framework: 1 paper (Savola)	• Gas turbine CCHP: 2 papers (Ghaebi, Ameri) • Large-scale CCHP micro-grid: 2 papers (Ameri, Savola)	• Absorption: 2 papers (Ghaebi, Ameri) • Electric: 1 paper (Ameri) • None: 1 paper (Savola)	None: 2 papers (Ghaebi, Ameri)	Optimal scheduling with: • Genetic algorithm: 1 paper (Ghaebi) • MILP: 1 paper (Ameri) • MINLP: 1 paper (Savola)
(Andiappan, 2017), 10 papers were of interest in this review article. Only 2 met the scope of this tabular analysis	• Simulation in *CPLEX*: 2 papers (Bischi, Yokoyama)	• Large-scale CCHP micro-grid: 1 paper (Bischi) • Small-scale CCHP: 1 paper (Yokoyama)	Electric and absorption: 2 papers (Bischi, Yokoyama)	• General storage: 1 paper (Bischi) • None: 1 paper (Yokoyama)	MILP for system planning and operation: 2 papers (Bischi, Yokoyama)
(Gu et al., 2017)	Simulation in *MATLAB-GUROBI* framework	• Medium-scale CCHP for a building • Gas turbine CHP, wind turbine, photovoltaic, back-up boiler	Electric and absorption	Mixed thermal storage	MILP for online optimal operation
(Zhang et al., 2017)	Simulation	• Medium-scale CCHP • Gas turbine CHP	Absorption	None	Linear MPC for optimal scheduling

	Simulation in a *Python-CPLEX* framework	•Micro-scale CHP •Gas engine CHP, photovoltaic and back-up boiler	None	Mixed thermal storage	MPC based combined control for PV-CHP hybrid system
(Kneiske et al., 2018)					
(Urbanucci, 2018), 4 papers were of interest in this review article. Only 1 met the scope of this tabular analysis	Simulation in *MATLAB-GAMS* framework: 1 paper (Carlos)	•Large-scale CCHP micro-grid for tourist resort: 1 paper (Carlos)	Electric and absorption: 1 paper (Carlos)	None: 1 paper (Carlos)	NLP: 1 paper (Carlos)

B. INES trigeneration set-up

This section provides the technical documentation used for the planning and operation of the INES trigeneration plant and extracts of product data, which are referenced in the main body of the dissertation. The following sub-sections are presented:

B.1 Piping and instrumentation diagram

B.2 Product data

    B.2.1 Adsorption chiller (AdC)

    B.2.2 Combined heating and power (CHP)

    B.2.3 Outdoor coil (OC)

    B.2.4 Reversible heat pump (RHP)

    B.2.5 Storage tanks

B.3 Operation modes

B.4 Functional description for the lower-level controller

B.1 Piping and instrumentation diagram
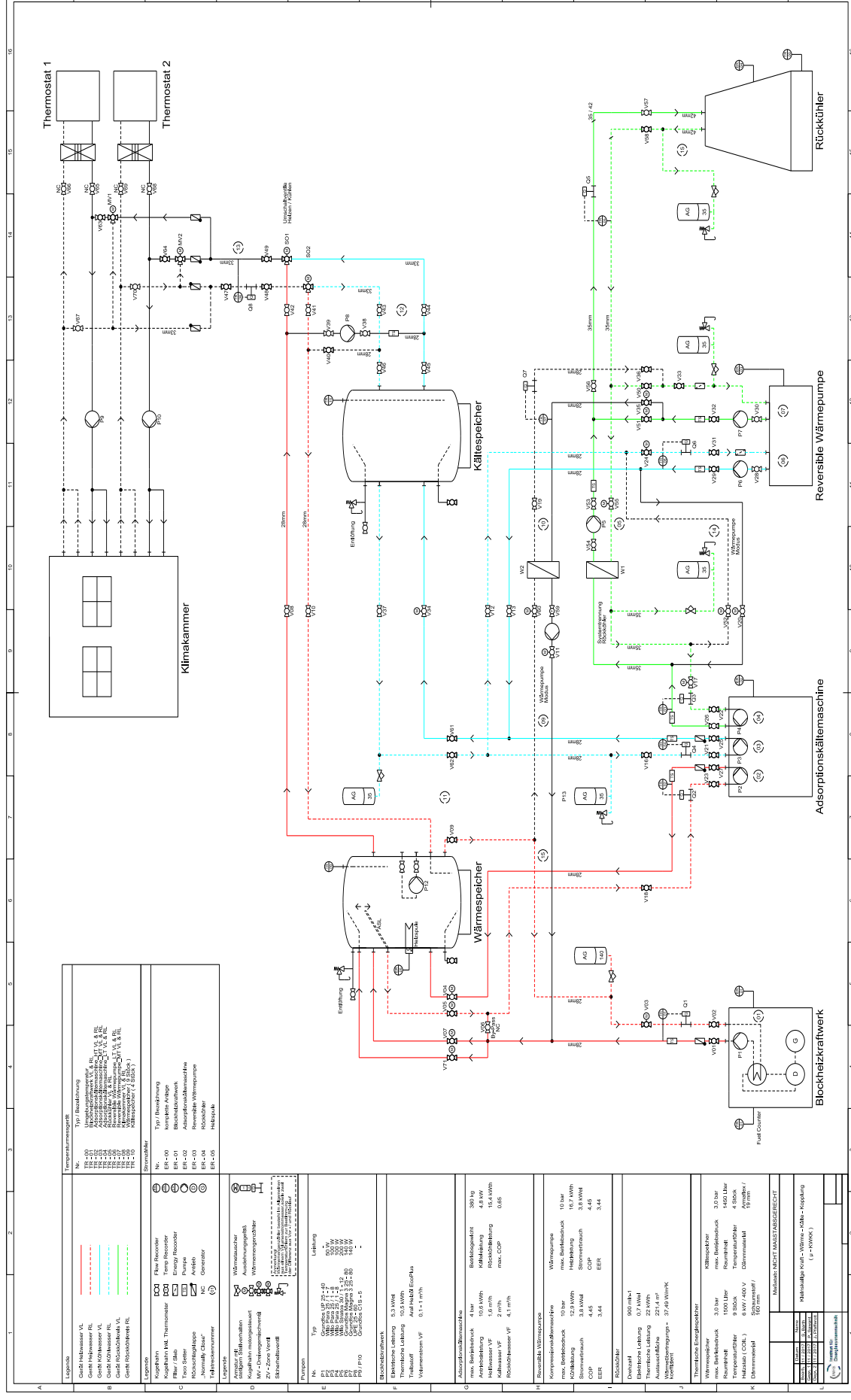
Figure 1 Piping and instrumentation diagram for the INES trigeneration lab

B.2   Product data

Manufacturer's product catalogues, data sheets, component installation and operation manuals are together referred to as product data. These provide information on nominal capacities, operation ranges, and safety limits for the components. The extracts of product data used for parameterisation of the models and setting up the MPC are presented for each component individually.

B.2.1 Adsorption chiller (AdC)

Adsorptionskälteaggregat eCoo

Energieeffizientes Kühlen und Heizen mit SorTech

Technische Daten eCoo

Einsatzbereich	
Heißwassertemperatur	55 – 95 °C
Rückkühlwassertemperatur	max. 45 °C
Kaltwassertemperatur	min. 8 °C
Heizwassertemperatur	freies Heizen: 25 – 70 °C
Rückkühlwassertemperatur	freies Kühlen: min. 5 °C

Leistungseckdaten	
Kälteleistung	bis zu 12 kW
Heizleistung	bis zu 40 kW
COP therm.	max. 0,65

Abmessungen	
BxTxH	840 x 811 x 1.345 mm
Aufstellfläche	0,68 m²

Elektr. Leistungsaufnahme/Anschluss	
Ohne Pumpengruppe	6 W (Ø)
Bei Druckverlusten eCoo	120 W
Bei Inanspruchnahme der max. Förderhöhe	410 W
Elektrischer Anschluss	230 V, 50/60 Hz

Gewicht	
Betriebsgewicht	ca. 325 kg*/380 kg**

*Ohne / **Mit Pumpengruppe und Verkleidung.*

Heißwasserkreislauf	
Volumenstrom	1.600 l/h
Druckverlust eCoo	120 mbar
Max. zusätzliche Förderhöhe	520 mbar
Max. Betriebsdruck	4 bar
Anschluss	1 ¼" AG

Rückkühlwasserkreislauf/Heizwasserkreislauf	
Volumenstrom	4.100 l/h
Druckverlust eCoo	275mbar
Max. zusätzliche Förderhöhe	345 mbar
Max. Betriebsdruck	4 bar
Anschluss	1 ½" AG

Kaltwasserkreislauf	
Volumenstrom	2.000 l/h
Druckverlust eCoo	280 mbar
Max. zusätzliche Förderhöhe	440 mbar
Max. Betriebsdruck	4 bar
Anschluss	1 ¼" AG

Frontansicht eCoo

Schrägansicht eCoo

Profil eCoo

Rückansicht eCoo

Figure 2 Extract of AdC's technical datasheet (in German only)
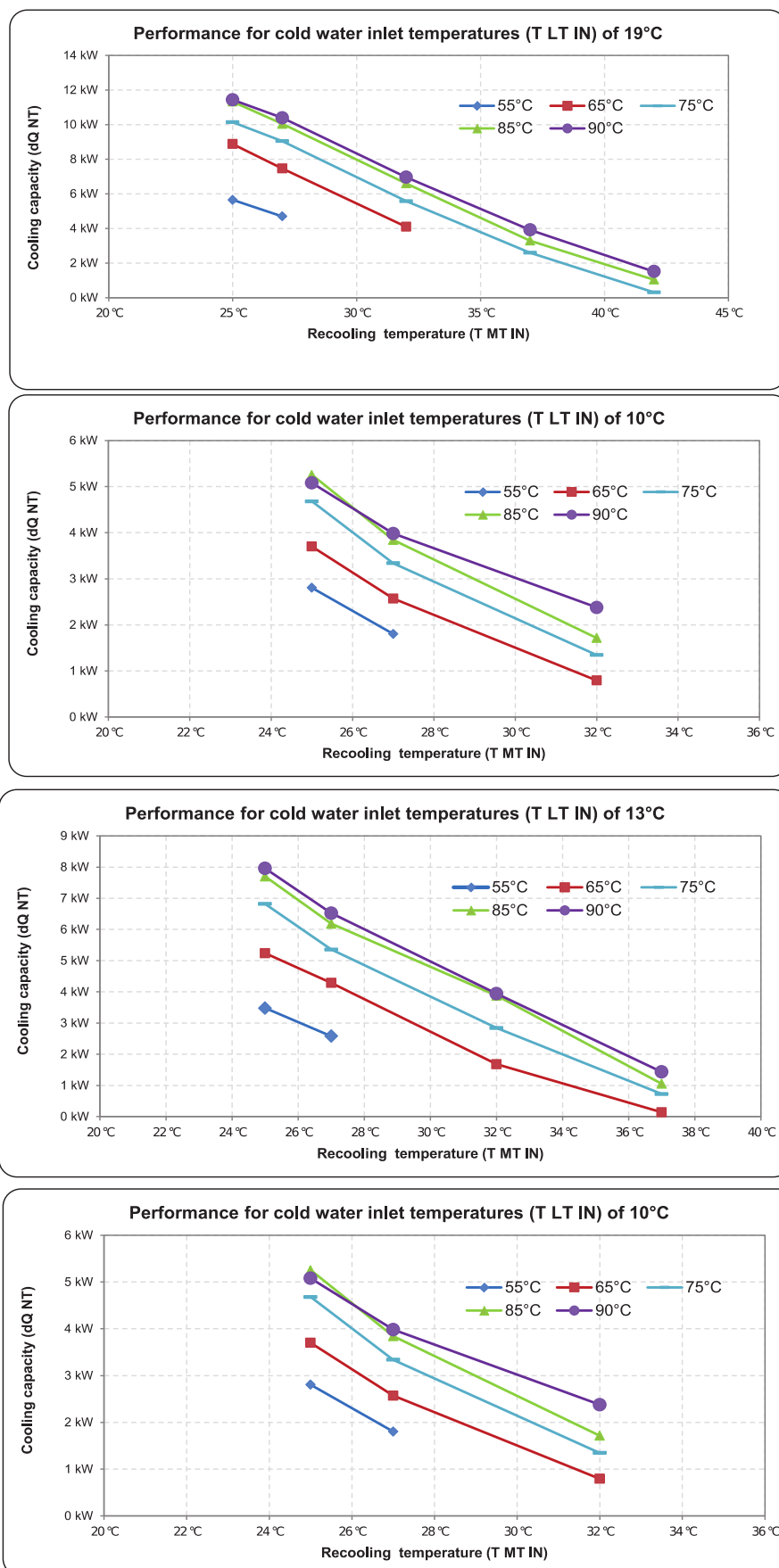
Figure 3 Characteristic curves for cooling capacity based on inlet temperatures from AdC's operation manual
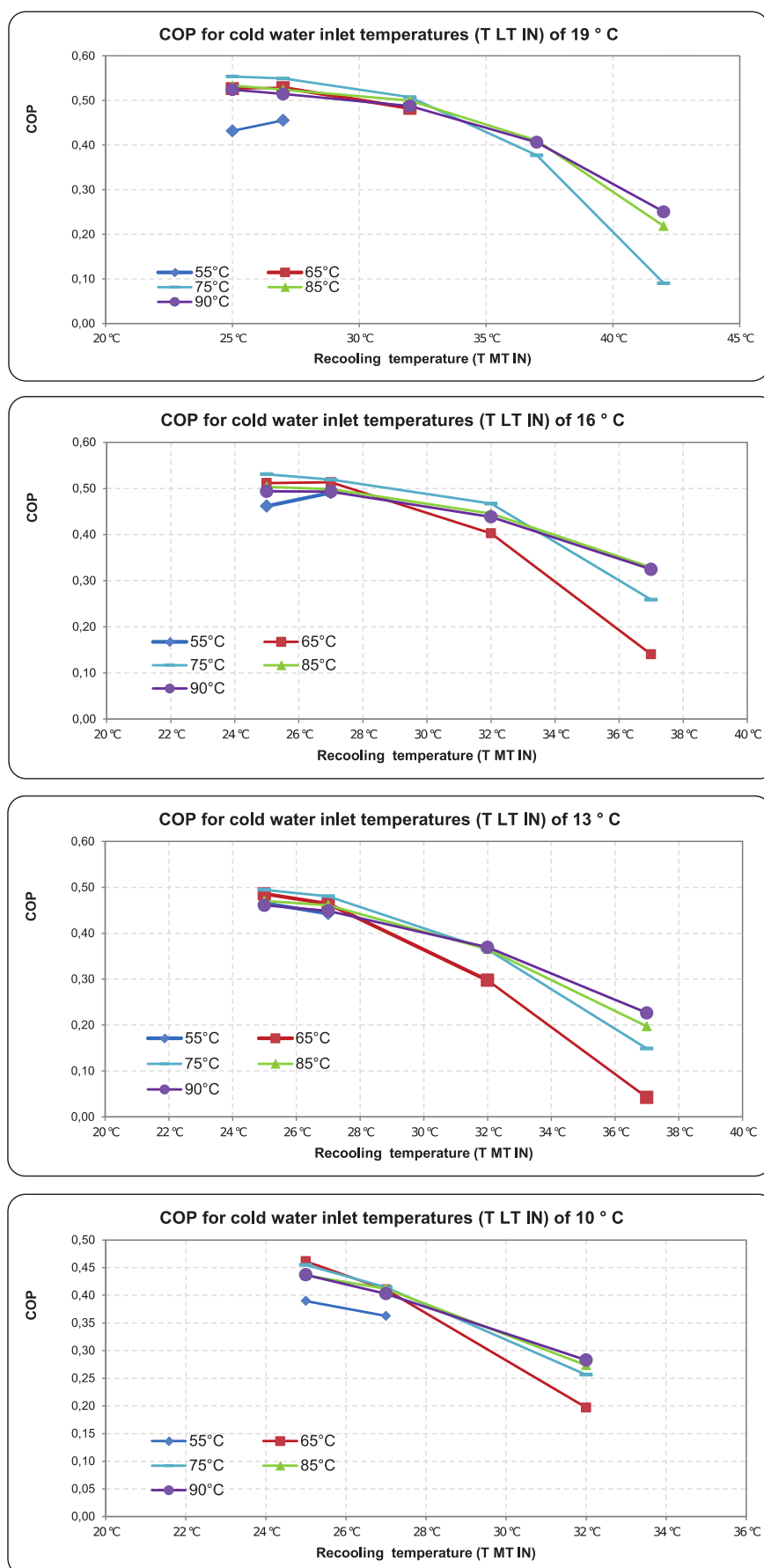
Figure 4 Characteristic curves for COP based on inlet temperatures from AdC's operation manual

B.2.2 Combined heating and power (CHP)

e Daten

[s ¹⁾]	G 5.5	G 5.5	G 5.0 Low NOx	G 5.0 Low NOx	F 5.5 Low NOx	F 5.5 Low NOx	HR 5.3	HR 5.3	HR 5.3	HR 5.3
	Standard ⁵⁾	Brennwert ²⁾	Standard ⁵⁾	Brennwert ²⁾	Standard ⁵⁾	Brennwert ²⁾	Standard ⁵⁾	Brennwert ²⁾	Standard ⁵⁾	Brennwert ²⁾
	Erdgas		Erdgas		Flüssiggas		Heizöl EL ³⁾		Biodiesel (RME)	
elektrische Leistung [kW] ⁴⁾	5,5		5,0		5,5		5,3			
thermische Leistung [kW]	12,5	14,8	12,3	14,6	12,5	14,8	10,5	11,9	10,3	11,7
Leistungsaufnahme [kW] ⁶⁾	20,5		19,6		20,5		17,9		17,6	
Hilfsenergie im Betrieb [kW$_{el.}$] ⁷⁾	0,12						0,14			
max. Vorlauftemperatur	83 °C									
max. Rücklauftemperatur	70 °C									
Spannung / Frequenz	3 ~ 230 V / 400 V 50 Hz									
Wirkungsgrade:										
- elektrisch	27%		26%		27%		30%			
- thermisch	61%	72%	63%	74%	61%	72%	59%	66%	59%	66%
- Brennstoffnutzung	88%	99%	89%	100%	88%	99%	89%	96%	89%	97%
Stromkennzahl	0,44		0,41		0,44		0,50		0,51	
Schallemission [dB(A)] nach DIN 45635-01	52 - 56						54 - 58			
Abgasemission < TA-Luft	X		X		X		-		-	
Wartung [Betriebsstunden]	3.500		3.500		3.500		2.700		1.400	
Minimum Methanzahl ⁸⁾	35		35		35		-		-	
Abgasführung	Gemeinsame Abgasführung mit Heizkessel möglich; Abgasleitung mit oder ohne Nebenluftzuführung									
Aufstellort	Nach den Regeln der Feuerstättenverordnung									
Maße [cm] und Gewicht [kg]:	Breite (ohne Regler): 72 cm / Länge: 107 cm / Höhe: 100 cm / Gewicht: 530 kg									
Platzbedarf (Breite/Tiefe) [cm]:	Dachs: min. 192/182 Dachs Brennwert: min. 192/202 Dachs SE Brennwert: min. 290/202									

¹⁾ der Dachs erfüllt das Hocheff zienzkriterium gemäß Kraft-Wärme-Kopplungsgesetz; ²⁾ mit externen Abgaswärmetauscher (Dachs Kondenser) bei einer Rücklauftemperatur von 30°C; ³⁾ ohne aschebildende Additive; Empfehlung: schwefelarm; ⁴⁾ Leistung nach DIN ISO 3046, gemessen an den Generatorklemmen, abweichende Werte je nach Aufstellhöhe und Umgebungs- und Einsatzbedingungen; ⁵⁾ Werte aus Typ-/Bauteilprüfbericht bei einer Rücklauftemperatur von 60 °C; ⁶⁾ Werte aus Typ-/Bauteilprüfbericht bei einer Rücklauftemperatur von 60 °C bezogen auf H$_i$, Toleranz +/- 5%; ⁷⁾ Toleranz +/- 10% bei 230V~, Berechnungswerte für EnEV; ⁸⁾ mit Einstellung und Düsenanpassung vor Ort

Einsatzfälle

Ein- und Mehrfamilienhäuser, Handwerksbetriebe, Bäckereien, Metzgereien, Werkstätten, Autohäuser, Hotels und Pensionen, Alten- und Pf egeheime, Schulen, Kindergärten, Sporthallen, Gemeindezentren, Hallenbäder, landwirtschaftliche Betriebe, kirchliche Einrichtungen

Prüfungen

Typprüfung durch TÜV Bayern (mit Prüfzeichen), DVGW Qualitätszeichen, Konformität mit den Anforderungen für Eigenerzeugungsanlagen am Niederspannungsnetz, CE Zertif zierung
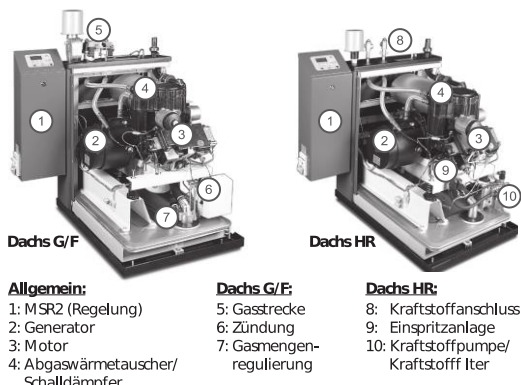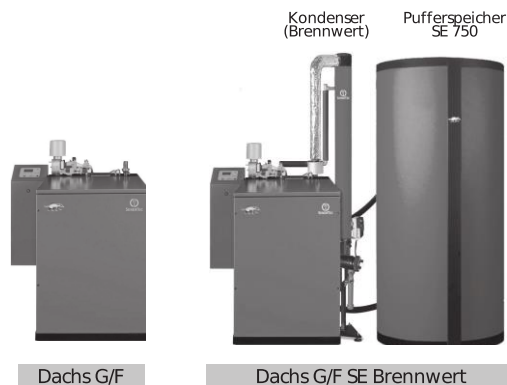
Kondenser (Brennwert)   Pufferspeicher SE 750

Dachs G/F   Dachs G/F SE Brennwert

Dachs G/F   Dachs HR

Allgemein:
1: MSR2 (Regelung)
2: Generator
3: Motor
4: Abgaswärmetauscher/ Schalldämpfer

Dachs G/F:
5: Gasstrecke
6: Zündung
7: Gasmengen- regulierung

Dachs HR:
8: Kraftstoffanschluss
9: Einspritzanlage
10: Kraftstoffpumpe/ Kraftstofff lter

Figure 5: Extract of CHP's technical data sheet (in German only)

B.2.3 Outdoor coil (OC)

SorTech Rückkühler

Technische Daten eRis 20 WV

Leistungseckdaten	
Leistung Rückkühlstrang	bis zu 58 kW
Rückkühlmedium	Ethylenglykol 34%
Wassertemperatur Eintritt/Austritt	30,6/25°C
Nennvolumenstrom	9,6 m³/h
Max. Betriebsdruck	4 bar
Wasserverbrauch	max. 9 m³/Jahr
Temperatur Lufteintritt/Luftaustritt	21,5/26,5°C
Luftvolumenstrom	35.000 m³/h
Druckverlust	310 mbar

Ventilatoren	
Ventilatoren	03xEC Ventilatoren
Schalldruckpegel in 10 m	36 dB(A)

Gewicht	
Leergewicht	ca. 630 kg

Abmessungen	
BxTxH	6.130 x 1.050 x 1.260 mm
Aufstellfläche	6,44 m²

Elektr. Leistungsaufnahme/Anschluss	
Elektrische Leistungsaufnahme	0,93 kW
Elektrischer Anschluss	230 V, 50 Hz

Der Rückkühler eRis 20 WV ist optimiert ausgelegt für den Betrieb mit Adsorptionskältemaschine Typ eCoo 20 IPS. Rückkühler mit stromsparender EC-Technologie. Regelung zur temperaturgeführten, stufenlosen Variation der Lüfterdrehzahl im Schaltschrank, komplett verkabelt und montiert. Der Rückkühler enthält ein Besprühsystem (Sprühmedium: Wasser), dass zum temporären Besprühen der Lamellen ausgelegt ist zur Spitzenlastabdeckung. Die Aufstellung erfolgt vertikal nur mit einem Kran oder Gabelstapler.

* Nicht förderfähig nach BAFA Vorgaben.

Figure 6 Extract of the OC's data sheet with photograph of the component installed outside the building

B.2.4 Reversible heat pump (RHP)

⚠DAIKIN • Single Unit • EWWP-KBW1N

Specifications

2-1 Technical Specifications				EWWP01 4KBW1N	EWWP02 2KBW1N	EWWP02 8KBW1N	EWWP03 5KBW1N	EWWP04 5KBW1N	EWWP05 5KBW1N	EWWP06 5KBW1N	EWWP09 0KBW1N	EWWP10 0KBW1N
Cooling capacity	Nom.		kW	12.9	21.4	27.8	32.3	42.8	55.7	64.7	85.7	98.6
Heating capacity	Nom.		kW	16.7	27.5	35.6	41.5	55.0	71.7	83.0	110.0	127.0
Power input	Cooling	Nom.	kW	3.8	6.1	7.8	9.1	12.2	16.0	18.2	24.2	28.0
	Heating	Nom.	kW	3.8	6.1	7.8	9.1	12.2	16.0	18.2	24.2	28.0
Capacity steps number				1				2			4	
EER				3.44	3.49	3.54		3.51	3.48	3.55	3.54	3.52
COP				4.45	4.49	4.54	4.55	4.51	4.48	4.56	4.55	4.54
Space heating general	Other	Capacity control		Inverter							-	
		Cdh (Degradation heating)		1.00							-	
		Pck (Crankcase heater mode)	kW	0.0080	0.0090	0.0080		0.0060	0.0080			
		Poff (Off mode)	kW	0.175	0.317	0.338	0.382	0.480	0.496	0.882		-
		Psb (Standby mode)	kW	0.0080	0.0090	0.0080					-	
		Pto (Thermostat off)	kW	0.00							-	
	Integrated supplementary heater	NOx emission	mg/kWh	0.00							-	
		Psup	kW	0.00							-	
		Type of energy input		Electrical							-	

Figure 7 Extract of RHP's product catalogue with technical data (INES Model = EWWP01 4KBW1N)

DAIKIN • Single Unit • EWWP-KBW1N

Capacity tables
Cooling/Heating Capacity Tables

EWWP014-035KBW1N

LWC		20			25			30			35			40			45			50			55		
LWE	Model	CC	HC	PI	CC	HC	PI	CC	HC	PI	CC	HC	PI	CC	HC	PI	CC	HC	PI	CC	HC	PI	CC	HC	PI
-10	014	7,95	10,9	2,88	7,48	10,6	3,09	6,94	10,3	3,34	6,34	10,0	3,63	5,67	9,64	3,96	4,93	9,28	4,33						
	022	12,3	16,2	3,89	12,1	16,4	4,36	11,4	16,3	4,86	10,6	16,0	5,41	9,6	15,6	6,00	8,5	15,1	6,63						
	028	16,2	21,8	5,55	16,3	22,4	6,17	15,9	22,7	6,87	15,1	22,8	7,66	14,1	22,6	8,54	12,7	22,3	9,51						
	035	20,7	27,3	6,49	20,6	27,7	7,06	20,4	28,2	7,78	19,5	28,2	8,64	18,0	27,8	9,66	16,1	27,0	10,8						
-5	014	9,83	12,7	2,89	9,33	12,5	3,11	8,79	12,2	3,37	8,20	11,9	3,70	7,56	11,6	4,01	6,88	11,3	4,38	6,15	10,9	4,77			
	022	15,8	19,9	4,11	15,2	19,8	4,59	14,6	19,7	5,11	13,7	19,4	5,67	12,8	19,0	6,29	11,6	18,6	6,94	10,3	18,0	7,65			
	028	19,9	25,6	5,72	19,9	26,2	6,31	19,6	26,6	6,99	18,7	26,5	7,77	17,9	26,6	8,63	16,6	26,2	9,59	15,2	25,8	10,6			
	035	24,2	30,9	6,62	24,1	31,4	7,21	24,0	32,0	7,93	23,1	32,0	8,79	21,8	31,7	9,79	20,1	31,1	11,0	17,8	30,0	12,2			
0	014	11,8	14,8	2,91	11,4	14,5	3,14	10,8	14,3	3,41	10,3	14,0	3,74	9,59	13,7	4,07	8,86	13,3	4,47	8,07	13,0	4,87	7,21	12,6	5,37
	022	18,6	23,0	4,35	18,2	23,0	4,80	17,4	22,7	5,31	16,7	22,6	5,88	15,7	22,2	6,52	14,5	21,7	7,22	13,2	21,2	7,97	11,9	20,7	8,79
	028	23,5	29,4	5,83	23,5	29,9	6,37	23,2	30,3	7,00	22,4	30,2	7,74	21,7	30,3	8,58	20,4	30,0	9,51	19,1	29,6	10,5	17,0	28,7	11,7
	035	27,7	34,4	6,60	27,6	34,9	7,24	27,5	35,6	7,99	26,7	35,7	8,86	25,6	35,5	9,84	23,9	35,1	11,1	21,8	34,0	12,1	19,3	32,9	13,5
4	014	13,0	15,9	2,87	12,8	16,0	3,12	12,4	15,9	3,42	12,0	15,8	3,77	11,4	15,5	4,11	10,7	15,2	4,51	9,92	14,9	4,93	9,04	14,5	5,43
	022	20,6	25,1	4,40	20,4	25,3	4,88	20,0	25,5	5,42	19,6	25,6	6,01	18,6	25,3	6,65	17,5	24,8	7,35	16,2	24,3	8,09	14,4	23,3	8,90
	028	26,5	32,4	5,88	26,5	32,9	6,42	26,2	33,3	7,07	25,5	33,4	7,86	24,7	33,4	8,66	23,5	33,1	9,59	22,0	32,6	10,6	20,1	32,0	11,8
	035	30,6	37,5	6,81	30,6	38,1	7,46	30,4	38,7	8,22	29,8	38,9	9,08	28,7	38,9	10,1	27,3	38,6	11,2	25,5	37,9	12,4	23,3	37,0	13,6
7	014	14,2	17,2	2,90	13,9	17,1	3,14	13,4	16,9	3,43	12,9	16,7	3,75	12,3	16,4	4,12	11,6	16,1	4,51	10,8	15,8	4,98	10,0	15,5	5,47
	022	22,5	27,1	4,57	22,3	27,3	5,00	22,0	27,6	5,51	21,4	27,5	6,13	20,4	27,0	6,69	19,0	26,4	7,34	17,4	25,5	8,09	15,5	24,5	9,02
	028	28,7	34,6	5,93	28,7	35,2	6,48	28,4	35,6	7,13	27,8	35,6	7,85	27,0	35,7	8,73	25,8	35,4	9,62	24,3	35,0	10,7	22,4	34,2	11,8
	035	32,9	39,9	6,89	32,8	40,5	7,56	32,8	41,2	8,32	32,3	41,5	9,12	31,3	41,6	10,2	29,9	41,2	11,3	27,9	40,5	12,5	25,5	39,3	13,7
10	014	15,4	18,3	2,90	15,0	18,2	3,17	14,7	18,2	3,47	14,2	18,0	3,78	13,7	17,9	4,19	13,0	17,6	4,60	12,2	17,3	5,06	11,2	16,7	5,49
	022	24,4	29,0	4,56	24,3	29,3	5,01	23,9	29,4	5,53	23,2	29,3	6,11	22,2	28,9	6,74	20,9	28,3	7,43	19,3	27,5	8,19	17,4	26,5	9,03
	028	30,2	36,1	5,93	30,2	36,6	6,49	30,0	37,1	7,15	29,5	37,4	7,90	28,8	37,5	8,73	27,8	37,4	9,67	26,4	37,1	10,7	24,7	36,5	11,8
	035	34,3	41,4	6,98	34,2	42,0	7,66	34,1	42,6	8,42	33,5	42,9	9,27	32,6	42,9	10,3	31,2	42,6	11,3	29,4	42,0	12,5	27,3	41,1	13,7
14	014	16,1	19,0	2,89	16,1	19,3	3,20	16,2	19,7	3,52	16,0	19,8	3,81	15,6	19,8	4,26	14,9	19,6	4,69	14,0	19,1	5,16	12,8	18,3	5,51
	022	26,2	30,7	4,53	26,2	31,2	5,02	26,0	31,6	5,55	25,6	31,6	6,08	24,6	31,4	6,80	23,4	30,9	7,52	21,8	30,2	8,31	20,1	29,1	9,02
	028	32,1	38,0	5,93	32,0	38,5	6,50	32,0	39,1	7,15	31,7	39,6	7,92	31,2	40,0	8,74	30,4	40,1	9,66	29,3	39,9	10,7	27,7	39,5	11,9
	035	38,2	45,3	7,04	38,1	45,9	7,72	37,8	46,4	8,49	37,2	46,7	9,37	36,3	46,7	10,3	35,0	46,5	11,4	33,5	46,1	12,5	30,8	44,6	13,7
16	014	16,7	19,6	2,88	16,6	19,8	3,20	16,6	20,1	3,52	16,5	20,3	3,82	16,1	20,4	4,26	15,6	20,3	4,69	14,7	19,9	5,15	13,6	19,1	5,51
	022	27,0	31,6	4,52	27,0	32,0	5,01	26,9	32,4	5,53	26,5	32,6	6,07	25,7	32,5	6,78	24,6	32,1	7,51	23,1	31,4	8,30	21,3	30,3	9,02
	028	32,4	38,4	5,94	32,4	38,9	6,52	32,3	39,5	7,19	32,1	40,1	7,95	31,7	40,5	8,78	31,0	40,7	9,71	30,0	40,8	10,7	28,7	40,6	11,9
	035	38,6	45,8	7,07	38,6	46,4	7,76	38,3	46,9	8,54	37,9	47,4	9,43	37,1	47,5	10,4	36,0	47,4	11,4	34,5	47,1	12,5	32,7	46,6	13,8
20	014	17,5	20,4	2,87	17,5	20,7	3,19	17,5	21,0	3,52	17,4	21,3	3,83	17,3	21,6	4,26	16,9	21,6	4,68	16,3	21,4	5,13	15,3	20,8	5,50
	022	28,7	33,2	4,50	28,6	33,6	4,98	28,6	34,1	5,51	28,3	34,4	6,05	27,8	34,6	6,75	26,9	34,4	7,47	25,6	33,9	8,26	23,8	32,8	9,01
	028	33,1	39,0	5,95	33,0	39,6	6,56	33,0	40,2	7,25	33,0	41,0	8,00	32,7	41,6	8,86	32,3	42,1	9,79	31,6	42,4	10,8	30,8	42,7	11,9
	035	40,7	47,8	7,04	40,6	48,4	7,75	40,6	49,2	8,54	40,5	50,1	9,46	40,5	50,9	10,4	40,4	51,9	11,4	39,0	51,6	12,5	37,2	51,2	13,9

CONDITIONS

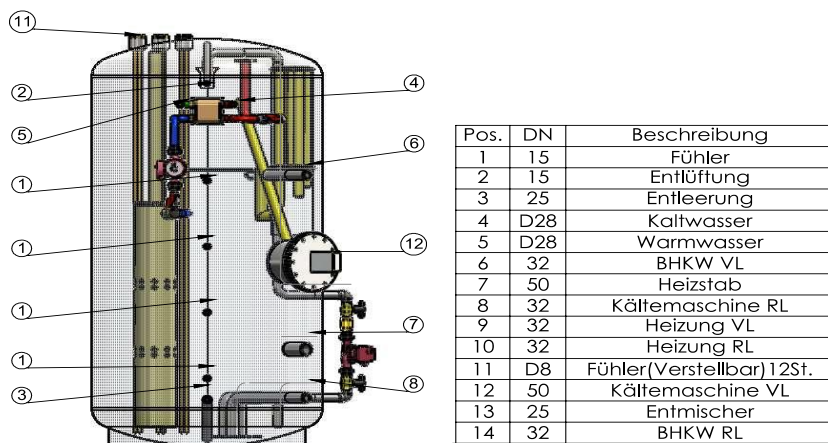1. Cooling capacity is according to EN14511:2011 and valid for chilled water range Dt = 3~8°C
2. Heating capacity is according to EN14511:2011 and valid for chilled water range Dt = 3~8°C
3. Power input is total input according to EN14511:2011

SYMBOLS

CC : Cooling capacity (kW)
HC : Heating capacity (kW)
PI : Power input (kW)
LWE : Leaving Water Evaporator (°C)
LWC : Leaving Water Condenser (°C)

Figure 8 Extract of RHP's operation manual with capacity tables for cooling and heating capacity based on circuit temperatures

B.2.5 Storage tanks

Pos.	DN	Beschreibung
1	15	Fühler
2	15	Entlüftung
3	25	Entleerung
4	D28	Kaltwasser
5	D28	Warmwasser
6	32	BHKW VL
7	50	Heizstab
8	32	Kältemaschine RL
9	32	Heizung VL
10	32	Heizung RL
11	D8	Fühler(Verstellbar)12St.
12	50	Kältemaschine VL
13	25	Entmischer
14	32	BHKW RL

Heizungspufferspeicher mit Frischwasserstation

Pufferspeicher mit Frischwasserstation

Pufferspeicher mit Frischwasserstation

Pufferspeicher für Heizungswasser in stehender zylindrischer
Ausführung, aus schwarzem Stahlblech St 37.1, elektrisch geschweißt,
mit gewölbten Böden, innen roh, außen rostschutzgrundiert mit
Gütenachweis.

Kompl. mit Füßen, Anschlüssen und Einbauten wie folgt:
1x Rücklaufeinschichtrohr DN 200 / DN 4 für FWST.
1x Kaskadeneinschichtrohr DN 300
1x Schichtentnahmerohr mit Stellmotor DN 40
1x Entmischungseinrichtung mit Pumpe
2x Anschluss   DN 50
2x Anschluss   DN 32
2x Anschluss   DN 15
4x Muffenanschluss   R1/2"
1x Entleerung   R 3/4"
1x Entlüftung   R 1/2"

Inhalt 1.500 Liter, PN 3
3x Messsonden a 4x10mm Ø Cu über Pufferhöhe

Mit integrierter in einer trockenen Tasche montierten Frischwasserstation
zur Brauchwasserbereitung, Leistung 40 L/min. Das Brauchwasser wird
durch den Plattenwärmetauscher im Gegenstromprinzip trägheitsfrei
erwärmt.
Lieferumfang:
Plattenwärmetauscher
Mehrstrahlflügelradzähler Qn 2,5 mit Impulsgeber
Ladepumpe Mircrocontroller Regelung inkl.
3 Temperatursensoren 1 Temperatursensor aus V4A
ohne Hülse mit Klemmverschraubung, Ausgleichszeit 2 sec.
Display 2 digitale Ausgänge, 1 digitaler Ausgang, 2 digitale Eingänge.

Technische Daten:
Höhe ohne Dämmung: ca. 2.200 mm
Höhe mit Dämmung: ca. 2.360 mm
Durchmesser ohne Dämmung: ca. 1.000 mm
Durchmesser mit Dämmung: ca. 1.320 mm
max. Druck: 3,0 bar Betriebsdruck
**Dämmung für vorstehende beschriebenen Heizungspufferspeicher -
160 mm**

Dämmung für vorstehende beschriebenen Heizungpufferspeicher
bestehend aus Schaumstoff (160 mm)
darüber eine Lage PVC-Folie s = 2 mm
Stöße mit Schienen abgedeckt, einschl. Deckel
Heizstab 400 V - Leistung 6 kW

Heizstab 400 V - Leistung 6 kW
mit Regelung und Sicherheitsthermostat

Figure 9 Extract of HTES design and catalogue data (in Germany only)
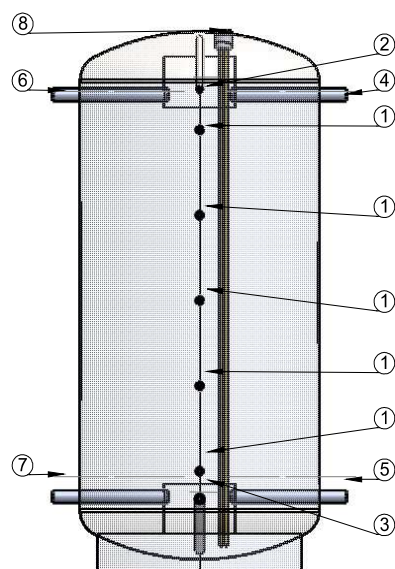
Pos.	DN	Beschreibung
1	15	Fühler
2	15	Entlüftung
3	25	Entleerung
4	32	Kältemaschine RL
5	32	KältemaschineVL
6	32	Netz RL
7	32	Netz VL
8	D8	Fühler(Vertellbar)12St.

Kältepufferspeicher

Pufferspeicher für Kaltwasser 1.450 l

Pufferspeicher für Kaltwasser in stehender zylindrischer Ausführung,
aus schwarzem Stahlblech St 37.1, elektrisch geschweißt, mit gewölbten
Böden, innen roh, außen rostschutzgrundiert mit Gütenachweis,

Kompl. mit Füßen, Anschlüssen und Einbauten wie folgt:
    2x Verteilertopf   DN 200
    4x Flanschanschluss   DN 32
    5x Muffenanschluss für Fühler R 1/2"
    1x Entlüftung   R 1/2"
    1x Entleerung   R 1"

Inhalt 1.450 Liter
1x Messsonden a 4x10mm Ø Cu über Pufferhöhe
Technische Daten:
Höhe ohne Dämmung: ca. 2.200 mm
Höhe mit Dämmung: ca. 2.219 mm
Durchmesser ohne Dämmung: ca. 1.000 mm
Durchmesser mit Dämmung: ca. 1.038 mm
max. Druck: 3,0 bar Betriebsdruck

Dämmung für Kältepufferspeicher 19 mm

Dämmung für vorstehende beschriebenen Kältepufferspeicher
Ausführung: 19 mm Armaflex diffusionsdicht,
               vollflächig verklebt

Figure 10 Extract of CTES design and catalogue data (in Germany only)

B.3 Operation modes

Seven different operation modes (*Figure 11* to *Figure 17*) are possible in the INES lab and the status of the components in these operation modes is shown in *Table. 2* .

Table. 2 Status of components in the operation mode

Operation mode	CHP	AdC	HP	CC
1	Off	Off	Off	Off
2	On	Off	Off	Off
3	On	On	Off	Off
4	Off	Off	Off	On
5	Off	Off	On	Off
6	Off	On	Off	Off
7	On	Off	Off	On

Operation mode 1: No components are turned on. Depending on the load profile, the HL or CL is satisfied by the stored energy in the tanks and the EL is covered by the GRID.
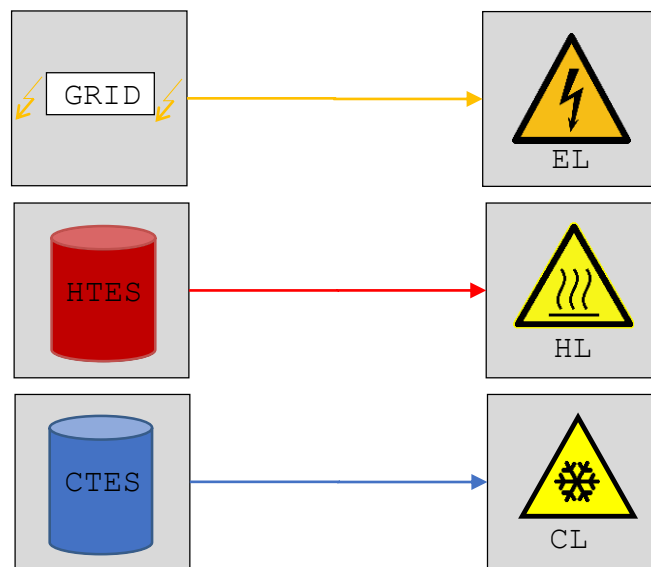
Figure 11 Operation mode 1 with no components running and loads satisfied over tanks and grid

Operation mode 2: Only the CHP is turned on. Its thermal power covers the HL or charges the stratified HTES. Its electrical power first satisfies the EL and any excess electricity is then fed into the GRID. However, if the CHP is off or EL is greater than CHPs electrical power then electricity is purchased from the grid.

This mode operates mostly in winter and is called the winter electricity production (WEP) mode.
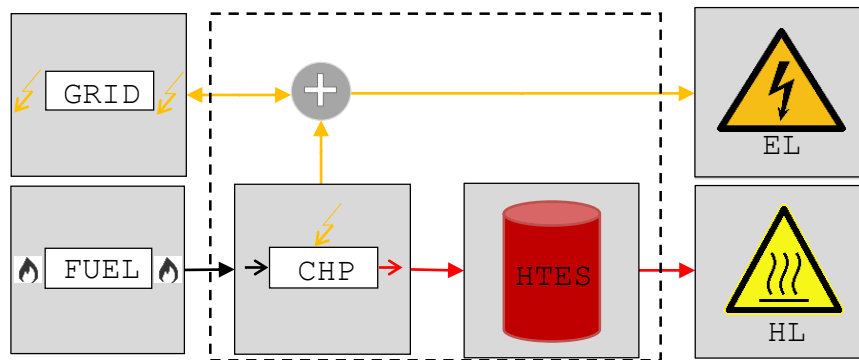
Figure 12 Operation mode 2 with only CHP running

Operation mode 3: The CHP, AdC, OC, and relevant pumps are turned on. The CHP's thermal power charges the HTES and this high temperature water is used to drive the AdC. The AdC's cooling power covers the CL or charges the CTES. The AdC emits its process heat to the environment through the OC. The OC and all the relevant pumps for this mode are controlled by an embedded controller in the AdC. The electricity balance is same as in operation mode 2. In technical terminology, the mode is called thermal bottoming cooling cycle as the cooling generation of AdC is cascaded to the heat generation of the CHP.

This mode operates mostly in summer and is called the summer electricity production (SEP) mode.
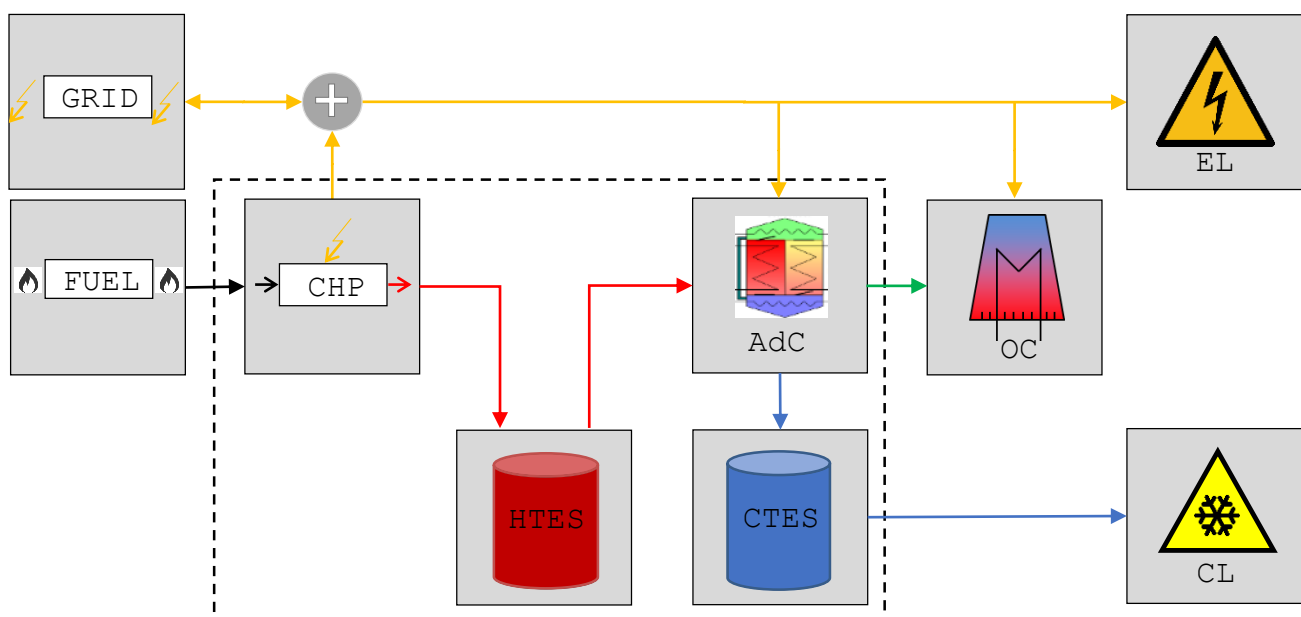
Figure 13 Operation mode 3 with CHP and AdC running

Operation mode 4: The CC, OC, and relevant pumps are turned on. CC's thermal power covers the CL or charges the CTES. The entire EL is covered by electricity purchased from the GRID. The hydraulic connections for this mode are planned such that the evaporator of the RHP gets connected to the CTES and the condenser gets connected to the OC. The OC is controlled using a PID controller developed in the framework of this work (*cf. Chapter 5*) to maintain a set temperature in the condenser input. The external pumps

operate to maintain constant nominal volume flows in the evaporator and condenser circuits.

This mode operates mostly in summer and is called the summer electricity consumption (SEC) mode.
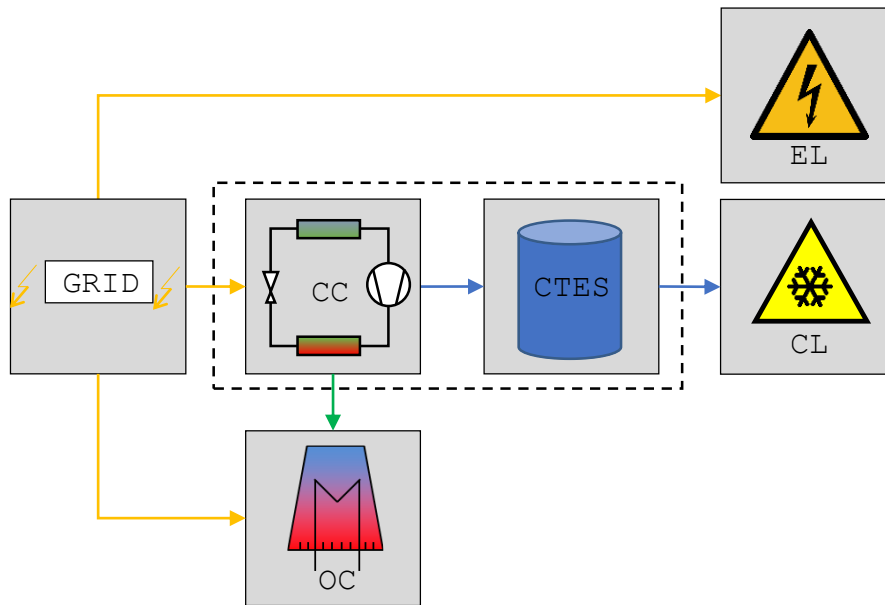
Figure 14 Operation mode 4 with only CC running

Operation mode 5: The HP, OC, and relevant pumps are turned on and this mode mirrors the operation in mode 4. Its thermal power covers the HL or charges the HTES. The entire EL is covered by electricity bought from the GRID. The hydraulic connections for this mode are planned such that the evaporator of the RHP gets connected to the OC and the condenser gets connected to the HTES. The OC operates at its maximum speed RPM_{max} and the relevant pumps are running to maintain constant nominal volume flows.

This mode operates mostly in winter and is called the winter electricity consumption (WEC) mode.
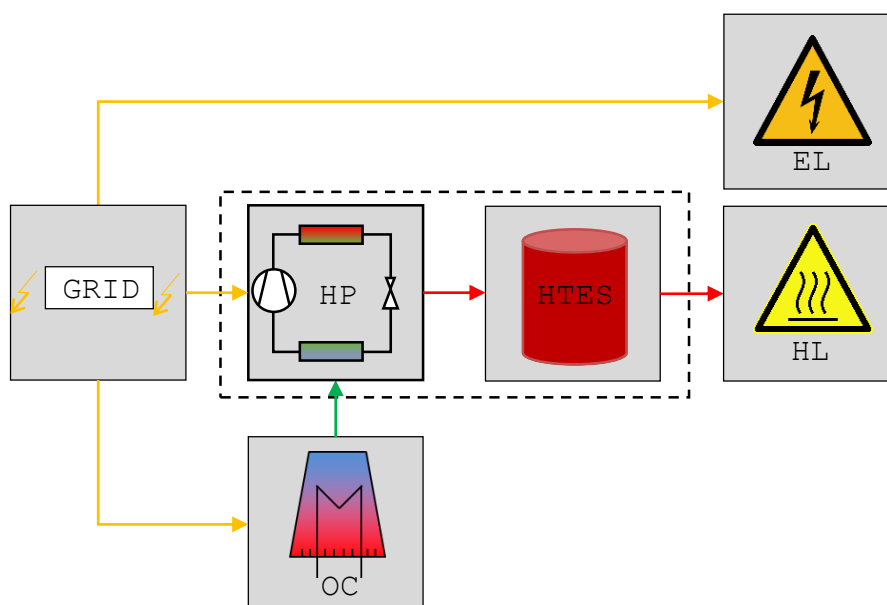
Figure 15 Operation mode 5 with only HP running

Operation mode 6: Is a sub-mode of the operation mode 3. Only the AdC is turned on and the CHP remains off. The AdC's cooling power covers the CL or charges the CTES. The entire EL is covered by electricity bought from the GRID.
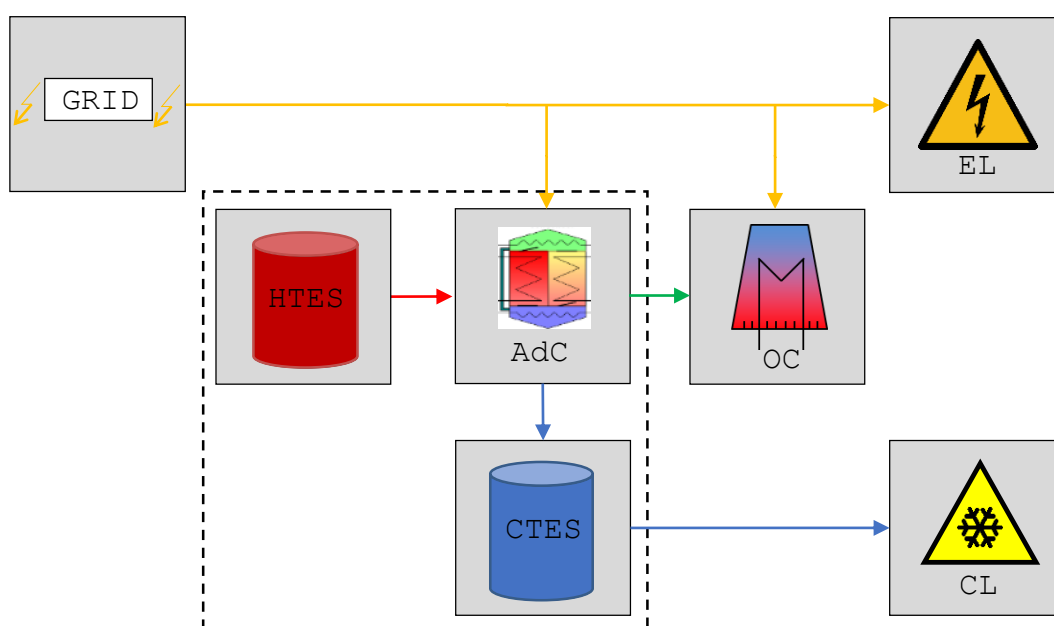
Figure 16 Operation mode 6 with only AdC running

Operation mode 7: Is an extension of the operation mode 4. In addition to the CC, the CHP is also turned on. Technically, it is called the electric bottoming cooling cycle as the

cooling generation is cascaded to the electricity generation of the CHP. The EL is partly covered by the CHP and remaining electricity is bought from the GRID.
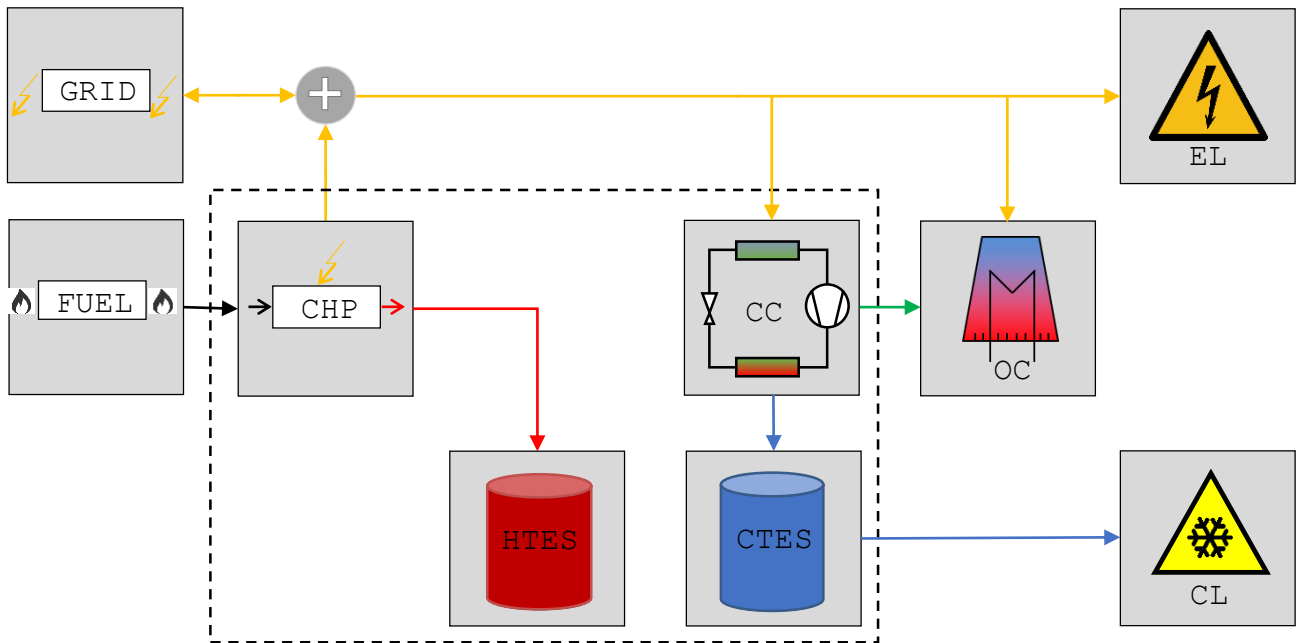
Figure 17 Operation mode 7 with CHP and CC running

Further relevant information regarding the operating modes is summarised below:

- Irrespective of the operation mode, it is possible to cover only the HL or CL at a time since switchover valves are installed between the tanks and the load circuit (*cf. Appendix B.1*).
- The changeover operation from one mode to another takes 140 seconds.

B.4 Functional description for the lower-level controller

The HMI on the workstation is used for selection, switching, visualisation, and monitoring of the trigeneration lab. One of the following four operation scenarios can be selected:

- HAND: Operation of the plant by hand using the component, valve, and pump switches on the HMI,
- AUTO: Automatic operation based on control signal from climate chamber,
- SEMI-AUTO: Selection of one of the 7 operation modes by hand on the HMI,
- REMOTE: Selection of one of the 7 operation modes by the supervisory controller (MPC or reference).

B.4.1 Switching logic for operation modes

Operation mode 1 (Off): Immediately after selection of operation mode 1,
- turn off P5, P6, P7, P13, AdC, CC, HP, OC, and CHP
- open and close valves as per *Table. 3*

- wait 140 seconds[1].

Operation mode 2 (CHP only): Immediately after selection of operation mode 2,

- turn off P5, P6, P7, P13, AdC, CC, HP and OC
- open and close valves as per *Table. 3*
- wait 140 seconds

Switch-on condition for CHP

- In SEMI-AUTO or AUTO: If $HT6 < M2\_HT6_{,min}$
- In REMOTE: Always

Switch-on procedure

- Turn on CHP
- Safety shut-down logic (*Section B.4.3*) switches to operation mode 1.

Switch-off condition for CHP

- In SEMI-AUTO or AUTO: If $HT1 > M2\_HT1_{,max}$
- In Remote: Never

Switch-off procedure

- Turn off CHP
- Valve positions remain unchanged

Both the temperature limits (here $M2\_HT6_{,min}$ and $M2\_HT1_{,max}$) can be changed on the HMI.

Operation mode 3 (CHP + AdC): This operation mode has the switch-on conditions for multiple components. Immediately after selection of operation mode 3,

- turn off P6, P7, P13, CC, and HP
- open and close valves as per *Table. 3*
- wait 140 seconds

Switch-on condition for CHP

- In SEMI-AUTO or AUTO: If $HT6 < M3\_HT6_{,min}$
- In REMOTE: Always

Switch-on procedure

- Turn on CHP
- Safety shut-down logic (*Section B.4.3*) switches to operation mode 1.

Switch-off condition for CHP

- In SEMI-AUTO or AUTO: If $HT1 > M3\_HT1_{,max}$
- In Remote: Never

Switch-off procedure

- Turn off CHP
- Valve positions remain unchanged

---

[1] Positioning time for actuator is 130 s

Switch-on condition for AdC, OC, and P5

- In SEMI-AUTO or AUTO: If $CT1 > M3\_CT1_{,max}$
- In REMOTE: Always

Switch-on procedure

- Turn on AdC, OC, and P5 ($V_{oc,set}$ for OC is given by AdC's embedded controller)
- Safety shut-down logic (*Section B.4.3*) switches to operation mode 1.

Switch-off condition for AdC, OC, and P5

- In SEMI-AUTO or AUTO: If $CT4 < M3\_CT4_{,min}$
- In Remote: Never

Switch-off procedure

- Turn off AdC, OC, and P5
- Valve positions remain unchanged.

All the temperature limits (here $M3\_HT6_{,min}$, $M3\_HT1_{,max}$, $M3\_CT1_{,max}$, and $M3\_CT4_{,min}$) can be changed on the HMI.

Operation mode 4 (CC only): Immediately after selection of operation mode 4,

- turn off P5, P13, AdC, HP, and CHP
- open and close valves as per *Table. 3*
- wait 140 seconds

Switch-on condition for CC, OC, P6, and P7

- In SEMI-AUTO or AUTO: If $CT1 > M4\_CT1_{,max}$
- In REMOTE: Always

Switch-on procedure

- Turn on P6, P7, CC, and OC ($V_{OC,set}$ for OC is given by the PID controller which is automatically activated in operation mode 4)
- Safety shut-down logic (*Section B.4.3*) switches to operation mode 1

Switch-off condition for CC, OC, P6, and P7

- In SEMI-AUTO or AUTO: If $CT4 < M4\_CT4_{,min}$
- In Remote: Never

Switch-off procedure

- Turn off CC
- After 20 s turn off P6, P7, and OC
- Valve positions remain unchanged

Both the temperature limits (here $M4\_CT1_{,max}$ and $M4\_CT4_{,min}$) can be changed on the HMI.

Operation mode 5 (HP only): Immediately after selection of operation mode 5,

- turn off CC, CHP, and AdC
- open and close valves as per *Table. 3*
- wait 140 seconds

Switch-on condition for HP, P5, P6, P7, P13, and OC
- In SEMI-AUTO or AUTO: If HT6 < M5_HT6,$_{min}$
- In REMOTE: Always

Switch-on procedure
- Turn on P5, P6, P7, P13, and OC ($V_{oc,set}$ for OC is fixed at 10 V)
- After 60 s turn on HP
- Safety shut-down logic (*Section B.4.3*) switches to operation mode 1.

Switch-off condition for HP, P5, P6, P7, P13, and OC
- In SEMI-AUTO or AUTO: If HT1 > M5_HT1,$_{max}$
- In Remote: Never

Switch-off procedure
- Turn off HP
- After 20 s turn off P5, P6, P7, P13, and OC
- Valve positions remain unchanged

Both the temperature limits (here M5_HT1,$_{max}$ and M5_HT6,$_{min}$) can be changed on the HMI.

Operation mode 6 (AdC Only): Immediately after selection of operation mode 6,
- turn off P6, P7, P13, CC, CHP, and HP
- open and close valves as per *Table. 3*
- wait 140 seconds

Switch-on condition for AdC, OC, and P5
- In SEMI-AUTO or AUTO: If CT1 > M6_CT1,$_{max}$ AND HT8 > M6_HT8,$_{set}$
- In REMOTE: Always

Switch-on procedure
- Turn on AdC, OC, and P5 ($V_{oc,set}$ for OC is given by AdC's embedded controller)
- Safety shut-down logic (*Section B.4.3*) switches to operation mode 1.

Switch-off condition for AdC, OC, and P5
- In SEMI-AUTO or AUTO: If CT4 < M6_CT4,$_{min}$ OR HT8 < M6_HT8,$_{min}$
- In Remote: Never

Switch-off procedure
- Turn off AdC, OC, and P5
- Valve positions remain unchanged.

The temperature limits (here M6_CT1,$_{max}$, M6_CT4,$_{min}$, M6_HT8,$_{set}$, and M6_HT8,$_{min}$) can be changed on the HMI.

Operation mode 7 (CHP + CC): This operation mode has the switch-on conditions for multiple components. Immediately after selection of operation mode 7,
- turn off P5, P13, AdC, and HP
- open and close valves as per *Table. 3*

- wait 140 seconds

<u>Switch-on condition for CHP</u>

- In SEMI-AUTO or AUTO: If HT6 < M7_HT6,$_{min}$
- In REMOTE: Always

<u>Switch-on procedure</u>

- Turn on CHP
- Safety shut-down logic (*Section B.4.3*) switches to operation mode 1.

<u>Switch-off condition for CHP</u>

- In SEMI-AUTO or AUTO: If HT1 > M7_HT1,$_{max}$
- In Remote: Never

<u>Switch-off procedure</u>

- Turn off CHP
- Valve positions remain unchanged.

<u>Switch-on condition for CC, OC, P6, and P7</u>

- In SEMI-AUTO or AUTO: If CT1 > M7_CT1,$_{max}$
- In REMOTE: Always

<u>Switch-on procedure</u>

- Turn on P6, P7, CC, and OC ($V_{oc,set}$ for OC is given by the PID controller which is automatically activated in operation mode 4)
- Safety shut-down logic (*Section B.4.3*) switches to operation mode 1

<u>Switch-off condition for CC, OC, P6, and P7</u>

- In SEMI-AUTO or AUTO: If CT4 < M7_CT4,$_{min}$
- In Remote: Never

<u>Switch-off procedure</u>

- Turn off CC
- After 20 s turn off P6, P7, and OC
- Valve positions remain unchanged

All the temperature limits (here M7_HT6,$_{min}$, M7_HT1,$_{max}$, M7_CT1,$_{max}$, and M7_CT4,$_{min}$) can be changed on the HMI.

B.4.2 Default valve positions

The valve control program sets the true or false signals for positioning the valves according to operation mode.

Table. 3 Position of the motorised valves in different operation modes. 1 - open and 0 - close

Mode(↓) & Valve(→) number	Valve position														
	3	4	5	7	11	17	20	24	34	35	51	52	55	60	71
1	1	0	0	0	0	1	0	1	1	0	0	0	1	0	1
2	1	0	0	0	0	1	0	1	1	0	0	0	1	0	1
3	1	1	1	0	0	1	0	0	1	0	0	0	1	0	1
4	1	0	0	0	0	1	0	1	1	0	1	0	0	0	1
5	1	0	0	1	1	0	1	1	0	1	0	1	1	1	0
6	1	1	1	0	0	1	0	0	1	0	0	0	1	0	1
7	1	0	0	0	0	1	0	1	1	0	1	0	0	0	1

B.4.3 Safety shut-down and warnings

Shut-down due to volume flow errors:

- If CHP = On AND $\dot{v}_{\text{CHP}}$< 0.05 m³/h, then safety shut down. First check after 900 seconds of turning on CHP and then check regularly
- If P5 = On AND $\dot{v}_{\text{OC}}$< 1 m³/h, then safety shut down. First check after 90 seconds of turning on the P5 and then check regularly
- If P6 = On AND$\dot{v}_{\text{RHP,e}}$ < 1 m³/h, then safety shut down. First check after 90 seconds of turning on the P6 and then check regularly
- If P7 = On AND $\dot{v}_{\text{OC}}$ OR $\dot{v}_{\text{RHP,c}}$ < 1 m³/h, then safety shut down. Loop test after 90 seconds of turning on the P7 and then check regularly
- If AdC = On AND $\dot{v}_{\text{AdC,L}}$ OR $\dot{v}_{\text{AdC,M}}$ OR $\dot{v}_{\text{AdC,H}}$ < 0.05 m³/h, then safety shut down. Loop test after 300 seconds of turning on the AdC and then check regularly
- If CC = On AND $\dot{v}_{\text{RHP,e}}$ OR $\dot{v}_{\text{RHP,c}}$ < 1 m³/h, then safety shut down. Loop test after 90 seconds of turning on the CC and then check regularly
- If HP = On AND $\dot{v}_{\text{RHP,e}}$ OR $\dot{v}_{\text{RHP,c}}$ OR $\dot{v}_{\text{OC}}$ < 1 m³/h, then safety shut down. Loop test after 90 seconds of turning on the HP and then check regularly

Shut-down due to temperature limit:

- If CHP = On AND $T_{\text{r,CHP}}$ > 80 °C, then safety shut down. Loop test after 120 seconds of turning on the CHP and then check regularly

Warnings:

- If CHP = On AND $P_{\text{el,CHP}}$ < 0.05 kW$_{\text{el}}$. Loop test after 900 seconds of turning on the CHP and then check regularly
- If HP OR CC = On AND $P_{\text{el,RHP}}$ < 0.05 kW$_{\text{el}}$. Loop test after 60 seconds of turning on the HP OR CC and then check regularly
- If AdC = On AND $P_{\text{el,AdC}}$ < 0.005 kW$_{\text{el}}$. Loop test after 300 seconds of turning on the AdC and then check regularly

- If HP = On AND $P_{el,OC}$ < 0.5 kW$_{el}$. Loop test after 300 seconds of turning on the HP and then check regularly
- If $T_{f,TC}$ > 60 °C
- If $\dot{v}_{RHP,e}$ OR $\dot{v}_{RHP,c}$ OR $\dot{v}_{AdC,L}$ OR $\dot{v}_{AdC,M}$ OR $\dot{v}_{AdC,H}$ OR $\dot{v}_{CHP}$ < - 0.2 m^3/h. Check every 30 seconds
- If COIL = On AND $P_{el,COIL}$ < 0.05 kW$_{el}$. Loop test after 60 seconds of turning on COIL.
- If T_{HT3} > 85 °C AND COIL = ON

B.4.4 Setting temperature limits

The temperature parameters or limits used in conventional control of the plant were selected after multiple tuning experiments and discussions with the component manufacturers. The aim was to ensure adequate tank temperature for heating or cooling, program a hysteresis to avoid frequent switching of the components, and utilise the entire volume of tank. These values could be adjusted directly on the HMI screen or in the Python code of the conventional controller.

For instance, in summer, the $T_{CT1,max}$ was set at 12 °C to ensure that T_{CT1} (temperature at bottom of CTES) is always lower than the set feed-line temperature in the TC circuit ($T_{f,TC,set}$ = 14 °C). $T_{CT4,min}$ was set at 12 °C to introduce a hysteresis over T_{CT4} (temperature at top of CTES) and use the maximum storage capacity of the tank.

Similarly, in winter, $T_{HT1,CHP,max}$ was set at 70 °C to ensure that T_{HT1} is always lower than $T_{r,CHP,max}$ = 73 °C when CHP is running and $T_{HT1,HP,max}$ was set at 43 °C to ensure that T_{HT1} is always lower than $T_{r,HP,c,max}$ = 45 °C when HP is running. $T_{HT6,min}$ was set at 70 °C to introduce a hysteresis over T_{HT6} and ensure that T_{HT6} *(temperature going to load) was always higher than* $T_{f,TC,set}$ = 40 °C.

Table. 4 Default values for temperature parameters / limits to implement the conventional controller in different modes

Parameter	Function	Default value (°C)
M2_HT6$_{,min}$	Used in operation mode 2. Read at HT6, which is located at load layer of the tank. If the current value is below the set value then CHP ON	70
M2_HT1$_{,max}$	Used in operation mode 2. Read at HT1, which is located at bottom of the tank. If the current value is above the set value then CHP OFF	70
M3_HT6$_{,min}$	Used in operation mode 3. Read at HT6, which is located at load layer of the tank. If the current value is below the set value then CHP ON	70
M3_HT1$_{,max}$	Used in operation mode 3. Read at HT1, which is located at bottom of the tank. If the current value is above the set value then CHP OFF	70

M3_CT4$_{,min}$	Used in operation mode 3. Read at CT4, which is located at top of the tank. If the current value is below the set value then AdC OFF	12
M3_CT1$_{,max}$	Used in operation mode 3. Read at CT1, which is located at bottom of the tank. If the current value is above the set value then AdC ON	12
M4_CT4$_{,min}$	Used in operation mode 4. Read at CT4, which is located at top of the tank. If the current value is below the set value then CC OFF	12
M4_CT1$_{,max}$	Used in operation mode 4. Read at CT1, which is located at bottom of the tank. If the current value is above the set value then CC ON	12
M5_HT6$_{,min}$	Used in operation mode 5. Read at HT6, which is located at load layer of the tank. If the current value is below the set value then HP ON	43
M5_HT1$_{,max}$	Used in operation mode 5. Read at HT1, which is located at bottom of the tank. If the current value is above the set value then HP OFF	43
M6_CT4$_{,min}$	Used in operation mode 6. Read at CT4, which is located at top of the tank. If the current value is below the set value then AdC OFF	12
M6_CT1$_{,max}$	Used in operation mode 6. Read at CT1, which is located at bottom of the tank. If the current value is above the set value then AdC ON	12
M6_HT8$_{,set}$	Used in operation mode 6. Read at HT8, which is located at AdC feed layer of the hot tank. If the current value is above the set value then AdC ON	52
M6_HT8$_{,min}$	Used in operation mode 6. Read at HT8, which is located at AdC feed layer of the hot tank. If the current value is below the set value then AdC OFF	50
M7_HT6$_{,min}$	Used in operation mode 7. Read at HT6, which is located at load layer of the tank. If the current value is below the set value then CHP ON	70
M7_HT1$_{,max}$	Used in operation mode 7. Read at HT1, which is located at bottom of the tank. If the current value is above the set value then CHP OFF	70
M7_CT4$_{,min}$	Used in operation mode 7. Read at CT4, which is located at top of the tank. If the current value is below the set value then CC OFF	12
M7_CT1$_{,max}$	Used in operation mode 7. Read at CT1, which is located at bottom of the tank. If the current value is above the set value then CC ON	12

C. Load profiles for application scenarios

Table. 5 List of CCHP related studies identified in this work for extracting 24-hour electrical and thermal, seasonal load profiles

Type of building	Aim of study	System specification	Peak summer loads	Peak winter loads	Peak transition loads	Ref.
Hospital-1	Optimisation for optimal capacities of a CCHP	•300 bed hospital •Load profiles for typical workday •No work day with constant load	•EL ~ 0.5 MW_{el} •HL ~ 0.58 MW_{th} •CL ~ 0.9 MW_{th}	•NA	•NA	(Kavvadias and Maroulis, 2010)
Hospital-2	CCHP operation optimisation	•CHP: 4.0 MW_{el} •CC: 4.2 MW_{th} •Boiler: 3.5 MW_{th} •Absorption chiller: 4.2 MW_{th} •Average hourly demands	•EL ~ 2.0 MW_{el} •HL ~ 2.0 MW_{th} •CL ~ 4.0 MW_{th}	•EL ~ 2.0 MW_{el} •HL ~ 3.5 MW_{th} •CL ~ 0.0 MW_{th}	•EL ~ 2.0 MW_{el} •HL ~ 2.3 MW_{th} •CL ~ 0.0 MW_{th}	(Facci et al., 2014)
Hospital-3	Sensitivity analysis of energy demands on optimal capacities of CCHP system	•Area: 83,745 m² •Demand from four independent buildings •Representative days in different seasons	•EL ~ 2.0 MW_{el} •HL ~ 2.0 MW_{th} •CL ~ 4.0 MW_{th}	•EL ~ 2.0 MW_{el} •HL ~ 3.5 MW_{th} •CL ~ 0.0 MW_{th}	•EL ~ 2.0 MW_{el} •HL ~ 2.3 MW_{th} •CL ~ 0.0 MW_{th}	(Li et al., 2008)
Hotel-1	Influence of part-load behaviour on optimal design and operation of CCHP	•Area: 60,000 m² •CHP: 1.46 MW_{el} •Boiler: 0.96 MW_{th} •Absorption chiller: 1.3 MW_{th} •Hourly demands of representative days	•EL ~ 2.1 MW_{el} •HL ~ 1.3 MW_{th} •CL ~ 4.7 MW_{th}	•EL ~ 1.7 MW_{el} •HL ~ 4.7 MW_{th} •CL ~ 0.6 MW_{th}	•EL ~ 1.8 MW_{el} •HL ~ 1.0 MW_{th} •CL ~ 1.7 MW_{th}	(Zhou et al., 2013)
Hotel-2	Influence of average and peak energy demands and uncertainties on CCHP performance	•Area: 78,200 m² •CHP: 2 MW_{el} and 3.5 MW_{th} •CC: 2 MW_{th} •Boiler: 1.5 MW_{th} •Absorption chiller: 3.2 MW_{th} •Average hourly demands	•EL ~ 1.9 MW_{el} •HL ~ 1.8 MW_{th} •CL ~ 3.7 MW_{th}	•EL ~ 1.5 MW_{el} •HL ~ 4.2 MW_{th} •CL ~ 0.6 MW_{th}	•EL ~ 1.5 MW_{el} •HL ~ 2.4 MW_{th} •CL ~ 1.4 MW_{th}	(Li et al., 2008)
Hotel-3	Short review and energy systems	•Area: 60,000 m² •CHP: 1.42 MW_{el}	•EL ~ 1.2 MW_{el}	•EL ~ 0.7 MW_{el}	•EL ~ 0.7 MW_{el}	(P. Liu et al., 2013)

	engineering approach to modelling and optimisation of micro-grids	•Heat pumps: 3.45 MW_{th} •Absorption chiller: 2.58 MW_{th} •Hourly demands of representative days for different months	•HL ~ 0.58 MW_{th} CL ~ 6.1 MW_{th}	•HL ~ 5.2 MW_{th} •CL ~ 0.0 MW_{th}	•HL ~ 0.5 MW_{th} •CL ~ 0.0 MW_{th}	
Industrial dairy unit	Optimisation of CCHP configuration for various energy price policies	•Industrial dairy •Load profile for typical workday and holiday	•EL ~ 3.2 MW_{el} •HL ~ 13.1 MW_{th} •CL ~ 14.9 MW_{th}	•NA	•NA	(Tichi et al., 2010)
Office building	Sensitivity analysis of trigeneration primary energy savings ratio	•CHP: 330 kW_{el} •CC: 560 kW_{th} •Boiler: 515 kW_{th} •AdC: 515 kW_{th}	•EL ~ 280 kW_{el} •HL ~ 0.9 kW_{th} •CL ~ 500 kW_{th}	•EL ~ 280 kW_{el} •HL ~ 335 kW_{th} •CL ~ 150 kW_{th}	•EL ~ 280 kW_{el} •HL ~ 224 kW_{th} •CL ~ 400 kW_{th}	(Chicco and Mancarella, 2007)
One family house	Optimal sizing of a CHP	•Area: 250 m² •CHP: 1-2 kW_{el} •CC: Not specified •Boiler: Not specified •Average hourly demands	•EL ~ 0.0 kW_{el} •HL ~ 0.0 kW_{th} •CL ~ 0.0 kW_{th}	•EL ~ 0.0 kW_{el} •HL ~ 0.0 kW_{th} •CL ~ 0.0 kW_{th}	•EL ~ 3.6 kW_{el} •HL ~ 5.5 kW_{th} •CL ~ 0.4 kW_{th}	(Ren et al., 2008)
University campus-1	Micro-CCHP real-time operation optimisation	•Area: 279 m² •CHP: 15 kW_{el} •AdC: 35 kW_{th} •TRNSYS generated hourly demands	•EL ~ 9.8 kW_{el} •HL ~ 0.0 kW_{th} •CL ~ 12.9 kW_{th}	•EL ~ 6.2 kW_{el} •HL ~ 11.2 kW_{th} •CL ~ 0.0 kW_{th}	•EL ~ 9.8 kW_{el} •HL ~ 3.0 kW_{th} •CL ~ 2.9 kW_{th}	(Cho et al., 2009a)
University campus-2	Design a supervisory control strategy to utilise higher energy and economic efficiency potential of CCHP systems	•Average cooling requirement = 315 MWh_{th}/day •Average heating requirement = 17 MWh_{th} •Average electricity requirement = 15 MW_{el} •CHP: 19.1 MW_{el}	•EL ~ 15.5 MW_{el} •HL ~ 0.0 kW_{th} •CL ~ 24.5 kW_{th}	•NA	•NA	(Chandan et al., 2012)
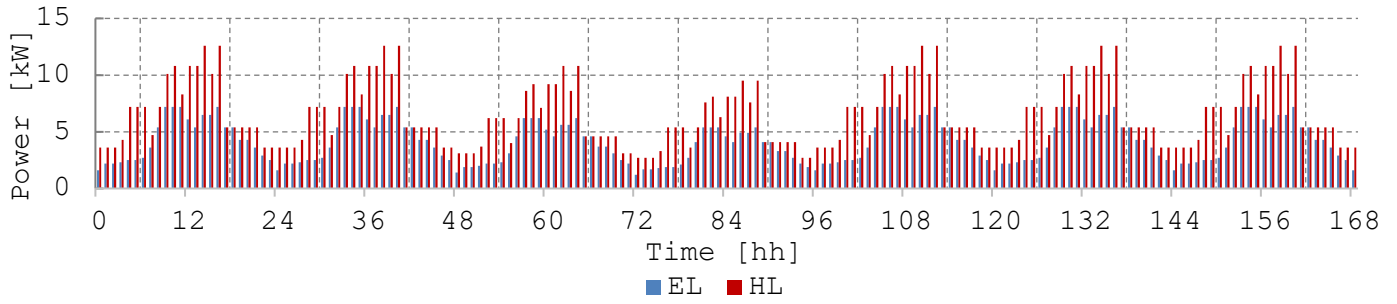
Figure 18 Hospital-2 load profile for a winter week starting on a Thursday midnight and scaled using peak HL of 12.5 kW$_{th}$ (125% of CHP's maximum thermal output) and weekend ~ weekday for hospitals
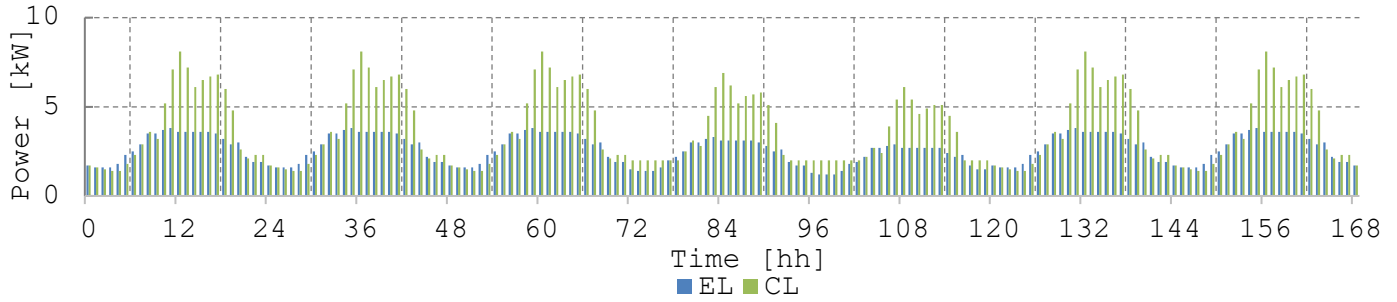
Figure 19 Hotel-1 load profile for a summer week starting on a Wednesday midnight and scaled using peak CL of 8 kW$_{th}$ (Peak load for 16/21 °C operation in TABS circuit) and weekend ~ weekday for hotels
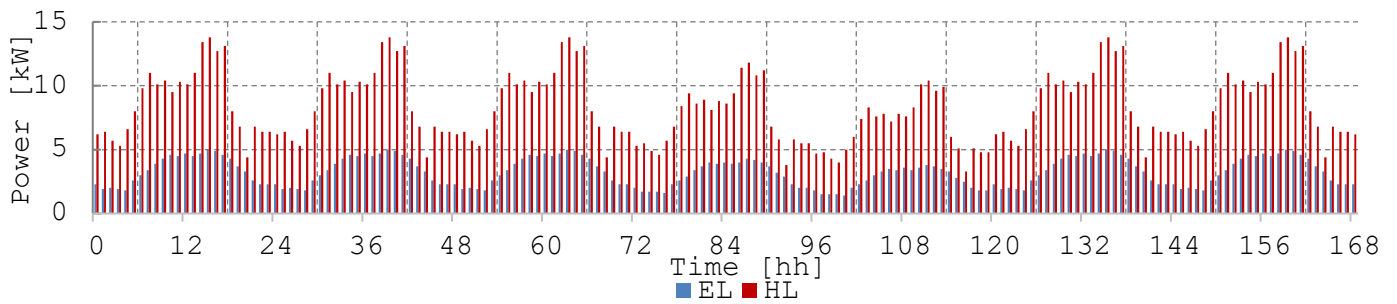
Figure 20 Hotel-1 load profile for a winter week starting on a Wednesday midnight and scaled using peak HL of 14 kW$_{th}$ (maximum possible with thermostat and test chamber in winter) and weekend ~ weekday for hotels
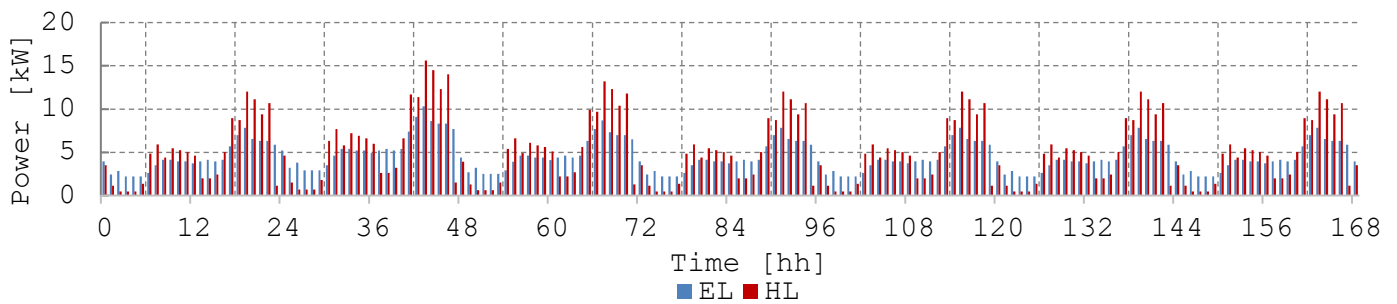
Figure 21 Residential load profile for a transition week starting on a Friday midnight and scaled using peak HL of 12.5 kW$_{th}$ (125% of CHP's maximum thermal output) and weekend > weekday for residence

D. Regression coefficients for the grey-box models

Table. 6 Values of regression coefficients programmed as model-parameters for the INES components

Parameter	Value	Parameter	Value	Parameter	Value	Parameter	Value	Parameter	Value
AdC:		CHP:		RHP:2nd degree		RHP:1st degree		OC:	
a_1	1.662	c_1	0.265	e_1	12.574	e_1^*	13.199	h_1	14
a_2	0.490	c_2	−0.0092	e_2	0.325	e_2^*	0.385	h_2	0.56
a_3	0.252	c_3	0.00019	e_3	0.033	e_3^*	−0.042		
a_4	−0.635	d_1	560.79	e_4	0.002	f_1^*	11.637		
a_5	0.010			e_5	−0.001	f_2^*	0.379		
a_6	−0.004			e_6	−0.001	f_3^*	−0.116		
a_7	−0.029			f_1	10.099	g_1^*	1.683		
a_8	0.003			f_2	0.331	g_2^*	0.006		
a_9	−0.000			f_3	0.011	g_3^*	0.069		
a_{10}	0.0148			f_4	0.002				
b_{10}	0.423			f_5	−0.001				
b_{10}	−0.022			f_6	−0.002				
b_{10}	0.006			g_1	2.369				
b_{10}	0.002			g_2	−0.004				
b_{10}	0.000			g_3	0.023				
b_{10}	0.000			g_4	0.000				
b_{10}	0.002			g_5	0.000				
b_{10}	−0.001			g_6	0.000				
b_{10}	−0.000								
b_{10}	−0.001								

E. List of experiments

Table. 7 Summary of experiments performed to compare a reference controller with MPC

Experiment name	Starting date and time for each controller	Load and elect. profile	Scaling factors	Ref. controller set-up	MPC set-up 1	MPC set-up 2	Duration of test for each controller	Avg. initial tank temperature [°C]	Avg. ambient temp. [°C]	Remarks
Sim 8kW_2019.08.20	• Ref. = 12.08.2019 / 10:15 • MPC = 20.08.2019 / 10:15	• Hotel-1 starting on Thursday • EWERK two-price tariff	• INES peak = 8 kW$_{th}$ cool • Saturday = 0.85×Workday • Sunday = 0.75×Workday	• $T_{HTG,min} = 70$ °C • $T_{HT1,CHP,max} = 70$ °C • $T_{CT1,max} = 12$ °C • $T_{CT4,min} = 12$ °C • Switch = 4.5 kW$_{th}$ • $T_{E,TC,set} = 14$ °C	• $T_{HT,min} = 95$ °C • $T_{HT,max} = 5$ °C • $T_{CT,max} = 30$ °C • $T_{CT,min} = 8$ °C • $T_{E,TC,set} = 14$ °C • $T_{E,CHP,max} = 68$ °C • $T_{L,AC,H,min} = 52$ °C	• MPC version = MINLP_V3.7 • IPOPT max iterations = 1500 • IPOPT acceptable tol. = 0.2 • IPOPT max CPU time = NA • Slack weights = 1e3 • Pycombina max CPU time = 60s	• Ref. = ca. 4.5 days • MPC = ca. 60 hours	• Ref. = CT(14),HT(62) • MPC = CT(13),HT(62)	• Ref. = 19 • MPC = 18	• Low pressure alarm in CC resulted in shorter MPC test
Sim 8kW_2019.08.28	• Ref. = 12.08.2019 / 10:30 • MPC = 28.08.2019 / 10:30	• Hotel-1 starting on Thursday • EWERK two-price tariff	• INES peak = 8 kW$_{th}$ cool • Saturday = 0.85×Workday • Sunday = 0.75×Workday	• $T_{HTG,min} = 70$ °C • $T_{HT1,CHP,max} = 70$ °C • $T_{CT1,max} = 12$ °C • $T_{CT4,min} = 12$ °C • Switch = 4.5 kW$_{th}$ • $T_{E,TC,set} = 14$ °C	• $T_{HT,min} = 95$ °C • $T_{HT,max} = 5$ °C • $T_{CT,max} = 30$ °C • $T_{CT,min} = 8$ °C • $T_{E,TC,set} = 14$ °C • $T_{E,CHP,max} = 68$ °C • $T_{L,AC,H,min} = 52$ °C	• MPC version = MINLP_V3.7 • IPOPT max iterations = 10000 • IPOPT acceptable tol. = 0.01 • IPOPT max CPU time = 180s • Slack weights = 1e3 • Pycombina max CPU time = 180s	• Ref. = ca. 4.5 days • MPC = ca. 4.5 days	• Ref. = CT(14),HT(63) • MPC = CT(15),HT(64)	• Ref. = 20 • MPC = 26	• NA
Sim 8kW_2019.09.10	• Ref. = 04.09.2019 / 14:00 • MPC = 10.09.2019 / 14:00	• Office building starting on Thursday • EPEX Spot SE day-ahead	• INES peak = 8 kW$_{th}$ cool • Saturday = 0.5×Workday • Sunday = 0.45×Workday	• $T_{HTG,min} = 70$ °C • $T_{HT1,CHP,max} = 70$ °C • $T_{CT1,max} = 12$ °C • $T_{CT4,min} = 12$ °C • Switch = 4.5 kW$_{th}$ • $T_{E,TC,set} = 14$ °C	• $T_{HT,min} = 95$ °C • $T_{HT,max} = 5$ °C • $T_{CT,max} = 30$ °C • $T_{CT,min} = 5$ °C • $T_{E,TC,set} = 14$ °C • $T_{E,CHP,max} = 73$ °C	• MPC version = MINLP_V3.8 • IPOPT max iterations = 10000 • IPOPT acceptable tol. = 0.01 • IPOPT max CPU time = 60s	• Ref. = ca. 5 days • MPC = ca. 5 days	• Ref. = CT(15),HT(68) • MPC = CT(14),HT(70)	• Ref. = 17 • MPC = 19	• NA

	Dates	Building / Tariff	INES peak / Profile	Parameters 1	Parameters 2	Solver settings	Runtime	CT/HT	Ref./MPC	Notes
Sim_8kW_2019.09.16	• Ref. = 16.09.2019 / 11:00 • MPC = 18.09.2019 / 11:00	• Office building starting NA • EWERK two-price tariff	• INES peak = 8 kW$_{th}$ cool • Holiday = Constant 2 kW$_{th}$	• $T_{HT,min} = 70$ °C • $T_{HT,CHP,max} = 70$ °C • $T_{CT1,max} = 12$ °C • $T_{CT4,min} = 12$ °C • Switch = 4.5 kW$_{th}$ • $T_{E,TC,set} = 14$ °C	• $T_{HT,min} = 95$ °C • $T_{HT,max} = 10$ °C • $T_{CT,max} = 30$ °C • $T_{CT,min} = 8$ °C • $T_{E,TC,set} = 14$ °C • $T_{r,CHP,max} = 68$ °C • $T_{r,AC,H,min} = 52$ °C	• MPC version = MINLP V3.9 • IPOPT max iterations = 10000 • IPOPT acceptable tol. = 0.01 • IPOPT max CPU time = 30s • Slack weights = 1e3 • Pycombina max CPU time = 30s	• Ref. = ca. 2 days • MPC = ca. 2 days	• Ref. = CT(13),HT(72) • MPC = CT(12),HT(69)	• Ref. = 12 • MPC = 13	• Load profile Weekday-Holiday-Weekday
Sim_12kW_2019.09.23	• Ref. = 23.09.2019 / 14:00 • MPC = 27.09.2019 / 14:00	• Hospital-2 starting on Thursday • EWERK two-price tariff	• INES peak = 12 kW$_{th}$ cool • Saturday = 0.85×Workday • Sunday = 0.75×Workday	• $T_{HT,min} = 70$ °C • $T_{HT,CHP,max} = 70$ °C • $T_{CT1,max} = 12$ °C • $T_{CT4,min} = 12$ °C • Switch = 6.5 kW$_{th}$ • $T_{E,TC,set} = 14$ °C	• $T_{HT,min} = 95$ °C • $T_{HT,max} = 5$ °C • $T_{CT,max} = 30$ °C • $T_{CT,min} = 5$ °C • $T_{E,TC,set} = 14$ °C • $T_{r,CHP,max} = 73$ °C • $T_{r,AC,H,min} = 55$ °C	• MPC version = MINLP V3.9 • IPOPT max iterations = 10000 • IPOPT acceptable tol. = 0.01 • IPOPT max CPU time = 30s • Slack weights = 1e3 • Pycombina max CPU time = 30s	• Ref. = ca. 4 days • MPC = ca. 1.1 days	• Ref. = CT(13),HT(62) • MPC = CT(13),HT(63)	• Ref. = 16 • MPC = 17	• RAM overload due to 300 DPI images in Spyder resulted in shorter MPC test
Sim_12kW_2019.10.01	• Ref. = 23.09.2019 / 14:00 • MPC = 01.09.2019 / 14:00	• Hospital-2 starting on Thursday • EWERK two-price tariff	• INES peak = 12 kW$_{th}$ cool • Saturday = 0.85×Workday • Sunday = 0.75×Workday	• $T_{HT,min} = 70$ °C • $T_{HT,CHP,max} = 70$ °C • $T_{CT1,max} = 12$ °C • $T_{CT4,min} = 12$ °C • Switch = 6.5 kW$_{th}$ • $T_{E,TC,set} = 14$ °C	• $T_{HT,min} = 95$ °C • $T_{HT,max} = 5$ °C • $T_{CT,max} = 30$ °C • $T_{CT,min} = 5$ °C • $T_{E,TC,set} = 14$ °C • $T_{r,CHP,max} = 73$ °C • $T_{r,AC,H,min} = 55$ °C	• MPC version = MINLP V3.9 • IPOPT max iterations = 10000 • IPOPT acceptable tol. = 0.01 • IPOPT max CPU time = 30s • Slack weights = 1e5 • Pycombina max CPU time = 30s	• Ref. = ca. 4 days • MPC = ca. 4 days	• Ref. = CT(13),HT(56) • MPC = CT(15),HT(56)	• Ref. = 17 • MPC = 13	• NA
Tra_25kW_2019.10.11	• Ref. = 11.10.2019 / 15:00 • MPC = 14.10.2019 / 15:00	• Hotel-1 starting on Monday • EPEX Spot SE day-ahead	• INES peak = 25 kW$_{th}$ cool for summer • Saturday = 0.85×Workday • Sunday = 0.75×Workday	• $T_{HT,min} = 70$ °C • $T_{HT,CHP,max} = 70$ °C • $T_{CT1,max} = 12$ °C • $T_{CT4,min} = 12$ °C • Switch = 4.5 kW$_{th}$ • $T_{E,TC,set} = 14$ °C	• $T_{HT,min} = 95$ °C • $T_{HT,max} = 5$ °C • $T_{CT,max} = 30$ °C • $T_{CT,min} = 5$ °C • $T_{E,TC,set} = 14$ °C • $T_{r,CHP,max} = 73$ °C • $T_{r,AC,H,min} = 55$ °C	• MPC version = MINLP V3.10 • IPOPT max iterations = 10000 • IPOPT acceptable tol. = 0.01 • IPOPT max CPU time = 30s • Slack weights = 1e3	• Ref. = ca. 3 days • MPC = ca. 1.5 days	• Ref. = CT(14),HT(48) • MPC = CT(13),HT(47)	• Ref. = 18 • MPC = 17	• OPC/UA client crashed resulting in shorter MPC test

Appendix

	Timing	Site / Tariff	Load	Temperatures 1	Temperatures 2	Solver settings	Duration	Violations	Switches	Notes
Tra_25kw 2019.10.16	• Ref. = 11.10.2019 / 14:30 • MPC = 16.10.2019 / 14:30	• Hotel-1 starting on Monday • EPEX Spot SE day-ahead	• INES peak = 25 kW$_{th}$ cool for summer and 12.5 kW$_{el}$ • Saturday = 0.85×Workday • Sunday = 0.75×Workday	• $T_{HT5,min}$ = 70 °C • $T_{HT1,CHP,max}$ = 70 °C • $T_{CT1,max}$ = 12 °C • $T_{CT4,min}$ = 12 °C • Switch = 4.5 kW$_{th}$ • $T_{E,TC,set}$ = 14 °C	• $T_{HT,min}$ = 95 °C • $T_{HP,max}$ = 5 °C • $T_{CT,max}$ = 30 °C • $T_{CT,min}$ = 5 °C • $T_{E,TC,set}$ = 14 °C • $T_{r,CHP,max}$ = 73 °C • $T_{r,AcT,H,min}$ = 55 °C	• MPC version = MINLP_V3.10 • IPOPT max iterations = 10000 • IPOPT acceptable tol. = 0.01 • IPOPT max CPU time = 30s • Slack weights = 1e3 • Pycombina max CPU time = 30s	• Ref. = ca. 3 days • MPC = ca. 3 days	• Ref. = CT(14),HT(48) • MPC = CT(13),HT(48)	• Ref. = 18 • MPC = 16	• NA
Tra_25kw 2019.10.21	• Ref. = 11.10.2019 / 14:30 • MPC = 21.10.2019 / 14:30	• Hotel-1 starting on Monday • EPEX Spot SE day-ahead	• INES peak = 25 kW$_{th}$ cool for summer and 6.3 kW$_{el}$ • Saturday = 0.85×Workday • Sunday = 0.75×Workday	• $T_{HT5,min}$ = 70 °C • $T_{HT1,CHP,max}$ = 70 °C • $T_{CT1,max}$ = 12 °C • $T_{CT4,min}$ = 12 °C • Switch = 4.5 kW$_{th}$ • $T_{E,TC,set}$ = 14 °C	• $T_{HT,min}$ = 95 °C • $T_{HP,max}$ = 5 °C • $T_{CT,max}$ = 30 °C • $T_{CT,min}$ = 5 °C • $T_{E,TC,set}$ = 14 °C • $T_{r,CHP,max}$ = 73 °C • $T_{r,AcT,H,min}$ = 55 °C	• MPC version = MINLP_V3.10 • IPOPT max iterations = 10000 • IPOPT acceptable tol. = 0.01 • IPOPT max CPU time = 30s • Slack weights = 1e3 • Pycombina max CPU time = 30s	• Ref. = ca. 22 hours • MPC = ca. 3 days	• Ref. = CT(14),HT(48) • MPC = CT(13),HT(49)	• Ref. = 18 • MPC = 13	• NA
Win_16kw 2019.11.13	• Ref. = 13.11.2019 / 16:30 • MPC = 26.11.2019 / 16:30	• Hotel-1 starting on Wednesday • EMERK two-price tariff	• INES peak = 16 kW$_{th}$ heat • Saturday = 0.85×Workday • Sunday = 0.75×Workday	• $T_{HT5,min}$ = 43 °C • $T_{HT1,CHP,max}$ = 70 °C • $T_{HT1,HP,max}$ = 43 °C • Switch = 10 kW$_{th}$ • $T_{E,TC,set}$ = 40 °C	• $T_{HT,min}$ = 95 °C • $T_{HP,max}$ = 10 °C • $T_{E,TC,set}$ = 40 °C • $T_{r,CHP,max}$ = 73°C • $T_{r,HP,Cmax}$ = 45°C	• MPC version = MINLPWinterV1.0 • IPOPT max iterations = 10000 • IPOPT acceptable tol. = 0.01 • IPOPT max CPU time = 30s • Slack weights = 1e3 • Pycombina max CPU time = 30s	• Ref. = 22 hours • MPC = ca. 3 days	• Ref. = HT(74) • MPC = HT(63)	• Ref. = 5 • MPC = 10	• HP had freeze alarm resulting in shorter ref. controller test
Win_16kw 2019.11.20	• Ref. = 20.11.2019 / 16:00 • MPC = 26.11.2019 / 16:00	• Hotel-1 starting on Wednesday • EMERK two-price tariff	• INES peak = 16 kW$_{th}$ heat • Saturday = 0.85×Workday • Sunday = 0.75×Workday	• $T_{HT5,min}$ = 43 °C • $T_{HT1,CHP,max}$ = 70 °C • $T_{HT1,HP,max}$ = 43 °C • Switch = 10 kW$_{th}$ • $T_{E,TC,set}$ = 40 °C	• $T_{HT,min}$ = 95 °C • $T_{HP,max}$ = 10 °C • $T_{E,TC,set}$ = 40 °C • $T_{r,CHP,max}$ = 73°C • $T_{r,HP,Cmax}$ = 45°C	• MPC version = MINLPWinterV1.0 • IPOPT max iterations = 10000 • IPOPT acceptable tol. = 0.01 • Slack weights = 1e3	• Ref. = 24 hours • MPC = ca. 3 days	• Ref. = HT(70) • MPC = HT(72)	• Ref. = 7 • MPC = 10	• HP had freeze alarm resulting in shorter ref. controller test

Test / Dates	Building	INES peak	Temperatures (1)	Temperatures (2)	MPC version & solver	Duration	HT	Count	Notes
Win_12kW_2019.12.02 • Ref. = 02.12.2019 / 18:15 • MPC = 06.12.2019 / 18:15	• Office building starting on Monday • EWERK two-price tariff	• INES peak = 12.5kW$_{th}$ heat • Saturday = 0.50×Workday • Sunday = 0.45×Workday	• $T_{HT,min}$ = 43 °C • $T_{HT,CHP,max}$ = 70 °C • $T_{HT,HP,max}$ = 43 °C • Switch = 10 kW$_{th}$ • $T_{f,TC,set}$ = 40 °C	• $T_{HT,min}$ = 95 °C • $T_{HP,max}$ = 10 °C • $T_{f,TC,set}$ = 40 °C • $T_{r,CHP,max}$ = 73°C • $T_{r,HP,C,max}$ = 45°C	• MPC version = MINLPWinterV1.2 • IPOPT max iterations = 10000 • IPOPT acceptable tol. = 0.01 • IPOPT max CPU time = 30s • Slack weights = 1e3 • Pycombina max CPU time = 30s	• Ref. = ca. 64 hours • MPC = ca. 72 hours	• Ref. = HT(61) • MPC = HT(60)	• Ref. = 0.8 • MPC = 0	• HP had freeze alarm resulting in shorter ref. controller test
Win_16kW_2019.12.11 • Ref. = 11.12.2019 / 16:00 • MPC = 16.12.2019 / 16:00	• Hospital-2 starting on Thursday • EPEX Spot SE day-ahead	• INES peak = 16 kW$_{th}$ heat • Saturday = 0.85×Workday • Sunday = 0.75×Workday	• $T_{HTS,min}$ = 43 °C • $T_{HT1,CHP,max}$ = 70 °C • $T_{HT1,HP,max}$ = 43 °C • Switch = 10 kW$_{th}$ • $T_{f,TC,set}$ = 40 °C	• $T_{HT,min}$ = 95 °C • $T_{HP,max}$ = 10 °C • $T_{f,TC,set}$ = 40 °C • $T_{r,CHP,max}$ = 73°C • $T_{r,HP,C,max}$ = 45°C	• MPC version = MINLPWinterV1.3 • IPOPT max iterations = 10000 • IPOPT acceptable tol. = 0.01 • IPOPT max CPU time = 30s • Slack weights = 1e3 • Pycombina max CPU time = 30s	• Ref. = ca. 94 hours • MPC = ca. 94 hours	• Ref. = HT(49) • MPC = HT(49)	• Ref. = 6 • MPC = 7	• NA
Win_08kW_2020.01.03 • Ref. = 03.01.2020 / 15:00 • MPC = 07.01.2020 / 15:00	• Office building starting on Thursday • EWERK two-price tariff	• INES peak = 8 kW$_{th}$ heat • Saturday = 0.5×Workday • Sunday = 0.45×Workday	• $T_{HTS,min}$ = 43 °C • $T_{HT1,CHP,max}$ = 70 °C • $T_{HT1,HP,max}$ = 43 °C • Switch = 10 kW$_{th}$ • $T_{f,TC,set}$ = 40 °C	• $T_{HT,min}$ = 95 °C • $T_{HP,max}$ = 10 °C • $T_{f,TC,set}$ = 40 °C • $T_{r,CHP,max}$ = 73°C • $T_{r,HP,C,max}$ = 45°C	• MPC version = MINLPWinterV1.4 • IPOPT max iterations = 10000 • IPOPT acceptable tol. = 0.01 • IPOPT max CPU time = 30s • Slack weights = 1e3 • Pycombina max CPU time = 30s	• Ref. = ca. 92 hours • MPC = ca. 7 days	• Ref. = HT(66) • MPC = HT(66)	• Ref. = 4 • MPC = 8	• NA
Win_12kW_2020.01.22 • Ref. = 22.01.2020 / 16:45 • MPC = 26.01.2020 / 16:45	• Hotel-1 starting on Monday • EPEX Spot SE day-ahead	• INES peak = 12.5kW$_{th}$ heat • Saturday = 0.85×Workday • Sunday = 0.75×Workday	• $T_{HTS,min}$ = 43 °C • $T_{HT1,CHP,max}$ = 70 °C • $T_{HT1,HP,max}$ = 43 °C • Switch = 10 kW$_{th}$ • $T_{f,TC,set}$ = 40 °C	• $T_{HT,min}$ = 95 °C • $T_{HP,max}$ = 10 °C • $T_{f,TC,set}$ = 40 °C • $T_{r,CHP,max}$ = 73°C	• MPC version = MINLPWinterV1.4 • IPOPT max iterations = 10000 • IPOPT acceptable tol. = 0.01	• Ref. = ca. 92 hours • MPC = ca. 92 hours	• Ref. = HT(44) • MPC = HT(50)	• Ref. = 0 • MPC = 7	• NA

Win_12kw_2020.02.07	• Ref. = 07.02.2020 / 14:45 • MPC = 13.02.2020 / 14:45	• Office building starting on Wednesday • EWERK two-price tariff	• INES peak = 12.5kW$_{th}$ heat • Saturday = 0.85×Workday • Sunday = 0.75×Workday	• $T_{INS,min}$ = 43 °C • $T_{HT1,CHP,max}$ = 70 °C • $T_{HT1,HP,max}$ = 43 °C • Switch = 10 kW$_{th}$ • $T_{r,TC,set}$ = 40 °C	• $T_{HT,min}$ = 95 °C • $T_{HT,max}$ = 10 °C • $T_{r,TC,set}$ = 40 °C • $T_{r,CHP,max}$ = 73°C • $T_{r,HP,C,max}$ = 45°C	• MPC version = MINLPWinterV1.4 • IPOPT max iterations = 10000 • IPOPT acceptable tol. = 0.01 • IPOPT max CPU time = 30s • Slack weights = 1e3 • Pycombina max CPU time = 30s	• Ref. = ca. 115 hours • MPC = ca. 130 hours
						• Ref. = HT(72) • MPC = HT(70)	• Ref. = 8 • MPC = 10
							• NA
Win_16kw_2020.03.31	• Ref. = 31.03.2020 / 15:00 • MPC = 02.04.2020 / 15:00	• Hotel-1 starting on Monday • EWERK two-price tariff	• INES peak = 16 kW$_{th}$ heat • Saturday = 0.85×Workday • Sunday = 0.75×Workday	• $T_{INS,min}$ = 43 °C • $T_{HT1,CHP,max}$ = 70 °C • $T_{HT1,HP,max}$ = 43 °C • Switch = 10 kW$_{th}$ • $T_{r,TC,set}$ = 40 °C	• $T_{HT,min}$ = 95 °C • $T_{HT,max}$ = 10 °C • $T_{r,TC,set}$ = 40 °C • $T_{r,CHP,max}$ = 73°C • $T_{r,HP,C,max}$ = 45°C	• MPC version = MINLPWinterV1.4 • IPOPT max iterations = 10000 • IPOPT acceptable tol. = 0.01 • IPOPT max CPU time = 30s • Slack weights = 1e3 • Pycombina max CPU time = 30s	• Ref. = ca. 23 hours • MPC = ca. 23 hours
						• Ref. = HT(58) • MPC = HT(60)	• Ref. = 5 • MPC = 9
							• NA
Win_16kw_2020.04.08	• Ref. = 08.04.2020 / 13:30 • MPC = 16.04.2020 / 13:30	• Hotel-1 starting on Thursday • EPEX SPOT SE day-ahead	• INES peak = 16 kW$_{th}$ heat • Saturday = 0.85×Workday • Sunday = 0.75×Workday	• $T_{INS,min}$ = 43 °C • $T_{HT1,CHP,max}$ = 70 °C • $T_{HT1,HP,max}$ = 43 °C • Switch = 10 kW$_{th}$ • $T_{r,TC,set}$ = 40 °C	• $T_{HT,min}$ = 95 °C • $T_{HT,max}$ = 10 °C • $T_{r,TC,set}$ = 40 °C • $T_{r,CHP,max}$ = 73°C • $T_{r,HP,C,max}$ = 45°C	• MPC version = MINLPWinterV1.5 • IPOPT max iterations = 10000 • IPOPT acceptable tol. = 0.01 • IPOPT max CPU time = 30s • Slack weights = 1e3 • Pycombina max CPU time = 30s	• Ref. = ca. 4 days • MPC = ca. 3 days
						• Ref. = HT(55) • MPC = HT(55)	• Ref. = 16 • MPC = 18
							• ca. 3 days of optimal control and CHP had maintenance alarm
Win_16kw_2020.04.20	• Ref. = 20.04.2020 / 12:45 • MPC = 23.04.2020 / 12:45	• Hotel-1 starting on Thursday • Load forecast disturbed	• INES peak = 16 kW$_{th}$ heat • Saturday = 0.85×Workday • Sunday = 0.75×Workday	• $T_{INS,min}$ = 43 °C • $T_{HT1,CHP,max}$ = 70 °C • $T_{HT1,HP,max}$ = 43 °C • Switch = 10 kW$_{th}$ • $T_{r,TC,set}$ = 40 °C	• $T_{HT,min}$ = 95 °C • $T_{HT,max}$ = 10 °C • $T_{r,TC,set}$ = 40 °C • $T_{r,CHP,max}$ = 73°C • $T_{r,HP,C,max}$ = 45°C	• MPC version = MINLPWinterV1.5 • IPOPT max iterations = 10000 • IPOPT acceptable tol. = 0.01 • IPOPT max CPU time = 30s • Slack weights = 1e3	• Ref. = ca. 3 days • MPC = ca. 8 days
						• Ref. = HT(55) • MPC = HT(55)	• Ref. = 16 • MPC = 18
							• Same manual disturbance to forecast applied to both tests